



HAL
open science

Study of the mechanisms of action of asphaltene deposition inhibitors.

Jawad El Ghazouani

► **To cite this version:**

Jawad El Ghazouani. Study of the mechanisms of action of asphaltene deposition inhibitors.. Chemical and Process Engineering. Université de Pau et des Pays de l'Adour, 2023. English. NNT: 2023PAUU3057 . tel-04690888

HAL Id: tel-04690888

<https://theses.hal.science/tel-04690888v1>

Submitted on 6 Sep 2024

HAL is a multi-disciplinary open access archive for the deposit and dissemination of scientific research documents, whether they are published or not. The documents may come from teaching and research institutions in France or abroad, or from public or private research centers.

L'archive ouverte pluridisciplinaire **HAL**, est destinée au dépôt et à la diffusion de documents scientifiques de niveau recherche, publiés ou non, émanant des établissements d'enseignement et de recherche français ou étrangers, des laboratoires publics ou privés.

UNIVERSITE DE PAU ET DES PAYS DE L'ADOUR

DOCTORAL THESIS

Study of the Mechanism(s) of Action of Asphaltene Deposition Inhibitors

by
Jawad El ghazouani

*A thesis submitted in fulfillment of the requirements
for the degree of Doctor of Philosophy (Process Engineering)
in the Université de Pau et de Pays de l'Adour (UPPA)*

Laboratoire des fluides complexes et leurs réservoirs (LFCR) - UMR5150
École doctorale des sciences exactes et leurs applications

Dissertation defended on November 23rd, 2023 to the doctoral committee:

Prof. Hervé CARRIER	UPPA	Committee Chair
Dr. Christine DALMAZZONE	IFPEN	Rapporteur
Prof. Lamia GOUAL	University of Wyoming	Rapporteur
Dr. Nicolas PASSADE-BOUPAT	TotalEnergies	Examiner
Prof. Jean-Luc DARIDON	UPPA	PhD Advisor



Declaration of Authorship

I, Jawad EL GHAZOUANI, declare that this thesis titled, “Study of the Mechanism(s) of Action of Asphaltene Deposition Inhibitors” and the work presented in it are my own. I confirm that:

- This work was done wholly or mainly while in candidature for a research degree at this University.
- Where any part of this thesis has previously been submitted for a degree or any other qualification at this University or any other institution, this has been clearly stated.
- Where I have consulted the published work of others, this is always clearly attributed.
- Where I have quoted from the work of others, the source is always given. With the exception of such quotations, this thesis is entirely my own work.
- I have acknowledged all main sources of help.
- Where the thesis is based on work done by myself jointly with others, I have made clear exactly what was done by others and what I have contributed myself.

Signed: Jawad El ghazouani

Date: 20/12/2023

Abstract

[ENGLISH VERSION]

Understanding the mechanisms of action of asphaltene deposition inhibitors is crucial for the petroleum industry, in order to design custom chemical additives tailored to different oil reservoirs and their specific issues. Scientists have strived to offer insights into the interactions between asphaltenes and a range of different chemical additives. However, the majority of these studies have been conducted on model systems (extracted asphaltenes) and under conditions far from actual operational conditions, often involving excessive use of antisolvents.

This thesis work proposes a study of the effects of different chemical additives on asphaltene destabilization, aggregation, and deposition. To achieve this, several complementary techniques were employed to characterize the impact of chemical additives on destabilization and deposition mechanisms, spanning scales from nanometers to micrometers. They include a mechanical technique such as centrifugation, an acoustic method based on a quartz crystal resonator, and optical devices underworking at atmospheric pressure. The combined use of these methods, which involve indirect detection and direct visualization, enabled the evaluation of the effectiveness of a commercial chemical additive, particularly its ability to shift the asphaltene destabilization threshold towards higher antisolvent compositions and reduce the amount of deposition on the quartz disk surface.

Subsequently, the interactions of alkylbenzene-derived compounds with asphaltenes were studied in nondiluted asphaltene-containing oil to assess their ability to shift the destabilization threshold of asphaltenes and inhibit deposition on the walls of equipment used for producing unstable asphaltenes beyond the destabilization threshold. The impact of the polarity of the functional group and the effect of the chain length of these compounds were examined using the aforementioned experimental methods. The results obtained through all these techniques revealed that the presence of a polar group is necessary for the amphiphile to interact with asphaltenes. Furthermore, it has been demonstrated that increasing the length of the alkyl chain contributes to enhanced stabilization of asphaltenes. However, beyond approximately ten carbons in this chain, this improvement appears to reach a plateau.

An investigation into the mechanisms of action of a commercial asphaltene deposition inhibitor and its chemical precursors was also carried out. To understand the mechanism of these chemical additives on the deposition phenomenon, a model of diffusion-limited mass transfer was considered assuming laminar flow between parallel planes. The input parameters for this model, namely the quantity of unstable asphaltenes available in the liquid phase and the rate of deposition of unstable asphaltenes on the surface, were obtained from experimental centrifugation results and continuous titration of the oil with n-heptane using a quartz crystal resonator. The combined use of the mass transfer model and experimental measurements allowed the determination, through inverse techniques, of the diffusion coefficient and the hydrodynamic radius of unstable asphaltene particles. Access to the hydrodynamic radius of unstable asphaltene particles highlighted that the presence of chemical additives affects the size of unstable particles, however, on average, the particles contributing to deposition accumulation exhibit sizes of the same order of magnitude as nanoaggregates and stable clusters (<20 nm). Additionally, the results demonstrate that in the presence of chemical additives, the mass transfer phenomenon remains diffusion-limited. Thus, deposition inhibitors have the effect of stabilizing asphaltenes, reducing the quantity of unstable particles available for diffusion, in addition to impacting the size of the depositing particles.

[VERSION FRANCAISE]

La compréhension des mécanismes d'action des inhibiteurs de dépôt d'asphaltène est essentielle pour l'industrie pétrolière, afin de concevoir des additifs chimiques sur mesure adaptés aux différents réservoirs pétroliers et à leurs problèmes spécifiques. Les chercheurs se sont efforcés de fournir des réponses concernant les interactions entre les asphaltènes et divers additifs chimiques, qu'ils soient commerciaux ou non. Cependant, la majorité de ces recherches ont été menées sur des systèmes modèles (asphaltènes extraits) et dans des conditions très éloignées des conditions opérationnelles réelles, avec par exemple l'utilisation excessive d'antisolvant.

Ce travail de thèse propose une étude des effets de différents additifs chimiques sur la déstabilisation, l'agrégation et la déposition des asphaltènes. Pour cela, plusieurs techniques complémentaires ont été utilisées afin de caractériser l'effet des additifs chimiques sur les mécanismes de déstabilisation et déposition qui couvrent des échelles allant du nanomètre au micromètre. Une technique mécanique : la centrifugation, une méthode acoustique basée sur un résonateur à cristal de quartz et des dispositifs optiques ont ainsi été employés à pression atmosphérique. L'emploi conjoint de ces méthodes de détection indirecte et de visualisation directe a permis d'évaluer l'efficacité d'un additif chimique commercial et notamment sa capacité à décaler le seuil de la déstabilisation des asphaltènes vers des compositions en antisolvant plus élevées et à réduire la quantité de dépôt à la surface du disque de quartz.

Les interactions des composés de type alkylbenzène avec les asphaltènes ont ensuite été étudiées dans une huile asphalténique non diluée afin d'évaluer leur capacité à déplacer le seuil de déstabilisation des asphaltènes et à inhiber la déposition sur les parois des équipements de production des asphaltènes instables au-delà du seuil de déstabilisation. L'impact de la polarité du groupement fonctionnel et l'effet de la longueur de la chaîne de ces composés ont été examinés à l'aide des méthodes expérimentales mentionnées précédemment. Les résultats obtenus par l'ensemble de ces techniques ont révélé que la présence d'un groupement polaire est nécessaire pour que l'amphiphile puisse interagir avec les asphaltènes. De plus, il a été montré qu'une augmentation de la longueur de la chaîne alkyle permet d'améliorer la stabilisation des

asphaltènes. Toutefois, au-delà d'une dizaine de carbones dans cette chaîne, cette amélioration semble atteindre un plateau.

Une étude sur les mécanismes d'action d'un inhibiteur de dépôt d'asphaltène commercial et de ses précurseurs chimiques a aussi été menée. Afin de comprendre les mécanismes d'action de ces additifs chimiques sur le phénomène de déposition, un modèle de transfert de masse contrôlé par diffusion, en postulant un écoulement laminaire entre plans parallèles, a été utilisé. Les paramètres d'entrée de ce modèle, à savoir la quantité d'asphaltènes instables disponible dans la phase liquide et la vitesse de déposition des asphaltènes instables sur la surface, ont été obtenus à partir de résultats expérimentaux de centrifugation ainsi que du titrage continu de l'huile par le n-heptane en utilisant un résonateur à cristal de quartz. L'utilisation conjointe du modèle de transfert de masse et des mesures expérimentales a permis de déterminer par technique inverse le coefficient de diffusion ainsi que le rayon hydrodynamique des particules d'asphaltène instables. L'accès au rayon hydrodynamique des particules d'asphaltènes instables a permis de mettre en évidence qu'en présence d'additifs chimiques, la taille des particules instables est affectée, mais en moyenne, les particules contribuant à l'accumulation de dépôt présentent des tailles du même ordre de grandeur que les nanoagrégats et les clusters stables (<20 nm). De plus, les résultats démontrent qu'en présence d'additifs chimiques, le phénomène de transfert de matière reste limité par la diffusion. Les inhibiteurs de dépôt ont donc pour effet de stabiliser les asphaltènes, réduisant ainsi la quantité de particules instables disponible pour la diffusion, en plus d'impacter la taille des particules qui déposent.

Acknowledgements

Ce travail de thèse a été une expérience inoubliable, gravée à jamais dans ma mémoire. J'ai pleinement conscience de la chance qui m'a été donnée de mener cette recherche à la croisée du monde universitaire, à l'Université de Pau et des Pays de l'Adour, et du secteur industriel au sein de TotalEnergies.

Je suis profondément reconnaissant envers toutes les personnes qui ont contribué à la réalisation de ce projet. Ces trois années ont été une aventure riche en rencontres et en apprentissages, tant sur le plan intellectuel que personnel.

Tout d'abord, je tiens à exprimer ma gratitude au Professeur Jean-Luc Daridon pour sa supervision de ce travail de recherche. Sa patience et sa disponibilité ont été d'une aide précieuse. J'ai énormément appris à ses côtés, ses connaissances pointues dans le domaine théorique et expérimental ont été une source inestimable de savoir pour moi. Sa confiance et son ouverture à de nouvelles idées m'ont permis de m'épanouir totalement au cours de cette thèse.

Un immense merci également à Mohamed Saidoun, un mentor exceptionnel, dont les conseils avisés m'ont inculqué un esprit critique et une rigueur qui seront précieux pour la suite de ma carrière. Sa capacité à aborder les problèmes sous un nouvel angle et à proposer des hypothèses a été extrêmement bénéfique tout au long de ce projet de recherche.

Je tiens à adresser mes remerciements particuliers à Moussa Kane et Julien Guerin pour leur suivi attentif de mon travail de recherche, ainsi que pour leur soutien précieux du côté industriel. Je suis profondément reconnaissant envers toute l'équipe du Hall 6, en particulier Marianne Pedelabat-Lartigau, David Mayou, Didier Laurensen, Roel Belt, ainsi que toutes les équipes de TotalEnergies du PERL et du CSTJF, pour leur accueil chaleureux, leur esprit d'équipe et leur solidarité. Un merci tout particulier à Leticia Ligiero, qui m'a offert l'opportunité de découvrir le monde de la recherche en entreprise lors de mon stage au laboratoire d'analyse du PERL. Cette expérience a confirmé ma volonté de poursuivre avec une thèse à la fin de mon master.

Au Laboratoire des Fluides Complexes et leurs Réservoirs, j'ai eu la chance de travailler aux côtés de personnes hautement compétentes et humainement exceptionnelles. Un remerciement spécial à Nelson et José, des collègues formidables devenus des amis, qui ont grandement contribué à mon intégration au sein de l'équipe LFCR. Leur expérience et leurs conseils m'ont énormément aidé pour la prise en main des différents montages expérimentaux. Mes remerciements vont également à toutes les personnes ayant facilité mon travail par leur soutien technique et administratif, notamment Djamel Nasri, Jean-Patrick Bazile, Catherine Urrea, Patricia Lafont, Blandine Gaio, Romain Vermorel et Isabel Boisard.

Je souhaite exprimer ma reconnaissance envers Madame Christine Dalmazzone et la Professeure Lamia Goual pour leur intérêt manifesté envers ce travail de recherche et leurs retours positifs lors de la soutenance de thèse. De même, je remercie chaleureusement le Professeur Hervé Carrier et Nicolas Passade-Boupat pour leur présence et nos échanges enrichissants.

À chacune des personnes mentionnées, je vous souhaite une route éclairée de succès et de bonheur. Vous êtes tous des personnes remarquables et je suis honoré d'avoir pu croiser votre chemin.

Enfin, je dédie ce travail de thèse à ma famille, et spécialement à mes parents dont le soutien constant a toujours été mon moteur pour tous mes projets.

Contents

Abstract	vi
Contents	xi
List of Figures	xv
List of Tables	xxiii
List of Abbreviations and Symbols	xxv
List of Abbreviations.....	xxv
List of Symbols.....	xxvii
Introduction	1
Chapter 1. State of the Art	4
1. Introduction.....	4
2. Asphaltenes and their environment.....	7
2.1. Composition and physical properties.....	7
2.2. Molecular structure of asphaltenes.....	9
2.3. Aggregation state of asphaltenes in good solvent.....	12
2.4. Asphaltenes destabilization.....	13
3. Asphaltenes management.....	18
3.1. Flow assurance issues related to asphaltenes.....	18
3.2. Prevention methods.....	20
3.3. Remediation methods.....	32
4. State of the Art summary.....	36
5. References.....	37
Chapter 2. Experimental Methods	47
1. Laboratory methods for evaluating behavior of asphaltene in the liquid phase and their deposition.....	47
5.1. Liquid phase tests.....	48
1.2. Deposition tests.....	52
1.3. Screening laboratory methods for evaluating chemical additives.....	54
1.4. Conclusions on the literature review.....	56
2. Experimental Methods.....	57
2.1. The quartz crystal resonator as an acoustic sensor.....	57

2.2. Centrifugation experiment.....	73
2.3. Optical microscopy techniques.....	78
2.4. Turbidity experiment	81
3. Definition of the oil and chemicals	81
4. Sample preparation	83
5. References.....	84
Chapter 3. Experimental evaluation method of chemical additive efficacy at atmospheric pressure using a fully immersed Quartz Crystal Resonator, centrifugation and optical microscopy techniques.....	91
1. Introduction.....	91
2. Chemicals.....	92
3. Results and discussion	93
3.1. Turbidity experiment	93
3.2. QCR experiment – Chemical additive effect on crude oil: Raw data (Δf and $\Delta \Gamma n$) analysis	94
3.3. Centrifugation experiment	103
3.4. SWIR microscopy	104
3.5. Detection Time experiment.....	106
3. Conclusions.....	107
4. References.....	109
Chapter 4. Effect of the chemical structure of alkylbenzene-derived amphiphiles on asphaltene destabilization, aggregation and deposition	112
1. Introduction.....	112
2. Chemicals.....	114
3. Results and discussion	115
3.1. Effect of functional group of amphiphilic molecules	115
3.2. Effect of alkyl chain length of amphiphilic molecules.....	123
4. Conclusions.....	128
5. References.....	129
Chapter 5. Understanding the mechanism of action of chemical additives on asphaltene deposition.....	132
1. Introduction.....	132
2. Materials and methods	135
2.1. Materials	135
2.2. Methods	137
3. Results and discussion	146

3.1. Evaluation of the chemical additive's interaction with QCR surface	146
3.2. Concentration of unstable asphaltenes	147
3.3. Modeling deposition rate of unstable asphaltene particles by adjusting the diffusion coefficient	154
3.4. Effect of chemical additives	158
3.5. Discussions	166
4. Conclusions.....	172
5. References.....	174
Conclusions and Perspectives	177
References.....	180

List of Figures

Chapter 1. State of the Art

Figure 1. Evolution in selected energy price indicators since September 2020. Sources: IEA analysis based on Argus Media (2022); ICIS (2022); BNEF (2022).....	5
Figure 2. Global direct primary energy consumption in 2021. Data obtained from BP's Statistical Review of World Energy (2022).....	6
Figure 3. Density correlation (Equation 1) compared to density of asphaltene cuts from four samples at 23 °C (reprinted from Barrera et al. ¹⁰).	9
Figure 4. Schematic of island and archipelago structures (reproduced from Hoepfner ¹³).	10
Figure 5. AFM measurements (scale bars: 5 Å) and assigned structures from various asphaltene samples (reprinted from Shuler et al. ¹²).	11
Figure 6. Schematic illustration of results on the molecular order of asphaltene obtained by X-ray scattering (reprinted from Hoepfner ¹³).	12
Figure 7. Typical Pressure-Temperature Asphaltene Phase Envelope (reproduced from Akbarzadeh et al. ⁴¹).	14
Figure 8. Interaction forces between asphaltene surfaces in various solvents (reprinted from Wang et al. ⁴²).	15
Figure 9. Schematic of the structural reorganization of asphaltene clusters in n-heptane (reprinted from Hoepfner ¹³).	16
Figure 10. Multiscale destabilization and aggregation of asphaltene.	16
Figure 11. Asphaltene deposition in production tubing in an oilfield in the Gulf of Mexico (reprinted from Borden ⁴⁷).	19

Figure 12. (a) ASCI as a function of the density of crude oils at reservoir conditions. (b) ASCI risk evaluation method (reprinted from Rondon et al.⁵⁹). P_{ini} is the pressure at reservoir conditions P_b are theoretical bubble points. 25

Figure 13. Comparison between different models in predicting asphaltene destabilization versus pressure for (A) oil sample; and (B) oil sample 6 (reprinted from Daryasafar et al.⁷⁶). 29

Chapter 2. Experimental Methods

Figure 1. Results of the relationship between the DPE^{15} of commercial dispersants at 70 ppm and the corresponding amount of deposition measured using a multi-section packed bed system at 70 vol% n-heptane and ambient conditions in (A) crude oil S ; (B) crude oil R (60 ppm of dispersant) (reprinted from Kuang et al.²⁴). 55

Figure 2. Quartz crystal resonator Thickness Shear Mode. 58

Figure 3. Schematic of a quartz crystal resonator immersed in a liquid. 59

Figure 4. Measurement of frequency and impedance shifts in air and in an oil-type liquid. 64

Figure 5. Theoretical conductance spectra a) usable harmonic signal with small n b) inharmonics that interfere with the resonance signal with large n. 66

Figure 6. Atmospheric pressure experimental titration QCR set-up..... 67

Figure 7. Red symbols are experimental frequency shifts (3rd overtone) obtained during continuous addition of a) toluene at 20°C and b) n-heptane at 60°C; solid line corresponds to the dilution model calculated using Equation 20 (reported by Saidoun et al.⁴³). 70

Figure 8. Shift of dissipation (3rd harmonic) recorded during experimental titration of a) a non-diluted crude oil and b) a diluted oil; solid lines correspond to the dilution model. 71

Figure 9. Percent deviation of the measured data from the calculated dilution curve; the symbols in green (○) correspond to the non-diluted crude oil and the symbols in blue (◆) correspond to the diluted crude oil. 72

Figure 10. Deposited mass at the surface au the QCR calculated using Equation 21 during continuous addition n-heptane in a crude oil at 60°C. 73

Figure 11. Concentration of unstable asphaltene aggregates larger than 200 nm separated by centrifugation as a function of the aging time for oil X titrated with 71.0 vol % of n-heptane.... 74

Figure 12. Calculated separation efficiency as a function of the particle size for several centrifuge run-times. 78

Figure 13. Detection time measurement for a mixture at a constant oil-heptane ratio. 79

Figure 14. SWIR camera capture at X50 magnification of crude oil X at A) 40 vol % of n-heptane B) 83 vol % of n-heptane. 80

Chapter 3. Experimental evaluation method of chemical additive efficacy at atmospheric pressure using a fully immersed Quartz Crystal Resonator, centrifugation and optical microscopy techniques

Figure 1. Chemical structure of additive A..... 92

Figure 2. Relative absorbance of Oil X in presence of chemical additive A at different concentrations: (red ×) 0 ppm, (black ○) 10 ppm, (yellow ■) 30 ppm, (purple ▲) 100 ppm, (green ◆) 300 ppm, (blue ●) 1000 ppm, (grey □) 3000 ppm..... 94

Figure 3. Determination of "onset" from resonance frequency measurements. 95

Figure 4. Shift of resonance frequency (3rd harmonic) recorded during experimental titration of crude oil X + chemical additive A at different concentrations as a function of the volume fraction of n-heptane: (red ×) 0 ppm, (green ◆) 300 ppm, (blue ●) 1000 ppm, (grey □) 3000 ppm, (brown ○) 5000 ppm, (yellow ✱) 10,000 ppm, (purple △) 20,000 ppm. A zoom of the frequency shift between 0.5 and 0.75 volume fraction of n-heptane is shown in the inner box..... 96

Figure 5. Shift of dissipation (3rd harmonic) recorded during experimental titration of crude oil X + chemical additive A at different concentrations as a function of the volume fraction of n-heptane: (red ×) 0 ppm, (green ◆) 300 ppm, (blue ●) 1000 ppm, (grey □) 3000 ppm, (brown ○) 5000 ppm, (yellow ✱) 10,000 ppm, (purple △) 20,000 ppm. 99

Figure 6. Apparent viscosity of the surrounding fluid calculated during experimental titration of crude oil X + chemical additive A at different concentrations as a function of the volume fraction of heptane: (black -) theoretical viscosity, (red ×) 0 ppm, (green ◆) 300 ppm, (blue ●) 1000 ppm, (grey □) 3000 ppm, (brown ○) 5000 ppm, (yellow ✱) 10,000 ppm, (purple △) 20,000 ppm. 100

Figure 7. Deposited mass calculated during experimental titration of crude oil X + chemical additive A at different concentrations as a function of the volume fraction of n-heptane: (red ×) 0 ppm, (green ◆) 300 ppm, (blue ●) 1000 ppm, (grey □) 3000 ppm, (brown ○) 5000 ppm, (yellow ✱) 10,000 ppm, (purple △) 20,000 ppm..... 101

Figure 8. Concentration of unstable asphaltenes larger than 200 nm separated by centrifugation as a function of the aging time of prepared blends of crude Oil X and n-heptane: (red ○) nontreated Oil X + 61.1 vol % of n-C7, (orange △) Oil X + chemical additive A (3000 ppmv) + 61.1 vol % of n-C7. The dotted lines are made to facilitate the reading of the trends. 103

Figure 9. SWIR camera capture at X50 magnification of crude oil X + chemical additive A samples at 83 vol % n-heptane: (A) 0 ppm, (B) 1000 ppm, (C) 3000 ppm, (D) 5000 ppm, (E) 10,000 ppm, (F) 20,000 ppm..... 105

Figure 10. Necessary aging time to detect particles by visual microscopy observations as function of the volume fraction of n-heptane in heptane-oil blends: (red ●) nontreated oil X, (orange ▲) oil X + chemical additive A at 3000 ppmv..... 106

Chapter 4. Effect of the chemical structure of alkylbenzene-derived amphiphiles on asphaltene destabilization, aggregation and deposition

Figure 1. Amphiphilic structure with X: the active functional group; R: the alkyl chain and the benzene ring circled in red..... 112

Figure 2. Necessary aging time to detect particles by visual microscopy observations as function of the volume fraction of n-heptane in heptane-oil blends: (red ●) nontreated oil X, (purple ▲) oil X + NB at 3000 ppm, (yellow ■) oil X + DDBSA at 3000 ppm and (grey ◇) oil X + DP at 3000 ppm. 117

Figure 3. Concentration of unstable asphaltenes larger than 200 nm separated by centrifugation as a function of the aging time of prepared blends of crude Oil X + 60 vol % ± 0.3% n-heptane: (red ●) nontreated oil X, (purple ▲) oil X + NB at 3000 ppm, (yellow ■) oil X + DDBSA at 3000 ppm and (grey ◇) oil X + DP at 3000 ppm. The solid lines are made to facilitate the reading of the trends. 118

Figure 4. (a) shift of resonance frequency (3rd harmonic) recorded during continuous titration of crude oil X as a function of the volume fraction of n-heptane: (red ●) nontreated oil X, (purple ▲) oil X + NB at 3000 ppm, (yellow ■) oil X + DDBSA at 3000 ppm and (grey ◇) oil X + DP at 3000 ppm. (b) zoom of the frequency shift between 0.55 and 0.75 volume fraction of n-heptane. 119

Figure 5. (a) deposited mass and (b) deposition rate, calculated during experimental titration of crude oil X with n-heptane. (red ●) nontreated oil X, (purple ▲) oil X + NB at 3000 ppm, (yellow ■) oil X + DDBSA at 3000 ppm and (grey ◇) oil X + DP at 3000 ppm. 121

Figure 6. (a) shift of resonance frequency (3rd harmonic) and (b) deposited mass, during continuous titration of crude oil X as a function of the volume fraction of n-heptane. (red ●) nontreated oil X, (blue ○) oil X + DDBSA at 300 ppm, (yellow ■) oil X + DDBSA at 3000 ppm and (black +) oil X + DDBSA at 10,000 ppm. 122

Figure 7. Necessary aging time to detect particles by visual microscopy observations as function of the volume fraction of n-heptane in heptane-oil blends: (red ●) nontreated oil X, (green ×) oil X + EP at 3000 ppm, (blue ○) oil X + NP at 3000 ppm and (grey ◇) oil X + DP at 3000 ppm. 124

Figure 8. Concentration of unstable asphaltenes larger than 200 nm separated by centrifugation as a function of the aging time of prepared blends of crude Oil X + 60 vol % ± 0.3% n-heptane: (red ●) nontreated oil X, (green ×) oil X + EP at 3000 ppm, (blue ○) oil X + NP at 3000 ppm and (grey ◇) oil X + DP at 3000 ppm. The solid lines are made to facilitate the reading of the trends. 125

Figure 9. (a) shift of resonance frequency (3rd harmonic) recorded during continuous titration of crude oil X as a function of the volume fraction of n-heptane: (red ●) nontreated oil X, (green ×) oil X + EP at 3000 ppm, (blue ○) oil X + NP at 3000 ppm and (grey ◇) oil X + DP at 3000 ppm. (b) zoom of the frequency shift between 0.55 and 0.75 volume fraction of n-heptane. 126

Figure 10. (a) deposited mass and (b) deposition rate, calculated during experimental titration of crude oil X with n-heptane. (red ●) nontreated oil X, (green ×) oil X + EP at 3000 ppm, (blue ○) oil X + NP at 3000 ppm and (grey ◇) oil X + DP at 3000 ppm. 127

Chapter 5. Understanding the mechanism of action of chemical additives on asphaltene deposition

Figure 1. Comparison of structure of chemical additive A with B and C. 137

Figure 2. Kinetics of asphaltenes destabilization and aggregation. 138

Figure 3. Schematic of unstable asphaltenes particles travelling at a velocity $U_x(x,y)$ in the momentum boundary layer (green dashed line) over a parallel solid surface and depositing through a mass-transfer boundary layer (red dashed line) controlled by the mass transfer coefficient k_c . $C_{A,d}$, liquid and $C_{A,s}$, surface are the liquid and surface concentrations of unstable asphaltenes particles respectively. 143

Figure 4. Average superficial velocities U_0 as a function of the revolution speed of the magnetic stirrer (reprinted from Saidoun et al.⁵). 145

Figure 5. Ratio of the shifts of resonance frequency and dissipation (3rd harmonic), for QCR immersed in pure toluene (black \diamond), toluene + 3000 ppmv of chemical additive A (orange \blacksquare), toluene + 3000 ppmv of chemical additive B (blue \blacktriangle), toluene + 3000 ppmv of chemical additive C (purple \ast), toluene + 3000 ppmv of chemical additive D (yellow \circ), as a function of time at 60 °C and atmospheric pressure. 147

Figure 6. Concentration of unstable asphaltenes larger than 200 nm for nontreated oil X as function of aging time at multiple n-heptane volume fractions: (grey \blacksquare) 56.2 vol% n-C₇, (yellow \bullet) 61.1 vol% n-C₇, (blue \square) 66.0 vol% n-C₇, (green \triangle) 71.0 vol% n-C₇, (purple \blacktriangle) 80.7 vol% n-C₇. The dashed lines are calculated from Equation 6. 148

Figure 7. (a) Equilibrium concentration of unstable asphaltenes as a function of n-heptane volume fraction for nontreated oil X. The symbols correspond to the experimental data obtained by centrifugation measurements and the red solid line is calculated from Equation 8. (b) Characteristic time of equilibration τ as a function of n-heptane volume fraction for nontreated oil X. The symbols correspond to the experimental data obtained by centrifugation measurements and the red solid line is calculated from Equation 7. 150

Figure 8. The red solid line is the concentration of unstable asphaltenes for the nontreated oil X as a function of n-heptane volume fraction calculated using Equation 6 for a 3.5h aged mixture. The symbols represent the experimental data obtained by centrifugation with the same aging time for nontreated oil X. 151

Figure 9. Generation rate of unstable asphaltenes dC_A/dt as a function of n-heptane volume fraction in nontreated oil X during continuous addition of n-heptane. 154

Figure 10. Asphaltene deposition rate (a) and deposited mass (b) on QCR sensor surface as a function of time during continuous titration of oil X with n-heptane. Symbols are experimental data and the solid lines are the computed values using Equations 32 (a) and 21 (b) with a fixed RA of 9.5 nm. 156

Figure 11. Symbols are experimental data obtained by QCR and the solid lines are the computed values of (a) the deposition rate using Equation 32 and (b) the cumulative mass of deposited asphaltenes using Equation 21 ; both as a function of time during continuous n-heptane addition and with a fitted RA. 157

Figure 12. Mean hydrodynamic radius of diffusing primary particles during the continuous titration of oil X with n-heptane. 157

Figure 13. (a) Shift of resonance frequency (3rd harmonic) recorded during experimental titration of different crude oil X + chemical additive systems as a function of the volume fraction of n-heptane: (red ●) nontreated oil X, (orange ▲) chemical additive A at 3000 ppmv, (blue ■) chemical additive B at 3000 ppmv, (purple ×) chemical additive C at 3000 ppmv and (green ◆) chemical additive D at 3000 ppmv. A zoom of the frequency shift between 0.50 and 0.70 volume fraction of n-heptane is shown in the right-hand figure (b). 159

Figure 14. (a) Equilibrium concentration of unstable asphaltenes as a function of n-heptane volume fraction. The symbols correspond to the experimental data obtained by centrifugation measurements and the solid lines are calculated from Equation 8. (b) Characteristic time of equilibration τ as a function of n-heptane volume fraction. The symbols correspond to the experimental data obtained by centrifugation measurements and the solid lines are calculated from Equation (7).(red ●) nontreated oil X, (orange ▲) chemical additive A at 3000 ppmv, (blue ■) chemical additive B at 3000 ppmv, (purple ×) chemical additive C at 3000 ppmv and (green ◆) chemical additive D at 3000 ppmv.161

Figure 15. Symbols are experimental data obtained by QCR and solid lines are computed deposition rate with a fitted mean hydrodynamic radius. 162

Figure 16. (a) deposition rate and (b) cumulative deposited mass as a function of n-heptane volume fraction in presence of the chemical additives. 164

Figure 17. Mean hydrodynamic radius of diffusing primary particles as a function of n-heptane volume fraction in presence of chemical additives. 165

Figure 18. Results for oil X treated with 3000 ppmv of chemical additive B: (I) resonant frequency changes raw data obtained from the QCR; (II) experimental (symbols) and modeled data (lines) of the concentration of unstable asphaltenes obtained through centrifugation for $t = 3.5$ h (III) deposition rate measured by the QCR; and (IV) the hydrodynamic radius fitted using the diffusion limited model. 167

Figure 19. Results for oil X treated with 3000 ppmv of chemical additive D: (I) resonant frequency changes raw data obtained from the QCR; (II) experimental (symbols) and modeled data (lines) of the concentration of unstable asphaltenes obtained through centrifugation for $t = 3.5$ h (III) deposition rate measured by the QCR; and (IV) the hydrodynamic radius fitted using the diffusion limited model. 168

Figure 20. Results for oil X treated with 3000 ppmv of chemical additive C: (I) resonant frequency changes raw data obtained from the QCR; (II) experimental (symbols) and modeled data (lines) of the concentration of unstable asphaltenes obtained through centrifugation for $t = 3.5$ h (III) deposition rate measured by the QCR; and (IV) the hydrodynamic radius fitted using the diffusion limited model. 170

Figure 21. Results for oil X treated with 3000 ppmv of chemical additive A: (I) resonant frequency changes raw data obtained from the QCR; (II) experimental (symbols) and modeled data (lines) of the concentration of unstable asphaltenes obtained through centrifugation for $t = 3.5$ h (III) deposition rate measured by the QCR; and (IV) the hydrodynamic radius fitted using the diffusion limited model. 171

List of Tables

Chapter 1. State of the Art

Table 1. Asphaltenes PVT lab experiments (GEOMARK, 2013 ⁵⁴).	21
Table 2. Hansen Solubility Parameter (MPa ^{1/2}) ⁸⁶	35

Chapter 2. Experimental Methods

Table 1. Oil-heptane mixture properties at 60°C.	77
Table 2. Properties of crude oil X.	82

Chapter 3. Experimental evaluation method of chemical additive efficacy at atmospheric pressure using a fully immersed Quartz Crystal Resonator, centrifugation and optical microscopy techniques

Table 1. Properties of chemical additive A.	92
Table 2. Deposition inhibition efficiency of the oil treated by chemical additive A at 80 vol % n-heptane composition.	102

Chapter 4. Effect of the chemical structure of alkylbenzene-derived amphiphiles on asphaltene destabilization, aggregation and deposition

Table 1. Chemical structures of amphiphilic compounds.	115
Table 2. Instantaneous detection time of asphaltene particles larger than 0.5 μm	117
Table 3. “Onset” of destabilization from resonant frequency measurements.	120
Table 4. Instantaneous detection time of asphaltene particles larger than 0.5 μm	124
Table 5. “Onset” of destabilization from resonant frequency measurements.	127

Chapter 5. Understanding the mechanism of action of chemical additives on asphaltene deposition

Table 1. Structures of chemical additives.	136
Table 2. “Onset” of destabilization from resonant frequency measurements.	159

List of Abbreviations and Symbols

List of Abbreviations

AD	Asphaltene Dispersant
ADT	Asphaltene Dispersion Test
AFM	Atomic Force Microscopy
AOP	Asphaltene Onset Pressure
ASCI	Asphaltene Solubility Class Index
C-EOS	Cubic Equations Of State
CCC	Critical Cluster Concentration
CCE	Constant Composition Expansion
CII	Colloidal Instability Index
CNAC	Critical Nano Aggregate Concentration
CPA	Cubic-Plus-Association
CSI	Colloidal Stability Index
DLD	Diffusion Limited Deposition
DL	Differential Liberation
DPE	Dispersing Performance Efficiency
EOS	Equation of State
EU	European Union
FH	Flory Huggins
FT-ICR	Fourier Transform Ion Cyclotron Resonance
HPHT	High-Pressure High-Temperature
HPM	High-Pressure Microscope
HRTEM	High-Resolution Transmission Electron Microscopy

IEA	International Energy Agency
LDI	Laser Desorption Ionization
LNG	Liquified Natural Gaz
MD	Molecular Dynamics
MS	Mass Spectrometry
NIR	Near Infrared
NMR	Nuclear Magnetic Resonance
OBM	Oil Base Mud
OCM	Oil Compatibility Model
PAH	Polycyclic Aromatic Hydrocarbon
PC-SAFT	Perturbed Chain - Statistical Associating Fluid Theory
PR	Peng-Robinson
PVT	Pressure-Volume-Temperature
QCM	Quartz Crystal Microbalance
QCR	Quartz Crystal Resonator
RCF	Relative Centrifugal Force
RPM	Revolution Per Minute
RST	Regular Solution Theory
SANS	Small Angle Neutron Scattering
SARA	Saturates Aromatics Resins Asphaltenes
SAXS	Small Angle X-ray Scattering
SDS	Solid Detection System
SEM	Scanning Electron Microscopy
SLD	Shear Limited Deposition
SRK	Soave-Redlich-Kwong
SP	Stankiewicz Plot

STO	Stock-tank Oil
SWIR	Short-Wave Infrared
TSM	Thickness Shear Mode
USAXS	Ultra-Small Angle X-ray Scattering
WAT	Wax Appearance Temperature
WAXS	Wide Angle X-ray Scattering

List of Symbols

δ	Solubility parameter	MPa ^{1/2}
δ_p	Penetration length of the acoustic wave in the contacting media	m
Γ	Resonance dissipation	Hz
Δ	Difference	-
η	Dynamic viscosity	mPa.s ⁻¹
λ	Wavelength	m
ρ	Density	kg.m ⁻³
τ	Characteristic time to reach equilibrium	h
v_m	Molar volume	cm ³ .mol ⁻¹
ϕ	Volume fraction	-
ψ	Correction factor of trapped liquid in asphaltenes deposit	-
ω	Angular speed	rad.s ⁻¹
C_7	Heptane	-
C_i	Concentration of i component	kg. m ⁻³
C_m	Sauerbrey coefficient	m ² .kg ⁻¹ .s ⁻¹
D_A	Diffusion coefficient of depositing asphaltenes	m ² .s ⁻¹

D_f	Fractal dimension	-
d_i	Diameter of i particle	m
f	Resonance frequency	Hz
f_0	Fundamental resonance frequency	Hz
F_{df}	Frictional forces	kg.m.s ⁻²
f_n	Resonance frequency from the overtone number of resonance n	Hz
F_{obj}	Objective function	-
G	Adjusted parameter of the Grunberg-Nissan equation	-
h	Thickness of the deposited film on the quartz resonator	m
H_L	Height of the liquid in the centrifugation tube	m
h_{layer}	Elastic virtual thickness	m
h_q	Thickness of the quartz disc	m
H_{vap}	Enthalpy of vaporization	J
k_c	Convective mass transfer coefficient	m.s ⁻¹
k_D	Generation rate constant of unstable asphaltenes	s ⁻¹
k_r	Reaction rate constant	s ⁻¹
L	Characteristic length	m
L_c	Length of the capillary	m
m	Masse	kg
MW	Molecular weight	g.mol ⁻¹
n	Overtone number of resonance	-
n_D	Refractive index	-
P	Pressure	bar
Q	Volumetric flow rate	m ³ .s ⁻¹
R	Empirical term in the Sauerbrey equation	-
r_1	Destabilization rate of asphaltenes	kg.m ⁻³ .s ⁻¹

R_A	Hydrodynamic radius of unstable asphaltenes	nm
$Rate_{dep}$	Deposition rate	kg.s ⁻¹
R_c	Radius of the capillary	m
R_p	Hydrodynamic radius of primary particles	nm
r_i	Residual value	-
S_c	Schmidt dimensionless number	-
Sh	Sherwood dimensionless number	-
S_{QCR}	Quartz sensor surface area	m ²
t	Time	s
u	Particle velocity	m.s ⁻¹
U_0	Fluid superficial velocity	m.s ⁻¹
V	Volume	m ³
v_q	Propagation velocity of the acoustic wave in the quartz resonator	m.s ⁻¹
x	Mass fraction	-

X_0	Property at the reference conditions
X_∞	Property at equilibrium
X_A	Property of unstable asphaltenes
X_{asph}	Property of the asphaltenes
$X_{A,d,liquid}$	Property of contributing asphaltenes to deposition in the liquid phase
X_{dep}	Property of the deposit
X_{eff}	Effective property
X_f	Final property
X_i	Initial property

X_{liquid}	Property of the liquid phase
X_{oil}	Property of the oil
X_q	Property of the quartz crystal

Introduction

The global energy demand continues to grow, and the challenges of energy transition are more important than ever. Increasing the share of decarbonized energies in the energy mix is essential to limit greenhouse gas emissions. However, the evolution of the energy mix faces geopolitical, demographic, economic, and social constraints of countries and regions. Moreover, there exists a pressing need to fulfill today's energy requirements while proactively strategizing for the energy needs of tomorrow. Currently, the global energy landscape still heavily relies on fossil fuels, accounting for approximately 85% of the energy mix in 2021. To address this energy demand, oil companies have expanded their operations beyond conventional deposits to deep offshore fields, where they encounter complex temperature and pressure conditions.

These operational conditions make hydrocarbon supply more challenging. This is particularly true for oil and its components, which are sensitive to their environment. Asphaltenes represent the most polar and heaviest fraction of oil. Asphaltenes destabilize with changes in temperature, pressure, and/or composition, leading to self-association and deposition on the surfaces of reservoir rocks or pipelines. These deposits impact oil extraction and flow, and in the worst cases, they can completely block pipelines, halting production. One of the preferred solutions by the oil industry is the injection of asphaltene deposition inhibitors to prevent or reduce deposit formation. However, to design tailored chemical additives for each reservoir, it's essential to understand the mechanisms of action of these chemistries. The objectives of this thesis work are to elucidate the mechanisms of action of asphaltene deposition inhibitors and to propose a workflow for assessing the efficacy of these chemical additives.

This manuscript is divided into 5 chapters, in addition to this introduction.

Chapter 1 provides a state of the art on the nature of asphaltenes and the industrial problems they cause at all stages of the oil supply chain.

Chapter 2 provides a concise overview of commonly used experimental techniques in the literature for characterizing asphaltene destabilization in the liquid phase and their deposition on surfaces.

The complementary experimental methods selected for this work are detailed, along with the properties of the oil and solvents used.

Chapter 3 presents a workflow for evaluating the effect of a commercial asphaltene deposition inhibitor. The effect of the deposition inhibitor is investigated from nanoscale to micrometer scale destabilization, aggregation, and deposition. A quartz crystal resonator (QCR) fully immersed in crude oil (nondiluted in a solvent) is used to detect asphaltene destabilization and surface deposition during continuous titration of an antisolvent (n-heptane) in the presence or absence of the chemical additive. A preliminary study on the effect of concentration identified an appropriate working concentration for further investigations. In addition to the results obtained with the acoustic sensor, the concentration of destabilized asphaltenes is evaluated through centrifugation, and aggregation kinetics are characterized through optical microscope observations.

Chapter 4 presents the results of a study on the effect of the chemical structure of alkylbenzene-derived amphiphiles in oil. The effect of polar groups and alkyl chain length on destabilization, aggregation, and deposition is studied using the workflow proposed in the previous chapter.

Chapter 5 investigates the mechanisms of action of a commercial chemical additive and its precursors on the deposition of unstable asphaltenes on a surface. The liquid phase is characterized through centrifugation measurements, and deposition is quantified using the QCR during continuous titration of n-heptane. The concentration of available unstable asphaltenes obtained through centrifugation, as well as the deposition rate obtained with the acoustic sensor, are then used in a diffusion-limited model to evaluate the evolution of the hydrodynamic radius of particles diffusing to the surface during continuous addition of n-heptane.

Finally, the last section presents conclusions drawn from the previous chapters and establishes a workflow for investigating the effect of a chemical additive. Recommendations for further research to confirm and complement the results are put forward.

At the end of each chapter, a list of references is provided.

Chapter 1. State of the Art

1. Introduction

The world is currently grappling with a confluence of crises that have had a profound impact on the global energy landscape. The COVID-19 pandemic has resulted in far-reaching consequences on energy demand and the energy mix. Lockdown measures and economic slowdowns led to a significant decrease in energy consumption, particularly within transportation and industrial sectors. According to the BP's *Statistical Review of World Energy 2021*, global energy demand fell by 4.5% in 2020, marking the largest decline since World War II. The decline in oil demand was particularly striking, with daily global oil demand plummeting by around 9 million barrels at the peak of the pandemic. Geopolitical tensions, exemplified by Russia's invasion of Ukraine, have added another layer of complexity to the global energy landscape. In 2021, Russian natural gas imports via pipeline and liquefied natural gas (LNG) accounted for nearly 40% of the total natural gas consumption in the European Union (EU). Russia's actions have had a direct impact on energy markets, especially in Europe. Gas supplies have been disrupted, leading to higher energy prices and concerns about energy security. According to European Commission, from January to November 2022, Russia's contribution, encompassing both pipeline gas and LNG imports, accounted for less than 25% of the EU's total gas imports. The decrease in Russian gas deliveries to the EU has compelled European countries to pursue alternative sources and diversify their energy mix to ensure a more secure and resilient supply.

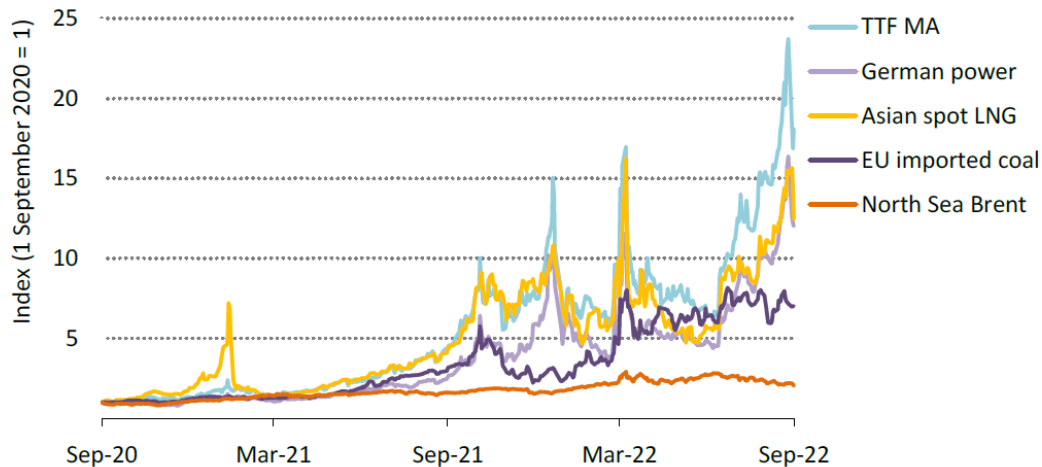


Figure 1. Evolution in selected energy price indicators since September 2020.
 Note: TTF MA = Title Transfer Facility month-ahead prices; LNG=liquified natural gas; Brent=Brent crude oil benchmark. Sources: IEA analysis based on Argus Media (2022); ICIS (2022); BNEF (2022).

Despite the push for renewable energy sources, oil continues to play a crucial role in meeting global energy demand. After the pandemic-induced recession, demand for all fossil fuels has risen by at least 5% in 2021. As of the most recent data available, oil remains the world's primary source of energy, accounting for approximately 32% of total energy consumption in 2021 (Figure 2). It is indispensable in various sectors, particularly transportation, where alternatives to oil-based fuels are still under development. The International Energy Agency (IEA) forecasts that oil demand will continue to grow until at least 2040, albeit at a slower pace, driven by emerging economies and increasing mobility needs.

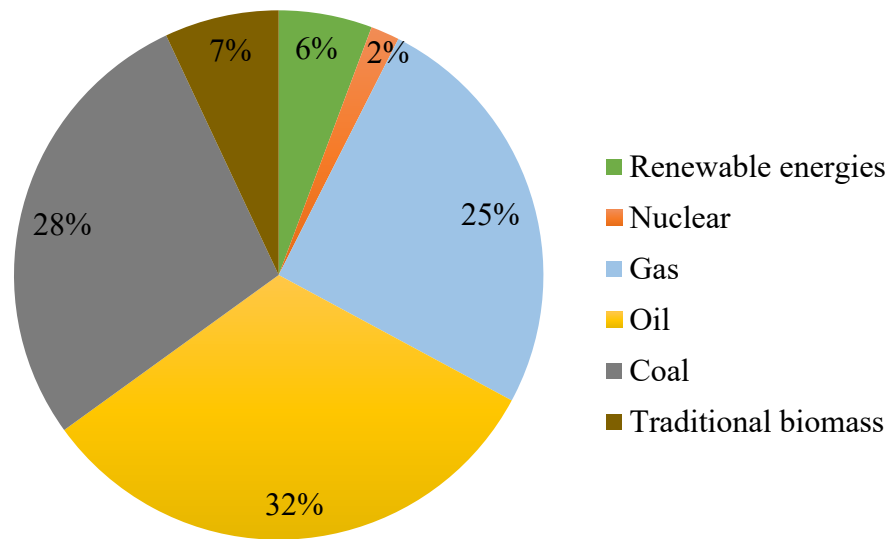


Figure 2. Global direct primary energy consumption in 2021. Data obtained from [BP's Statistical Review of World Energy \(2022\)](#).

While there is a growing imperative to reduce dependence on fossil fuels, including oil, a complete and immediate transition to renewable energies is not yet feasible. Renewable technologies, such as wind and solar, have made significant progress but still face challenges related to intermittency, energy storage, and scalability. Oil, therefore, serves as a vital bridge in the energy transition, supporting the development and deployment of renewable energy technologies. Additionally, oil revenues can be utilized to fund research and development efforts aimed at advancing renewable energy solutions.

In this context, the supply of hydrocarbons is a crucial issue in order to meet the energy needs of populations, especially in emerging countries experiencing rapid economic and demographic growth. To meet this energy demand, oil companies have expanded their operations beyond conventional onshore reservoirs to deep offshore reservoirs with complex temperature and pressure conditions. The smooth flow of hydrocarbons from the reservoirs to the sales points is ensured by engineering processes known as flow assurance. The term "flow assurance" was introduced in the 1990s by Petrobras in portuguese as "*Garantia do Escoamento*" literally meaning

“guarantee of flow”. Flow assurance encompasses several operational and technical aspects. It considers environmental factors, such as temperature or pressure in subsea production areas, which can influence the fluidity of hydrocarbons. Modeling and analysis studies are carried out to assess potential risks, design appropriate production systems, and implement suitable flow management strategies. The second aspect involves the prevention of issues related to wax, inorganic compounds (scale), gas hydrates and asphaltenes¹.

This research is focused on asphaltenes, which are complex organic compounds found in crude oil. In fact, when asphaltenes present in crude oils are destabilized due to changes in temperature, composition or pressure, they tend to aggregate and sediment or form solid deposits on equipment surfaces, leading to flow restrictions, reduced production rates, equipment damage, and costly operational disruptions². Managing asphaltene-related issues requires a comprehensive approach, including advanced monitoring and modeling techniques, mechanical methods and chemical treatments to control or prevent deposition.

2. Asphaltenes and their environment

2.1. Composition and physical properties

The oil is generally described through four distinct fractions with solubility properties or affinity with different chromatography matrices: saturates, aromatics, resins, and finally asphaltenes (SARA). The procedure for separating these fractions is standardized^{3;4}. The first step involves adding an excess of a light alkane such as n-heptane or n-pentane to separate the insoluble asphaltenes from this solvent, unlike the other fractions grouped under the name of maltenes (saturates, aromatics, resins). This is followed by a separation of the maltenes through liquid chromatography using solvents of different polarities.

Operationally, asphaltenes are described by a solubility class. They represent the petroleum fraction that is insoluble in n-alkanes (typically n-heptane or n-pentane) and soluble in aromatic hydrocarbon solvents (usually toluene or xylene). The choice of the n-alkane has an impact on the

asphaltene subfraction that is destabilized. A shorter n-alkane will destabilize a larger fraction of sticky asphaltenes, whereas a longer n-alkane leads to powdery asphaltenes that are more aromatic compared to those destabilized by shorter n-alkanes^{5,6}. This operational definition of asphaltenes does not describe a specific chemical entity per se, but rather a wide distribution of chemical species and structures of complexity.

Asphaltenes are the heaviest and most polar fraction of crude oils. They are composed of over a hundred thousand molecules⁷ and are rich in heteroatoms (N, O, S) as well as trace amounts (in ppm) of heavy metals such as nickel and vanadium⁸. These heteroatoms undoubtedly have an effect on the polarity of asphaltenes and can influence their solubility⁹.

Barrera et al.¹⁰ proposed a power law correlation between asphaltene density and molecular weight based on a dataset of measured densities and molecular weights of n-C₇ asphaltenes. The authors used a conventional mixing rule to calculate the density of extracted asphaltenes in toluene, and the molecular weight was measured in toluene using a vapor pressure osmometer.

The power law correlation proposed by Barrera et al.¹⁰ is expressed as follows,

$$\rho = 1100 + 100 \left(1 - \exp \left(-\frac{MW}{3850} \right) \right) \quad (1)$$

Where ρ is the density (kg/m³) and MW is the molecular weight (g/mol) of the asphaltene cut at 10 g/L asphaltene concentration.

A good agreement with experimental data was observed using the proposed correlated power law (Figure 3), although the authors noted that the deviations might be due to the fact that the correlation does not explicitly consider the mass fraction of non-associating components.

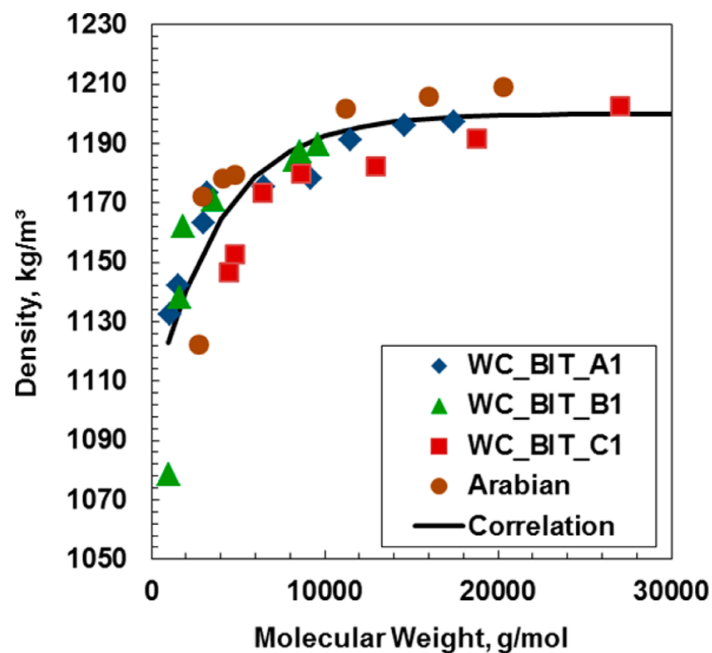


Figure 3. Density correlation (Equation 1) compared to density of asphaltene cuts from four samples at 23 °C (reprinted from Barrera et al.¹⁰).

2.2. Molecular structure of asphaltenes

In the literature, two molecular structures have long been the subject of debate^{11;12}:

- The island structure, characterized by a single polycyclic aromatic hydrocarbon (PAH) core and a shell of alkyl side chains.
- The archipelago-like structure, on the other hand, consists of multiple aromatic cores linked together by alkyl chains.

Figure 4 shows schematics of both structures.

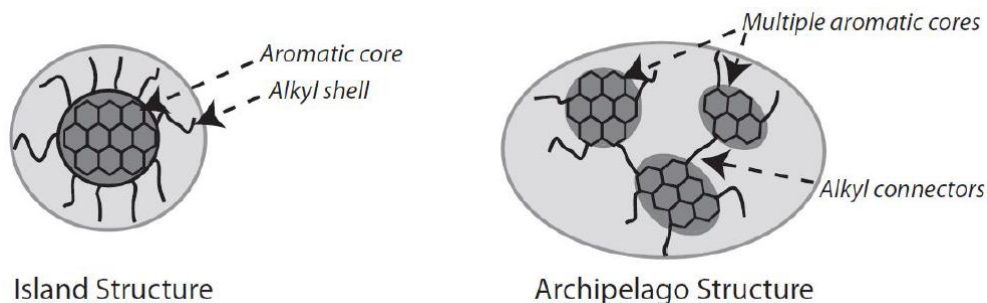


Figure 4. Schematic of island and archipelago structures (reproduced from Hoepfner¹³).

Various techniques have been employed to study asphaltene structures. Time-resolved fluorescence depolarization^{14;15} experiments and mass spectrometry methods, including laser desorption ionization mass spectrometry (LDI-MS)¹⁶ and Fourier transform ion cyclotron resonance mass spectrometry (FT-ICR MS)^{17;18}, have provided valuable insights. These studies have revealed that asphaltene molecules are not polymeric with large molecular weights, as previously believed. Instead, their average molecular weights are around 700-750 g/mol^{14;15}. This consensus on the molecular weight alone excludes the archipelago-like structure due to the high molecular weight that these structures would theoretically have.

The dominant structure observed in asphaltenes is the "island" architecture, characterized by a predominance of molecules with a single PAH core containing approximately seven aromatic rings^{11;15;19}. Asphaltenes exhibit a roughly equal distribution of aromatic and aliphatic carbons, consistent with their island architecture. Molecular orbital calculations coupled with measured optical data showed that the width of the asphaltene PAH distribution ranges from 4 to 15 fused rings^{19;20}.

Atomic force microscopy (AFM) imaging of isolated asphaltene molecules has provided direct confirmation of their structural properties²¹ (Figure 5). Images obtained from diverse asphaltene samples have supported the prevalence of the island molecular architecture. No archipelago structure was observed in any of the 10 samples. The authors then synthesized a model archipelago structure to confirm its visualization by AFM and successfully dispelled any possible doubts. However, another type of molecular structure called "aryl-linked core", showed in Figure 5. B1.2, has been identified at a lower concentration, characterized by two or more aromatic moieties linked

by an aryl linkage. Schuler describes this third type of structure as having a single, contiguous sp^2 hybridized carbon network containing one or more aryl linkages in which adjacent aromatic rings are directly bonded together but do not share a common bond in a ring.

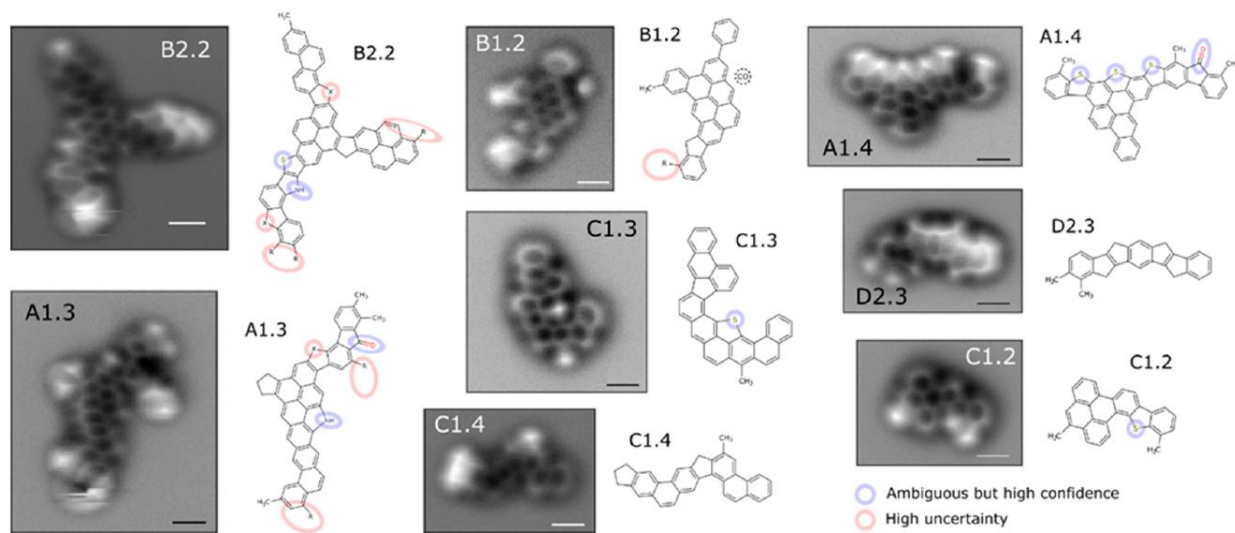


Figure 5. AFM measurements (scale bars: 5 Å) and assigned structures from various asphaltenes samples (reprinted from Shuler et al.¹²).

In conclusion, the structure of asphaltenes is predominantly characterized by simple aromatic core systems in which the core is typically fully fused (island) and occasionally contains one or two aryl-linked cores. This structural characteristic aligns with the observed behavior of asphaltenes forming nanoaggregates.

2.3. Aggregation state of asphaltenes in good solvent

Asphaltene molecules, due to their aromatic and polar character, have a tendency to self-associate and form nanoaggregates structures. Numerous techniques have been used to characterize the size and shape of nanoaggregates such as centrifugation^{22,23}, static light scattering²⁴, direct-current conductivity^{23;25;26}, nuclear magnetic resonance (NMR)^{27;28}, small angle X-ray scattering and neutron scattering (SAXS/SANS)^{24;29;30}. Fluorescence measurements indicate that the initial aggregation of asphaltenes occurs at approximately 50 mg/L³¹, whereas the critical nanoaggregate concentration (CNAC), at which nanoaggregates stop growing, converges to a value ranging from 50 mg/L to 150 mg/L^{32;33}. Hoepfner¹³ used X-ray scattering (SAXS/SANS and WAXS) to study the structural characteristics of asphaltene aggregates in the nanometer range. Figure 6 provides an illustrative representation of the geometrical properties observed in Hoepfner's investigation. The organization of polydisperse asphaltene nanoaggregates is described as a stack, with an average diameter of 1-2 nm³⁴, composed of 5 to 9 asphaltene molecules^{35;36;37} created by the $\pi - \pi$ interaction of the aromatic cores and limited by the steric repulsion generated by the peripheral alkyl chains³³. The molar mass of the nanoaggregates varies within the range of 3000 to 10000 g/mol^{30;38}, depending on the degree of association and their fractal dimension is commonly measured to be around 1.7^{30;39}, indicating a high level of solvation.

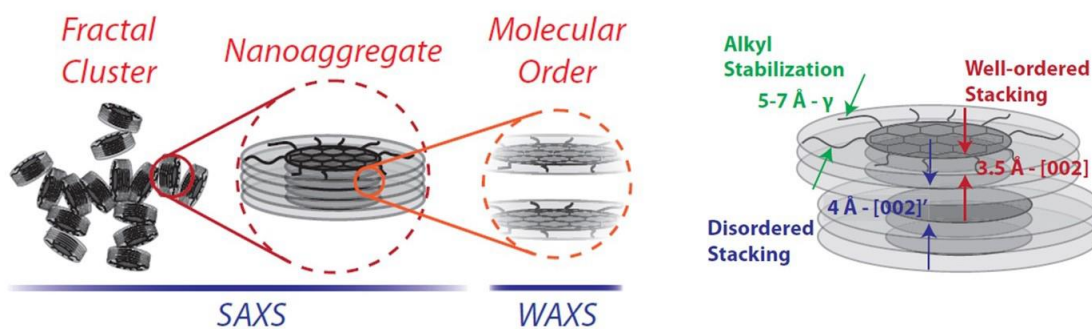


Figure 6. Schematic illustration of results on the molecular order of asphaltenes obtained by X-ray scattering (reprinted from Hoepfner¹³).

A second level of aggregation was observed at higher asphaltene concentrations in good solvent for asphaltene described as clusters. Goual et al.²³ determined, through DC conductivity studies, the critical cluster concentration (CCC) of asphaltenes at approximately 1.5-2 g/L in toluene. Clusters consist of less than 12 nanoaggregates and have an average diameter of 5-10 nm⁴⁰. They are characterized by a molar mass ranging from 50,000 to 100,000 g/mol, and they exhibit a fractal dimension of up to $D_f \sim 2$, indicating the presence of loosely packed particles with trapped solvent^{13;38}. The growth of self-associated asphaltene structures is limited to the nanoscale in good solvents, leaving them in suspension subject to Brownian motion and to hydrodynamic forces. Further meso-scale aggregation of clusters is synonym to a commencing destabilization of asphaltenes usually called asphaltene flocculation.

2.4. Asphaltenes destabilization

A pressure-temperature phase diagram reproduced from Akbarzadeh et al.⁴¹ is presented in Figure 7. At reservoir conditions (represented by a red point), the asphaltenes are stable. Considering a constant mass expansion starting from the reservoir pressure along an isotherm (indicated by the blue arrow), the state of asphaltene stability is described. When the asphaltene-phase envelope (APE) is reached (continuous red line), the less soluble asphaltenes destabilize due to the expansion of the molar volume of light alkanes such as methane. Further pressure reduction results in additional asphaltene separation until the bubble point pressure is reached. From the bubble point, the light alkanes leave the oil phase, which then becomes a better solvent for asphaltenes, allowing for their redissolution.

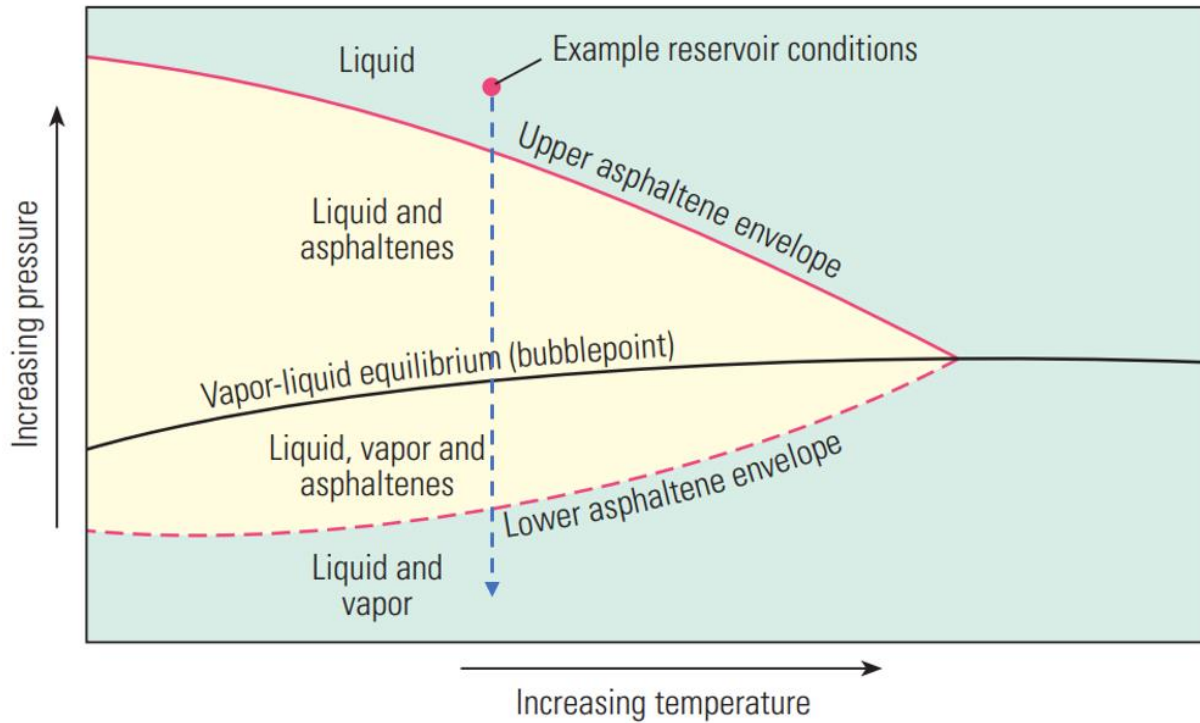


Figure 7. Typical Pressure-Temperature Asphaltene Phase Envelope (reproduced from Akbarzadeh et al.⁴¹).

In order to enhance the understanding of the mechanisms of asphaltene destabilization and deposition, the majority of laboratory tests simulate the expansion of light alkanes by injecting asphaltene antisolvents (mainly n-heptane and n-pentane) at atmospheric pressure. This allows for the study of the impact of solvent quality on the state of asphaltene destabilization in simple and safe systems.

Wang et al.⁴² used AFM to measure the colloidal forces between asphaltene surfaces in heptol (a mixture of n-heptane and toluene), with an asphaltene peripheral side being attached to a silica substrate. The results of the interaction forces, along with a schematic representation of the molecular configuration of asphaltenes in different solvents, are presented in Figure 8. In pure toluene, a steric long-range repulsion was observed, and this repulsion can be accurately described by the scaling theory of polymer brushes. However, when n-heptane was added to the system, the steric repulsion weakened and transformed into a weak attraction. The authors attributed this attraction to van der Waals forces, which are believed to facilitate asphaltene aggregation.

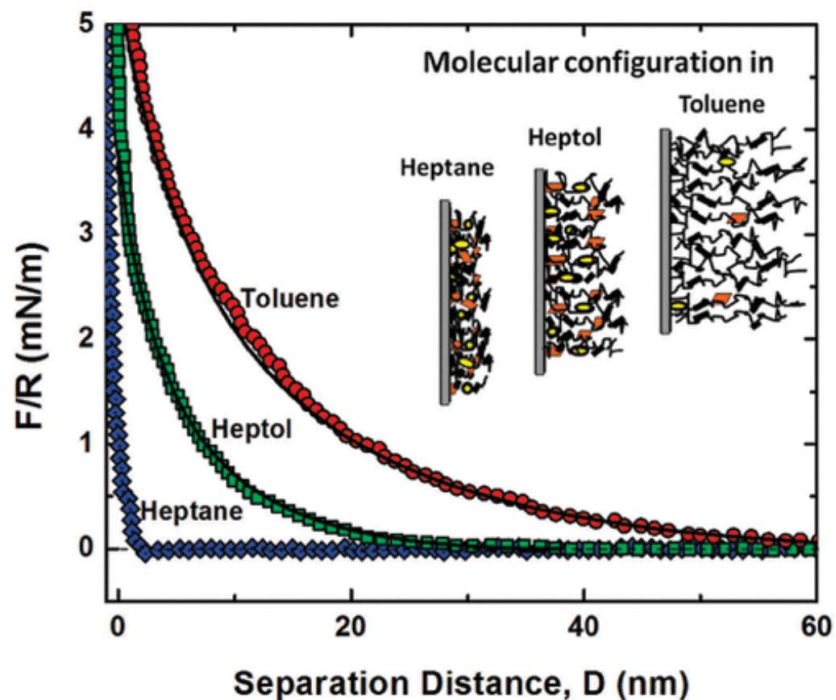


Figure 8. Interaction forces between asphaltene surfaces in various solvents (reprinted from Wang et al.⁴²).

Hoepfner¹³ showed, using X-ray scattering measurements, that the asphaltenes which undergo destabilization with a minimal amount of antisolvent addition exhibit the formation of larger fractal clusters. Among the range of asphaltene sizes, the larger ones, characterized by higher polydispersity, are considered the least stable. These larger asphaltenes experience stronger interaggregate attractions or weaker repulsion forces. Consequently, they tend to associate preferentially with one another, primarily due to the influence of inter-aggregate attractions such as the London dispersion force. After destabilization, the insoluble clusters formed exhibit a notably higher fractal dimension compared to the soluble ones as shown in Figure 9. This change in fractal dimension arises from a modification in the packing arrangement of individual asphaltene nanoaggregates. These aggregates adopt a more solid-like structure by expelling the solvent trapped within them, resulting in a denser and more compact arrangement.

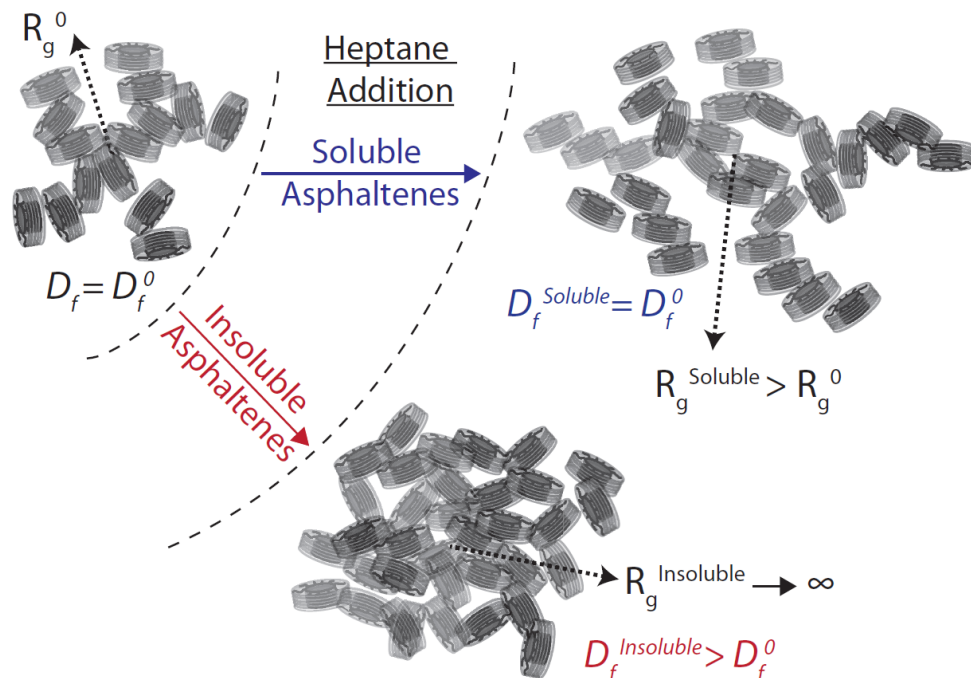


Figure 9. Schematic of the structural reorganization of asphaltene clusters in n-heptane (reprinted from Hoepfner¹³).

Asphaltenes represent a fraction of oil that stands out due to its complexity, attributed to their wide polydispersity and sensitivity to their surrounding fluid and their associated self-association mechanisms. Asphaltene follow complex destabilization mechanisms that involve multiscale aggregation phenomena occur from a few nanometers to hundreds of micrometers. A schematic in Figure 10 illustrates the processes of asphaltene destabilization and aggregation.

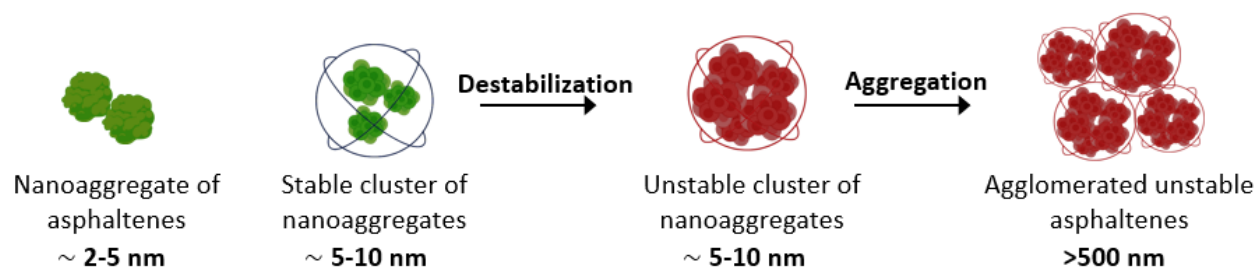


Figure 10. Multiscale destabilization and aggregation of asphaltenes.

According to Figure 10, the following terminology will be adopted in this manuscript to describe the processes to which asphaltenes are subjected:

- Nanoaggregates of asphaltenes form stable nanoaggregate clusters.
- These stable nanoaggregate clusters, in the presence of an antisolvent, undergo destabilization and become unstable clusters.
- These unstable clusters grow in the liquid phase to form larger aggregates at the micrometer scale, which characterizes flocculation or they diffuse on surfaces and form a deposition layer.
- Once the aggregates reach a size too large to remain suspended in the liquid phase, they will sediment.

Despite decades of debate on the nature of asphaltenes and their destabilization processes, the petroleum industry has firmly established the connection between asphaltenes presence in reservoir fluids and flow assurance issues. To address the issues related to asphaltenes, the oil industry has implemented prevention and remediation solutions, which will be detailed in the following section.

3. Asphaltenes management

3.1. Flow assurance issues related to asphaltenes

Long before its widespread use in the daily lives of populations, oil in its most primitive form was used daily as fuel for illumination⁴³. The modern era of petroleum production began in 1859 in Pennsylvania, United States, when Edwin L. Drake, a former railroad employee, achieved a significant breakthrough by drilling the first commercial oil well using a hollow iron rod^{43;44}. The discovery of the first commercial oil well marked a major turning point, paving the way for large-scale oil exploration and exploitation. It also led to significant technological advancements, such as improved drilling techniques and the introduction of pipelines for transporting oil over long distances.

The Oil & Gas industry can be divided into 3 segments based on the operation stage in the supply chain: Upstream, Midstream, and Downstream. Upstream refers to activities related to the exploration and production of oil from onshore or increasingly deep offshore fields. Midstream refers to the activities of transportation, storage, and intermediate processing of hydrocarbons produced during the upstream stage. This includes the transportation of oil and gas through pipelines, storage in tanks, and processing facilities to remove impurities and separate different products. Finally, downstream encompasses the activities of refining, distribution, and marketing of final petroleum products. The challenges associated with asphaltenes are present at each stage across the Oil & Gas industry's supply chain.

When asphaltenes become destabilized and tend to aggregate, they can deposit and obstruct the porosity, reducing the rock's permeability and limiting oil extraction yield⁴⁵. The upstream issue of asphaltene deposition extends beyond the reservoir and can affect the production column by partially or completely blocking the production tubing (Figure 11). As early as 1965, Haskett and Taretra⁴⁶ reported the case of tubing totally clogged with asphaltene deposits in several wells in the Hassi Messaoud field, requiring tubing cleaning at a high frequency. Juyan and Yen² reported the example of oil fields in the Gulf of Mexico, where problems related to asphaltene deposition can cost up to a hundred million dollars when the surface-controlled subsurface safety valve becomes fouled and a well shut-in is implemented. Considering a production rate of 10,000 barrels

per day at \$75 per barrel (approximately the price of Brent crude oil in May 2023), a total production shutdown results in the loss of \$0.75 million per day.



Figure 11. Asphaltene deposition in production tubing in an oilfield in the Gulf of Mexico (reprinted from Borden⁴⁷).

In addition, a subfraction of asphaltenes contribute to the formation of stable water-in-oil emulsions, which affects the oil/water separation process⁴⁸.

The high viscosity of a heavy oil sample is affected by the asphaltene content. At higher asphaltene concentrations, the strong attractive interactions between asphaltene aggregates result in a significant increase in the viscosity of the heavy oil making it more challenging to operate⁴⁹.

In the midstream, during transportation, the blending of oils with different compositions can render them incompatible and lead to the destabilization of the asphaltene fraction. Wiehe⁵⁰ discusses the phenomenon where certain crudes, which may initially be compatible at their source, can encounter incompatibility issues during transportation to refineries. When a low solubility blending number crude⁵¹ (crude oil with limited compatibility with other types of crude oils when mixed together) is transported in the same pipeline or tanker that previously contained a high insolubility number crude⁵¹ (low solubility), it can lead to the destabilization of initially stable asphaltenes. The author indicates that generally in such conditions, these micro-aggregate

asphaltenes are carried by the fluid without sedimentation or deposition. However, if these asphaltenes encounter a heat source above 300°C, they can melt and adhere to the wall in the form of coke, causing fouling problems.

Furthermore, several issues in downstream can be caused by asphaltenes. During the hydro processing of heavy oils, at high temperature, most asphaltenes are converted into coke, which can limit the conversion of heavy oil by accumulating in the catalyst, downstream separators, heat exchangers, and fractionating towers⁵². Additionally, the metals present in the structure of asphaltenes can deactivate the catalyst during the hydro processing reaction⁵³.

All these issues related to asphaltenes result in significant economic costs. Prevention and remediation techniques are implemented to ensure proper flow and transportation of the oil.

3.2. Prevention methods

In new development projects, it is essential to assess oil stability in relation to asphaltene destabilization risks. However, evaluating asphaltene stability under reservoir conditions can be prohibitively expensive and, at times, impractical due to challenges in obtaining representative oil samples. Table 1 presents the pricing of GEOMARK in 2013 for Pressure-Volume-Temperature (PVT) analysis. A standard study for an oil used to be billed at \$23,815, to which several thousand dollars were added for specific asphaltene characterization.

Table 1. Asphaltenes PVT lab experiments (GEOMARK, 2013⁵⁴).

Experiment	Price, \$
Opening pressure at ambient temperature	240
Sample restoration (agitation/heating for 5 days)	1650
Single stage flash of fluid sample	1950
C ₁₅₊ gas analysis	675
C ₃₀₊ liquid analysis	1500
OBM ^a analyses for EOS ^b tuning (C ₃₀₊ analysis, CCE ^y , viscosities)	2100
OBM contamination estimation and calculation of mudd-free API gravity and GOR	200
CCE at reservoir temperature	1600
CCE at reference temperature	1600
DL ^δ (6 to 8 pressure steps)	3700
Two-stage separator test with gas and residual oil compositions	2400
Live fluid viscosity profile	2500
STO ^ε package	2100
EOS decontaminated calculated PVT report	1600
Standard black oil PVT study price	23815
Live fluid AOP by near infra-red at specified temperature	2625
HP/HT filtration for quantification of asphaltenes	1575

Fluid compatibility test (test for asphaltene destabilization from titration) at P & T by NIR	3150
^α Oil Base Mud, ^β Equation of State, ^γ Constant Composition Expansion, ^δ Differential Liberation, ^ε Stock-tank Oil	

Consequently, to assess oil stability, the utilization of experimental or numerical methods has become crucial in overcoming financial and logistical constraints related to asphaltene analysis under real conditions. These alternative approaches enable the petroleum industry to make informed decisions while managing costs and optimizing the time required to evaluate project viability.

3.2.1. Risk assessment methods

3.2.1.1. Instability Index

These methods, based on the analysis of the composition of oil blends, derived from the SARA analysis, are intended to evaluate an asphaltene instability index to assess asphaltene instability risks. Among these methods, mention can be made of the Colloidal Instability Index (CII)^{51;55} and its derivative, the Colloidal Stability Index (CSI)⁵⁵, Stankiewicz Plot (SP)⁵⁶, or the Sepulveda Stability Criterion⁵⁶. CII method involves assessing the ratio of the considered unstable fractions in the blend (asphaltenes, saturates) to the considered stabilizing fractions (resins, aromatics).

$$CII = \frac{Asphaltenes(wt\%) + Saturates(wt\%)}{Resin(wt\%) + Aromatics(wt\%)} \quad (2)$$

Asomaning and Watkinson⁵⁵ defined the ranges of the CII index as follows: a CII value higher than 0.9 indicates an unstable asphaltene fraction. For values between 0.7 and 0.9, the stability is considered uncertain. Lastly, a CII value below 0.7 represents a stable asphaltene fraction.

However, the accuracy of these techniques remains partial, especially when determining the incompatibility of a blend⁵⁷.

3.2.1.2. Oil compatibility Model

Regarding experimental methods, the Oil Compatibility Model (OCM)^{50;51} can be mentioned. The OCM is based on two key hypotheses⁵¹. Firstly, it assumes that asphaltenes flocculate from crude oil at the same mixture solubility parameter, regardless of whether the oil is blended with other liquids or other oils. Secondly, it posits that the solubility parameter of a mixture can be determined as the volumetric average solubility parameter. The OCM assesses stability using two parameters: the insolubility number (I_N) and the solubility blend number (S_{BN}). The I_N represents the degree of asphaltenes insolubility, ranging from 0 for complete solubility to 100 for minimal solubility. The S_{BN} measures the crude oil's similarity to n-heptane as a solvent, with values ranging from 0 for weak solvents to 100 for solvents similar to toluene. By analyzing the minimum volume of toluene required to keep asphaltenes in solution at different volume ratios of oil to toluene-heptane mixtures, the OCM predicts the stability of crude oils. Wiehe⁵⁸ introduced a criterion that utilizes the insolubility number and solubility blend number to establish the correct proportions and order of blending oils to ensure compatibility. This criterion states that in order to achieve compatibility, the solubility blending number of the oil mixture must exceed the insolubility number of every individual oil present in the blend.

3.2.1.3. ASCI method

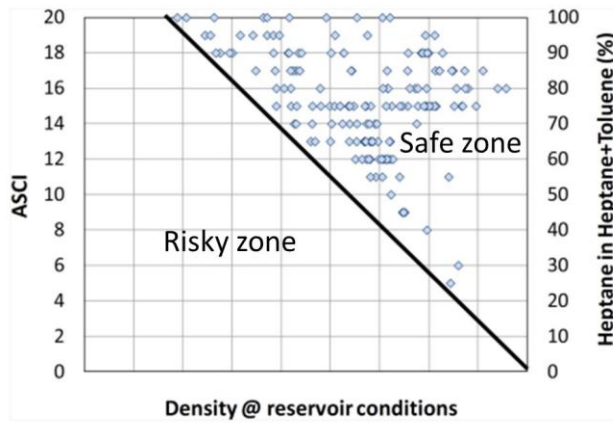
The Asphaltene Solubility Class Index (ASCI)^{59;60} is a rating method to evaluate the instantaneous flocculation of asphaltene in n-heptane/toluene mixtures at different ratios. The n-heptane/toluene mixtures are classified with integer number ranging from 0 to 20 depending on the ratio of each solvent. An ASCI of 0 corresponds to 100 wt % toluene, while an ASCI of 20 corresponds to 100 wt % n-heptane. A droplet of crude oil is then added to the n-heptane/toluene mixtures at a temperature of 50°C and the aging process is observed for 48H. The ASCI rating is established when the visual flocculation of asphaltene is observed according to this relation,

$$ASCI = 100 \frac{\phi_{C_7,detection}}{5} \quad (3)$$

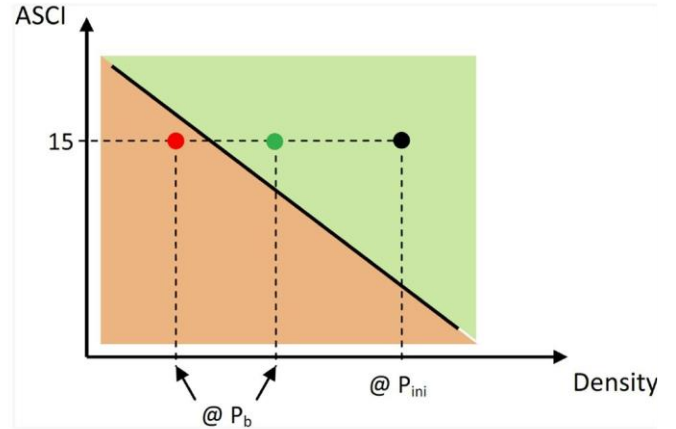
where $\phi_{C_7,detection}$, is the minimum volume concentration of n-heptane to achieve the visual detection of solid and black particles.

The amount of antisolvent at the detection threshold is commonly referred to as the "onset" ("onset" of flocculation, "onset" of deposition). It is essential to keep in mind that the "onset" is dependent on the system's aging time and the detection threshold of the equipment used. However, the term "onset" will be used in this manuscript in quotation marks because it remains a convenient comparative tool widely reported in the literature.

The higher the ASCI value, the higher the stability of the asphaltene fraction. Figure 12.a. shows the stability border obtained from multiple reservoirs fluids data at given density. Figure 12.b. shows the risk evaluation method for a given ASCI rating. At reservoir conditions (indicated by the black point), the fluid with an ASCI rating of 15 poses no risk as long as its density remains above the risky boundary. However, if the density decreases during oil production and crosses the stability border, the risk of asphaltene destabilization is initiated (represented by the red point).



(a)



(b)

Figure 12. (a) ASCI as a function of the density of crude oils at reservoir conditions. (b) ASCI risk evaluation method (reprinted from Rondon et al.⁵⁹). P_{ini} is the pressure at reservoir conditions P_b are theoretical bubble points.

This risk assessment method offers clear advantages, particularly in terms of simplicity and speed. However, the method is not quantitative, and the observation of the flocculation threshold relies on the operator's eyes judgment.

3.2.2. Asphaltene stability modeling

Another method used to assess the risk of asphaltene destabilization is by modeling asphaltene stability in oil as a function of oil composition and external parameters such as temperature, pressure, and injection of antisolvents. For most asphaltene models, their primary objective is to predict the "onset" of asphaltene instability. There are two approaches commonly found in the literature to model asphaltene destabilization in the bulk^{61;62;63;64}.

- The colloidal model⁶⁵: asphaltenes are considered as particles stabilized by resins adsorbed on their surface. The asphaltene + resin system forms colloids, where the transfer of peptizing agents from the colloid to the bulk phase leads to asphaltene flocculation.
- The solubility model: asphaltenes are dissolved in crude oil, and flocculation occurs when their solubility drops below a certain threshold level.

The solubility-based approach is currently the most widely used, and two main solubility theory approaches can be distinguished: Regular Solution Theory (RST) models and Equation of State (EOS).

The solubility models treat the oil system as a pseudo-binary mixture consisting of a bulk oil solvent and asphaltene solute.

The RST, was originally developed to describe the thermodynamics of nonpolar component solutions⁵. It assumes zero excess entropy, meaning the entropy of mixing is equal to that of an ideal solution. The RST utilize solubility parameters to derive the activity of a single component in a binary mixture. This approach allows direct calculation of asphaltene solubility using pure component data. From the RST, other theories or models more specific to asphaltenes have emerged.

Using the Flory-Huggins Theory several authors^{66;67} assumes asphaltenes has the form of a flexible chain of segments and that each segment is equal in size to a solvent molecule. In this theory, asphaltenes are considered as homogeneous structure with averaged properties. However, in such approaches, the solubility of asphaltenes can be overestimated in the presence of a high amount of solvent, and these models may not accurately determine the amount of flocculated asphaltenes

under high pressures⁶³. The Scott-Magat model⁶⁸ follow the same concept of the Flory-Huggins theory but it considers the polydispersity of asphaltenes. The Yarranton and Masliyah model⁶⁹ employs a solid-liquid equilibrium approach to describe the solubility of asphaltenes. It utilizes K -values derived from the Scatchard-Hildebrand solubility theory and incorporates the Flory-Huggins entropy of mixing. In this model, asphaltenes are characterized as a series of polyaromatic hydrocarbons with randomly distributed functional groups. The model is able to predict both the “onset” and quantity of destabilized asphaltenes.

RST models are focused on predicting solubility limits and do not explicitly consider fluid compressibility.

In contrast to RST models, EOS encompass both solubility limits and fluid compressibility. In the variety of available EOS in the literature, two main families are commonly used for modeling asphaltene destabilization: cubic equations and SAFT-type EOS.

Cubic equations of state (C-EOS), such as Soave-Redlich-Kwong (SRK) and Peng-Robinson (PR), are widely used in the oil industry to describe fluid, mixture, and solid properties⁶⁴. These equations consider L-V, L-L and L-S equilibria. In this approach asphaltenes behavior is considered homogenous. Molecular geometry, structure and interactions are not considered (e.g. asphaltene particles aggregation, hydrogen bonding). Several models have been developed based on C-EOS, including the Nghiem et al. model⁷⁰ which divides the heaviest component in the oil into a non-flocculating and a flocculating component. Asphaltenes are treated as a pure dense phase, referred to as the asphalt phase (asphaltene + resin), which can exist in either liquid or solid form. The Sabbagh et al.⁷¹ model adapts the PR equation of state to consider asphaltene self-association. In order to simulate the wide molar mass distribution of asphaltenes, the authors divided them into thirty subfractions. The model utilizes temperature, pressure, and mole fraction data for each pseudo component and the average molar mass of asphaltenes as a fitting parameter in order to predict the “onset” and amount of asphaltene flocculated. It considers L-L equilibrium, with only asphaltenes partitioning into the dense phase. Maltenes are treated as single pseudo-components. The model successfully matches asphaltene yields for n-alkane diluted bitumen, but it encounters difficulties in accurately fitting yields from n-pentane-diluted bitumen systems at high dilution ratios.

Li and Firoozabadi^{72;73} utilized the cubic-plus-association (CPA) equation of state to model asphaltene destabilization. This approach combines the PR equation of state with an additional association part derived from thermodynamic perturbation theory. In their model, they assumed that asphaltenes separate in the form of a liquid phase leading to liquid-liquid phase equilibria.

The PC-SAFT (Perturbed Chain - Statistical Associating Fluid Theory) model⁷⁴ is based on the SAFT theory, which is a statistical theory that describes the thermodynamic properties of fluids using associating chain molecules. The SAFT theory models a molecule as a chain of spherical segments bonded together like a pearl necklace. This model incorporates various contributions to the residual free Helmholtz energy.

The PC-SAFT model incorporates perturbative interactions to account for the effects of large and complex-shaped molecules, such as asphaltenes. In PC-SAFT, three parameters are required for each non-associating component:

- the number of segments per molecule (m)
- the diameter or volume of each segment in a molecule (σ)
- the segment-segment interaction energy (ε/k).

These parameters are then determined for each of the pseudo component based on correlations with corresponding molecular weights.

Daryasafar et al.⁷⁵ proposed a comparative study of various thermodynamic models to predict asphaltene destabilization. Five different models were compared, namely the cubic plus association (CPA) model, the PC-SAFT model incorporating an association term, a solid model, the Flory Huggins Theory (FH), and a modified version of the Flory Huggins Theory (MFH). The investigation involved a total of 12 oil samples. For the characterization of the C+ fraction, a set of 12 pseudo-components was utilized. It was assumed that asphaltene possesses a homogeneous structure. To align with the experimental data, the critical properties, acentric factor, and binary interaction parameters of the asphaltenes were adjusted accordingly. Results are presented in Figure 13.

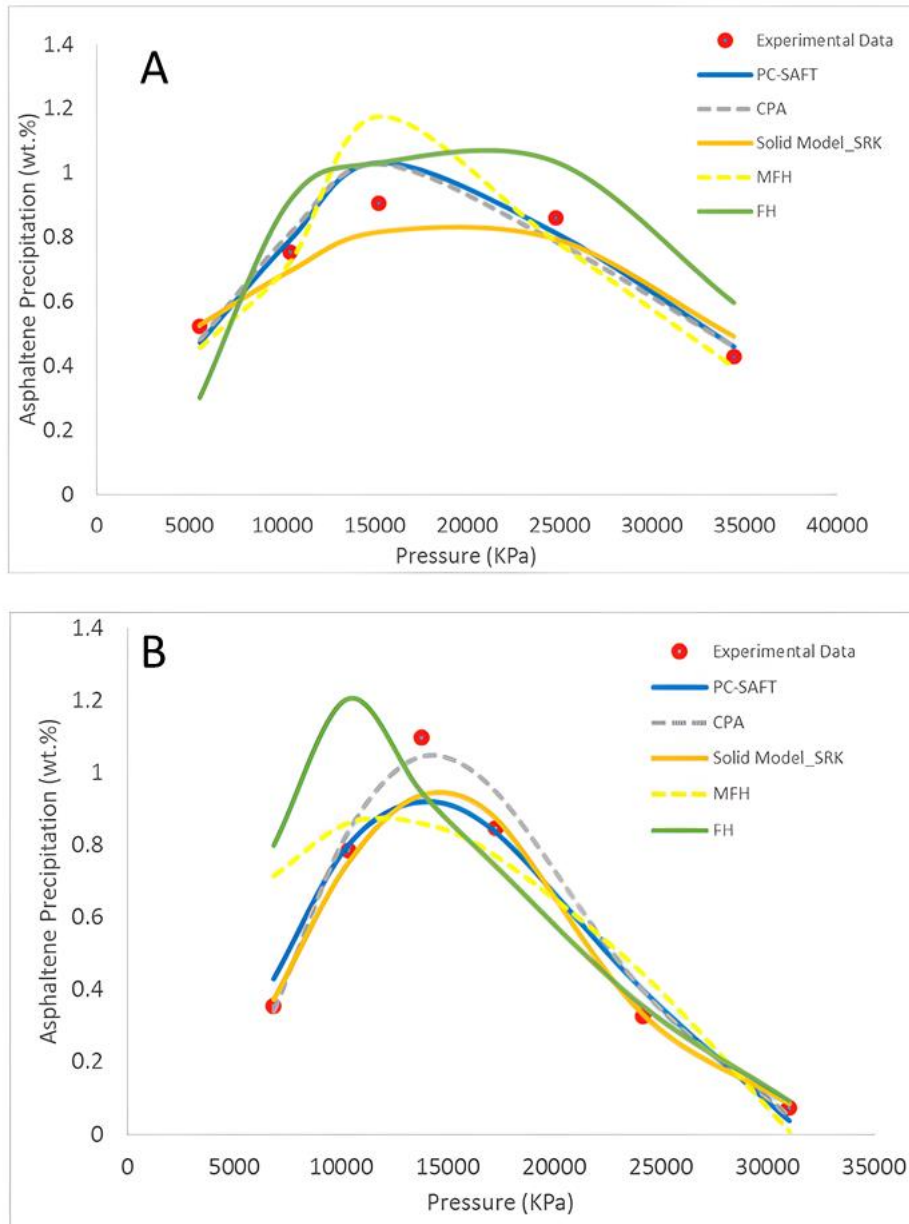


Figure 13. Comparison between different models in predicting asphaltene destabilization versus pressure for (A) oil sample 4; and (B) oil sample 6 (reprinted from Daryasafar et al.⁷⁵).

Results from different models demonstrated that the PC-SAFT and CPA models are the most accurate in predicting asphaltene destabilization during depressurization and hydrocarbon gas injection into the studied oil samples. Tuned variables were considered, including physical parameters of the lumped pseudo-component, association terms, and binary interaction parameters. Sensitivity analysis was performed by using Monte-Carlo algorithm and it was showed

that the cross-association energy between asphaltene and hydrocarbon for the PC-SAFT model, the self-association energy of asphaltene for the CPA model, and the binary interaction parameter between asphaltene and CO₂ for the solid model had the highest influence on the model outputs. The adjusted binary interaction coefficients revealed that, in certain instances, the values of binary interaction parameters between components approached unity. This indicates that the interaction between specific components, such as resin and asphaltene, becomes significant due to their high polarity and complex nature. As a result, the value of the binary interaction parameter increases, reflecting the enhanced interaction between these components.

In the last decades, several attempts have been made for modeling and predicting asphaltene destabilization. A comparison of modeling works indicates that destabilization modeling using PC-SAFT EoS is promising. Additionally, improvements in fluid characterization techniques and the consideration of asphaltene poly-dispersity are seen to play an important role in improving the quality of predictions. As Andersen and Speight stated⁷⁶, "*The more realistic the model becomes, the more complex it will be. The complexity also leads to an increase in unknown parameters, which in turn need to be estimated or fitted to experimental data.*". Unless precise measurements or accurate calculations of input parameters are available, all models are likely to rely on fitting procedures.

3.2.3. Chemical additives

The terminology for characterizing a chemical additive used as an asphaltene inhibitor does not appear to be universal in the literature. Firstly, one may question what the term "inhibitor" means in the context of asphaltenes. Does it refer to a chemistry with the ability to reduce the amount of asphaltenes deposited on a surface, enhance the dispersion of asphaltenes in the liquid, or delay the "onset" of asphaltene destabilization? Additionally, designating a chemical additive by its function seems inappropriate since its effectiveness depends on the system in which it is injected. For example, a chemical additive may be commercially referred to as an asphaltene dispersant (AD), but this dispersion effect is not universal and relies on the properties of asphaltenes and the system's conditions. To avoid any ambiguity in the rest of the manuscript, the

term "chemical additive" will be used, and the specific effect will be clarified when established (e.g., dispersant, deposition inhibitor).

The efficient control of asphaltene deposition is crucial for maximizing oilfield production. In Middle Eastern fields, the cost of chemical additive injection per well ranges from \$31,000 to \$46,000 annually⁷⁷. Meanwhile, in the Gulf of Mexico, for wells with typical production rates of 10,000 barrels per day, the cost can reach approximately \$330,000 to \$390,000 per well per year⁷⁷. Thus, it becomes imperative to find a cost-effective chemical inhibitor to effectively manage asphaltene deposition and minimize production-related expenses.

Chemical additives are injected into petroleum reservoirs and wellbores to mitigate the detrimental effects of asphaltenes during oil production. These chemical additives are injected using various methods, such as formation squeeze, batch injection, and continuous injection⁷⁸. Formation squeeze injection involves forcing the inhibitor into the formation surrounding the wellbore, creating a barrier against asphaltene deposition. Batch injection delivers a predetermined volume of chemical additive solution into the wellbore to prevent agglomeration and sedimentation. Continuous injection ensures a steady supply of chemical additives during production, maintaining flow assurance and productivity.

The biggest challenge in the use of chemical additives as asphaltene deposition inhibitors is that their effectiveness depends on the properties of the asphaltenes (such as their aromaticity, polarity, or molecular weight) they act upon. In other words, a chemical additive that proves efficient in limiting asphaltene deposition in a specific oilfield may be ineffective or even exacerbate deposition in another field⁷⁹. As a result, these chemical additives must be custom-designed, and their efficacy must be assessed and proven before on-site injection.

In *Chapter 2*, a review of the most common methods for screening asphaltene inhibitors will be presented in the first part. In *Chapter 4*, the chemical structure and role of asphaltene dispersants will be discussed.

3.3. Remediation methods

3.3.1. Mechanical removal

Mechanical methods are commonly employed for the removal of asphaltene deposits in wellbores. These methods involve the use of mechanical force to scrape off the deposits. They include techniques such as wire line unit operations and hydro-blasting with a coiled tubing unit^{80;81}. Wireline and coiled tubing are widely used for in-situ cleaning of vertical and horizontal wells, respectively. They allow for data collection, tool delivery, and the dislodging of deposits within the wellbore. Hydro-blasting, carried out with coiled tubing, is a prevalent mechanical removal method where high-pressure water jets disintegrate deposit and extract them, often assisted by cleanout fluids to facilitate solid dissociation⁸¹.

More challenging cleaning methods involve drilling, scraping, and brushing operations. Hydraulically or electrically powered tools equipped with various bits, blades, and bristles are used to dislodge deposited solids from well casings⁵. These tools are delivered downhole via coiled tubing or wireline. To perform these cleaning operations, wells need to be shut down, leading to a loss in production.

Pigging, which involves the use of plug-like devices known as pigs, is another mechanical removal technique. Pigs are introduced into live pipelines and driven downline by fluid flow to remove deposits. They can be equipped with wire bristles and scraper blades for effective cleaning. Mechanical removal techniques, including pigging, carry risks, such as the possibility of pigs getting stuck in the flowline⁸².

However, the efficacy of mechanical removal techniques alone is often limited. Evidence suggests that mechanical scraping operations may not result in significant increases in production and can even lead to production loss in some cases⁵. Moreover, mechanical methods may not be suitable

for removing deposits from the formation face and may not reach regions where asphaltene deposition occurs beyond their intervention capabilities.

Therefore, while mechanical methods play a vital role in minimizing the impact of asphaltene deposition, they are often used in conjunction with other approaches, such as solvent treatments, to achieve more effective results.

3.3.2. Solvent Wash

Solvent washing using aromatic solvents is a commonly employed method for dissolving asphaltene deposits in wellbore and near-wellbore areas. The evaluation of solvents' solubility parameters is used to identify the most appropriate solvent for remediation of asphaltenes in the oil production process. The solubility parameter serves as a means to compare the relative solvency characteristics of various solvents.

Hildebrand and Scott⁸³ describe the solubility parameter (δ) as the square root of the cohesive energy density:

$$\delta = \sqrt{\frac{\Delta H_{vap} - RT}{v_m}} \quad (4)$$

where ΔH_{vap} is the energy of vaporization and v_m is the molar volume.

Building upon the work of these authors, Hansen⁸⁴ postulates that the total cohesive energy of a compound is equal to the sum of the dispersion energy (δ_d), polar energy (δ_p) and hydrogen bonding energy (δ_h) according to the following form,

$$\delta = (\delta_d + \delta_p + \delta_h)^{1/2} \quad (5)$$

The intermolecular interaction present in a liquid solvent is then related to the vaporization energy as follows,

$$\delta = \left(\frac{E}{v_m} \right)^{1/2} \quad (6)$$

where E is the sum of the total cohesive energy of the compound given (experimentally) by the energy of vaporization.

Solvents with a solubility parameter close to that of asphaltenes are considered as good solvents capable of dissolving them. To calculate the solubility parameter of various chemicals, simple empirical correlations have been established based on measurements of their refractive indices, densities, or viscosities⁸⁵.

Wang and Buckley⁸⁶ proposed a correlation to determine the solubility parameter of non-polar hydrocarbons using experimental refractive index (n_D) measurements at ambient conditions, given by,

$$\delta = 52.042 \left(\frac{n_D^2 - 1}{n_D^2 + 2} \right) + 2.904 \quad (7)$$

Reported values^{5;85} for the overall asphaltene solubility parameter are ranging from 20 MPa^{1/2} to 26 MPa^{1/2}. Hansen solubility parameter (HSB) of some solvent⁸⁴ are listed in Table 2. Light aromatics, although having a similar HSB to that of asphaltenes, pose safety and health risks and have a harmful impact on the environment. Typically, xylene is preferred due to its higher flash point (28°C) and is blended with cosolvents to enhance its effectiveness^{5;87}.

However, solvent washing is often expensive due to the large dosages of solvent required. In addition, the use of aromatic solvents is becoming less attractive due to increasingly restrictive governmental regulations on their usage, disposal, volatile emissions, as well as concerns regarding flammability, acute toxicity, and environmental contamination.

Table 2. Hansen Solubility Parameter (MPa^{1/2})⁸⁴.

Solvent	δ_d	δ_p	δ_h	δ
Benzene	18.4	0	2.0	18.5
Naphthalene	19.2	2.0	5.9	20.2
Phenol	18.0	5.9	14.9	24.1
Pyridine	19.0	8.8	5.9	21.8
Toluene	18.0	1.4	2.0	18.2
Xylene	17.6	1.0	3.1	17.9
<i>n</i> -pentane	14.5	0	0	14.5
<i>n</i> -heptane	15.3	0	0	15.3

4. State of the Art summary

Asphaltenes constitute a complex fraction of petroleum due to their polydispersity and self-association mechanisms. Over the past decades, advancements in structural characterization and chemical composition have provided insights into asphaltene properties. Key elements are outlined below:

- Asphaltene represents the most polar fraction of petroleum.
- In the literature, the volumetric density of asphaltene is generally accepted to be 1200 kg/m³.
- Asphaltene consists of aromatic cycles and aliphatic chains.
- Heteroatoms and heavy metals are present in the chemical structure of asphaltene.
- In their stable state, asphaltene molecules form nanoaggregates (approximately 8 asphaltene molecules) of about 2-5 nm and clusters of nanoaggregates (comprising less than 10 nanoaggregates) with sizes ranging from 5 to 10 nm.
- When destabilized, asphaltene clusters grow until they reach a macroscopic size.

Asphaltenes represent a significant economic threat throughout the Oil & Gas supply chain. Various prevention methods have been developed to address the asphaltene challenge. In upstream operations, the preferred solution in most cases is the injection of chemical additives to prevent asphaltene deposition. To make this solution more eco-efficient (economically and environmentally), with minimal dosages and environmentally friendly chemistries, a better understanding of “asphaltene inhibitors” is crucial. However, the mechanisms of action of these chemical additives are not clearly identified. The objective of this thesis work is to shed light on the mechanisms of action of chemical additives concerning asphaltene deposition and to propose a workflow for evaluating these chemical additives.

5. References

- (1) Wang, Q. *Oil and Gas Chemistry Management Series, Flow Assurance*; Gulf Professional Publishing, 2022; Vol. 2.
- (2) Juyal, P.; Yen, A. T. Chapter 3 - Asphaltene Management. In *Flow Assurance*; Wang, Q., Ed.; Oil and Gas Chemistry Management Series; Gulf Professional Publishing, 2022; Vol. 1, pp 185–226. <https://doi.org/10.1016/B978-0-12-822010-8.00007-6>.
- (3) Corbett, L. W. *Composition of asphalt based on generic fractionation, using solvent deasphalting, elution-adsorption chromatography, and densimetric characterization*. ACS Publications. <https://doi.org/10.1021/ac60273a004>.
- (4) Jewell, D. M.; Albaugh, E. W.; Davis, B. E.; Ruberto, R. G. *Integration of Chromatographic and Spectroscopic Techniques for the Characterization of Residual Oils*. ACS Publications. <https://doi.org/10.1021/i160051a022>.
- (5) Vargas, F. M.; Tavakkoli, M. *Asphaltene Deposition: Fundamentals, Prediction, Prevention, and Remediation*; CRC Press, 2018.
- (6) Hammami, A.; Ratulowski, J. Precipitation and Deposition of Asphaltenes in Production Systems: A Flow Assurance Overview. In *Asphaltenes, Heavy Oils, and Petroleomics*; Mullins, O. C., Sheu, E. Y., Hammami, A., Marshall, A. G., Eds.; Springer: New York, NY, 2007; pp 617–660. https://doi.org/10.1007/0-387-68903-6_23.
- (7) Mohammadi, A. H.; Eslamimanesh, A.; Richon, D. Monodisperse Thermodynamic Model Based on Chemical + Flory–Huggins Polymer Solution Theories for Predicting Asphaltene Precipitation. *Ind. Eng. Chem. Res.* **2012**, *51* (10), 4041–4055. <https://doi.org/10.1021/ie202737p>.
- (8) Ancheyta, J.; Centeno, G.; Trejo, F.; Marroquín, G. Changes in Asphaltene Properties during Hydrotreating of Heavy Crudes. *Energy Fuels* **2003**, *17* (5), 1233–1238. <https://doi.org/10.1021/ef030023+>.
- (9) Kaminski, T. J.; Fogler, H. S.; Wolf, N.; Wattana, P.; Mairal, A. Classification of Asphaltenes via Fractionation and the Effect of Heteroatom Content on Dissolution Kinetics. *Energy Fuels* **2000**, *14* (1), 25–30. <https://doi.org/10.1021/ef990111n>.

- (10) Barrera, D. M.; Ortiz, D. P.; Yarranton, H. W. Molecular Weight and Density Distributions of Asphaltenes from Crude Oils. *Energy Fuels* **2013**, *27* (5), 2474–2487. <https://doi.org/10.1021/ef400142v>.
- (11) Chen, L.; Bertolini, A.; Dubost, F.; Achourov, V.; Betancourt, S.; Cañas, J. A.; Dumont, H.; Pomerantz, A. E.; Mullins, O. C. Yen–Mullins Model Applies to Oilfield Reservoirs. *Energy Fuels* **2020**, *34* (11), 14074–14093. <https://doi.org/10.1021/acs.energyfuels.0c02937>.
- (12) Schuler, B.; Zhang, Y.; Liu, F.; Pomerantz, A. E.; Andrews, A. B.; Gross, L.; Pauchard, V.; Banerjee, S.; Mullins, O. C. Overview of Asphaltene Nanostructures and Thermodynamic Applications. *Energy Fuels* **2020**, *34* (12), 15082–15105. <https://doi.org/10.1021/acs.energyfuels.0c00874>.
- (13) Hoepfner, M. P. Investigations into Asphaltene Deposition, Stability, and Structure. Thesis, 2013.
- (14) Groenzin, H.; Mullins, O. C. Asphaltene Molecular Size and Structure. *J. Phys. Chem. A* **1999**, *103* (50), 11237–11245. <https://doi.org/10.1021/jp992609w>.
- (15) Buch, L.; Groenzin, H.; Buenrostro-Gonzalez, E.; Andersen, S. I.; Lira-Galeana, C.; Mullins, O. C. Molecular Size of Asphaltene Fractions Obtained from Residuum Hydrotreatment☆. *Fuel* **2003**, *82* (9), 1075–1084. [https://doi.org/10.1016/S0016-2361\(03\)00006-1](https://doi.org/10.1016/S0016-2361(03)00006-1).
- (16) Hortal, A. R.; Hurtado, P.; Martínez-Haya, B.; Mullins, O. C. Molecular-Weight Distributions of Coal and Petroleum Asphaltenes from Laser Desorption/Ionization Experiments. *Energy Fuels* **2007**, *21* (5), 2863–2868. <https://doi.org/10.1021/ef700225s>.
- (17) Rodgers, R. P.; Marshall, A. G. Petroleomics: Advanced Characterization of Petroleum-Derived Materials by Fourier Transform Ion Cyclotron Resonance Mass Spectrometry (FT-ICR MS). In *Asphaltenes, Heavy Oils, and Petroleomics*; Mullins, O. C., Sheu, E. Y., Hammami, A., Marshall, A. G., Eds.; Springer: New York, NY, 2007; pp 63–93. https://doi.org/10.1007/0-387-68903-6_3.
- (18) McKenna, A. M.; Purcell, J. M.; Rodgers, R. P.; Marshall, A. G. Identification of Vanadyl Porphyrins in a Heavy Crude Oil and Raw Asphaltene by Atmospheric Pressure Photoionization Fourier Transform Ion Cyclotron Resonance (FT-ICR) Mass Spectrometry. *Energy Fuels* **2009**, *23* (4), 2122–2128. <https://doi.org/10.1021/ef800999e>.

- (19) Ruiz-Morales, Y.; Mullins, O. C. Measured and Simulated Electronic Absorption and Emission Spectra of Asphaltenes. *Energy Fuels* **2009**, *23* (3), 1169–1177. <https://doi.org/10.1021/ef800663w>.
- (20) Ruiz-Morales, Y. Molecular Orbital Calculations and Optical Transitions of PAHs and Asphaltenes. In *Asphaltenes, Heavy Oils, and Petroleomics*; Mullins, O. C., Sheu, E. Y., Hammami, A., Marshall, A. G., Eds.; Springer: New York, NY, 2007; pp 95–137. https://doi.org/10.1007/0-387-68903-6_4.
- (21) Schuler, B.; Fatayer, S.; Meyer, G.; Rogel, E.; Moir, M.; Zhang, Y.; Harper, M. R.; Pomerantz, A. E.; Bake, K. D.; Witt, M.; Peña, D.; Kushnerick, J. D.; Mullins, O. C.; Ovalles, C.; van den Berg, F. G. A.; Gross, L. Heavy Oil Based Mixtures of Different Origins and Treatments Studied by Atomic Force Microscopy. *Energy Fuels* **2017**, *31* (7), 6856–6861. <https://doi.org/10.1021/acs.energyfuels.7b00805>.
- (22) Mostowfi, F.; Indo, K.; Mullins, O. C.; McFarlane, R. Asphaltene Nanoaggregates Studied by Centrifugation. *Energy Fuels* **2009**, *23* (3), 1194–1200. <https://doi.org/10.1021/ef8006273>.
- (23) Goual, L.; Sedghi, M.; Zeng, H.; Mostowfi, F.; McFarlane, R.; Mullins, O. C. On the Formation and Properties of Asphaltene Nanoaggregates and Clusters by DC-Conductivity and Centrifugation. *Fuel* **2011**, *90* (7), 2480–2490. <https://doi.org/10.1016/j.fuel.2011.02.025>.
- (24) Eyssautier, J.; Frot, D.; Barré, L. Structure and Dynamic Properties of Colloidal Asphaltene Aggregates. *Langmuir* **2012**, *28* (33), 11997–12004. <https://doi.org/10.1021/la301707h>.
- (25) Goual, L. Impedance Spectroscopy of Petroleum Fluids at Low Frequency. *Energy Fuels* **2009**, *23* (4), 2090–2094. <https://doi.org/10.1021/ef800860x>.
- (26) Zeng, H.; Song, Y.-Q.; Johnson, D. L.; Mullins, O. C. Critical Nanoaggregate Concentration of Asphaltenes by Direct-Current (DC) Electrical Conductivity. *Energy Fuels* **2009**, *23* (3), 1201–1208. <https://doi.org/10.1021/ef800781a>.
- (27) Sheremata, J. M.; Gray, M. R.; Dettman, H. D.; McCaffrey, W. C. Quantitative Molecular Representation and Sequential Optimization of Athabasca Asphaltenes. *Energy Fuels* **2004**, *18* (5), 1377–1384. <https://doi.org/10.1021/ef049936+>.

- (28) Lisitza, N. V.; Freed, D. E.; Sen, P. N.; Song, Y.-Q. Study of Asphaltene Nanoaggregation by Nuclear Magnetic Resonance (NMR). *Energy Fuels* **2009**, *23* (3), 1189–1193. <https://doi.org/10.1021/ef800631a>.
- (29) Sheu, E. Y. Self-Association of Asphaltenes. In *Structures and Dynamics of Asphaltenes*; Mullins, O. C., Sheu, E. Y., Eds.; Springer US: Boston, MA, 1998; pp 115–144. https://doi.org/10.1007/978-1-4899-1615-0_4.
- (30) Hoepfner, M. P.; Fogler, H. S. Multiscale Scattering Investigations of Asphaltene Cluster Breakup, Nanoaggregate Dissociation, and Molecular Ordering. *Langmuir* **2013**, *29* (49), 15423–15432. <https://doi.org/10.1021/la403531w>.
- (31) Goncalves, S.; Castillo, J.; Fernández, A.; Hung, J. Absorbance and Fluorescence Spectroscopy on the Aggregation Behavior of Asphaltene–Toluene Solutions. *Fuel* **2004**, *83* (13), 1823–1828. <https://doi.org/10.1016/j.fuel.2004.03.009>.
- (32) Andreatta, G.; Bostrom, N.; Mullins, O. C. High-Q Ultrasonic Determination of the Critical Nanoaggregate Concentration of Asphaltenes and the Critical Micelle Concentration of Standard Surfactants. *Langmuir* **2005**, *21* (7), 2728–2736. <https://doi.org/10.1021/la048640t>.
- (33) Goual, L.; Sedghi, M.; Wang, X.; Zhu, Z. Asphaltene Aggregation and Impact of Alkylphenols. *Langmuir* **2014**, *30* (19), 5394–5403. <https://doi.org/10.1021/la500615k>.
- (34) Mullins, O. C.; Sabbah, H.; Eyssautier, J.; Pomerantz, A. E.; Barré, L.; Andrews, A. B.; Ruiz-Morales, Y.; Mostowfi, F.; McFarlane, R.; Goual, L.; Lepkowitz, R.; Cooper, T.; Orbulescu, J.; Leblanc, R. M.; Edwards, J.; Zare, R. N. Advances in Asphaltene Science and the Yen–Mullins Model. *Energy Fuels* **2012**, *26* (7), 3986–4003. <https://doi.org/10.1021/ef300185p>.
- (35) Schneider, M. H.; Andrews, A. B.; Mitra-Kirtley, S.; Mullins, O. C. Asphaltene Molecular Size by Fluorescence Correlation Spectroscopy. *Energy Fuels* **2007**, *21* (5), 2875–2882. <https://doi.org/10.1021/ef700216r>.
- (36) Tanaka, R.; Sato, E.; Hunt, J. E.; Winans, R. E.; Sato, S.; Takanohashi, T. Characterization of Asphaltene Aggregates Using X-Ray Diffraction and Small-Angle X-Ray Scattering. *Energy Fuels* **2004**, *18* (4), 1118–1125. <https://doi.org/10.1021/ef034082z>.
- (37) Wu, Q.; Pomerantz, A. E.; Mullins, O. C.; Zare, R. N. Laser-Based Mass Spectrometric Determination of Aggregation Numbers for Petroleum- and Coal-Derived Asphaltenes. *Energy Fuels* **2014**, *28* (1), 475–482. <https://doi.org/10.1021/ef401958n>.

- (38) Eyssautier, J.; Barré, L.; Levitz, P.; Espinat, D. Caractérisation et Modélisation des Asphaltènes en Conditions Réactionnelles d'Hydrotraitement. Thesis, 2012.
- (39) Fávero, C. V. B. An Investigation of the Destabilization, Aggregation, and Deposition of Asphaltenes. 168. Thesis, 2018.
- (40) Simon, S.; Jestin, J.; Palermo, T.; Barré, L. Relation between Solution and Interfacial Properties of Asphaltene Aggregates. *Energy Fuels* **2009**, *23* (1), 306–313. <https://doi.org/10.1021/ef800548b>.
- (41) Akbarzadeh, K.; Hammami, A.; Kharrat, A.; Zhang, D.; Allenson, S.; Creek, J.; Kabir, S.; Jamaluddin, A.; Marshall, A. G.; Rodgers, R.; Mullins, O.; Solbakken, T. Asphaltenes - Problematic but Rich in Potential. *Oilfield Review* **2007**, *19*, 22–43.
- (42) Wang, S.; Liu, J.; Zhang, L.; Masliyah, J.; Xu, Z. Interaction Forces between Asphaltene Surfaces in Organic Solvents. *Langmuir* **2010**, *26* (1), 183–190. <https://doi.org/10.1021/la9020004>.
- (43) Speight, J. G. *The Chemistry and Technology of Petroleum*, 5th ed.; CRC Press, 2014.
- (44) Maugeri, L. *The Age of Oil: The Mythology, History, and Future of the World's Most Controversial Resource*; Praeger, 2006; Vol. 44.
- (45) Nalwaya, V.; Tantayakom, V.; Piumsomboon, P.; Fogler, S. Studies on Asphaltenes through Analysis of Polar Fractions. *Ind. Eng. Chem. Res.* **1999**, *38* (3), 964–972. <https://doi.org/10.1021/ie9804428>.
- (46) Haskett, C. E.; Tartera, M. A Practical Solution to the Problem of Asphaltene Deposits-Hassi Messaoud Field, Algeria. *Journal of Petroleum Technology* **1965**, *17* (04), 387–391. <https://doi.org/10.2118/994-PA>.
- (47) Borden, K. The Challenges of Processing and Transporting Heavy Crude. *Oil and Gas Facilities* **2015**, *2* (05), 22–26. <https://doi.org/10.2118/1013-0022-OGF>.
- (48) Kilpatrick, P. K. Water-in-Crude Oil Emulsion Stabilization: Review and Unanswered Questions. *Energy Fuels* **2012**, *26* (7), 4017–4026. <https://doi.org/10.1021/ef3003262>.
- (49) Luo, P.; Gu, Y. Effects of Asphaltene Content on the Heavy Oil Viscosity at Different Temperatures. *Fuel* **2007**, *86* (7), 1069–1078. <https://doi.org/10.1016/j.fuel.2006.10.017>.

- (50) Wiehe, I. A. Asphaltene Solubility and Fluid Compatibility. *Energy Fuels* **2012**, *26* (7), 4004–4016. <https://doi.org/10.1021/ef300276x>.
- (51) Wiehe, I. A.; Kennedy, R. J. The Oil Compatibility Model and Crude Oil Incompatibility. *Energy Fuels* **2000**, *14* (1), 56–59. <https://doi.org/10.1021/ef990133+>.
- (52) Nguyen, M. T.; Nguyen, D. L. T.; Xia, C.; Nguyen, T. B.; Shokouhimehr, M.; Sana, S. S.; Grace, A. N.; Aghbashlo, M.; Tabatabaei, M.; Sonne, C.; Kim, S. Y.; Lam, S. S.; Le, Q. V. Recent Advances in Asphaltene Transformation in Heavy Oil Hydroprocessing: Progress, Challenges, and Future Perspectives. *Fuel Processing Technology* **2021**, *213*, 106681. <https://doi.org/10.1016/j.fuproc.2020.106681>.
- (53) Kohli, K.; Prajapati, R.; Maity, S. K.; Sau, M.; Garg, M. O. Deactivation of Hydrotreating Catalyst by Metals in Resin and Asphaltene Parts of Heavy Oil and Residues. *Fuel* **2016**, *175*, 264–273. <https://doi.org/10.1016/j.fuel.2016.02.036>.
- (54) GEOMARK RESEARCH, LTD. *Laboratory Services Capabilities & Price Schedule*. <https://docplayer.net/43082041-Geomark-research-ltd-laboratory-services-capabilities-price-schedule.html> (accessed 2023-07-15).
- (55) S. Asomaning, A. P. Watkinson. Petroleum Stability and Heteroatom Species Effects in Fouling of Heat Exchangers by Asphaltenes. *Heat Transfer Engineering* **2000**, *21* (3), 10–16. <https://doi.org/10.1080/014576300270852>.
- (56) Kumar, R.; Voolapalli, R. K.; Upadhyayula, S. Prediction of Crude Oil Blends Compatibility and Blend Optimization for Increasing Heavy Oil Processing. *Fuel Processing Technology* **2018**, *177*, 309–327. <https://doi.org/10.1016/j.fuproc.2018.05.008>.
- (57) Guzmán, R.; Ancheyta, J.; Trejo, F.; Rodríguez, S. Methods for Determining Asphaltene Stability in Crude Oils. *Fuel* **2017**, *188*, 530–543. <https://doi.org/10.1016/j.fuel.2016.10.012>.
- (58) Wiehe, I. A.; Kennedy, R. J. Application of the Oil Compatibility Model to Refinery Streams. *Energy Fuels* **2000**, *14* (1), 60–63. <https://doi.org/10.1021/ef9901342>.
- (59) Rondon-Gonzalez, M.; Kane, M.; Quintero, C.; Passade-Boupat, N.; Zhou, H. Developing A Field with Asphaltenes Risks: From Diagnosis to Cure; OnePetro, 2014. <https://doi.org/10.2118/171891-MS>.

- (60) Passade-Boupat, N.; Zhou, H.; Rondon-Gonzalez, M. Asphaltene Precipitation from Crude Oils: How to Predict It and to Anticipate Treatment?; OnePetro, 2013. <https://doi.org/10.2118/164184-MS>.
- (61) Cimino, R.; Corraera, S.; Del Bianco, A.; Lockhart, T. P. Solubility and Phase Behavior of Asphaltenes in Hydrocarbon Media. In *Asphaltenes: Fundamentals and Applications*; Sheu, E. Y., Mullins, O. C., Eds.; Springer US: Boston, MA, 1995; pp 97–130. https://doi.org/10.1007/978-1-4757-9293-5_3.
- (62) Macías, A.; Hernández, E. A.; Sámano, V.; Ancheyta, J. Simplified Regular Solution Model for Asphaltenes Precipitation in Crude Oil Blends. *Petroleum Science and Technology* **2023**, 1–15. <https://doi.org/10.1080/10916466.2023.2210164>.
- (63) Subramanian, S.; Simon, S.; Sjöblom, J. Asphaltene Precipitation Models: A Review. *Journal of Dispersion Science and Technology* **2016**, 37 (7), 1027–1049. <https://doi.org/10.1080/01932691.2015.1065418>.
- (64) Hernández, E. A.; Lira-Galeana, C.; Ancheyta, J. Analysis of Asphaltene Precipitation Models from Solubility and Thermodynamic-Colloidal Theories. *Processes* **2023**, 11 (3), 765. <https://doi.org/10.3390/pr11030765>.
- (65) Leontaritis, K. J.; Mansoori, G. A. Asphaltene Flocculation During Oil Production and Processing: A Thermodynamic Colloidal Model; OnePetro, 1987. <https://doi.org/10.2118/16258-MS>.
- (66) Flory, P. J. Thermodynamics of High Polymer Solutions. *The Journal of Chemical Physics* **2004**, 10 (1), 51–61. <https://doi.org/10.1063/1.1723621>.
- (67) Huggins, M. L. Solutions of Long Chain Compounds. *The Journal of Chemical Physics* **2004**, 9 (5), 440. <https://doi.org/10.1063/1.1750930>.
- (68) Scott, R. L.; Magat, M. The Thermodynamics of High-Polymer Solutions: I. The Free Energy of Mixing of Solvents and Polymers of Heterogeneous Distribution. *The Journal of Chemical Physics* **2004**, 13 (5), 172–177. <https://doi.org/10.1063/1.1724018>.
- (69) Yarranton, H. W.; Masliyah, J. H. Molar Mass Distribution and Solubility Modeling of Asphaltenes. *AIChE Journal* **1996**, 42 (12), 3533–3543. <https://doi.org/10.1002/aic.690421222>.

- (70) Nghiem, L. X.; Hassam, M. S.; Nutakki, R.; George, A. E. D. Efficient Modelling of Asphaltene Precipitation; OnePetro, 1993. <https://doi.org/10.2118/26642-MS>.
- (71) Sabbagh, O.; Akbarzadeh, K.; Badamchi-Zadeh, A.; Svrcek, W. Y.; Yarranton, H. W. Applying the PR-EoS to Asphaltene Precipitation from n-Alkane Diluted Heavy Oils and Bitumens. *Energy Fuels* **2006**, *20* (2), 625–634. <https://doi.org/10.1021/ef0502709>.
- (72) Li, Z.; Firoozabadi, A. Modeling Asphaltene Precipitation by N-Alkanes from Heavy Oils and Bitumens Using Cubic-Plus-Association Equation of State. *Energy Fuels* **2010**, *24* (2), 1106–1113. <https://doi.org/10.1021/ef9009857>.
- (73) Li, Z.; Firoozabadi, A. Cubic-Plus-Association Equation of State for Asphaltene Precipitation in Live Oils. *Energy Fuels* **2010**, *24* (5), 2956–2963. <https://doi.org/10.1021/ef9014263>.
- (74) Gross, J.; Sadowski, G. Perturbed-Chain SAFT: An Equation of State Based on a Perturbation Theory for Chain Molecules. *Industrial and Engineering Chemistry Research* **2001**, *40* (4), 1244–1260. <https://doi.org/10.1021/ie0003887>.
- (75) Daryasafar, A.; Masoudi, M.; Kord, S.; Madani, M. Evaluation of Different Thermodynamic Models in Predicting Asphaltene Precipitation: A Comparative Study. *Fluid Phase Equilibria* **2020**, *514*, 112557. <https://doi.org/10.1016/j.fluid.2020.112557>.
- (76) Andersen, S. I.; Speight, J. G. Thermodynamic Models for Asphaltene Solubility and Precipitation. *Journal of Petroleum Science and Engineering* **1999**, *22* (1), 53–66. [https://doi.org/10.1016/S0920-4105\(98\)00057-6](https://doi.org/10.1016/S0920-4105(98)00057-6).
- (77) Vargas, J. K., A. T. Khaleel, J. Yarbrough, P. Pourreau, M. Tavakkoli, F. M. Strategies for Mitigation and Remediation of Asphaltene Deposition. In *Asphaltene Deposition*; CRC Press, 2018.
- (78) Manek, M. B. Asphaltene Dispersants as Demulsification Aids; OnePetro, 1995. <https://doi.org/10.2118/28972-MS>.
- (79) Khaleel, A. T.; Abutaqiya, M. I. L.; Sisco, C. J.; Vargas, F. M. Mitigation of Asphaltene Deposition by Re-Injection of Dead Oil. *Fluid Phase Equilibria* **2020**, *514*, 112552. <https://doi.org/10.1016/j.fluid.2020.112552>.
- (80) Akbar, S. H.; Saleh, A. A. A Comprehensive Approach To Solve Asphaltene Deposition Problem in Some Deep Wells; OnePetro, 1989. <https://doi.org/10.2118/17965-MS>.

- (81) Li, J.; Misselbrook, J.; Sach, M. Sand Cleanouts With Coiled Tubing: Choice of Process, Tools and Fluids. *Journal of Canadian Petroleum Technology* **2010**, *49* (08), 69–82. <https://doi.org/10.2118/113267-PA>.
- (82) Fung, G.; Backhaus, W. P.; McDaniel, S.; Erdogmus, M. To Pig or Not to Pig: The Marlin Experience With Stuck Pig; OnePetro, 2006. <https://doi.org/10.4043/18387-MS>.
- (83) Hildebrand, J. H.; Scott, R. L. The Solubility of Nonelectrolytes, Reinhold Pub. Co., *New York* **1950**, *3*.
- (84) Hansen, C. M. *Hansen Solubility Parameters: A User's Handbook, Second Edition*; CRC Press, 2007.
- (85) Verdier, S. C. R. Experimental Study and Modelling of Asphaltene Precipitation Caused by Gas Injection, Technical University of Denmark. Thesis, 2006.
- (86) Wang, J. X.; Buckley, J. S. A Two-Component Solubility Model of the Onset of Asphaltene Flocculation in Crude Oils. *Energy Fuels* **2001**, *15* (5), 1004–1012. <https://doi.org/10.1021/ef010012l>.
- (87) Gharbi, K.; Benyounes, K.; Khodja, M. Removal and Prevention of Asphaltene Deposition during Oil Production: A Literature Review. *Journal of Petroleum Science and Engineering* **2017**, *158*, 351–360. <https://doi.org/10.1016/j.petrol.2017.08.062>.

Chapter 2. Experimental Methods

Numerous methods have been proposed in the literature to investigate the destabilization, aggregation, and deposition of asphaltenes. These methods are used comparatively in the presence of chemical additives to, for instance, assess the shift in the detection threshold of unstable asphaltenes or the inhibition of deposition on a surface. In this chapter, a review of laboratory methods for studying asphaltene behavior in the liquid phase and their deposition onto surfaces is presented, and the advantages and disadvantages of each technique will be discussed. This will be followed by a detailed presentation of the experimental methods employed throughout this manuscript. Finally, information about the chemicals and the protocol for preparing the chemical additives will be provided in the last section.

1. Laboratory methods for evaluating behavior of asphaltene in the liquid phase and their deposition

In the literature, various techniques can be found for characterizing asphaltene flocculation or deposition. These methods can be applied using either live oil or dead oil samples. Live oil tests involve destabilizing asphaltenes through depressurization, while dead oil tests induce destabilization by adding an antisolvent such as n-pentane or n-heptane. Laboratory techniques can be categorized into two parts: techniques that characterize changes in asphaltene behavior in the liquid phase (e.g. flocculation) and techniques that assess asphaltene deposition on a surface.

5.1. Liquid phase tests

Many researchers have strived to introduce experimental methods for identifying the point of instant detection of unstable asphaltenes, frequently termed as "onset." Asphaltene destabilization is recognized when:

- (i) Asphaltenes have grown in size, forming micrometer-sized aggregates. This step is described as flocculation.
- (ii) The unstable aggregates, having become too large to remain suspended, leave the liquid phase and sediment.

As discussed in the previous chapter, the term "onset" corresponds the instantaneous detection of larger unstable particles and depends on the detection threshold of the technique used and the experimental conditions.

Various methods were employed to detect the "onset" of asphaltene destabilization or to study their aggregation kinetics in model oil, dead oil or live oil. These include physical properties measurement, visual observation by microscopy, NIR spectroscopy, acoustic sensor, gravimetric separation.

5.1.1. Physical properties measurement

Techniques that utilize the physical properties of the fluid can be applied to determine asphaltene separation from liquid (e.g. the emergence of mesoscale aggregates, flocs). For example, the viscometry method¹ involves monitoring the change in viscosity of an oil mixture upon the addition of an antisolvent. A noticeable increase in oil viscosity, attributed to the aggregation of unstable asphaltene clusters, characterizes the "onset" of asphaltene flocculation. The same principle was applied by assessing the change in density of oil mixtures at different n-heptane ratios². The break point in the slope of oil density versus the volume of antisolvent is considered to mark the "onset" of asphaltene flocculation. Viscosity or density-based techniques, despite their advantage of being applicable to dark dead or live oils, are hindered by the risk of

equipment fouling due to asphaltene particles, which presents a significant drawback of these methods.

Monitoring the variations in asphaltene conductivity during the addition of an antisolvent allows for the investigation of asphaltene aggregation³. Goual et al.⁴ conducted direct-current (DC) electrical conductivity measurements of asphaltene with impedance analysis in heptol. Analyzing the slope of asphaltene conductivity versus the antisolvent fraction enabled the authors to determine the “onset” of asphaltene flocculation at the first break point. Additionally, the “onset” of sedimentation occurs at the second breakpoint when the unstable asphaltene population decreases after phase separation.

5.1.2. Acoustic resonance technique

Acoustic resonance techniques were applied under atmospheric⁵ or high-pressure high-temperature (HPHT) conditions⁶ to observe changes in sonic wave velocity across various fluid phases in dark crude oils. By sending acoustic waves through fluids, the response indicates phase changes, such as from liquid to gas or liquid to solid (e.g. asphaltene particles). This method can detect the “asphaltene onset pressure” (AOP) during depressurization stages in live oil systems. The system employs an HPHT cylindrical resonator, with a transmitter sending waves through the fluid and a receiver capturing response signals. The normalized acoustic response can be plotted against pressure, revealing changes connected to the AOP and bubble pressure⁶. As pressure decreases, sonic speed drops until AOP, causing a dip in the curve due to flocculated solid particles. While this method offers valuable insights into fluid behavior during phase transitions, its capacity to identify the lower boundary of asphaltene destabilization is constrained⁷. This limitation arises from the gradual re-solubilization of asphaltene particles in oil below the bubble point pressure, a phenomenon not discerned by resonance frequency. In addition, acoustic resonance techniques does not allow for fluid mixing, leading to inaccurate identification of the “onset” point due to the non-uniform distribution of asphaltenes⁷.

1.1.3 Optical microscopy technique

Authors^{8;9;10} have proposed techniques relying on optical microscopy, both under atmospheric and high-pressure conditions, to identify the "onset" of asphaltene flocculation. Maqbool et al.⁸ proposed a method for evaluating asphaltene aggregation kinetics through an optical microscope. Various mixtures of oil + antisolvent are observed under an optical microscope at different aging times. The aging time at which the appearance of black asphaltene particles (>500 nm) is microscopically observable corresponds to the detection time. The time for unstable asphaltenes to reach a microscopic size varies linearly with the antisolvent content on a semi-logarithmic graph^{8;11}. Daridon et al.¹⁰ developed an experimental setup with a short-wave infrared (SWIR) microscope to investigate phase transitions (e.g. asphaltene flocculation) in a pressurized fluid loaded into a PVT cell equipped with sapphire windows. The details of these optical methods will be provided in the following section of this chapter, as we have adopted them for some of our tests.

1.1.4 Light scattering technique

Light scattering measurements were also used to determine the "onset" of flocculation of unstable asphaltenes. NIR spectroscopy is particularly well-suited for dark oil samples. Within the NIR range of the electromagnetic spectrum, which spans from 780 to 2500 nm¹², crude oil samples exhibit significantly lower optical density values than in the UV-vis range¹³. The process of asphaltene flocculation is discerned through a reduction in normalized light intensity, often indicated by decreased light transmittance. This decline in light intensity arises from the scattering of light resulting from the formation of aggregates formed by asphaltene particles. These aggregates act as barriers, obstructing the passage of light through the fluid, which can then be detected by a receiver or detector. Within the Solid Detection System (SDS)¹⁴, the fluid is introduced into a high-pressure sapphire cell. The SDS method enables real-time analysis of live oil samples under reservoir conditions (high pressure and temperature) to determine the AOP^{15;16}. Through isothermal depressurization experiments, asphaltene destabilization is induced by gradually reducing the pressure of the live crude sample from its initial reservoir pressure. During this process, NIR light transmittance is continuously monitored. Initially, light transmittance

increases as pressure drops, reflecting oil expansion (density reduction). However, upon reaching the AOP, an abrupt drop in light transmittance occurs, marked by an inflection point. This reduction stems from light scattering triggered by the presence of asphaltene aggregates. Light scattering is usually combined with a high-pressure microscope (HPM) to allow the visual inspection of flocs at the AOP.

1.1.5 Filtration technique

High-pressure filtration devices have also found application within PVT cells^{17;18}. During a constant-temperature depressurization process, the fluid is homogenized by a magnetic stirrer. Subsequently, the blended fluid is forced through a micrometer hydrophobic filter at elevated pressure and temperature. This filtration takes place under standard conditions. The back side of the filter is pressurized using a stable hydrocarbon gas to match the experimental pressure. By evaluating the weight percentages of unstable asphaltenes collected on a filter (utilizing SARA analysis) for different ratios of n-alkanes to bitumen, the authors have developed a graphical illustration that demonstrates the correlation between the weight percentage of flocculated asphaltenes and the antisolvent-to-bitumen ratio¹⁷. Subsequently, these data points are extended to the dilution ratio at which no solid materials would accumulate and this point marks the “onset” of flocculation. However, the mesh size of the filter is approximately $0.45 \mu\text{m}$, so the detection threshold of this technique does not account for the appearance of unstable asphaltene aggregates with sizes smaller than the mesh size.

1.1.6. Gravimetric technique: centrifugation

The gravimetric technique exploits the difference in weight between unstable asphaltene aggregates (larger than 100 nm) and the residual mixture of crude oil and antisolvent. After centrifugation, the unstable asphaltene aggregates are collected in the bottom of the vial. The lowest antisolvent fraction exhibiting asphaltene particles at the bottom marks the “onset” of flocculation. However, the main advantage of centrifugation is that it allows quantification of the

amount of unstable asphaltenes at a given antisolvent composition and aging time⁸. The experimental protocol for centrifugation separation will be detailed in the *Experimental Methods* section below.

1.2. Deposition tests

1.2.1. Capillary test

Brosetta et al.¹⁹ proposed a method to evaluate the “onset” of deposition and asphaltene deposition rate by monitoring the pressure drop caused by the formation of a deposit layer inside a metallic capillary loop. The experiment involves injecting an oil-antisolvent mixture (mixed upstream with a pump system and a T-junction) at a fixed flow rate and measuring the pressure drop across the capillary tube. The authors used the Hagen-Poiseuille law to express the pressure drop as a function of the flow rate:

$$\Delta P = \frac{8\eta}{\pi R_c^4} L_c Q \quad (1)$$

where R_c and L_c are, respectively, the radius and length of the capillary and η is the liquid viscosity.

The effective average hydrodynamic thickness of the deposited layer $e(t)$ at time t is given by,

$$\frac{\Delta P(t) - \Delta P_0}{\Delta P_0} = \frac{[R_{c_0} - e(t)]^{-4}}{R_{c_0}^{-4}} \approx 4 \frac{e(t)}{R_{c_0}} \quad (2)$$

where R_{c_0} is the initial radius of the capillary and ΔP_0 is the initial pressure drop.

The capillary deposition tests can be performed both at ambient and HPHT conditions. However, some authors using capillary loop devices have highlighted that the deposition is not uniformly distributed on the internal metal surface of the capillary. Scanning electron microscopy (SEM) observations have shown that the deposit thickness is greater at the capillary inlet rather than at its end^{20;21}. Kuang et al.²² proposed a method to evaluate the deposition profile along the capillary. In

their study, at the end of the run, the authors cut the capillary into ten equal sections and measured the cumulative deposit in each section by performing toluene washes. They observed a non-uniform deposition profile with larger deposit quantities at both the inlet and outlet of the capillary. Capillary loop devices are interesting, especially for characterizing deposit formation based on shear forces. However, relying solely on pressure drop measurements can lead to biased interpretations due to the deposition profile along the capillary.

1.2.2. Packed-bed apparatus

Recently, experimental setup using a packed bed have been reported in the literature^{23;24;25}. The experimental setup for a packed bed consists of a column filled with metallic beads, which serve as the surface for asphaltene deposition. An upstream injection and mixing systems are used to prepare the oil-antisolvent system and to flow the oil through the column. In such experiments, the quantity of asphaltene deposited is measured by comparing the weight of the beads before and after the test. The packed bed offers the advantage of conducting deposition tests under different flow regimes at ambient or HPHT conditions. However, Saidoun²⁶ report that the volumes required to obtain representative deposition measurement results using a packed bed apparatus are on the order of several liters of oil and take several days of continuous experiment.

1.2.3. Quartz crystal Microbalance

The use of Quartz Crystal Microbalance (QCM) in crude oil systems dates back to 2002 with a study by Ekholm et al.²⁷ on the interaction of asphaltenes and resins on a hydrophilic surface. Subsequently, many authors have employed the acoustic properties of QCM to investigate asphaltenes destabilization and deposition in various systems^{28;29;30;31;32}. The technique relies on the principle that the resonant frequency of quartz properties is responsive to its thickness, and consequently, to material adsorbed or deposited on its surface. Abudu and Goual²⁸ introduced the use of quartz properties for assessing asphaltene adsorption. Subsequently, Daridon et al.³¹ extended the application of the quartz sensor by correlating the changes in resonant frequency and dissipation to the deposition of unstable asphaltenes and the alterations in viscosity and density.

This was achieved through continuous antisolvent titration under both ambient conditions and HPHT in a PVT cell using a quartz sensor with both faces immersed in the fluid^{26;33}. The quartz method as an acoustic sensor will be detailed in the *Experimental Methods* section.

1.3. Screening laboratory methods for evaluating chemical additives

The methods presented above are commonly used comparatively to assess the effectiveness of chemical additives. The effectiveness of a chemical additive can be characterized by its ability to shift the “onset” of destabilization, its capacity to disperse asphaltene particles while limiting their size, or its capacity to reduce the formation of asphaltene deposition on a surface.

One can mention the Asphaltene Dispersion Test (ADT), which is one of the most common and widely used commercial techniques for assessing the efficiency of a chemical additive in dispersing asphaltenes. In this test, a chemical additive is introduced to an oil sample at a certain concentration, and the destabilization of asphaltenes is induced using an excess of antisolvent like n-heptane. Subsequently, normal gravimetric sedimentation is observed visually over a specific aging period. If the solution maintains its black color without any visible phase separation, it signifies that the chemical additive prevents the unstable asphaltene particles from settling by keeping them suspended. Other variations of this technique are used with more sophisticated detection systems in order to be less operator-dependent, such as the turbidity test^{34;35} in which the dispersion capacity is evaluated based on the measurement of the light transmittance, where a low transmittance value indicates good dispersion of asphaltene particles.

However, the ADT and turbidity tests are conducted with diluted crude oils (1–5% volume of crude oil to n-heptane) under static conditions, which is far from real industrial conditions. Optical techniques have detection thresholds in the micrometer range, completely ignoring asphaltene destabilization phenomena at the nanoscale. In reality, destabilized asphaltenes below these detection thresholds may exist and diffuse on surfaces, leading to deposit accumulation. Moreover, authors^{24;36} have highlighted that a chemical additive capable of keeping unstable asphaltene particles in suspension does not necessarily reduce deposition, and in certain cases, an increase was even observed.

Kuang et al.²⁴ evaluated the dispersing performance efficiency (DPE) of commercial chemical additives by measuring NIR transmittance and their ability to reduce deposition using a multi-section packed bed system. The authors used the DPE proposed by Melendez-Alvarez¹⁵ to rank the dispersing effect of the chemical additives in two oils named S and R. A higher value of DPE indicates a greater dispersing capacity of the chemical additive. The results obtained by the authors are presented in Figure 1. The dashed lines correspond to the deposition quantities on spheres for nontreated oils. First, it should be noted that the measured DPE is different depending on the oil, meaning that the dispersing capacity of a chemical additive depends on the properties of asphaltenes and the system. On the other hand, the I8 chemical additive, which exhibits the most effective dispersion of asphaltene particles in both oils, increases the deposition in oil S compared to the reference oil, while in oil R, it seems to have no effect if considering the standard error. The I15 chemical additive is considered the least effective dispersant in oil S, yet it reduces the deposition on the spheres by 47% compared to nontreated oil. Therefore, a chemical additive showing a dispersing effect is not necessarily a good asphaltene deposition inhibitor.

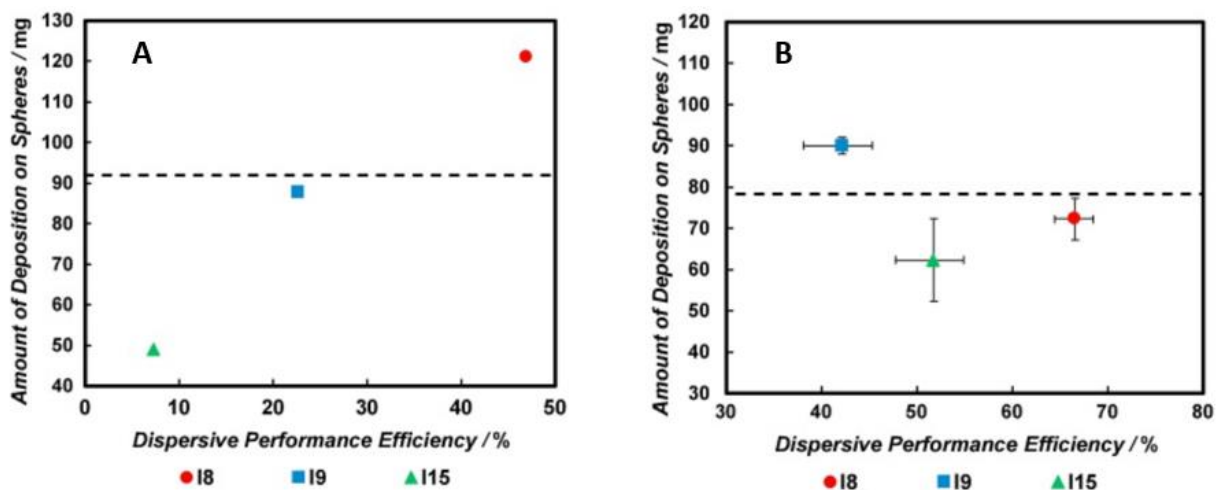


Figure 1. Results of the relationship between the DPE¹⁵ of commercial dispersants at 70 ppm and the corresponding amount of deposition measured using a multi-section packed bed system at 70 vol% n-heptane and ambient conditions in (A) crude oil S ; (B) crude oil R (60 ppm of dispersant) (reprinted from Kuang et al.²⁴).

Similarly, Joonaki et al.³⁶ evaluated three different chemical additives using ADT and NIR spectroscopy, and their ranking based on dispersion efficiency was completely opposite to the ranking obtained for deposition inhibition using a quartz crystal microbalance under high-pressure high-temperature conditions. Moreover, Montesi et al.³⁷ reported that the majority of commercial asphaltene dispersants injected in certain deepwater fields have shown limited effectiveness in mitigating the asphaltene deposition issue. Since the dispersing capacity of a chemical additive does not guarantee inhibition of the cumulative mass of asphaltenes on a surface, deposition measurement techniques are required.

1.4. Conclusions on the literature review

Nowadays, most commercial “asphaltene inhibitors” are marketed as dispersants, aiming to delay the sedimentation of asphaltene particles and/or reduce their aggregation kinetics. Screening methods, therefore, focus on the dispersing capability of chemical additives, relying on light absorption/scattering measurements or optical observation devices. However, the destabilization of asphaltenes is often induced using an excess of antisolvent and under conditions far from industrial conditions. Moreover, recent studies have questioned the evaluation of asphaltene inhibitors solely based on their dispersing ability. Indeed, the chemical additives’ capacity to disperse asphaltenes in the liquid is not correlated with their ability to reduce deposition on a surface. Recently, the industry has turned to screening methods based on the chemical additives’ capacity to reduce the deposit thickness or to delay its build-up period on a surface. For that purpose, in this work, it was chosen to employ several complementary experimental techniques: centrifugation, SWIR and time detection microscopy, quartz crystal resonator, to assess the effect of chemical additives on asphaltene destabilization, aggregation, and deposition. Centrifugation was used to quantify the separable amount of unstable asphaltenes. The time detection method proposed by Maqbool et al.⁸, involving optical microscopy and accounting for solution aging, was also employed. SWIR microscopy was used to observe the effect of a chemical additive on the size and morphology of micrometric unstable asphaltene aggregates. Finally, the quartz crystal resonator (QCR) was used at atmospheric pressure to investigate both asphaltene destabilization and deposition during the continuous titration of a dead oil. The acoustic sensor's sensitivity to

surface deposit at the nanogram level makes it a preferred technique for investigating the phenomena of destabilization and deposition of asphaltene particles, which occur at a similar scale²⁶.

2. Experimental Methods

2.1. The quartz crystal resonator as an acoustic sensor

2.1.1. Theoretical background

The quartz crystal resonator (QCR) consists of a crystalline quartz disc with electrodes deposited on both sides. Quartz exhibits piezoelectric properties, which were discovered by the Curie brothers in 1880. When a mechanical stress is applied to the quartz crystal, a displacement of electric charges occurs. Reversibly, when an electric voltage is applied to the quartz disc through the electrodes, the inverse piezoelectric effect induces a mechanical deformation of the crystal, leading to its oscillation at a specific resonant frequency. Quartz is not the only piezoelectric material (tourmaline, topaz); however, it has a very high quality factor (greater than 10^5), which represents the ratio of stored energy to energy dissipated in each oscillation cycle³⁸. Since quartz is an anisotropic material, its properties depend on how it is cut, particularly its thermal properties. The quartz we used for sensing is cut at an angle of 35.25° with respect to its optical axis Z, known as the "AT-cut," which shows a low impact of temperature changes on the resonance frequency³⁹. AT-cut quartz disc vibrates in a mode called the *Thickness Shear Mode* or TSM. This mode indicates that the movement of the quartz is perpendicular to its thickness (Figure 2). Applying an AC-voltage to the electrodes produces a tangential deformation (shear) inside the quartz disc. This deformation causes a displacement of the parallel surfaces in opposite directions. Stationary acoustic waves with vibration nodes (antinodes) on the surface are thus generated and propagate through the quartz disc (thickness mode) perpendicular to it (along the Y-axis).

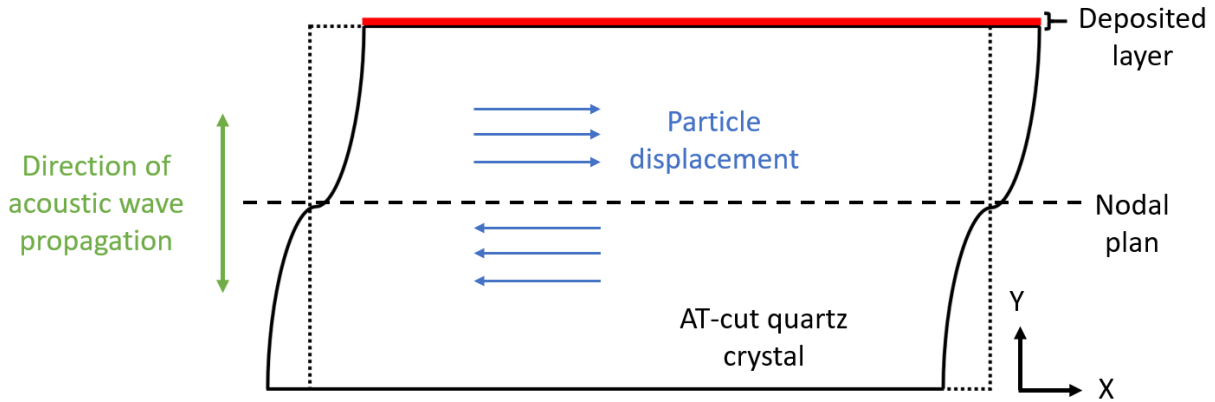


Figure 2. Quartz crystal resonator Thickness Shear Mode.

The wavelengths of these acoustic waves correspond to twice the thickness of the quartz resonator as shown in Figure 2. If a thin rigid film (homogeneous or not) is deposited on the surface of the quartz plate, it is considered by the resonator as part of its own thickness. Consequently, the wavelength, λ , increases, and the resonant frequency associated with a harmonic, f_n , decreases as a result.

$$f_n = \frac{nv_q}{\lambda_n} = \frac{nv_q}{2(h_q + h)} \quad (3)$$

where, v_q is the propagation velocity of the acoustic wave in the quartz resonator, h_q is the thickness of the quartz disc, and h is the thickness of the deposited film. The quartz crystal resonates when the wavelength is a multiple of twice the thickness of the quartz.

$$n\lambda_n = 2(h_q + h) \quad (4)$$

The frequency at which the amplitude of vibration of the acoustic wave is maximum corresponds to the fundamental resonance frequency of the quartz, f_0 . The oscillations of the quartz resonator are sensitive to changes occurring on its surface and in its immediate environment, which is why it is used as an acoustic sensor (Figure 3).

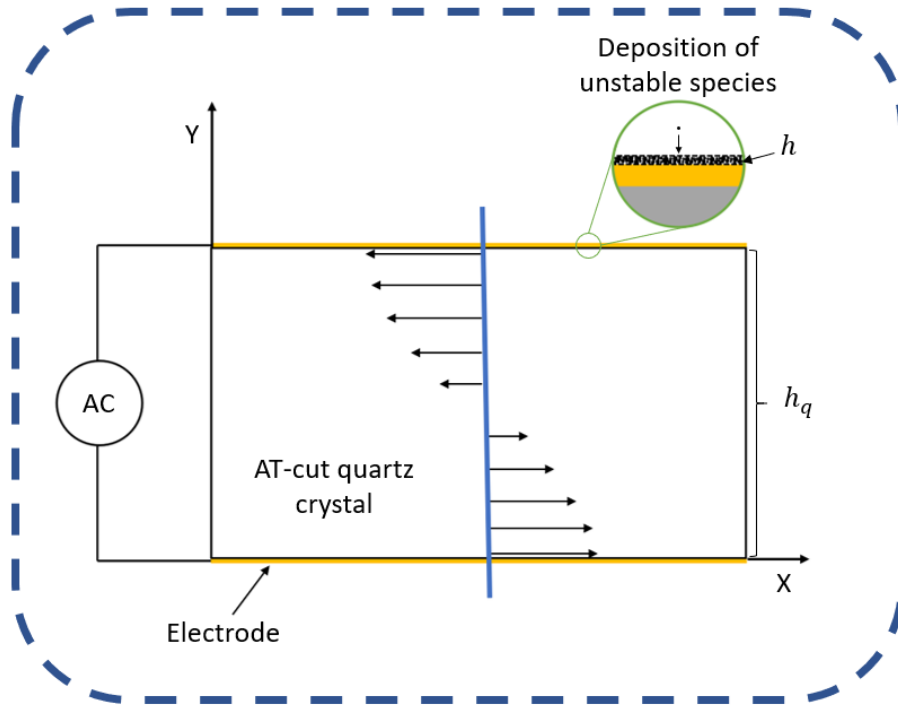


Figure 3. Schematic of a quartz crystal resonator immersed in a liquid.

Sauerbrey⁴⁰ pioneered the use of the quartz crystal resonator, in vacuum or in air, as a microbalance for weighing, hence the name "quartz crystal microbalance" or QCM usually used instead of quartz crystal resonator sensor. He demonstrated that when a thin rigid film is deposited on the surface of a quartz crystal, the excess thickness vibrates synchronously with the crystal, and the change in resonance frequency $\Delta f_{n,m}$ is related to the increase in thickness Δh by the Equation 5:

$$\frac{\Delta f_{n,m}}{f_0} = - \frac{\Delta h}{h_q} \quad (5)$$

where, h_q is the intrinsic thickness of the quartz crystal (without deposition), and f_0 is the resonance frequency of the fundamental.

The increase in quartz thickness due to the deposition of a thin rigid film leads to an increase in wavelength and therefore a decrease in resonance frequency. The sensitivity of the quartz resonator allows for the detection of Δh corresponding to deposited masses typically on the order of nanograms per square centimeter.

The change in resonance frequency can be expressed by the Sauerbrey equation⁴⁰ as follows:

$$\Delta f_{n,m} = -n2C_m\rho_D\Delta h \quad (6)$$

in this equation, ρ_D represent the density of the deposit and C_m corresponds to the Sauerbrey coefficient and its expressed as:

$$C_m = 2 \frac{f_0^2}{\sqrt{\rho_q\mu_q}} \quad (7)$$

where ρ_q and μ_q are the density and shear modulus of the quartz, respectively.

However, the application of the quartz resonator extends beyond solely measuring a deposited mass on its surface. When it is in contact with a liquid, it also provides information about the properties of the surrounding liquid. This is why we refer to it as a "quartz crystal resonator" (QCR) sensor.

The effects of viscosity (Δf_η) represent the interaction between the vibration of the quartz resonator and the surrounding viscous liquid. Kanazawa and Gordon⁴¹ showed that when the quartz resonator is in contact with a Newtonian fluid, the change in resonance frequency is proportional to the square root of the density (ρ_{liquid}) and viscosity (η_{liquid}) of the liquid, according to the Equation 8:

$$\Delta f_{n,\eta} = -\sqrt{n} \frac{C_m}{\sqrt{\pi f_0}} \sqrt{\rho_{liquid}\eta_{liquid}} \quad (8)$$

The viscosity effects not only impact the resonance frequency of the quartz but also result in energy dissipation of the acoustic wave, known as viscous damping. This viscous damping can be characterized by the bandwidth (Γ), which represents the half-width at half-maximum of the resonance peak.

When a quartz resonator with a deposited thin rigid film comes into contact with a liquid, several parameters can affect its oscillation. In addition to mass effects and those related to viscosity, parameters such as temperature (T), hydrostatic pressure (P), surface roughness (R_s), solid-liquid

surface slippage (G_s), and porosity with trapped liquid (P_o) can be considered. The effects related to temperature and hydrostatic pressure can be neglected when they are kept constant in both air and liquid environments. One approach to account for interfacial effects is to consider a virtual thin elastic layer between the quartz resonator and the surrounding liquid. This virtual layer, which is homogeneous and elastic, takes into account the deposition of material on the quartz resonator by considering interfacial effects (R_s, G_s, P_o). It is defined by two parameters: the virtual thickness, h_{layer} , and the shear modulus, G_A . The effects of roughness slippage and liquid trapped in pores are included in the first parameter, h_{layer} . The second parameter, G_A , takes into account the stiffness of the thin layer and is represented in the bandwidth equation ($\Delta\Gamma$) as a dimensionless number denoted by R . Interactions between mass effects (Δf_m) and viscosity effects (Δf_η) are considered negligible, and the frequency shift can be expressed as an additive form of these two contributions, according to the following equation:

$$\Delta f_n = \Delta f_{n,m} + \Delta f_{n,\eta} \quad (9)$$

By considering a "small loading" approach, which applies when the ratio of the resonance frequency change attributed to the deposition on the quartz resonator compared to the resonance frequency change of the quartz resonator without deposition is less than 2%²⁹, it becomes possible to express, with a simplified model, the changes in resonance frequency and bandwidth using the equations of Sauerbrey and Kanazawa. For the 3rd overtone of a 3 MHz QCR, this corresponds to a shift in frequency of 180 kHz. As the change in resonance frequency observed in our experiments does not exceed 25 kHz the small loading approximation holds and the shift in resonance frequency can be expressed as follows:

$$\Delta f_n = -n2C_m\rho_D h - \sqrt{n} \frac{C_m}{\sqrt{\pi f_0}} \sqrt{\rho_{liquid}\eta_{liquid}} \quad (10)$$

with $h = h_D + h_{layer}$

h_{layer} represents the thickness of the virtual layer that, as mentioned earlier, accounts for interfacial phenomena. This elastic virtual thickness can become negative when slip effects are significant.

The frequency shift (Δf_n) can be linearized by dividing Equation 10 by the harmonic (n).

$$\frac{\Delta f_n}{n} = -2C_m\rho_D h - \frac{1}{\sqrt{n}} \frac{C_m}{\sqrt{\pi f_0}} \sqrt{\rho_{liquid}\eta_{liquid}} \quad (11)$$

The slope represents the influence of the viscous effect as n approaches 1.

$$\frac{\Delta f_{n,\eta}}{n} = -\frac{C_m}{\sqrt{\pi f_0}} \sqrt{\rho_{liquid}\eta_{liquid}} \quad (12)$$

The y-intercept represents the deposited mass.

$$\frac{\Delta f_{n,m}}{n} = -2C_m\rho_D h \quad (13)$$

The half-width at half-maximum (Γ) take the following expression:

$$\Delta\Gamma_n = \sqrt{n} \frac{C_m}{\sqrt{\pi f_0}} \sqrt{\rho_{liquid}\eta_{liquid}} (1 + R) \quad (14)$$

$\Delta\Gamma_n$ is directly linear with the square root of the harmonic.

$$\Delta\Gamma_n = \Delta\Gamma_{n,\eta} \sqrt{n} \quad (15)$$

$$\Delta\Gamma_{n,\eta} = \frac{C_m}{\sqrt{\pi f_0}} \sqrt{\rho_{liquid}\eta_{liquid}} (1 + R) \quad (16)$$

From the resonance frequency shifts and changes in bandwidth measured for multiple harmonics and using the above equations, it becomes possible to obtain information about the deposited mass on the surface of the quartz resonator as well as the viscous properties of its surrounding environment.

In order to determine these parameters, we used a steady state method based on an impedance analysis that involves recording the electrical conductance G as a function of frequency, the conductance spectrum is obtained by applying an R_F voltage to the resonator using a network analyzer. As illustrated in Figure 4, the resonance frequency of each harmonic corresponds to the frequency at the peak conductance maximum. The bandwidth, which represents the half-width at half-maximum of the conductance peak, reflects the dissipation effect of the resonator. Immersing

the resonator in a fluid affects its resonance peaks as shown in Figure 4 for a given overtone n . It results in a negative resonance frequency shift Δf_n compared to its resonance frequency in vacuum. However, for practical reasons, it is preferred to use measurements in air as reference because the difference of quartz resonance behavior in air compared to the vacuum is minimal, and this ensures an identical apparatus configuration to those of the experiment:

$$\Delta f_n = f_{n,liquid} - f_{n,air} \quad (17)$$

$$\Delta \Gamma_n = \Gamma_{n,liquid} - \Gamma_{n,air} \quad (18)$$

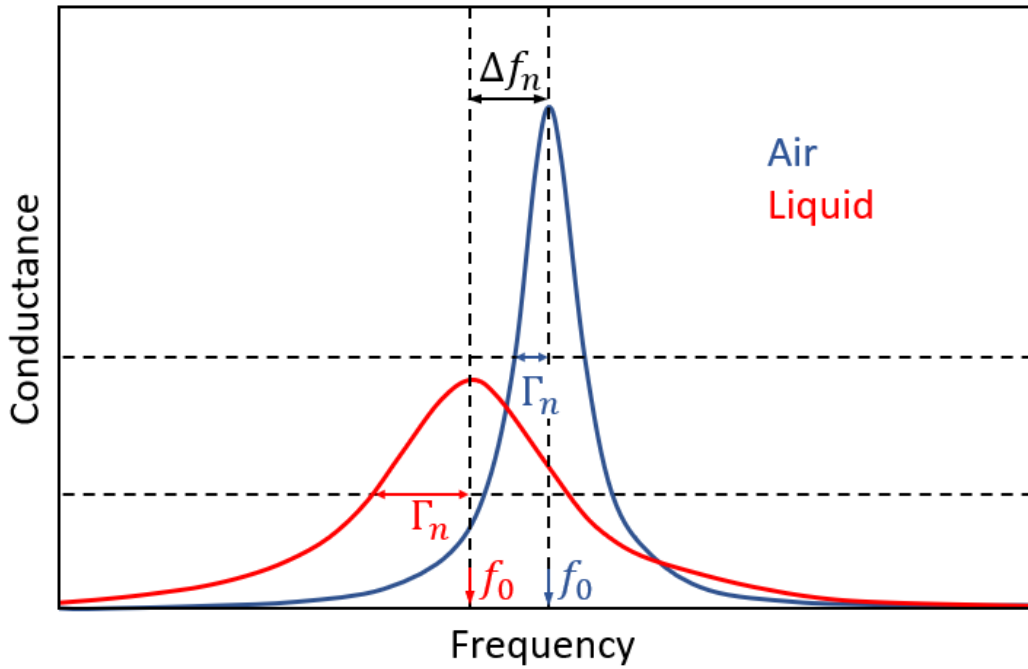


Figure 4. Measurement of frequency and impedance shifts in air and in an oil-type liquid.

The quartz crystal sensor has highly polished surfaces in order to minimize surface imperfections and closely correspond to the theoretical model. However, several intrinsic parasitic effects of quartz crystals (finite crystal boundary conditions, piezoelectric stiffening, energy trapping, inharmonic resonances) can significantly affect the resonance frequency and dissipation, even to the point of changing mass and viscosity effects. In order to minimize the disturbance of the

resonance signal by inharmonics and frequency jumps, the quartz disk is refined at the edges. This way, it can appear spherical with increased thickness at the center or beveled on one or both faces of the quartz, in order to trap the resonance energy at the center of the disk. Losses related to the support holding the resonator are thus minimized, and its oscillation is not restricted. Despite this particular geometry, the choice of harmonics remains limited. Indeed, the parasitic effects caused by the finite structure of the crystal and the interferences related to inharmonic modes reduce the range of valid experimental harmonics. Johannsmann³⁸ demonstrated that the lower harmonic orders, especially the fundamental, were affected by these intrinsic parameters of quartz crystals. Cassiède et al.⁴² performed impedance measurements on several harmonics using quartz crystals with different fundamental frequencies, up to 10 MHz. First of all, it appears that the first harmonic is particularly affected by the intrinsic parameters of quartz crystals such as piezoelectric stiffening and edge effects. Moreover, it was shown that inharmonic resonances interfere with the main resonance beyond a certain harmonic order, depending on each crystal, thus preventing the correct determination of both the resonance frequency and the bandwidth (Figure 5). The parasitic effect of inharmonics is even more significant for crystals vibrating at very high frequencies (above 6 MHz) because the difference between harmonic and inharmonic modes is inversely proportional to the crystal's fundamental frequency.

The acoustic sensor used for this work is a highly polished AT-cut quartz having a fundamental frequency of 3 MHz and a diameter of 13.6 mm with gold electrodes of 6.7 mm in diameter deposited on both sides. The fundamental resonance frequency as well as the geometry of the quartz was selected to allow the sensor to be operational in an extended overtone range (from 3 to 7) in full immersion in viscous oils.

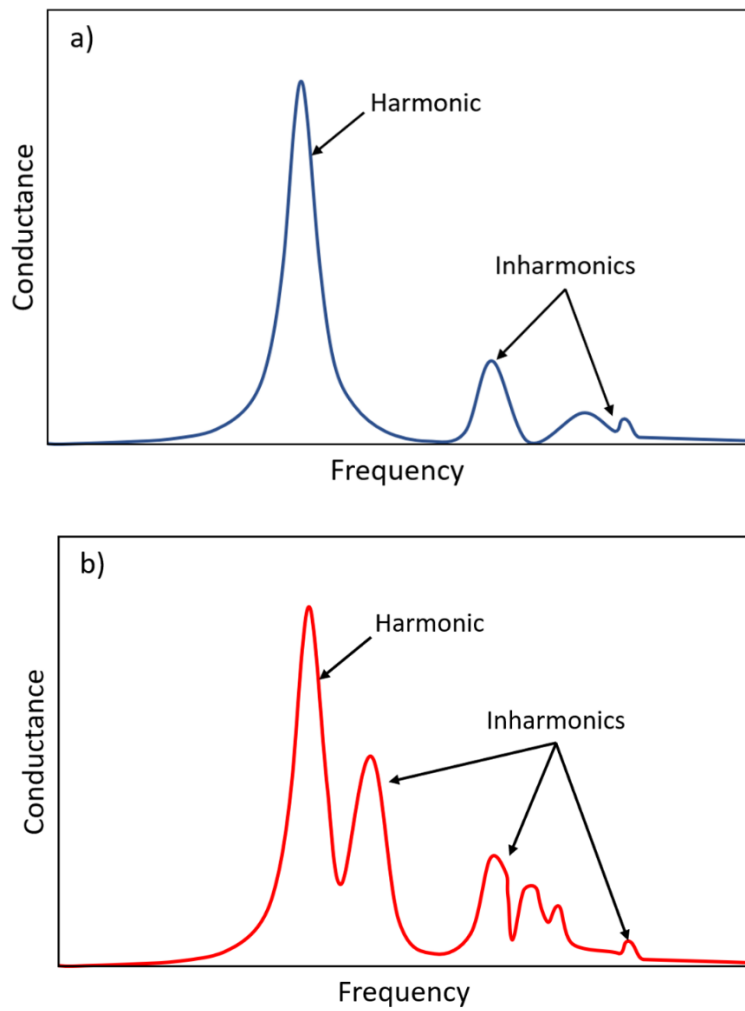


Figure 5. Theoretical conductance spectra a) usable harmonic signal with small n b) inharmonics that interfere with the resonance signal with large n .

2.1.2. Experimental antisolvent titration setup

The technique considered here to study asphaltene destabilization and deposition using a thickness shear mode acoustic sensor is based on a titration method. The titration system, which was presented in previous works^{31;43;44} is mainly composed of a stirred batch reactor working at varying volume with an inserted injection system. A schematic diagram of the full experimental setup is presented in Figure 6.

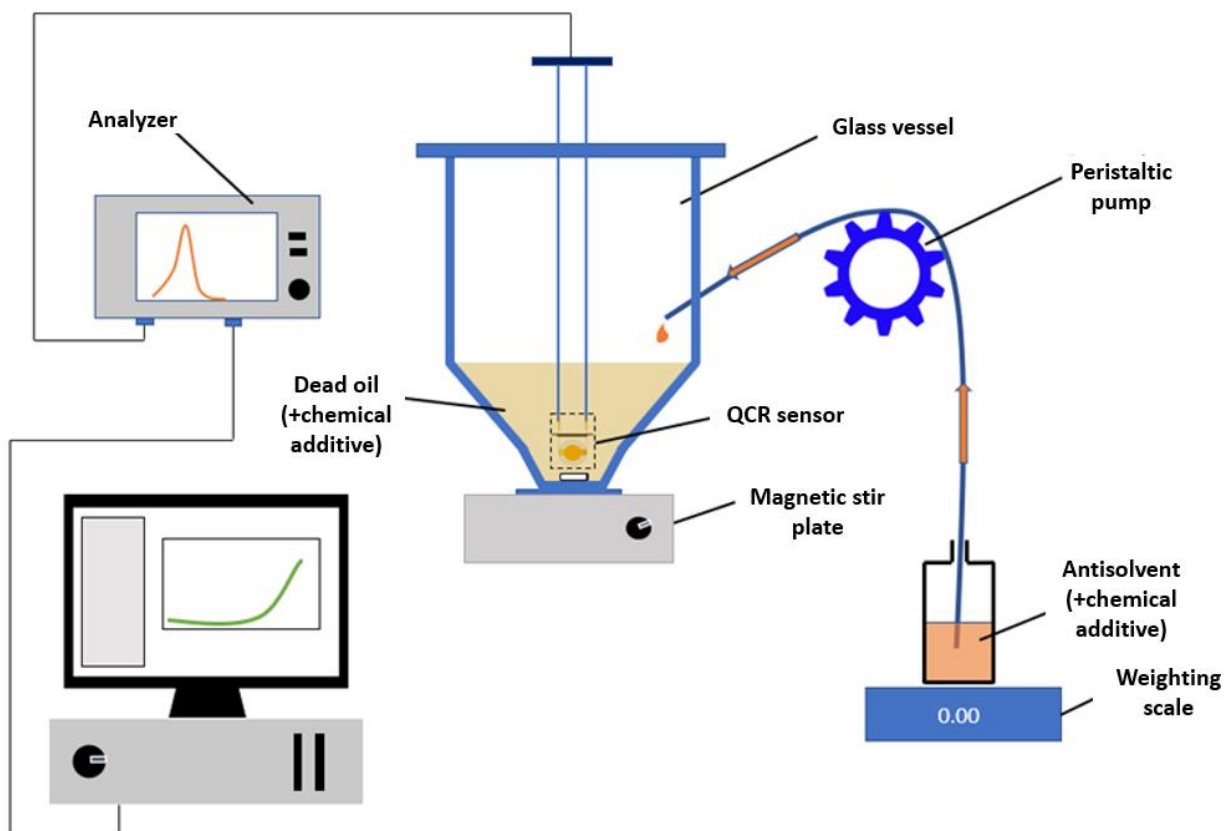


Figure 6. Atmospheric pressure experimental titration QCR set-up.

The temperature-controlled titration cell is a conical glass vessel to achieve an antisolvent injection reaching concentrations between 0 and 90 % in a single run. The antisolvent used in this manuscript is >99% pure grade n-heptane supplied by Sigma Aldrich. Antisolvent is added into the vessel at constant flow rate discharged by a peristaltic pump at constant rate chosen to avoid any local over concentration. The titrant is withdrawn from a container that has been placed on a

balance. The mass change in the container is continuously recorded, allowing a direct calculation of the composition of studied system as a function of time. To avoid radial or axial gradients in composition and temperature, the mixture is continuously stirred at a fixed speed of 470 rpm. The stirring speed is maximized while ensuring that the quartz remains fully immersed during the titration. The magnetic stirring bar is 25 mm long and has a diameter of 0.5 mm. Two electrical feedthroughs are used to plug and hold the acoustic sensor immersed in oil during the entire experiment at the bottom of the cell. QCR sensors are highly sensitive to their thickness, as well as to the thickness of the electrode, and particularly to their surface quality. It is completely impossible to manufacture two sensors with identical properties and therefore with the same resonance properties in air. Thus, it is preferable to use the same QCR for comparative studies. The same quartz disk was reused in this work to allow a reliable comparison of all experiments carried out. It was cleaned between each experiment by consecutive immersions in toluene vials located in an ultrasonic cleaner. Any direct contact of the quartz surface and a solid material is avoided during the washing and drying as well as the storage of the sensor between successive experiments to limit the risk of scratching and consequently changing the resonant properties of the resonator. Cleaning quality is verified by measuring the resonant properties of the unloading quartz disk at the same temperature before each new experiment. The cleanliness of quartz surfaces is validated only if the resonance frequency change does not exceed 10 Hz / 9 MHz.

A network analyser was used to apply a radio frequency voltage to the quartz sensor and to measure the input port voltage reflection coefficients which are used to calculate the conductance of the quartz over the frequency range from fundamental to 7th overtone. The obtained conductance spectra around the resonance of each overtone are digitalized in order to determine their resonance frequency f_n that correspond to the frequency at the maximum of a conductance peak. From this method, the resonance frequencies are estimated with an uncertainty of 4 Hz whereas the resonance half-band half-width Γ_n (related to resonator dissipation) is determined with a maximum error of 5 Hz. The unloaded reference values $f_{n,air}$ and $\Gamma_{n,air}$ are obtained by applying measurements in air at the same temperature prior to each experiment. Reference frequencies and dissipation are respectively used to calculate the shift in resonant properties caused by liquid immersion Δf_n and $\Delta \Gamma_n$.

In this work, each of the studied solutions were prepared as follows with a rigorously identical protocol to compare results with or without a chemical additive:

- i) 25 cm³ of the studied mixture is poured into the cell.
- ii) The crude + chemical additive mixture is left under stirring at the working temperature for 1 hour to achieve equilibrium between quartz sensor surface and the surrounding oil.
- iii) The n-heptane is injected at constant mass flow rate of 0.25 g/min.

For the interpretation of recorded data, the shift in resonant frequency and half-band half-width were calculated and plotted as a function of either time or volume fraction of n-heptane in the mixture ϕ_{C7} expressed as a function of the volume of each component:

$$\phi_{C7} = \frac{V_{C7}}{V_{C7} + V_{oil} + V_{chemical\ add}} \quad (19)$$

The volume of each component is calculated by converting masses into volumes using measured densities.

During the titration of an oil with a “good” asphaltene solvent such as toluene, the absence of asphaltene destabilization makes the term related to loaded mass on the sensor equal to zero. Thus, only viscosity effect caused by dilution is observed on the frequency shift. The viscosity of the mixture is reduced by the addition of the solvent. Daridon et al.³¹ proposed the following Grunberg-Nissan type equation to correlate the resonant frequency changes of a given overtone during the continuous addition of a solvent, considering a binary mixture of oil and solvent:

$$\Delta_{f_{mix}} = \exp(x \ln(\Delta_{f_{solvent}}) + (1 - x) \ln(\Delta_{f_{oil}}) + x(1 - x)G) \quad (20)$$

where x is the mass fraction of the solvent in the mixture, Δ_{f_i} is the resonant frequency of the component i and G is a Grunberg-Nissan adjustment parameter.

Saidoun et al.⁴³ followed the same approach by titrating an oil with toluene at 20°C, and the results are shown in Figure 7.a. An excellent match was found between the experimental data and the dilution model, with a deviation of less than 5%.

Results obtained by authors with an oil titrated by n-heptane at 60°C are shown in Figure 7.b. When an antisolvent, is added to asphaltene, they tend to destabilized and generate deposits on the

surface of the QCR. Consequently, the term related to mass becomes non-zero, and an inflection point on the resonance frequency curve becomes evident. At this point, the resonant behavior deviates from Kanazawa law associate to the simple dilution.

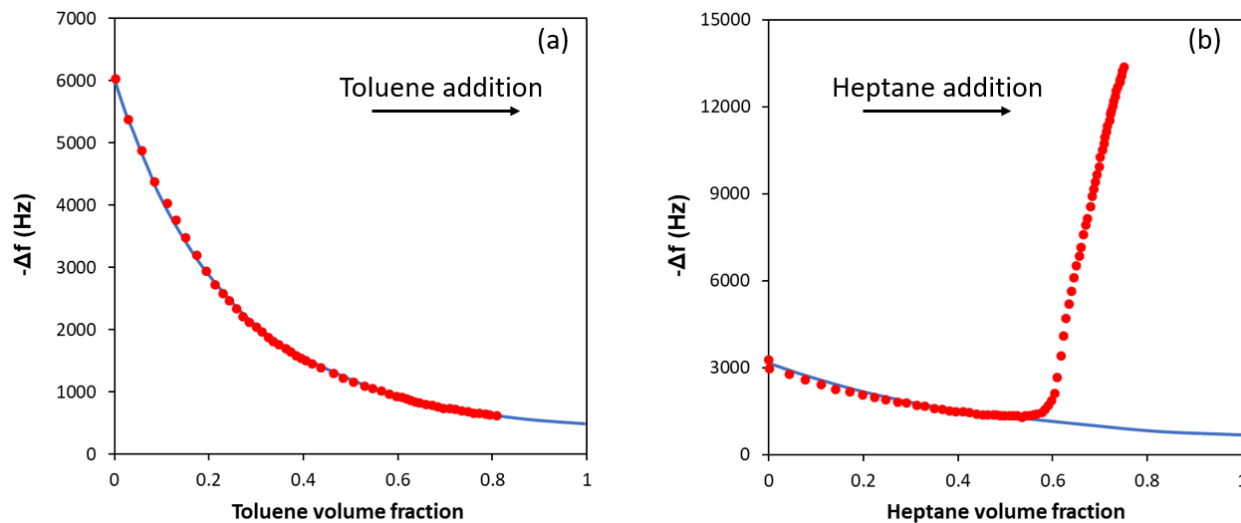


Figure 7. Red symbols are experimental frequency shifts (3rd overtone) obtained during continuous addition of a) toluene at 20°C and b) n-heptane at 60°C; solid line corresponds to the dilution model calculated using Equation 20 (reported by Saidoun et al.⁴³).

The shift in the bandwidth was recorded at 60°C during the continuous addition of n-heptane for a) a non-diluted crude oil and b) a diluted crude oil with a 1:19 oil/toluene ratio. The third overtone peak are plotted for both samples in Figure 8 and the dilution curves were calculated using the Grunberg-Nissan type equation. For both samples, titration curves first decrease because of the reduction in viscosity caused by the addition of n-heptane (dominating dilution effect). Then the increase in dissipation is related to the destabilization of the asphaltenes and the growth of asphaltene aggregates suspended around the sensor. The quartz disk therefore detects larger and/or more objects close to its surface.

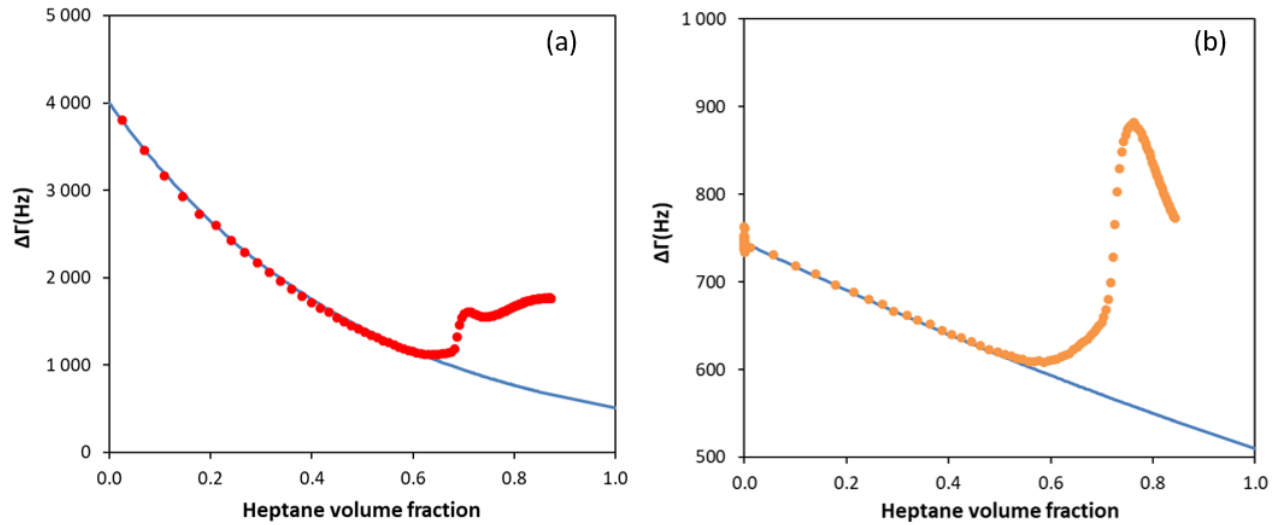


Figure 8. Shift of dissipation (3rd harmonic) recorded during experimental titration of a) a non-diluted crude oil and b) a diluted oil; solid lines correspond to the dilution model.

The percentage deviation of experimental data for both oils compared to the dilution model is shown in Figure 9. The results demonstrate a break in the horizontal trend and an increase in the percentage deviation during asphaltene destabilization. Although the effect seems more pronounced for diluted oil in Figure 9, it can be seen that the deviation is indeed more significant for the nondiluted oil as the asphaltene content is higher.

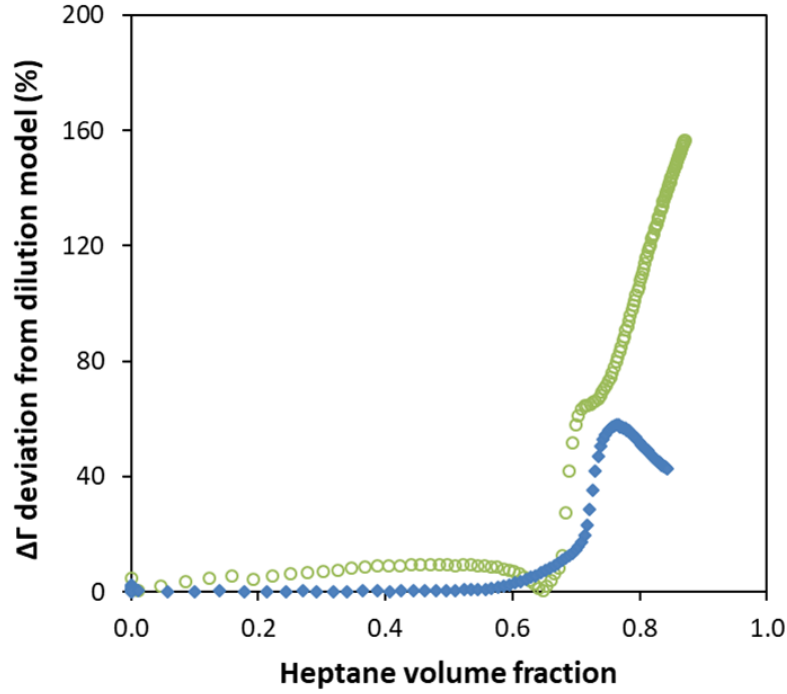


Figure 9. Percent deviation of the measured data from the calculated dilution curve; the symbols in green (○) correspond to the non-diluted crude oil and the symbols in blue (◆) correspond to the diluted crude oil.

During a titration experiment with continuous addition of antisolvent, the cumulative mass of deposited asphaltenes per unit surface area of the disc sensor is calculated using Equation 10.

$$\Delta m = \rho_D h = \frac{-\Delta f_{n,m}}{n2C_m} \quad (21)$$

where ρ_D is the density of the asphaltene deposit and is fixed to 1200 kg/m³.

As an example, the deposited mass per unit of area during a typical continuous titration is plotted in Figure 10.

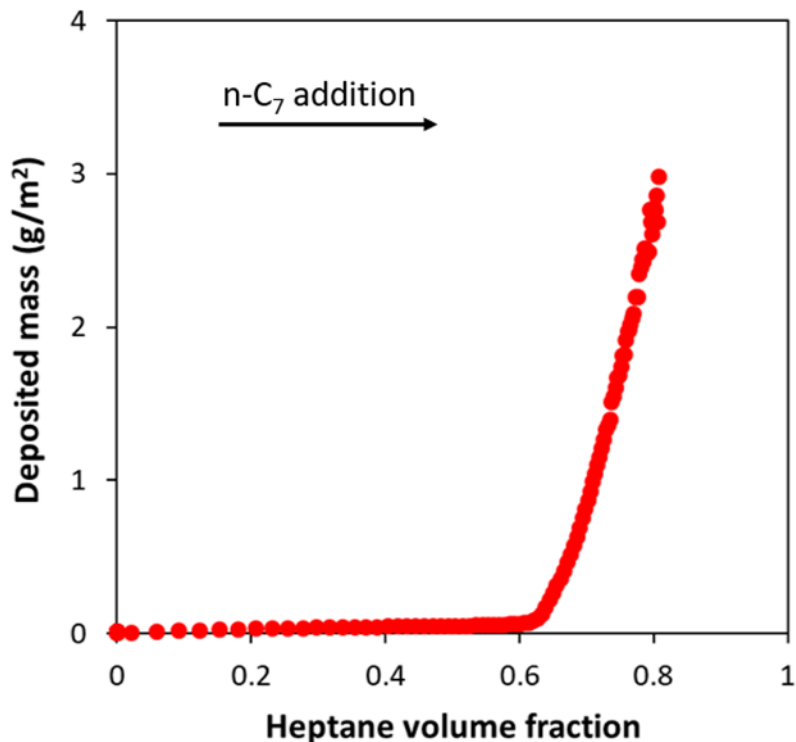


Figure 10. Deposited mass at the surface au the QCR calculated using Equation 21 during continuous addition n-heptane in a crude oil at 60°C.

2.2. Centrifugation experiment

2.2.1. Experimental protocol

The content of unstable asphaltenes per unit volume of crude oil at specific aging time $C_A(t)$ was measured by time-resolved centrifugation method proposed by Maqbool et al⁴⁵. The samples were prepared following the same protocol as presented for QCR experiments. Mixtures of non-treated oil and oil + chemical additive were prepared with various n-heptane content. After their preparation the samples were sealed and maintained under stirring at 470 rpm and 60°C during aging process. Aliquots of 1.5 ml were taken over time and centrifuged at 60°C with the *Rotina 380R* from *Hettich* at 15,000 rpm corresponding to a relative centrifugal force (RCF) of 24,400 g.

In this method, the supernatant is drained and recovered centrifuged pellets are collected as "wet" cakes containing unstable asphaltenes and trapped liquid solution. Then, pellets are washed with

n-heptane several times, re-dispersed and re-centrifuged until the supernatant remains transparent in order to remove the residual oil. Finally, the mass of dried cake is used to calculate the concentration of unstable asphaltene aggregates larger than a cut-off size per unit volume of initial crude oil. The concentration of separated unstable asphaltene aggregates $C_A(t)$ is plotted as a function of the aging time for different oil-heptane blend systems for the interpretation. $C_A(t)$ is expected to increase with the aging time for a fixed mixture and eventually tends to an equilibrium (plateau region represented by a red dotted line in Figure 11). The concentration of unstable asphaltenes at equilibrium, $C_{A\infty}$, and the time required to reach this equilibrium are determined using a reverse technique with the help of an equation (green solid line in Figure 11). The method will be detailed in the following chapters of the manuscript, and results will be presented.

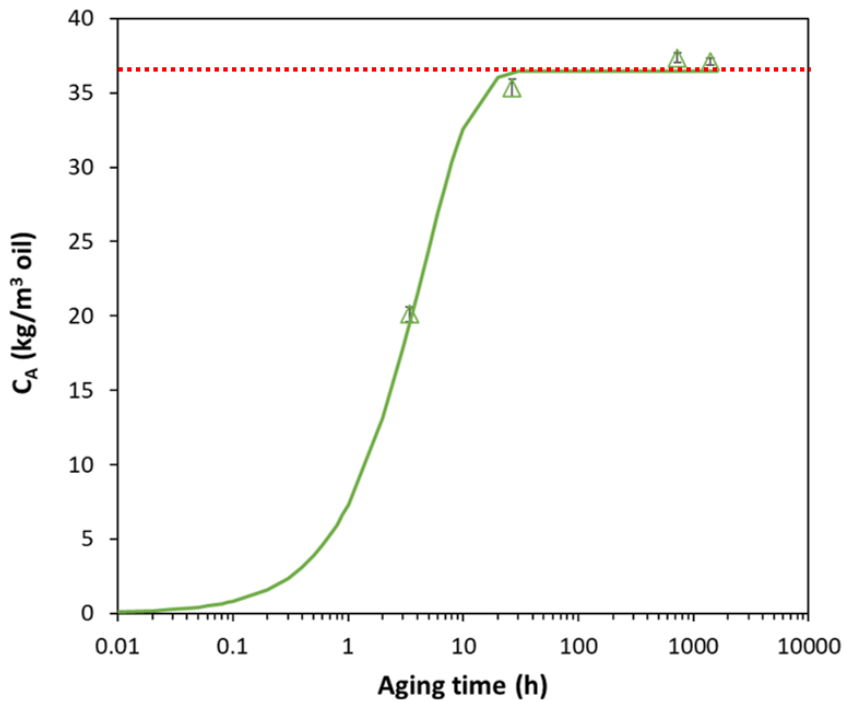


Figure 11. Concentration of unstable asphaltene aggregates larger than 200 nm separated by centrifugation as a function of the aging time for oil X titrated with 71.0 vol % of n-heptane.

2.2.2. Separation efficiency calculation method

The separation efficiency of aggregates of varying sizes depends on several parameters: the physical properties of the fluid (viscosity and density), the distance of particles from the rotating axis, the size and the density of the aggregates, and finally the revolution per minute (RPM) of the centrifuge rotor. Maqbool et al.⁴⁵ proposed a method to evaluate the efficiency of asphaltene aggregates separation in a liquid. Their method is presented below.

The oil-heptane mixture viscosity is estimated by applying Grunberg-Nissan mixing type equation⁴⁶ given by:

$$\eta_{liquid} = \exp^{x_{oil}\ln(\eta_{oil})+x_{C_7}\ln(\eta_{C_7})} \quad (22)$$

where x_i and η_i are the mass fraction and the dynamic viscosity of liquids respectively.

The density of the liquid mixture is calculated considering volume additivity by using the volume combining rule as follows:

$$\rho_{liquid} = \frac{1}{\frac{x_{oil}}{\rho_{oil}} + \frac{x_{C_7}}{\rho_{C_7}}} \quad (23)$$

Where ρ_i is the density of component i in the solution.

Considering a Stokes flow ($Re \ll 1$) and neglect particle collisions (dilute system), the frictional forces acting on an aggregate can be written as follows:

$$F_{df} = 3\pi d_k \eta_{liquid} u \quad (24)$$

where d_k is the diameter of the aggregate k , η_{liquid} is the viscosity of the liquid mixture and u represents the particle velocity.

The centrifugal force exerted on an aggregate k is given by:

$$F_{cent} = m_A \omega^2 x \quad (25)$$

with m_A being the apparent mass, which corresponds to the actual weight of the aggregate minus the buoyant force pushing upward (Equation 26), ω is the angular velocity, and x represents the distance between the aggregate particle and the center of rotation.

The apparent mass of the aggregate is expressed as follows:

$$m_A = m_R - m_B \quad (26)$$

The mass of the aggregate k is given by:

$$m_R = \frac{\pi d_k^3}{6} \phi_{solid} \rho_{asph} + \frac{\pi d_k^3}{6} (1 - \phi_{solid}) \rho_{liquid} \quad (27)$$

with ϕ_{solid} being the solid fraction in the asphaltene aggregate (composed of asphaltenes and trapped oil) and ρ_{asph} being the asphaltene density assumed equal to 1200 kg/m³.

Mass of displaced liquid is expressed as:

$$m_B = \frac{\pi d_k^3}{6} \rho_{liquid} \quad (28)$$

By combining Equations 26, 27 and 28, the apparent mass of the aggregate becomes:

$$m_A = \frac{\pi d_k^3}{6} \phi_{solid} (\rho_{asph} - \rho_{liquid}) = \frac{\pi d_k^3}{6} \phi_{solid} \Delta\rho \quad (29)$$

The balance of forces acting on an aggregate corresponds to the equalization of Equations 24 and 25:

$$m_A \omega^2 x = 3\pi d_k \eta_{liquid} u \quad (30)$$

with u being the velocity of the particle. The radial distance of the aggregate from the centrifugal axis at time t is represented by x . It is obtained by combining Equations 29 and 30

$$u = \frac{dx}{dt} = \phi_{solid} \Delta\rho \frac{d_k^2}{18\eta_{liquid}} \omega^2 x \quad (31)$$

Considering an aggregate k that moves from an initial position x_0 to a final position x_f at a time t , Equation 31 is integrated to obtain the distance traveled by a particle in time t :

$$\Delta_{x_k} = x_f - x_0 = x_f \left[1 - \exp\left(-\frac{\Delta\rho d_k^2 \phi_{solid} \omega^2 t}{18\eta_{liquid}}\right) \right] \quad (32)$$

For a homogeneous distribution of particles in the liquid, Maqbool et al.⁴⁵ defined the separation efficiency for a particle k as:

$$S_k = \frac{\Delta_{x_k}}{H_L} \text{ for } \Delta_{x_k} < H_L \quad (33)$$

$$S_k = 1 \text{ for } \Delta_{x_k} > H_L$$

When the particle's initial position is at the top of the liquid in the tube the difference in position between x_0 and x_f reaches its maximum value and is equal to H_L (the height of the liquid). For an aggregate of a specific size, efficient separation is achieved when the calculated distance (Δ_{x_k}) traveled exceeds the height of the liquid (H_L).

A sensitivity analysis of the separation efficiency for an oil-heptane mixture is presented in Figure 12. The RCF is set at 24,400 g. The properties of the liquid are given in Table 1.

Table 1. Oil-heptane mixture properties at 60°C

Property	Value
n-heptane fraction	50 wt %
Liquid density	760.2 kg/m ³
Liquid viscosity	1.84 mPa.s
Length of the liquid (H)	3.5 cm
ϕ_{solid}	0.637 ⁴⁵

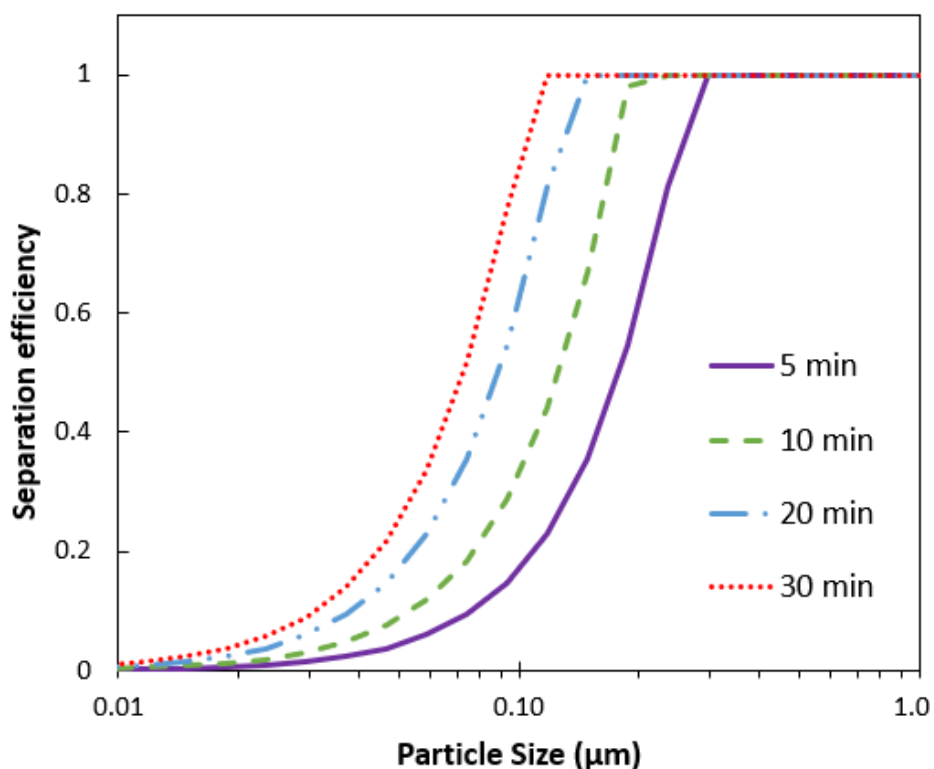


Figure 12. Calculated separation efficiency as a function of the particle size for several centrifuge run-times.

2.3. Optical microscopy techniques

The “onset” of asphaltene flocculation has been investigated by considering an aggregation kinetics proposed by Maqbool et al.⁸. Indeed, the detection threshold for the instantaneous appearance of asphaltene flocs depends on both the quantity of antisolvent present in the system and the aging time. In other words, at a given composition of antisolvent, it is possible to observe the appearance (e.g., under an optical microscope) of unstable asphaltene flocs below the instantaneous onset by waiting for a sufficient amount of time. Maqbool et al.⁸ proposed an optical detection method that takes into account both the quantity of n-heptane (or the solubility parameter of the solution) and the aging time.

2.3.1. Detection Time Experiment

Following the procedure introduced by Maqbool et al.⁸, the detection time of unstable asphaltenes in oil-heptane mixtures was measured with and without addition of chemical additives. Solutions were prepared with the same protocol described in earlier sections. When the desired volume fraction of n-heptane in the oil-heptane mixture was reached, the flask was sealed, and the mixture was kept in this condition at 60°C under constant stirring (at 470 rpm) for the time necessary to achieve the full study. Aliquots of each sample were taken at controlled aging times using a capillary and observed immediately after sampling under a microscope (*OLYMPUS BX-53*) with a magnification of x20 and mounted with a *SC50* camera. The detection time corresponds to the aging time after which asphaltene flocs ($>0.5\mu\text{m}$) are first observed and confirmed to further grow by microscopy, an example is given Figure 13. The experiment was repeated for multiple volume fractions of antisolvent with and without chemical additive. A plot of the detection time as a function of the volume fraction of heptane was obtained as a result the experiments. This plot is referred to as the detection time curve. It ranges from few minutes for large antisolvent fraction up to a hundred of hours for low antisolvent fraction. The lowest concentrations of antisolvent for which the detection-time is less than 5 minutes is considered as the instantaneous detection condition by microscopy.

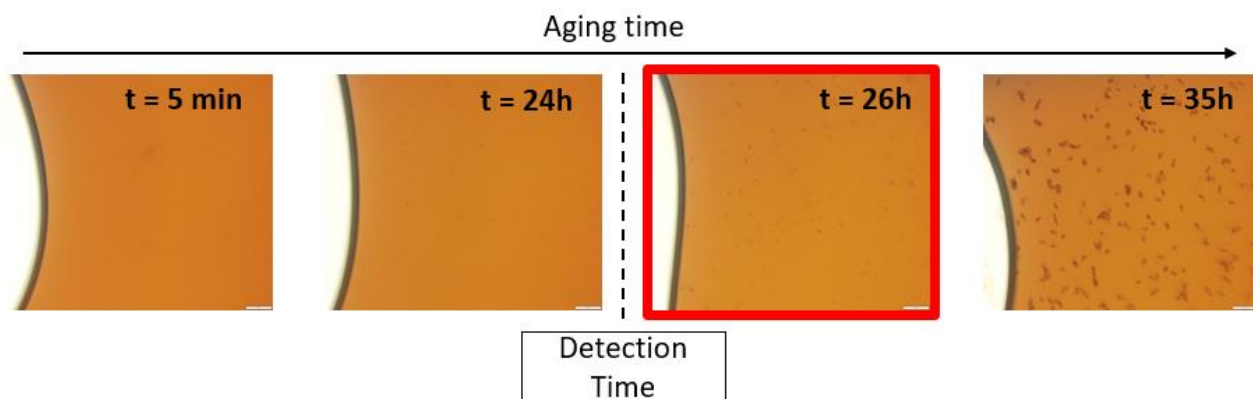


Figure 13. Detection time measurement for a mixture at a constant oil-heptane ratio.

2.3.2. SWIR Microscopy Experiment

Because of the darkness of the oil, it is difficult to observe the shape and size of aggregates using a standard microscope with a high magnification. In most crude oils, there is a minimum of absorbance around $1.6 \mu\text{m}$, which makes them nearly transparent in a spectral range near this wavelength⁴⁷. Therefore, a short-wave infrared (SWIR) camera coupled to a microscope was used at wavelengths where the absorption of light by heavy hydrocarbons is reduced. A custom optical assembly was used. It was developed around video microscope unit (VMU mitutoyo)¹⁰ paired with a x50 to x100 objectives with a long working distance and correction for infrared wavelengths. The long working distance objective lenses were used to focalize on specific objects (e.g. asphaltene flocs). A camera using an InGaAs sensor was mounted onto the VMU for measurement in the infrared bandwidth from 0.9 to $1.7 \mu\text{m}$. Samples of the mixture were taken at different n-heptane volume composition and placed in a two polished windows cell with a path length of 1mm for immediately observation under a microscope with X50 magnification. An example of the results obtained with the SWIR camera is provided in Figure 14.

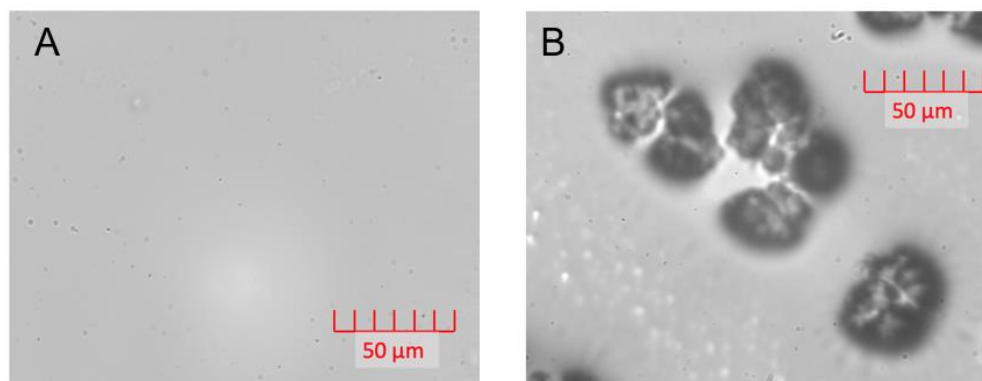


Figure 14. SWIR camera capture at X50 magnification of crude oil X at A) 40 vol % of n-heptane B) 83 vol % of n-heptane.

2.4. Turbidity experiment

As discussed at the beginning of this chapter, one of the most commonly used methods for screening chemical additives in industrial laboratories is the measurement of their dispersion capacity. The assessment of a chemical additive through turbidity measurements will be presented in *Chapter 3*, and the limitations of this technique will be discussed.

During the turbidity test performed in this work, the ability of dispersion is assessed by measuring the light transmittance, wherein a low transmittance value indicates effective dispersion of asphaltene particles. Asphaltenes were destabilized by adding 100 μL of crude oil sample with or without chemical additive to 3 mL of n-heptane in a vial. The mixture was manually homogenized and placed in a quartz cuvette. Then, the absorbance evolution of the blend was measured as a function of time. The presence of asphaltene can be detected in the visible region. The turbidity measurements were obtained using a *Cary 60 UV-Vis Spectrophotometer* from *Agilent* using a near-infrared light source of 800 nm.

3. Definition of the oil and chemicals

All the results presented in this manuscript were obtained using a dead oil, called oil X in this manuscript, provided by *TotalEnergies* from a field located in West Africa and already put in production. The oil was free from contamination of water, solid particles, production chemical additives or drilling fluids. Standard properties as well as SARA analysis of the dead oil are summarized in Table 2. To conduct this analysis, a sample of dead oil was obtained directly from the bottom tank and flashed in a cold trap. The dead oil was then topped at 323 K and 20 mbar to remove light ends (C15-). The residue was diluted in dichloromethane at a concentration of 15 mg/ml, and an Iatroscan instrument was used to measure saturates, aromatics, and polar fractions (resin + asphaltenes). Saturates were eluted using n-heptane, while aromatics were eluted using a solvent composed of 25 vol% dichloromethane and 75 vol% n-heptane. The content of asphaltenes was determined by destabilization, using n-pentane as an antisolvent with a weight/volume ratio

of 1:40. Before each experiment, the oil was previously heated at 60°C which is above the wax appearance temperature (WAT) of the crude when the oil sample is taken.

Table 2. Properties of crude oil X.

Property	Value	Technique/Apparatus
Average Mw (g/mol)	232	
Density (kg/m ³) @ 60°C	871	Viscometer Stabinger SVM 3000 – ASTM D7042
Viscosity (mPa.s) @ 60°C	12,5	Viscometer Stabinger SVM 3000 – ASTM D7042
Refractive index @ 60 °C	1.4967	Mettler Toledo RM40
Saturates (wt%)	31.9	
Aromatics (wt%)	46.6	
Resins (wt%)	21.5	
Asphaltenes (wt%)	10.7	
ASCI classification ⁴⁸	11	
Wax appearance temperature (°C)	41	Polarized Microscopy ⁴⁹

The experiments were conducted by titration in which the destabilization was induced by the continuous addition of n-heptane at 99+% purity supplied by Sigma Aldrich until the desired concentration of n-heptane was achieved.

4. Sample preparation

Since most of selected chemical additives are solid or too viscous at room temperature, they were first dissolved in toluene. The oil-chemical additive mixtures were prepared according to the following protocol:

- A stock solution of chemical additive + toluene was prepared with a concentration of 345,000 ppm in volume.
- The stock solution was homogenized in an ultrasonic bath until the chemical additive was completely dissolved in the toluene (within a few minutes).
- The stock solution was then withdrawn using a micropipette and injected into an oil volume preheated at 60°C to achieve a concentration of 3000 ppm in volume.
- The stock solution was also injected into n-heptane to reach a concentration of 3000 ppm by volume.

Each of the stock solutions, as well as the oil-stock solution mixtures or heptane-stock solution mixtures, were freshly prepared before each experiment, and the solutions were immediately used after preparation. In other words, there was no contact time before their utilization.

5. References

- (1) Escobedo, J.; Mansoori, G. A. Theory of Viscosity as a Criterion for Detection of Onset of Asphaltene Flocculation. **1994**.
- (2) Ekulu, G.; Magri, P.; Rogalski, M. Scanning Aggregation Phenomena in Crude Oils with Density Measurements. *Journal of Dispersion Science and Technology* **2004**, *25* (3), 321–331. <https://doi.org/10.1081/DIS-120037681>.
- (3) Fotland, P.; Anfindsen, H.; Fadnes, F. H. Detection of Asphaltene Precipitation and Amounts Precipitated by Measurement of Electrical Conductivity. *Fluid Phase Equilibria* **1993**, *82*, 157–164. [https://doi.org/10.1016/0378-3812\(93\)87139-R](https://doi.org/10.1016/0378-3812(93)87139-R).
- (4) Goual, L.; Sedghi, M.; Wang, X.; Zhu, Z. Asphaltene Aggregation and Impact of Alkylphenols. *Langmuir* **2014**, *30* (19), 5394–5403. <https://doi.org/10.1021/la500615k>.
- (5) Carrier, H.; Plantier, F.; Daridon, J.-L.; Lagourette, B.; Lu, Z. Acoustic Method for Measuring Asphaltene Flocculation in Crude Oils. *Journal of Petroleum Science and Engineering* **2000**, *27* (3), 111–117. [https://doi.org/10.1016/S0920-4105\(00\)00052-8](https://doi.org/10.1016/S0920-4105(00)00052-8).
- (6) Jamaluddin, A. K. M.; Creek, J.; Kabir, C. S.; McFadden, J. D.; D’Cruz, D.; Manakalathil, J.; Joshi, N.; Ross, B. Laboratory Techniques to Measure Thermodynamic Asphaltene Instability. *Journal of Canadian Petroleum Technology* **2002**, *41* (07). <https://doi.org/10.2118/02-07-04>.
- (7) Soleymanzadeh, A.; Yousefi, M.; Kord, S.; Mohammadzadeh, O. A Review on Methods of Determining Onset of Asphaltene Precipitation. *J Petrol Explor Prod Technol* **2019**, *9* (2), 1375–1396. <https://doi.org/10.1007/s13202-018-0533-5>.
- (8) Maqbool, T.; Balgoa, A. T.; Fogler, H. S. Revisiting Asphaltene Precipitation from Crude Oils: A Case of Neglected Kinetic Effects. *Energy Fuels* **2009**, *23* (7), 3681–3686. <https://doi.org/10.1021/ef9002236>.
- (9) Haji-Akbari, N.; Teeraphakul, P.; Balgoa, A. T.; Fogler, H. S. Effect of *n*-Alkane Precipitants on Aggregation Kinetics of Asphaltenes. *Energy Fuels* **2015**, *29* (4), 2190–2196. <https://doi.org/10.1021/ef502743g>.
- (10) Daridon, J.-L.; Lin, C.-W.; Carrier, H.; Pauly, J.; Fleming, F. P. Combined Investigations of Fluid Phase Equilibria and Fluid–Solid Phase Equilibria in Complex CO₂–Crude Oil Systems

- under High Pressure. *J. Chem. Eng. Data* **2020**, *65* (7), 3357–3372. <https://doi.org/10.1021/acs.jced.0c00144>.
- (11) Haji-Akbari, N.; Teeraphakul, P.; Balgoa, A. T.; Fogler, H. S. Effect of *n*-Alkane Precipitants on Aggregation Kinetics of Asphaltenes. *Energy Fuels* **2015**, *29* (4), 2190–2196. <https://doi.org/10.1021/ef502743g>.
- (12) Mahdi Hassanvand. Study of Temperature Effect on Asphaltene Precipitation by Visual and Quantitative Methods. *J. Yeast Fungal Res.* **2012**, *3* (2). <https://doi.org/10.5897/JPTAF11.035>.
- (13) Enayat, S.; Rajan Babu, N.; Kuang, J.; Rezaee, S.; Lu, H.; Tavakkoli, M.; Wang, J.; Vargas, F. M. On the Development of Experimental Methods to Determine the Rates of Asphaltene Precipitation, Aggregation, and Deposition. *Fuel* **2020**, *260*, 116250. <https://doi.org/10.1016/j.fuel.2019.116250>.
- (14) Khaleel, A.; Abutaqiya, M.; Tavakkoli, M.; Melendez-Alvarez, A. A.; Vargas, F. M. On the Prediction, Prevention and Remediation of Asphaltene Deposition. In *Day 1 Mon, November 09, 2015*; SPE: Abu Dhabi, UAE, 2015; p D011S013R003. <https://doi.org/10.2118/177941-MS>.
- (15) Melendez-Alvarez, A. A.; Garcia-Bermudes, M.; Tavakkoli, M.; Doherty, R. H.; Meng, S.; Abdallah, D. S.; Vargas, F. M. On the Evaluation of the Performance of Asphaltene Dispersants. *Fuel* **2016**, *179*, 210–220. <https://doi.org/10.1016/j.fuel.2016.03.056>.
- (16) Firoozinia, H.; Fouladi Hossein Abad, K.; Varamesh, A. A Comprehensive Experimental Evaluation of Asphaltene Dispersants for Injection under Reservoir Conditions. *Pet. Sci.* **2016**, *13* (2), 280–291. <https://doi.org/10.1007/s12182-016-0078-5>.
- (17) Kokal, S. L.; Najman, J.; Sayegh, S. G.; George, A. E. Measurement And Correlation Of Asphaltene Precipitation From Heavy Oils By Gas Injection. *Journal of Canadian Petroleum Technology* **1992**, *31* (04). <https://doi.org/10.2118/92-04-01>.
- (18) Leontaritis, K. J.; Amaefule, J. O.; Charles, R. E. A Systematic Approach for the Prevention and Treatment of Formation Damage Caused by Asphaltene Deposition. *SPE Production & Facilities* **1994**, *9* (03), 157–164. <https://doi.org/10.2118/23810-PA>.
- (19) Broseta, D.; Robin, M.; Savvidis, T.; Féjean, C.; Durandeau, M.; Zhou, H. Detection of Asphaltene Deposition by Capillary Flow Measurements; OnePetro, 2000. <https://doi.org/10.2118/59294-MS>.

- (20) Hoepfner, M. P.; Limsakoune, V.; Chuenmeechao, V.; Maqbool, T.; Fogler, H. S. A Fundamental Study of Asphaltene Deposition. *Energy Fuels* **2013**, *27* (2), 725–735. <https://doi.org/10.1021/ef3017392>.
- (21) Lawal, K. A.; Crawshaw, J. P.; Boek, E. S.; Vesovic, V. Experimental Investigation of Asphaltene Deposition in Capillary Flow. *Energy Fuels* **2012**, *26* (4), 2145–2153. <https://doi.org/10.1021/ef201874m>.
- (22) Kuang, J.; Tavakkoli, M.; Yarbrough, J.; Wang, J.; Jain, S.; Ashtekar, S.; Abdallah, D. S.; Punnapala, S.; Vargas, F. M. Investigation of Asphaltene Deposition at High Temperature and under Dynamic Conditions. *Energy & Fuels* **2018**. <https://doi.org/10.1021/acs.energyfuels.8b03318>.
- (23) Huffman, M.; Fogler, H. S. Asphaltene Destabilization in the Presence of Dodecylbenzene Sulfonic Acid and Dodecylphenol. *Fuel* **2021**, *304*, 121320. <https://doi.org/10.1016/j.fuel.2021.121320>.
- (24) Kuang, J.; Melendez-Alvarez, A. A.; Yarbrough, J.; Garcia-Bermudes, M.; Tavakkoli, M.; Abdallah, D. S.; Punnapala, S.; Vargas, F. M. Assessment of the Performance of Asphaltene Inhibitors Using a Multi-Section Packed Bed Column. *Fuel* **2019**, *241*, 247–254. <https://doi.org/10.1016/j.fuel.2018.11.059>.
- (25) Vilas Bôas Fávero, C.; Hanpan, A.; Phichphimok, P.; Binabdullah, K.; Fogler, H. S. Mechanistic Investigation of Asphaltene Deposition. *Energy Fuels* **2016**, *30* (11), 8915–8921. <https://doi.org/10.1021/acs.energyfuels.6b01289>.
- (26) Saidoun, M. Investigations into Asphaltenes Destabilization, Aggregation and Deposition. Thesis, 2020.
- (27) Ekholm, P.; Blomberg, E.; Claesson, P.; Auflem, I. H.; Sjöblom, J.; Kornfeldt, A. A Quartz Crystal Microbalance Study of the Adsorption of Asphaltenes and Resins onto a Hydrophilic Surface. *Journal of Colloid and Interface Science* **2002**, *247* (2), 342–350. <https://doi.org/10.1006/jcis.2002.8122>.
- (28) Abudu, A.; Goual, L. Adsorption of Crude Oil on Surfaces Using Quartz Crystal Microbalance with Dissipation (QCM-D) under Flow Conditions. *Energy Fuels* **2009**, *23* (3), 1237–1248. <https://doi.org/10.1021/ef800616x>.
- (29) De Souza Freire Orlandi, E. Following Asphaltenes Destabilization and Deposition by Quartz Crystal Resonator, Université de Pau et des Pays de l'Adour. Thesis, 2017.

- (30) Liu, F.; Hickman, S.; Maqbool, T.; Pauchard, V.; Banerjee, S. Study of Asphaltene Deposition onto Stainless-Steel Surfaces Using Quartz Crystal Microbalance with Dissipation. *Energy Fuels* **2020**, *34* (8), 9283–9295. <https://doi.org/10.1021/acs.energyfuels.0c00663>.
- (31) Daridon, J. L.; Cassiède, M.; Nasri, D.; Pauly, J.; Carrier, H. Probing Asphaltene Flocculation by a Quartz Crystal Resonator. *Energy Fuels* **2013**, *27* (8), 4639–4647. <https://doi.org/10.1021/ef400910v>.
- (32) Joonaki, E.; Burgass, R.; Hassanpouryouzband, A.; Tohidi, B. Comparison of Experimental Techniques for Evaluation of Chemistries against Asphaltene Aggregation and Deposition: New Application of High-Pressure and High-Temperature Quartz Crystal Microbalance. *Energy Fuels* **2018**, *32* (3), 2712–2721. <https://doi.org/10.1021/acs.energyfuels.7b02773>.
- (33) Cassiède, M.; Mejia, A.; Radji, S.; Carrier, H.; Daridon, J.-L.; Saidoun, M.; Tort, F. Evaluation of the Influence of a Chemical Inhibitor on Asphaltene Destabilization and Deposition Mechanisms under Atmospheric and Oil Production Conditions Using QCM and AFM Techniques. *Energy Fuels* **2021**, *35* (21), 17551–17565. <https://doi.org/10.1021/acs.energyfuels.1c02570>.
- (34) Shadman, M. M.; Vafaie-Sefti, M.; Ahmadi, S.; Assaf M. A.; Veisi, S. Effect of dispersants on the kinetics of asphaltene settling using turbidity measurement method, *Petroleum Science and Technology* **2016**, *34*(14), 1233–1239. <https://doi.org/10.1080/10916466.2016.1193519>
- (35) El Ghazouani, J.; Saidoun, M.; Tort, F.; Daridon, J.-L. Experimental Evaluation Method of Asphaltene Deposition Inhibitor's Efficacy at Atmospheric Pressure Using a Fully Immersed Quartz Crystal Resonator, Centrifugation, and Optical Microscopy Techniques. *Energy Fuels* **2023**, *37* (8), 5895–5904. <https://doi.org/10.1021/acs.energyfuels.3c00305>.
- (36) Joonaki, E.; Burgass, R.; Hassanpouryouzband, A.; Tohidi, B. Comparison of Experimental Techniques for Evaluation of Chemistries against Asphaltene Aggregation and Deposition: New Application of High-Pressure and High-Temperature Quartz Crystal Microbalance. *Energy Fuels* **2018**, *32* (3), 2712–2721. <https://doi.org/10.1021/acs.energyfuels.7b02773>.
- (37) Montesi, A.; Pinnick, R. A.; Subramanian, S.; Wang, J.; Creek, J. L. Asphaltene Management in GOM DW Subsea Development. In *Offshore Technology Conference*; OTC, 2011; p OTC-21587.
- (38) Johannsmann, D. *The Quartz Crystal Microbalance in Soft Matter Research: Fundamentals and Modeling*; Soft and Biological Matter; Springer International Publishing: Cham, 2015. <https://doi.org/10.1007/978-3-319-07836-6>.

- (39) Cerda, R. M. *Understanding Quartz Crystals and Oscillators*; Artech House microwave library; Artech House: Boston, 2014.
- (40) G, S. Use of the Vibrating Quartz for Thin Film Weighing and Microweighing. *Z. Phys.* **1959**, *155*, 206.
- (41) Keiji Kanazawa, K.; Gordon, J. G. The Oscillation Frequency of a Quartz Resonator in Contact with Liquid. *Analytica Chimica Acta* **1985**, *175*, 99–105. [https://doi.org/10.1016/S0003-2670\(00\)82721-X](https://doi.org/10.1016/S0003-2670(00)82721-X).
- (42) Cassiède, M.; Paillol, J. H.; Pauly, J.; Daridon, J.-L. Electrical Behaviour of AT-Cut Quartz Crystal Resonators as a Function of Overtone Number. *Sensors and Actuators A: Physical* **2010**, *159* (2), 174–183. <https://doi.org/10.1016/j.sna.2010.03.028>.
- (43) Saidoun, M.; Palermo, T.; Passade-Boupat, N.; Gingras, J.-P.; Carrier, H.; Daridon, J.-L. Revisiting Asphaltene Instability Predictions by Probing Destabilization Using a Fully Immersed Quartz Crystal Resonator. *Fuel* **2019**, *251*, 523–533. <https://doi.org/10.1016/j.fuel.2019.04.025>.
- (44) Acevedo, N.; Moulian, R.; Chacón-Patiño, M. L.; Mejia, A.; Radji, S.; Daridon, J.-L.; Barrère-Mangote, C.; Giusti, P.; Rodgers, R. P.; Piscitelli, V.; Castillo, J.; Carrier, H.; Bouyssiere, B. Understanding Asphaltene Fraction Behavior through Combined Quartz Crystal Resonator Sensor, FT-ICR MS, GPC ICP HR-MS, and AFM Characterization. Part I: Extrography Fractionations. *Energy Fuels* **2020**, *34* (11), 13903–13915. <https://doi.org/10.1021/acs.energyfuels.0c02687>.
- (45) Maqbool, T.; Raha, S.; Hoepfner, M. P.; Fogler, H. S. Modeling the Aggregation of Asphaltene Nanoaggregates in Crude Oil–Precipitant Systems. *Energy Fuels* **2011**, *25* (4), 1585–1596. <https://doi.org/10.1021/ef1014132>.
- (46) Grunberg, L.; Nissan, A. H. Mixture Law for Viscosity. *Nature* **1949**, *164* (4175), 799–800. <https://doi.org/10.1038/164799b0>.
- (47) Daridon, J.-L.; Lin, C.-W.; Carrier, H.; Pauly, J.; Fleming, F. P. Combined Investigations of Fluid Phase Equilibria and Fluid–Solid Phase Equilibria in Complex CO₂–Crude Oil Systems under High Pressure. *J. Chem. Eng. Data* **2020**, *65* (7), 3357–3372. <https://doi.org/10.1021/acs.jced.0c00144>.

- (48) Passade-Boupat, N.; Zhou, H.; Rondon-Gonzalez, M. Asphaltene Precipitation from Crude Oils: How to Predict It and to Anticipate Treatment?; 2013; p SPE-164184-MS. <https://doi.org/10.2118/164184-MS>.
- (49) Daridon, J.-L.; Pauly, J.; Milhet, M. High Pressure Solid-Liquid Phase Equilibria in Synthetic Waxes. *Physical Chemistry Chemical Physics* **2002**, *4* (18), 4458. <https://doi.org/10.1039/b205017j>.

Chapter 3. Experimental evaluation method of chemical additive efficacy at atmospheric pressure using a fully immersed Quartz Crystal Resonator, centrifugation and optical microscopy techniques

1. Introduction

The literature review on screening laboratory methods for evaluating chemical additives has highlighted that assessing a chemical additive solely based on its dispersant capabilities does not provide conclusive evidence regarding its inhibitory effect on deposition. Furthermore, the destabilization, aggregation, flocculation, or deposition processes of asphaltenes occur at nanoscale to macroscale levels. Therefore, it is essential for chemical additive screening methods to have sensitivity thresholds adapted to these scales. The objective of this chapter is to evaluate a multi-scale method based on the coupling of four experimental techniques (QCR, centrifugation, Microscopy detection time, SWIR microscopy) to investigate the effect of chemical additives on the destabilization and deposition of asphaltenes under conditions of non-diluted crude oil samples at atmospheric pressure. All these techniques were presented in detail in the previous chapter.

The role of an asphaltene deposition inhibitor's is to reduce deposit thickness or to delay its build-up period. However, the addition of a chemical additive does not systematically lead to a positive effect for preventing asphaltene deposition. Moreover, Barcenas et al.¹ demonstrated that increasing the amount of chemical additives injected does not always results in a higher interaction with asphaltenes. To evaluate the efficacy of a chemical additive, laboratory tests were conducted to identify the working concentration that shows a positive effect on asphaltene destabilization and on the diffusion deposition process trying to replicate driving forces of asphaltene destabilization in industrial operating conditions. The results of these tests are given below.

2. Chemicals

The commercial “asphaltene deposition inhibitor” used in this study was from *TotalEnergies Additives & Fuels Solutions*, named here as chemical additive A, and its properties are summarized in Table 1. It consists of an alkylphenol resin modified by an alkyl polyamine, the chemical structure is presented in Figure 1. This polymer was diluted in Solvarex 150 type of aromatic solvent at a concentration of 42.5% by mass of the active ingredient. In this manuscript, the level of ppm is defined as the ratio of volume concentrations of the mother solution (diluted active matter) in the studied mixtures. The characteristics of oil X and antisolvent were given in the previous chapter. The concentration of chemical additive in the mixture was kept constant throughout the respective experiments (chemical additive initially present in crude oil and in titrant) to avoid dilution effect as the titration progresses.

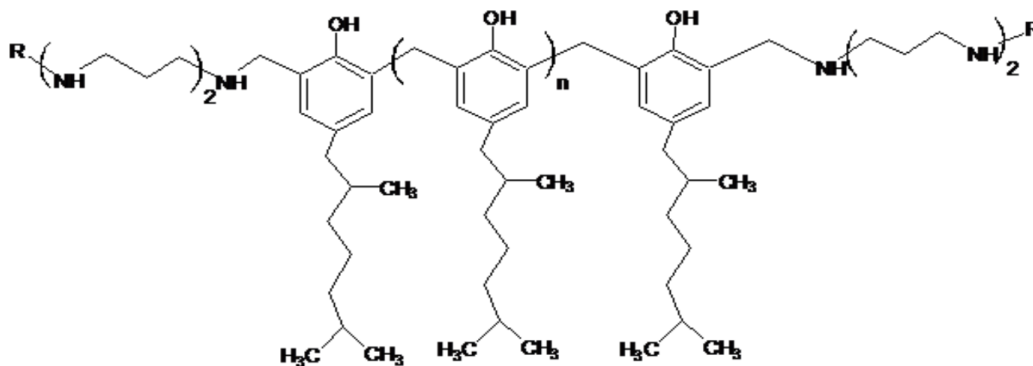


Figure 1. Chemical structure of additive A.

Table 1. Properties of chemical additive A

Property	Value	Technique/Apparatus
Density (kg/m ³) @ 15 °C	930	Viscometer Stabinger SVM 3000 – ASTM D7042
Refractive Index @ 60 °C	1.504	Mettler Toledo RM40

3. Results and discussion

3.1. Turbidity experiment

The turbidity test is one of the most common approaches used in laboratory for evaluating the effectiveness of chemical additives based on the dispersion efficiency of asphaltenes in presence of chemicals. This method evaluates the ability of a chemical additive to keep destabilized asphaltenes in suspension. The higher the absorbance, the more dispersed the asphaltenes. The results of absorbance measurements with concentrations ranging from 10 ppm to 3000 ppm (in volume) of chemical additives in oil/n-heptane mixtures are shown in Figure 2. From 100 ppm the absorbance is maintained at a higher value than for the nontreated reference oil. The unstable asphaltene aggregates are therefore maintained in suspension in the presence of the chemical additive A over this period of 1 h. The effect of the concentration above 300 ppm appears negligible. With this type of technique where the antisolvent/oil ratios have to be higher than 90% in volume and the medium remains static during the measurement, the question of representativeness with field conditions can be asked. Hence the need to resort to experiments with more realistic antisolvent/oil ratio conditions and focus on scales of measures that enable to more clearly discriminate the effectiveness of chemical additives.

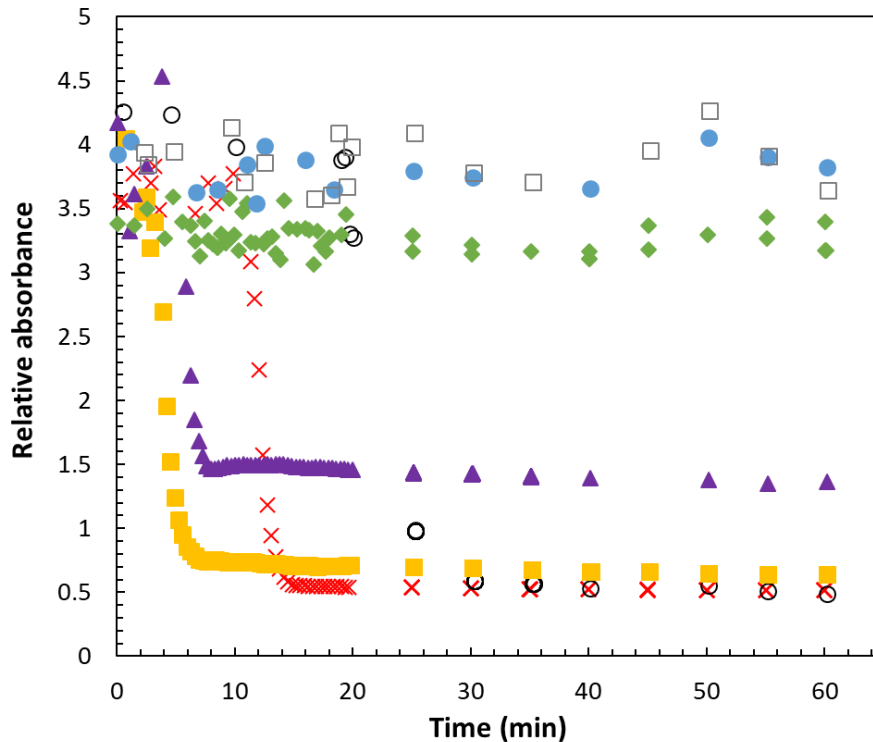


Figure 2. Relative absorbance of Oil X in presence of chemical additive A at different concentrations: (red \times) 0 ppm, (black \circ) 10 ppm, (yellow \blacksquare) 30 ppm, (purple \blacktriangle) 100 ppm, (green \blacklozenge) 300 ppm, (blue \bullet) 1000 ppm, (grey \square) 3000 ppm.

3.2. QCR experiment – Chemical additive effect on crude oil: Raw data (Δf and $\Delta \Gamma_n$) analysis

Titration experimentations of n-heptane in dead crude oil with an immersed QCR sensor were carried out with various chemical additive dosages and compared with crude oil free of chemical additives. During these experiments, both the shift in resonance frequency and changes in bandwidth along various overtones (1 to 7) of the resonating sensor were recorded and analyzed for comparison.

The major point of asphaltene destabilization, elsewhere referred to as “onset”, is defined as the intersect of the opposed slopes before and after the observed inflexion point of the resonance frequency (Figure 3). At this point, resonant behavior deviates from the simple dilution Kanazawa law. In practice, frequency signal of quartz crystal resonator appeared predominantly affected by

mass deposition of asphaltenes, if any, explaining the major change of slope of the frequency². Consequently, the shift in frequency plot was prefead to estimate the onset.

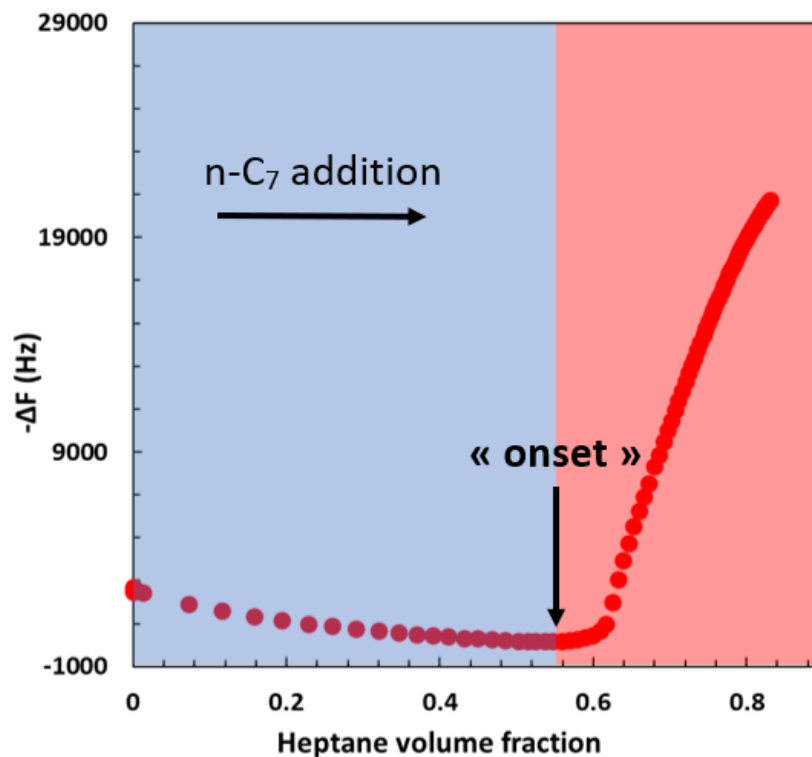


Figure 3. Determination of "onset" from resonance frequency measurements.

The change in resonance frequency of the third overtone peak measured by the quartz crystal immersed in pure crude oil and in the presence of chemical additive A with different contents ranging from 300 to 20,000 ppm (in volume) are shown in Figure 4. It can be noted in this figure that for an addition of 300 ppm of chemical additive A, the destabilization is shifted to a lower n-heptane composition in comparison to the shift in frequency of the free additive crude oil. No change was detected on the destabilization curve beyond the onset. At 1000 ppm, no significant effect was observed on the threshold, whereas a decrease in the amplitude of the shift in frequency was noted after the onset. From 3000 ppm the destabilization is slightly shifted toward higher compositions and this effect is more marked as the chemical additive concentration is important. For 3000 ppm we observe a shift in destabilization of +2.2 % in volume fraction compared to the reference measurement (pure crude oil) and +8.5 and +11.4 % for 10,000 ppm and 20,000 ppm,

respectively. These results show that more than 1000 ppm of chemical additive A is required to shift the destabilization of asphaltenes to a higher antisolvent composition. In addition, the onset shift is greater as the concentration of additive is increased but appears to reach a plateau value near 20,000 ppm.

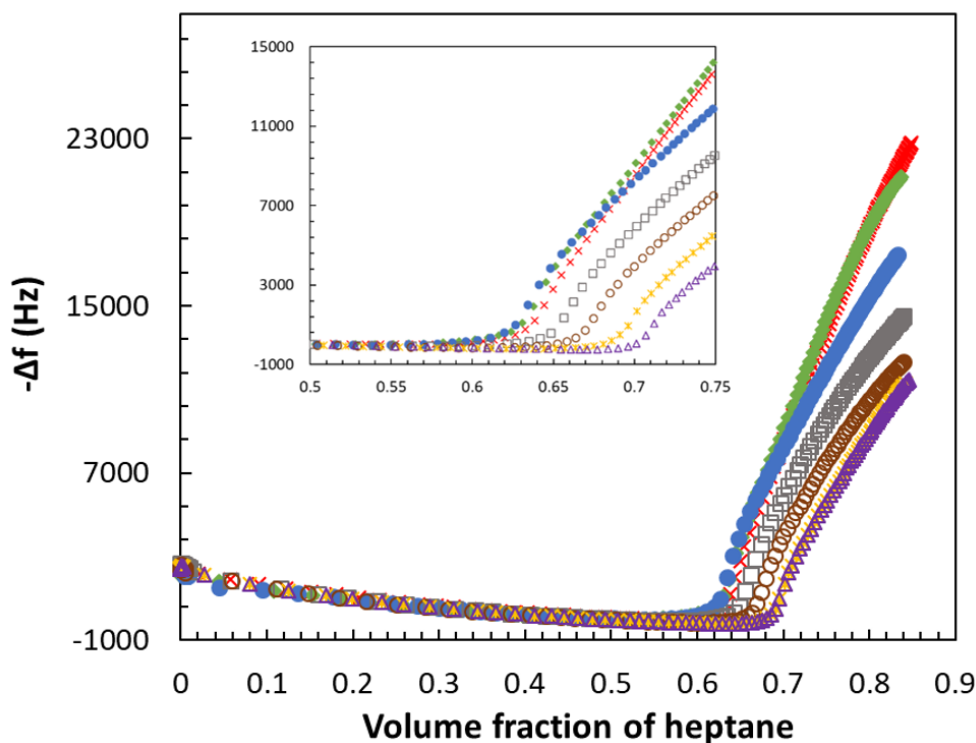


Figure 4. Shift of resonance frequency (3rd harmonic) recorded during experimental titration of crude oil X + chemical additive A at different concentrations as a function of the volume fraction of n-heptane: (red \times) 0 ppm, (green \blacklozenge) 300 ppm, (blue \bullet) 1000 ppm, (grey \square) 3000 ppm, (brown \circ) 5000 ppm, (yellow \ast) 10,000 ppm, (purple \triangle) 20,000 ppm. A zoom of the frequency shift between 0.5 and 0.75 volume fraction of n-heptane is shown in the inner box.

As for the change in resonance frequency, the shift in the bandwidth was only plotted for the third overtone peak in Figure 5. This figure shows for each concentrations an increase in dissipation with a maximum and then a decrease. Daridon et al.² demonstrated, using the simple Einstein viscosity equation, that for an oil with a viscosity similar to that of Oil X (10 mPa.s), small changes in $\Delta\Gamma$ can be associated with a change in volume fraction. The sensor is capable of detecting a minimum value equivalent to 1.1×10^{-3} for the 3rd harmonic, for a $\Delta\Gamma$ of 5 Hz. For all samples, titration curves first decrease because of the reduction in viscosity caused by the

addition of n-heptane (dominating dilution effect). Then, the increase in dissipation is related to the destabilization of the asphaltenes and the growth of asphaltene aggregates suspended around the sensor. The quartz disk therefore detects larger and/or more objects close to its surface. This increase in dissipation is shifted towards higher n-heptane compositions as the chemical additive concentration is increased. Furthermore, the amplitude of the dissipation peak increases as the chemical additive concentration in the solution is increased.

From these measurements and from Equations 1 and 2 it is possible to extract the mass deposited on the quartz surface as well as the change in density-viscosity product of the fluid in contact with the sensor.

$$\Delta f_n = -n2C_m\Delta m - \sqrt{n} \frac{C_m}{\sqrt{\pi f_0}} \sqrt{\rho_{liquid}\eta_{liquid}} \quad (1)$$

$$\Delta\Gamma_n = \sqrt{n} \frac{C_m}{\sqrt{\pi f_0}} \sqrt{\rho_{liquid}\eta_{liquid}} (1 + R) \quad (2)$$

The apparent viscosity is calculated according to the following equation:

$$(\rho\eta)_\Gamma = \frac{\pi f_0}{C_m^2} \left(\frac{\Delta\Gamma_n}{1 + R} \right)^2 \quad (3)$$

Where $\Delta\Gamma_n$ here is $\Delta\Gamma_3$ as a function of the square root of 3 (eq 2). Only the 3rd harmonic was used for several reasons. Firstly, it appears that the first harmonic is particularly affected by intrinsic properties of quartz crystals such as piezoelectric stiffening and edge effects³, which means that it behaves differently from other harmonics and cannot be used. For the largest harmonics, it has been shown that inharmonic resonances interfere with the main resonance peaks⁴. Finally, the 3rd harmonic has the greatest penetration length of the acoustic wave in the contacting media (Equation 4). The ratio $\frac{\Delta f_\eta}{\Delta f_m}$ is proportional to $\frac{1}{\sqrt{n}}$, which makes it possible to estimate the bulk viscosity-density product from 3rd harmonic peak with less impact from the properties of the deposited layer than with higher harmonics.

$$\delta_p = \sqrt{\frac{\mu_{liquid}}{n\pi f_0 \rho_{liquid}}} \quad (4)$$

The density is calculated using the molar mass/molar volume ratio of the mixture during continuous addition of n-heptane. Theoretical viscosity change with addition of n-heptane was calculated using the Grunberg-Nissan type of equation⁵ (Equation 5) assuming a binary mixture composed of crude oil + n-heptane.

$$\eta = \exp(x \ln(\eta_{C_7}) + (1 - x) \ln(\eta_{oil}) + x(1 - x)G) \quad (5)$$

In this expression, the Grunberg-Nissan parameter G was adjusted to match the apparent viscosity measured by QCR before asphaltene's destabilization.

The results in Figure 6 indicate that the aggregation of asphaltene after n-heptane addition promotes a slight increase of the viscosity. A shift in the increase in dissipation is observed in the presence of the chemical additive and it is proportional to its concentration.

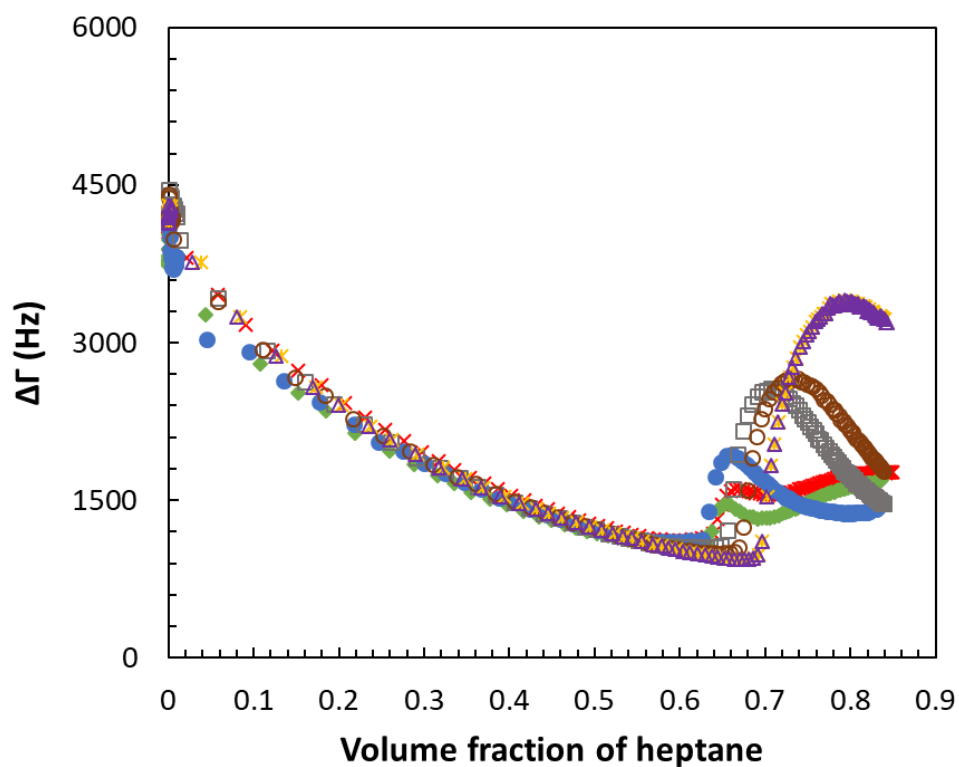


Figure 5. Shift of dissipation (3rd harmonic) recorded during experimental titration of crude oil X + chemical additive A at different concentrations as a function of the volume fraction of n-heptane: (red \times) 0 ppm, (green \blacklozenge) 300 ppm, (blue \bullet) 1000 ppm, (grey \square) 3000 ppm, (brown \circ) 5000 ppm, (yellow \ast) 10,000 ppm, (purple \triangle) 20,000 ppm.

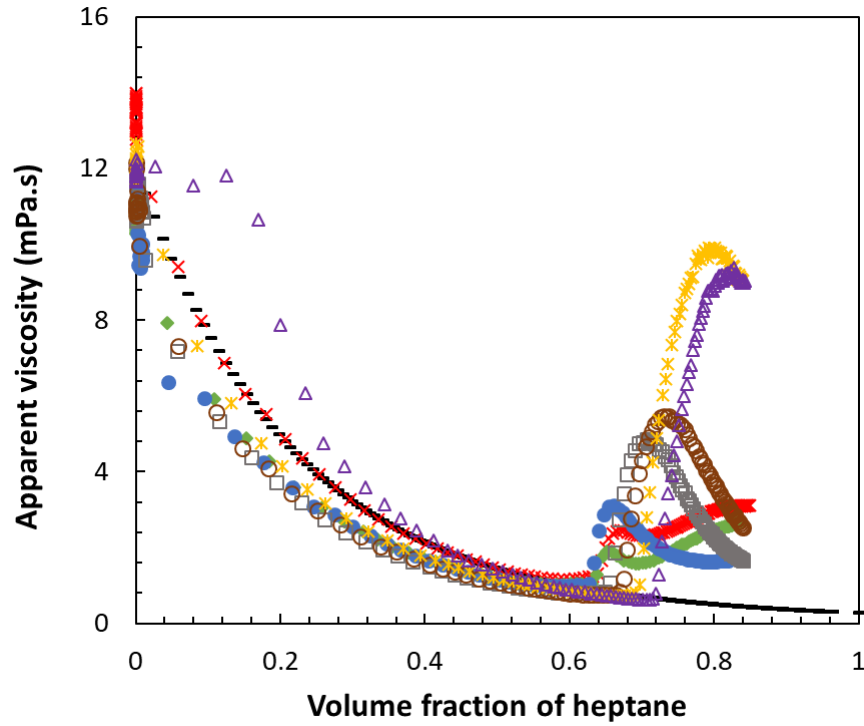


Figure 6. Apparent viscosity of the surrounding fluid calculated during experimental titration of crude oil X + chemical additive A at different concentrations as a function of the volume fraction of heptane: (black -) theoretical viscosity, (red \times) 0 ppm, (green \blacklozenge) 300 ppm, (blue \bullet) 1000 ppm, (grey \square) 3000 ppm, (brown \circ) 5000 ppm, (yellow \ast) 10,000 ppm, (purple \triangle) 20,000 ppm.

The deposited mass can be evaluated by expressing $\Delta f_n/n$ as a function of $\frac{1}{\sqrt{n}}$ and determining the y-intercept ⁶. The values obtained by this method during the titration are displayed in Figure 7. Starting from a concentration of 1000 ppm of chemical additive A, a clear decrease of the deposit compared to nontreated oil is shown.

For the purpose of evaluating and comparing the positive chemical additive effect on the deposition reduction, the deposition inhibition efficiency in the presence of chemical additive A at a volume concentration of 80 vol % was calculated according to the following equation:

$$\text{deposition inhibition \%} = \left(1 - \frac{\text{deposited mass @ 80 vol\% with chemical add.}}{\text{deposited mass @ 80 vol\% Pure Crude Oil}}\right) * 100 \quad (6)$$

The results are reported in Table 2. As it can be inferred from Table 2, very few effects were observed at a low concentration of chemical additive A (300 ppm). At excessive concentrations of chemical additive ($>10,000$ ppm) the effects seem to tend toward an inhibition efficiency of 90% at a volume composition of 80% in antisolvent. The subsequent working concentration was set at 3000 ppm for further evaluation of the chemical additive because at this concentration the deposition inhibition efficiency is sufficiently clear, and the concentration is not excessive in relation to the real use conditions in the industry.

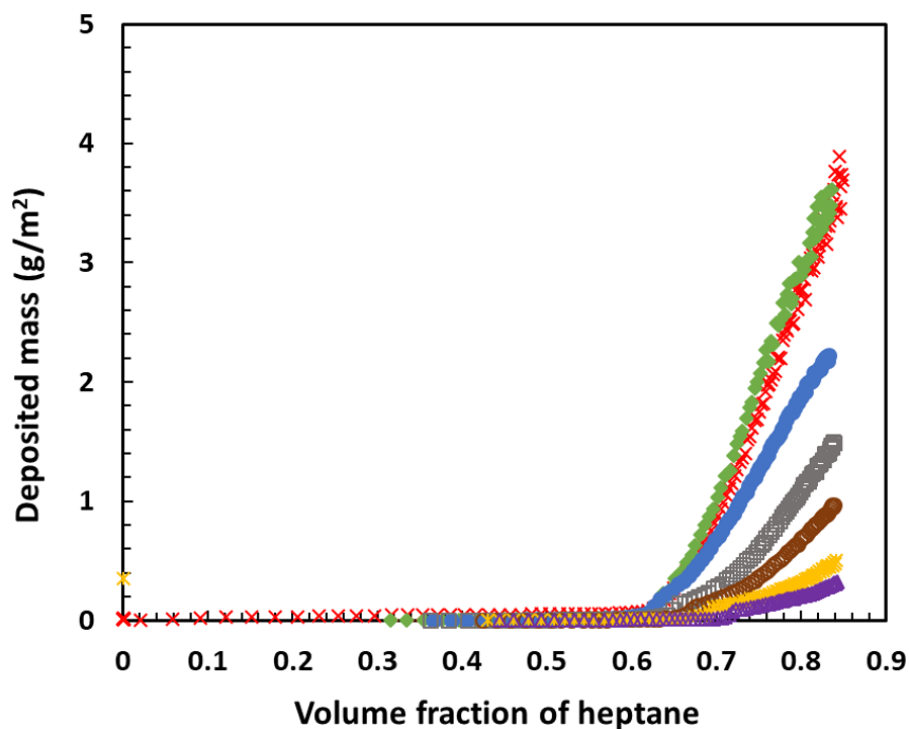


Figure 7. Deposited mass calculated during experimental titration of crude oil X + chemical additive A at different concentrations as a function of the volume fraction of n-heptane: (red \times) 0 ppm, (green \blacklozenge) 300 ppm, (blue \bullet) 1000 ppm, (grey \square) 3000 ppm, (brown \circ) 5000 ppm, (yellow \ast) 10,000 ppm, (purple \triangle) 20,000 ppm.

Table 2. Deposition inhibition efficiency of the oil treated by chemical additive A at 80 vol % n-heptane composition.

Chemical additive A concentration (ppm)	Deposition inhibition efficiency (%)
300	-5.91
1000	32.84
3000	60.96
5000	75.27
10,000	88.51
20,000	92.28

3.3. Centrifugation experiment

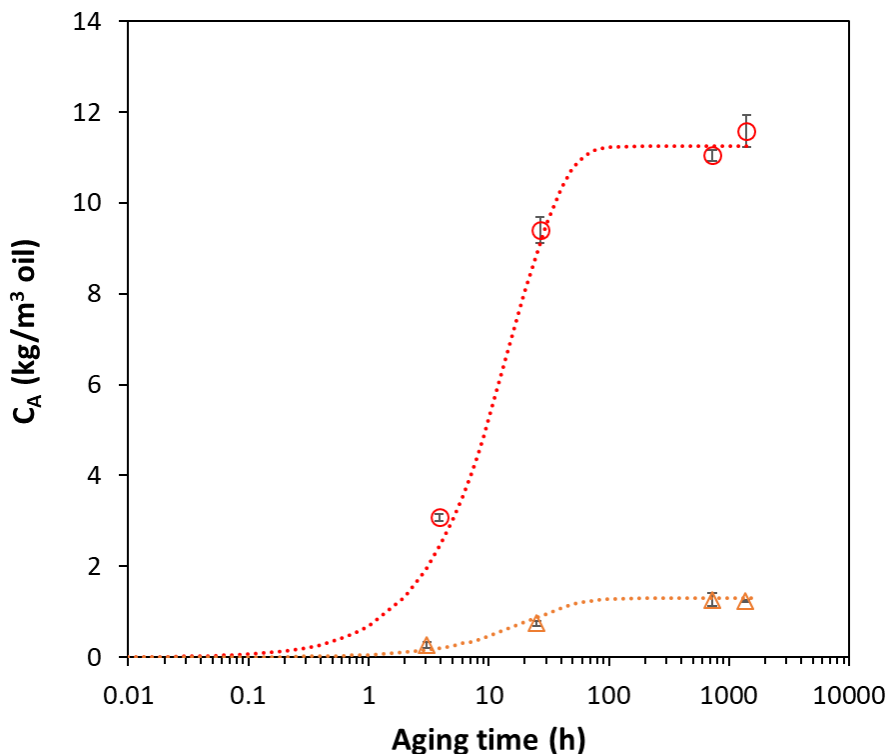


Figure 8. Concentration of unstable asphaltenes larger than 200 nm separated by centrifugation as a function of the aging time of prepared blends of crude Oil X and n-heptane: (red \circ) nontreated Oil X + 61.1 vol % of n-C7, (orange \triangle) Oil X + chemical additive A (3000 ppmv) + 61.1 vol % of n-C7. The dotted lines are made to facilitate the reading of the trends.

The concentration of unstable asphaltene aggregates larger than 200 nm centrifuged per unit of volume of crude oil at a specific aging time $C_A(t)$ is represented as function of the aging time of the crude oil-heptane mixture in Figure 8. The results show that the amount of separable asphaltenes destabilized from oil-heptane mixture is reduced by the presence of chemical additive A. Equilibrium plateau values are reached at aging times higher than 400 h; about 1.3 kg/m³ oil in the presence of additive chemical A compared to 11.2 kg/m³ oil for the nontreated oil.

3.4. SWIR microscopy

The titration tests carried out with the quartz crystal sensor indicated a delayed destabilization of asphaltenes, reduced mass deposition on quartz surfaces, and an increased dissipation of the signal in the presence of the chemical additive. This increase in dissipation (proportional to an apparent viscosity) can reflect a change in the morphology of the flocs formed far from the “onset” of destabilization. To observe this change in floc structures in the micrometer range SWIR microscopy observations were performed at the end of the titration. To make these observations comparable, a sample of titrated oil was taken instantaneously after the titration experiment and directly transferred to the glass cell of the microscope. All of the samples investigated corresponded to a n-heptane volume fraction of 0.83. The results are shown in Figure 9. Without chemical additive, the aggregates have a size between 25 and 45 μm in diameter and have a globular-like shape in this condition of sampling (Figure 9. A). A clear decrease in aggregate size is observed above 3000 ppm (Figure 9. C, D, E and F) in the same conditions of sampling. From 10,000 ppm the size of aggregates does not seem to decrease anymore. Moreover, as the concentration of chemical additive A is increased, the aggregates become less and less spherical and some aggregates with needle shapes are observed.

The reduction of the size of the aggregates observed in presence of the chemical additive at this micrometer scale is very likely related to the stabilization of aggregates by the amphiphilic properties of the chemical additive. Indeed, it was reported in the literature that amphiphiles with their polar head will react with the active sites of asphaltenes^{7,8,9}. Once attached to the asphaltenes, the hydrophobic tail of the amphiphiles will generate a steric repulsion and thus limit the size of the asphaltene aggregates^{8,10}. In *Chapter 4*, the effect of the chemistry of various amphiphilic structures on the liquid phase as well as on the deposition will be discussed.

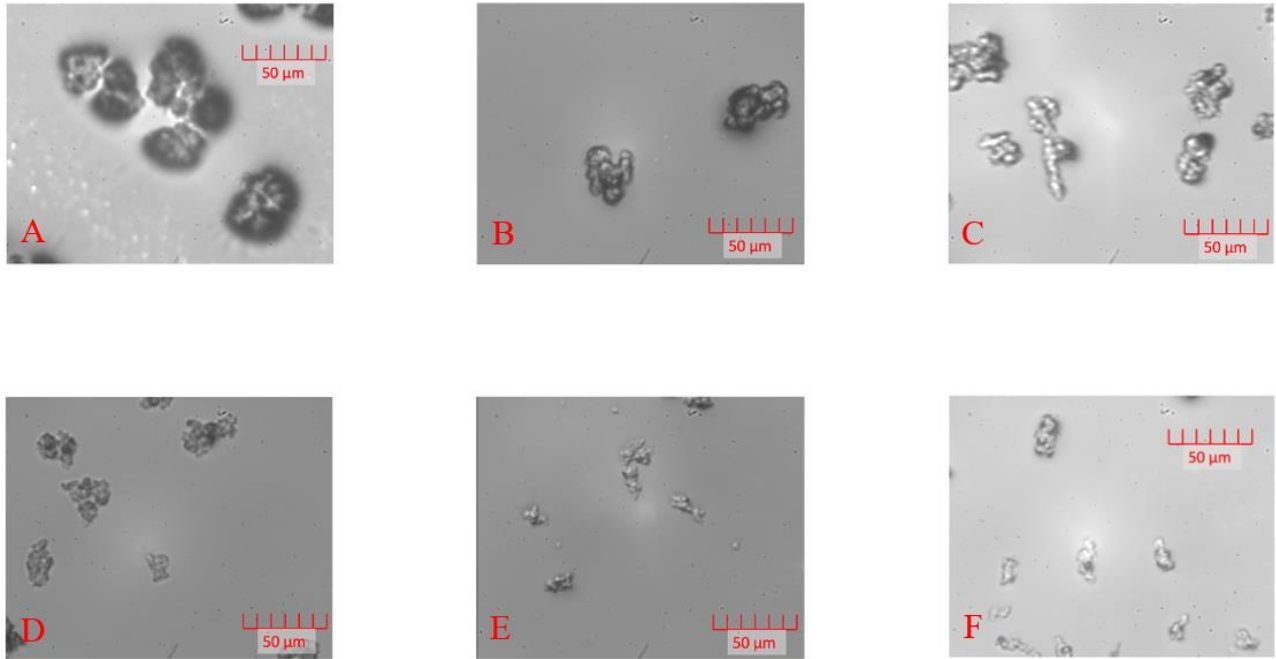


Figure 9. SWIR camera capture at X50 magnification of crude oil X + chemical additive A samples at 83 vol % n-heptane: (A) 0 ppm, (B) 1000 ppm, (C) 3000 ppm, (D) 5000 ppm, (E) 10,000 ppm, (F) 20,000 ppm.

3.5. Detection Time experiment

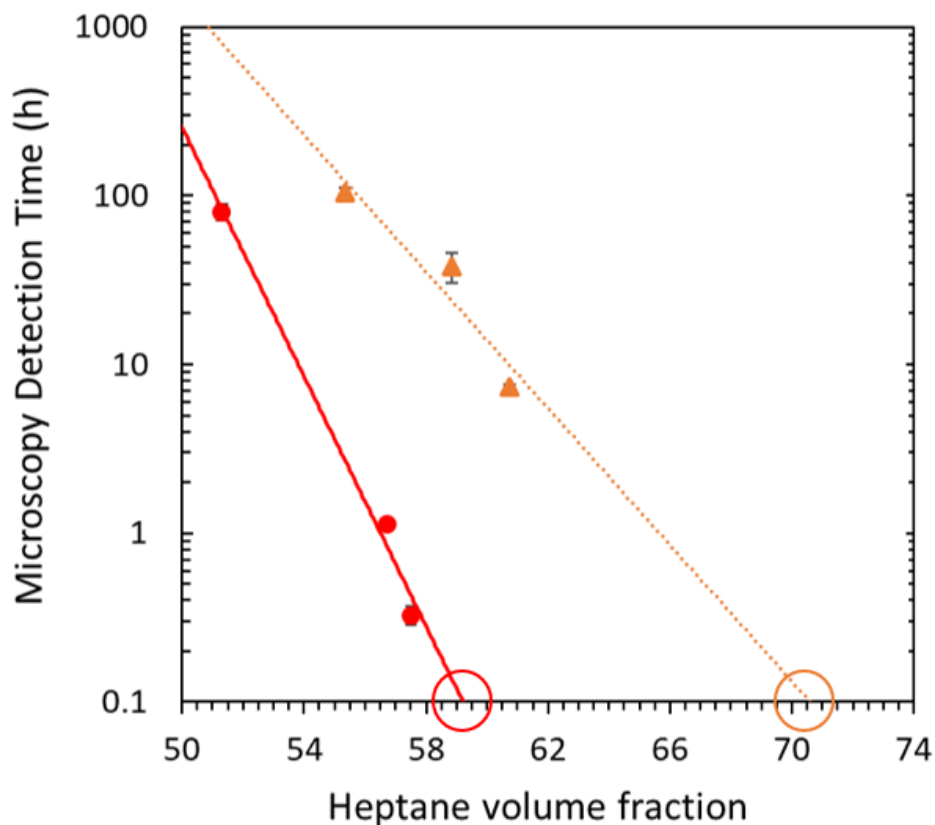


Figure 10. Necessary aging time to detect particles by visual microscopy observations as function of the volume fraction of n-heptane in heptane-oil blends: (red ●) nontreated oil X, (orange ▲) oil X + chemical additive A at 3000 ppmv.

The detection time curves are shown in Figure 10 for oil X as pure reference crude oil and the same oil treated by chemical additive A at 3000 ppm in volume. The instantaneous microscopy detection of asphaltene aggregates in oil X + n-heptane was observed at ~59.2 vol% of n-heptane and ~70.5 vol % for the oil treated with chemical additive A. This result is consistent with the observed minimum shift in frequency ($-\Delta f$) of the resonating immersed sensor; i.e., at 55.2 vol % of n-heptane in oil X and 58.7 vol % of n-heptane treated oil X with 3000 ppm of chemical additive A (refer to Figure 4). The difference in detection threshold between observation under the microscope and the QCR in the presence of chemical additive A is explained by the fact that destabilized asphaltenes take more time to grow large enough to be visible under the microscope compared to nontreated asphaltenes.

This way, the larger sensitivity of the quartz resonator compared to microscopy is also verified, as expected. Indeed, the microscope observations describe the appearance of aggregates larger than 500 nm, while the quartz allows the detection of nanometer level. Nevertheless, both techniques show a delay of the same order of magnitude in the observation destabilization of asphaltenes in the presence of the chemical additive at nanoscale and microscale.

The presence of chemical additive A in crude oil delays the observation of asphaltene aggregates by 1 to 2 orders of magnitudes at n-heptane fractions lesser than 60 vol % in oil X. The results suggest that chemical additive A stabilizes the asphaltene aggregates by keeping them in suspension.

3. Conclusions

Raw and processed data obtained from the QCR sensor were used to compare asphaltenes' destabilization and deposition during a titration of pure crude oil and crude oil with chemical additive. It allowed us to evaluate the efficacy of a chemical additive through measurements in the nanometer scale. The results show that chemical additive A shifted the destabilization toward higher antisolvent compositions with an increased effect as the concentration of additive in solution was increased. From 1000 ppm onwards, a decrease of the deposit with an increase of the chemical additive concentration was observed. This effect seems to be limited between 10,000 ppm and 20,000 ppm, and it can be assumed that there is a threshold above which the increase in chemical additive concentration no longer has a significant impact on deposition. Excessive chemical additive increase did not negatively impact the amount of deposition and no chemical additive self-assembly effect was observed. Moreover, the results obtained in QCR were supported by the results obtained in centrifugation, where a clear decrease in concentration of destabilized particles larger than 200 nm was observed in the presence of chemical additive. The effect of the chemical additive on the aggregation kinetics was also highlighted by the detection time measurements, with a delay in appearance of unstable asphaltene aggregates larger than 500 nm. These observations are consistent with the results obtained by the QCR and the effect of chemical additives on the response of quartz to dissipation. Indeed, it has been described previously that the increase in dissipation is linked to an increase in the viscosity of the crude-heptane mixture, which is itself linked to the appearance of flocs in the environment close to the quartz disk.

Absorbance measurements showed the capacity of the chemical additive to maintain these particles in suspension and thus to limit their size.

Increasing the concentration of chemical additive A showed a shift in the increase of viscosity compared to the pure crude oil, which is consistent with the shift in the appearance of aggregates under the microscope and shows the effect of the chemical additive in delaying the destabilization toward higher antisolvent compositions.

This research aims at providing solutions to the industry, confronted with problems related to the accumulation of asphaltene deposits on the walls of pipelines but also related to the accumulation of sedimented particles under static conditions. Hence, the results of this chapter show that evaluation of the effectiveness of a chemical additive in laboratories must study the deposition as well as the aggregation kinetics. In addition, the study of viscosity is interesting especially for the evaluation of the effectiveness of a “flow improver” chemical additive. Immersed resonating sensors and centrifugation (or microscopy) methods are showed to be complementary techniques for the screening of “asphaltene inhibitors”.

4. References

- (1) Barcenas, M.; Orea, P.; Buenrostro-González, E.; Zamudio-Rivera, L. S.; Duda, Y. Study of Medium Effect on Asphaltene Agglomeration Inhibitor Efficiency. *Energy Fuels* **2008**, *22* (3), 1917–1922. <https://doi.org/10.1021/ef700773m>.
- (2) Daridon, J.-L.; Carrier, H. Measurement of Phase Changes in Live Crude Oil Using an Acoustic Wave Sensor: Asphaltene Instability Envelope. *Energy Fuels* **2017**, *31* (9), 9255–9267. <https://doi.org/10.1021/acs.energyfuels.7b01655>.
- (3) Cassiède, M.; Paillol, J. H.; Pauly, J.; Daridon, J.-L. Electrical Behaviour of AT-Cut Quartz Crystal Resonators as a Function of Overtone Number. *Sensors and Actuators A: Physical* **2010**, *159* (2), 174–183. <https://doi.org/10.1016/j.sna.2010.03.028>.
- (4) Cassiède, M.; Daridon, J.-L.; Paillol, J. H.; Pauly, J. Characterization of the Behaviour of a Quartz Crystal Resonator Fully Immersed in a Newtonian Liquid by Impedance Analysis. *Sensors and Actuators A: Physical* **2011**, *167* (2), 317–326. <https://doi.org/10.1016/j.sna.2011.03.002>.
- (5) Grunberg, L.; Nissan, A. H. Mixture Law for Viscosity. *Nature* **1949**, *164* (4175), 799–800. <https://doi.org/10.1038/164799b0>.
- (6) Daridon, J. L.; Cassiède, M.; Nasri, D.; Pauly, J.; Carrier, H. Probing Asphaltene Flocculation by a Quartz Crystal Resonator. *Energy Fuels* **2013**, *27* (8), 4639–4647. <https://doi.org/10.1021/ef400910v>.
- (7) González, G.; Middea, A. Peptization of Asphaltene by Various Oil Soluble Amphiphiles. *Colloids and Surfaces* **1991**, *52*, 207–217. [https://doi.org/10.1016/0166-6622\(91\)80015-G](https://doi.org/10.1016/0166-6622(91)80015-G).
- (8) Chang, C.-L.; Fogler, H. S. Stabilization of Asphaltenes in Aliphatic Solvents Using Alkylbenzene-Derived Amphiphiles. 1. Effect of the Chemical Structure of Amphiphiles on Asphaltene Stabilization. *Langmuir* **1994**, *10* (6), 1749–1757. <https://doi.org/10.1021/la00018a022>.
- (9) Chang, C.-L.; Fogler, H. S. Stabilization of Asphaltenes in Aliphatic Solvents Using Alkylbenzene-Derived Amphiphiles. 2. Study of the Asphaltene-Amphiphile Interactions and Structures Using Fourier Transform Infrared Spectroscopy and Small-Angle X-Ray Scattering Techniques. *Langmuir* **1994**, *10* (6), 1758–1766. <https://doi.org/10.1021/la00018a023>.

- (10) León, O.; Rogel, E.; Urbina, A.; Andújar, A.; Lucas, A. Study of the Adsorption of Alkyl Benzene-Derived Amphiphiles on Asphaltene Particles. *Langmuir* **1999**, *15* (22), 7653–7657. <https://doi.org/10.1021/la9812370>.

Chapter 4. Effect of the chemical structure of alkylbenzene-derived amphiphiles on asphaltene destabilization, aggregation and deposition

1. Introduction

In order to displace or limit the deposition of asphaltenes on surfaces, the injection of chemical additives is a commonly applied solution in the industry. For this reason, many authors have studied the mechanism of asphaltene-chemical additive interaction¹⁻¹¹. The aggregation of unstable asphaltene particles that come into contact through Brownian motion is governed by two interactions: i) an energy barrier resulting from steric repulsion effects, which are caused by the naturally present alkyl chains in the structure of asphaltenes^{1;2} and ii) an attractive interaction related to Van der Waals forces^{3;4}.

From this standpoint, the idea of enhancing the stability of asphaltene clusters by increasing their steric repulsion emerges. One way to increase this steric repulsion is by introducing alkyl chains into the structure of stable asphaltene molecules or clusters. To achieve this, it has been proposed the use of amphiphilic structures as dispersants¹⁻¹¹. An amphiphilic structure, presented in Figure 1, consists of a polar anchoring group that interacts with the asphaltenes by forming a strong bond with a heteroatom^{5;6}. It is attached to a benzene ring that facilitates $\pi - \pi$ interactions with the aromatic cores of asphaltenes^{5;6}. Finally, an alkyl chain of varying length is attached at the opposite part of the benzene ring. Its function is to induce steric repulsion and prevents asphaltene aggregation⁷.

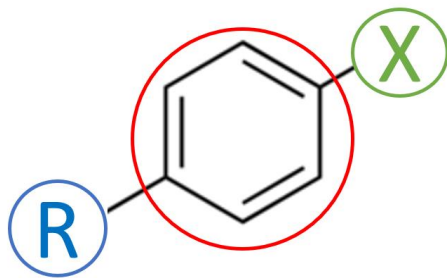


Figure 1. Amphiphilic structure with X: the active functional group; R: the alkyl chain and the benzene ring circled in red.

Chang and Fogler^{5,6} conducted experiments using various alkylbenzene-derived amphiphiles to assess their capacity to stabilize asphaltenes in aliphatic solvents. The authors suggested that the alkyl chain size should be at least 6 carbons to effectively stabilize asphaltenes and should not exceed 16 carbons to avoid crystallization. Furthermore, they demonstrated through FTIR spectroscopy measurements that the interaction between asphaltenes and amphiphiles depends on the polarity of the active functional group. They found that higher polarity leads to greater adsorption of amphiphiles on the surface of asphaltenes, resulting in better stabilization of asphaltenes (when using alkyl chains of equivalent length between 9 and 12 carbons).

Strong organic acids such as dodecyl benzene sulfonic acid (DDBSA) exhibit acid-base interactions with the heteroatoms present in asphaltenes (nitrogen, oxygen, and sulfur)⁸. In a recent study on several dead oils, Huffman et al.⁹ demonstrated through detection time measurements using an optical microscope that DDBSA could either accelerate or delay the asphaltene aggregation depending on the nature of the oil. Despite investigating the composition of destabilized asphaltenes from various oils in the presence of DDBSA, the authors were unable to establish a correlation between the chemical composition of the destabilized asphaltenes and the versatile behavior of DDBSA⁹.

Goual et al.⁷ conducted a study combining impedance analysis, high-resolution transmission electron microscopy (HRTEM), and molecular dynamics (MD) simulations on asphaltene systems extracted in heptol in the presence of p-alkylphenols. The results indicate that the difference in alkyl chain length between octylphenol (OP) and dodecylphenol (DP) does not affect the “onset” of asphaltene destabilization. However, the DC conductivity results show that OP and DP reduce the size of asphaltene aggregates by 15% and 20%, respectively. Moreover, MD simulations revealed that OP forms hydrogen bonds with asphaltenes. OP disperses asphaltenes by both saturating the H-bonding sites and generating steric repulsion with its alkyl chain. These conclusions are supported by HRTEM observations showing filamentous asphaltene aggregates, attributed to the interaction of OP at the periphery of asphaltenes. Additionally, the authors highlighted that the self-association of p-alkylphenols could reduce their dispersion effectiveness. Barcenas et al.¹⁰, through Monte Carlo computer modeling, also reported this self-association phenomenon of amphiphiles when their concentration is increased in toluene.

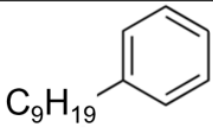
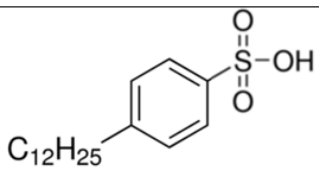
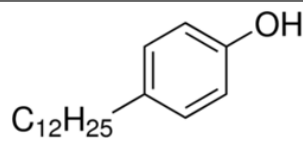
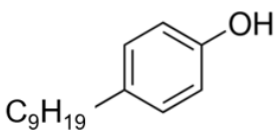
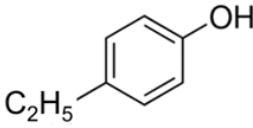
Ismail et al.¹¹ performed ultra-small-angle X-ray scattering (USAXS) measurements in the presence of DP on a model oil system (extracted asphaltene + toluene). The results indicate that DP reduces the growth rate of unstable (or insoluble) asphaltene clusters. Additionally, DP decreases the radius of gyration (R_g) of stable (or soluble) asphaltene clusters by up to 23% compared to nontreated asphaltenes. Moreover, the authors highlighted that the presence of DP slows down the transition from a fractal structure of unstable asphaltene clusters to that of a second phase with a rough surface.

However, the majority of studies on amphiphile-asphaltene interactions are conducted in model oil systems. Therefore, the objective of this chapter is to investigate the effect of the structure of alkylbenzene-derived compounds on the destabilization, aggregation, and deposition of asphaltenes in a dead oil. A combination of three methods presented in the *Chapter 2* was used in the presence of amphiphiles: (i) Quartz crystal resonator (QCR) to evaluate asphaltene destabilization and the mass deposited on the sensor at the nanogram scale; (ii) detection time using an optical microscope to study the aggregation kinetics of unstable asphaltenes clusters, and (iii) centrifugation to estimate the concentration of unstable asphaltene aggregates. The concentration of the amphiphiles was set at 3000 ppm in volume, and the sample preparation protocol is presented in *Chapter 2*.

2. Chemicals

The characteristics of oil and antisolvent were given in *Chapter 2*. The 4-dodecylphenol (>96.5%) was purchased from Pfaltz&Bauer, the 4-dodecylbenzenesulfonic acid (>95%) was purchased from Merck, nonylbenzene (>97%), 4-ethylphenol (>97%), and 4-nonylphenol (>98%) were purchased from Fisher Scientific. The chemical structures of alkylbenzene-derived amphiphiles are given in Table 1.

Table 1. Chemical structures of amphiphilic compounds.

Abbreviation	Structure
NB	
DDBSA	
DP	
NP	
EP	

3. Results and discussion

3.1. Effect of functional group of amphiphilic molecules

The Nonylbenzene (NB), dodecylphenol (DP), and dodecyl benzene sulfonic acid (DDBSA) were selected to study the effect of the amphiphile head groups. These amphiphiles were chosen because they present different functionalizations (or the absence of functionalization for NB) with distinct polarities. The amphiphiles are ranked in ascending order of polarity as follows: NB (without a polar group) < DP (with a phenolic group) < DDBSA (with a sulfonic acid group). According to the results obtained in the literature⁵, the difference of three carbon atoms in the alkyl chain between C₉ and C₁₂ doesn't show to have any impact on the stabilization of asphaltenes.

That's why NB is compared to NP and DDBSA. This assumption was also verified from measurements presented in the section on the effect of alkyl chain length.

3.1.1. Detection time experiments

The detection time curve for pure oil X as reference and oil X treated with 3000 ppm in volume of each NB, DP and DDBSA were obtained experimentally. The results are shown in Figure 2. The detection time curves in Figure 2 show that treating oil with NB results in no significant changes in detection time. The DDBSA and the DP shift the detection time in higher n-heptane composition, and the effect is more significant in the presence of DP. The extrapolation of experimental data using an exponential regression allows to estimate, the n-heptane composition at instantaneous microscopy detection (less than a few minutes) of asphaltene aggregates particles larger than $0.5 \mu\text{m}$ for each system. The results are presented in Table 2. Instantaneous detection time of asphaltenes particles larger than $0.5 \mu\text{m}$.

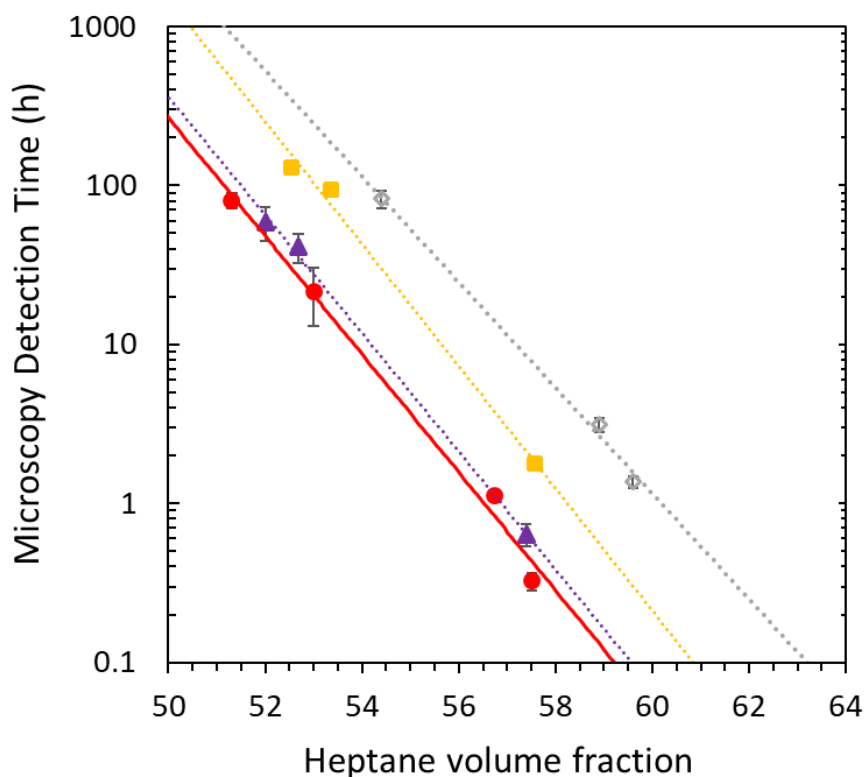


Figure 2. Necessary aging time to detect particles by visual microscopy observations as function of the volume fraction of n-heptane in heptane-oil blends: (red ●) nontreated oil X, (purple ▲) oil X + NB at 3000 ppm, (yellow ■) oil X + DDBSA at 3000 ppm and (grey ◇) oil X + DP at 3000 ppm.

Table 2. Instantaneous detection time of asphaltenes particles larger than 0.5 μm .

Sample	n-heptane composition at instantaneous detection time (%)
Oil X	59.2
Oil X + NB	59.5
Oil X + DP	63.1
Oil X + DDBSA	60.7

From the observation of this table, it appears that the presence of NB does not affect the aggregation kinetics of asphaltenes. Moreover, the nature of the polar head group impacts the aggregation kinetics specifically, DDBSA and DP delay the appearance of large particles, in other words, it is necessary to increase the amount of n-heptane to obtain a detection time similar to that of nontreated oil X. The effect observed in this case remains modest (4%).

3.1.2. Centrifugation experiments

As with previous measurements, the centrifugation experiments were performed with oil X as reference and oil X treated with 3000 ppm in volume of NB, DP and DDBSA. The concentration of unstable asphaltene aggregates larger than 200 nm centrifuged per unit of volume of crude oil as function of the aging time is represented for each system in Figure 3.

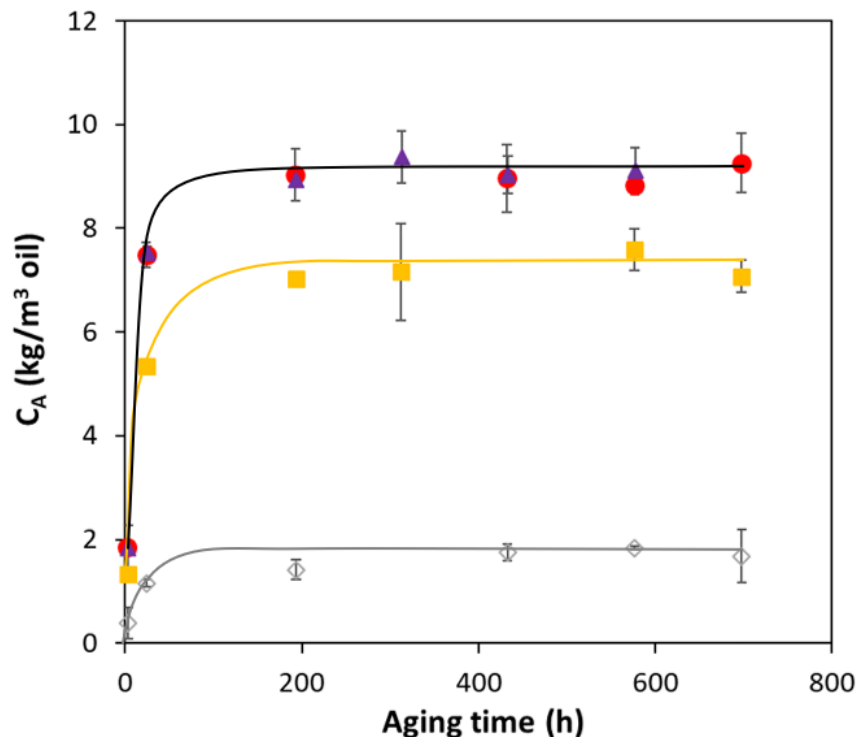


Figure 3. Concentration of unstable asphaltens larger than 200 nm separated by centrifugation as a function of the aging time of prepared blends of crude Oil X + 60 vol % \pm 0.3% n-heptane: (red ●) nontreated oil X, (purple ▲) oil X + NB at 3000 ppm, (yellow ■) oil X + DDBSA at 3000 ppm and (grey ◇) oil X + DP at 3000 ppm. The solid lines are made to facilitate the reading of the trends.

This figure indicates that the amount of unstable asphaltens separated by centrifugation is not affected by the presence of NB. However, the quantity of unstable asphaltens separated at equilibrium is reduced in the presence of DDBSA and DP by 21 % and 81 %, respectively, compared to the nontreated oil X. The presence of polar groups, therefore, allows for a strong enough interaction with asphaltene to affect the quantity of destabilized asphaltene. The effect of DDBSA and DP found here is far more significant than that observed with microscopy on the threshold of destabilization.

3.1.3. QCR experiments

Titration experimentations of n-heptane in dead crude oil X with an immersed QCR sensor were carried out with NB, DDBSA and DP. During these experiments, the shift in resonance frequency along various overtones (1 to 7) of the resonating sensor was recorded and the deposited mass and the deposition rate were calculated as presented in *Chapter 2*. The changes in resonance frequency of the third overtone peak measured by the QCR for each system are presented in Figure 4.

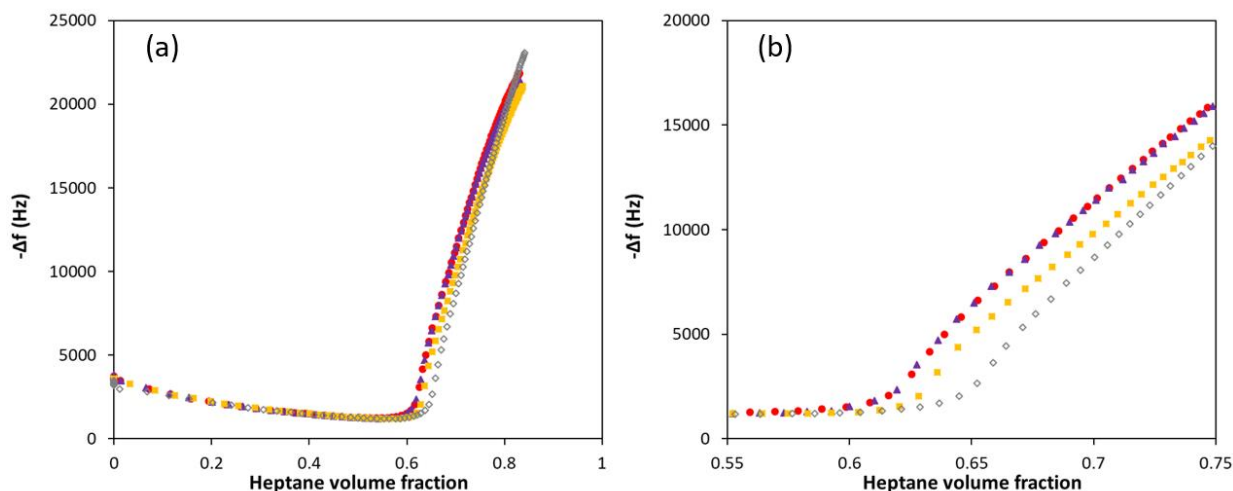


Figure 4. (a) shift of resonance frequency (3rd harmonic) recorded during continuous titration of crude oil X as a function of the volume fraction of n-heptane: (red ●) nontreated oil X, (purple ▲) oil X + NB at 3000 ppm, (yellow ■) oil X + DDBSA at 3000 ppm and (grey ◇) oil X + DP at 3000 ppm. (b) zoom of the frequency shift between 0.55 and 0.75 volume fraction of n-heptane.

The results show that the presence of NB does not impact the resonance frequency change compared to nontreated oil X. Additionally, in the presence of DP and DDBSA, the “onset” of asphaltene destabilization is shifted towards higher n-heptane compositions equivalently. The values for the destabilization detection threshold, measured from the resonance frequencies for the third harmonic, are provided in Table 3. A shift of +2.5% in volume fraction for the “onset” of destabilization is observed for oil treated with 3000 ppm volume of DP or DDBSA compared to the reference measurement of pure crude oil X.

Table 3. “Onset” of destabilization from resonant frequency measurements.

Sample	n-heptane composition at “onset” of destabilization (%)
Oil X	55.2
Oil X + NB	55.0
Oil X + DP	57.7
Oil X + DDBSA	57.5

The deposited mass and deposition rate during the continuous titration of n-heptane in the presence of NB, DDBSA, and DP are calculated based on experimental data obtained from the QCR and the simplified model presented in *Chapter 2*. The results are presented in Figure 5. The quantity of asphaltenes deposited on the sensor surface in the presence of NB is similar to the mass deposited for nontreated oil X. A decrease in the deposited mass is observed in the presence of DDBSA and DP, with a more significant inhibition of cumulative deposition in the presence of DP compared to DDBSA, up to approximately 76 vol% of n-heptane, as seen in Figure 5.a. However, at 69 vol% of n-heptane, the deposition rate becomes higher for the oil treated with DP compared to that treated with DDBSA, as seen in Figure 5.b. Furthermore, the maximum deposition rate, although shifted towards a higher n-heptane composition, is higher and maintained for a longer time in the presence of DP compared to DDBSA, with respective values of 4.9 and 4.5 g/m²/day.

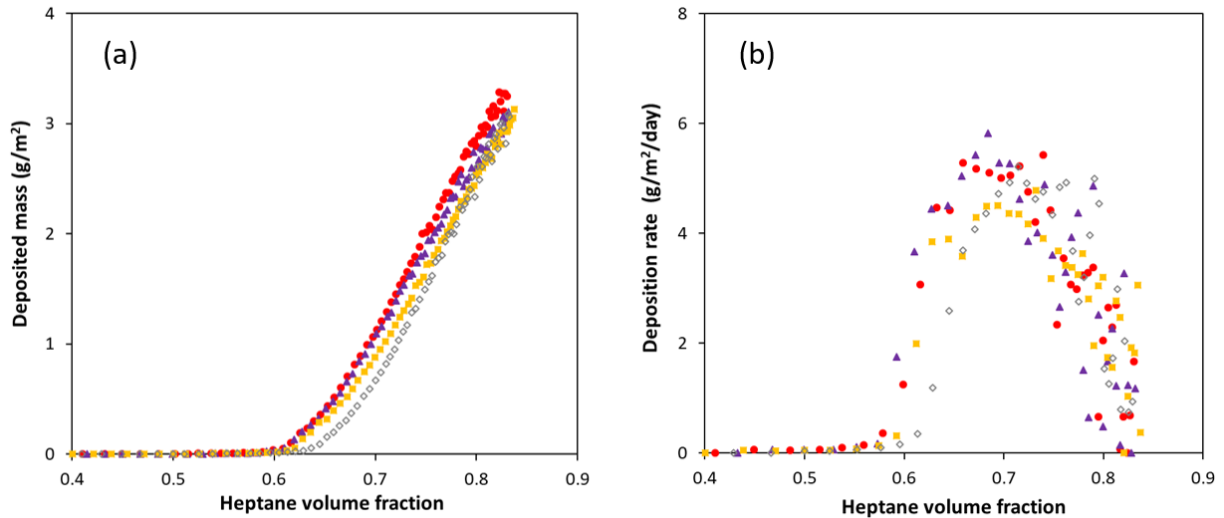


Figure 5. (a) deposited mass and (b) deposition rate, calculated during experimental titration of crude oil X with n-heptane. (red ●) nontreated oil X, (purple ▲) oil X + NB at 3000 ppm, (yellow ■) oil X + DDBSA at 3000 ppm and (grey ◇) oil X + DP at 3000 ppm.

Huffman et al.⁹ reported that DDBSA had a versatile effect and that for certain dead oils, the presence of this amphiphile could increase the deposited mass. In order to investigate this effect, additional measurements were carried out on the QCR at several concentrations of DDBSA in oil X. The results are presented in Figure 6. The results indicate that at low concentration (300 ppm), the “onset” of destabilization is not significantly shifted compared to nontreated oil; however, the cumulative deposition at the end of the titration is the same as the mixture with 3000 ppm. Furthermore, at 10,000 ppm of DDBSA, the “onset” shift and the inhibition of deposition are more pronounced compared to the previous concentrations. For the dead oil studied, DDBSA does not promote asphaltene destabilization and deposition within the tested concentration range. On the

contrary, we observed both a positive shift in the destabilization threshold and a decrease in deposited mass caused by the addition of DDBSA whatever its concentration.

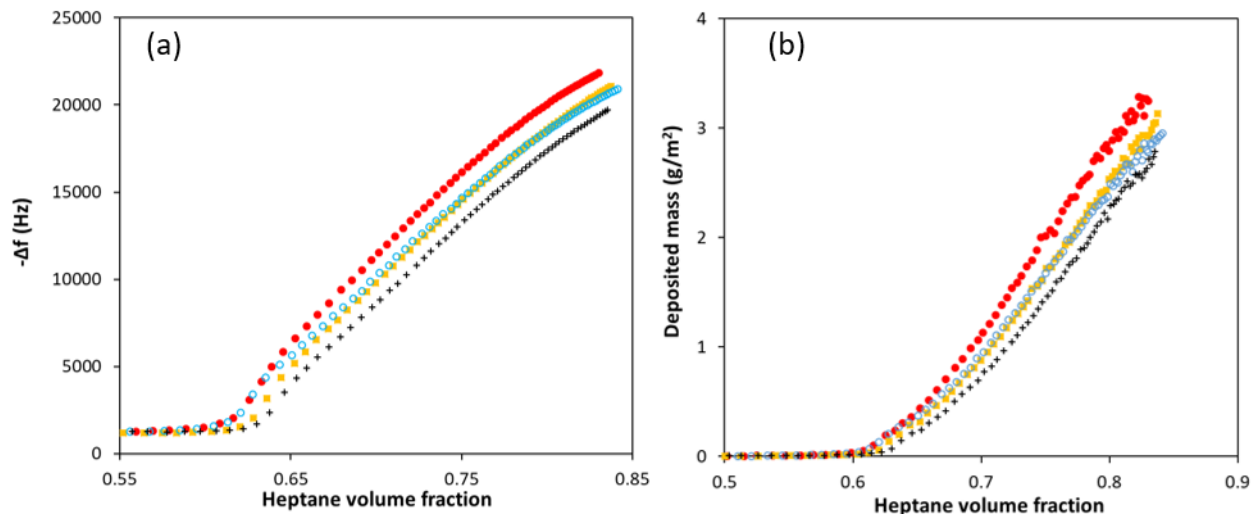


Figure 6. (a) shift of resonance frequency (3rd harmonic) and (b) deposited mass, during continuous titration of crude oil X as a function of the volume fraction of n-heptane. (red ●) nontreated oil X, (blue ○) oil X + DDBSA at 300 ppm, (yellow ■) oil X + DDBSA at 3000 ppm and (black +) oil X + DDBSA at 10,000 ppm.

3.1.4. Discussions

All the methods used indicate that NB does not affect the destabilization, aggregation and deposition of asphaltene. It is therefore concluded that NB does not interact with asphaltene. On the other hand, in the presence of DDBSA and DP, the destabilization, aggregation, and deposition of asphaltene are affected. DDBSA and DP shift the destabilization of asphaltene in higher antisolvent composition and slow down the aggregation kinetics. Moreover, in the presence of DDBSA and DP, the cumulative deposition amount on the surface of the acoustic sensor is reduced compared to nontreated oil. Thus, these concomitant measurements confirm that a polar headgroup is required for the amphiphile to interact with asphaltene.

3.2. Effect of alkyl chain length of amphiphilic molecules

Given the good results obtained with DP, alkylphenols were used in this second part to study the influence of alkyl chain length. Three p-alkylphenols were selected with chain lengths ranging from 2 to 12 carbons. The objective was to compare the impact of the alkyl chain on the stabilization of asphaltenes in a dead oil using the combination of the three experiments.

3.2.1. Detection time experiments

The detection time curves for pure oil X as a reference and oil X treated with 3000 ppm in volume of each EP, NP, and DP were obtained experimentally. The results are presented in Figure 7. The detection time curves in Figure 7 demonstrate that in the presence of EP, the appearance of asphaltene particles with sizes above the microscope detection threshold is shifted towards a higher n-heptane composition compared to nontreated oil. Similarly, a shift is observed in the presence of NP and DP; however, the detection time curves are nearly identical, and the n-heptane composition at instantaneous detection time is also similar, as shown in Table 4. The microscope observations suggest that the aggregation kinetics of asphaltenes is affected in the presence of EP, despite its alkyl chain being only 2 carbons long. The influence of the additive increases as the alkyl chain lengthens from 2 to 9, but the increase from 9 to 12 does not significantly impact the aggregation kinetics of unstable asphaltenes.

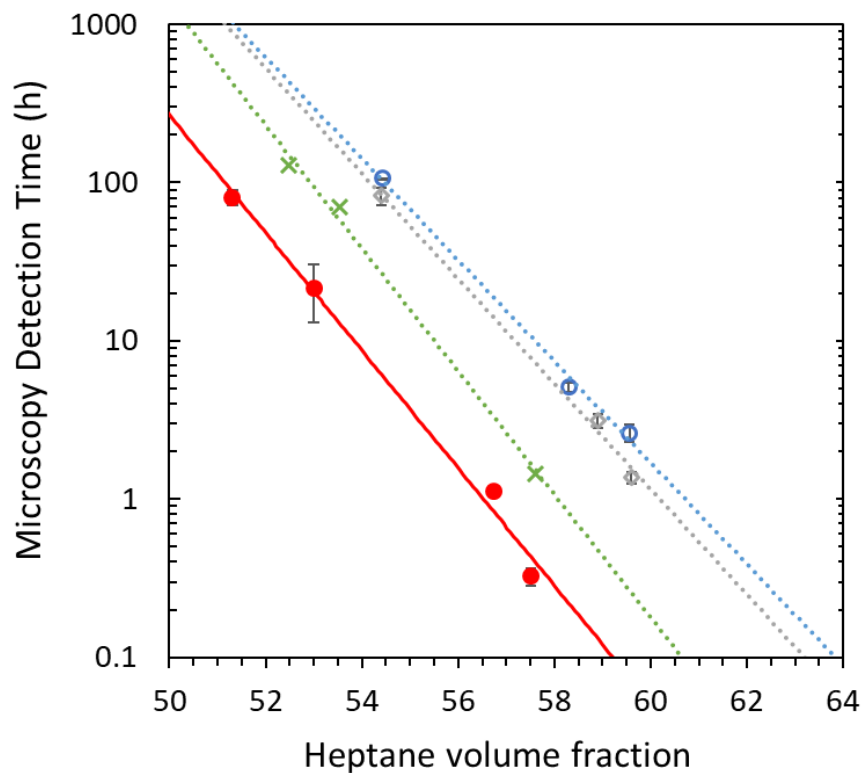


Figure 7. Necessary aging time to detect particles by visual microscopy observations as function of the volume fraction of n-heptane in heptane-oil blends: (red ●) nontreated oil X, (green ×) oil X + EP at 3000 ppm, (blue ○) oil X + NP at 3000 ppm and (grey ◇) oil X + DP at 3000 ppm.

Table 4. Instantaneous detection time of asphaltenes particles larger than $0.5 \mu\text{m}$.

Sample	n-heptane composition at instantaneous detection time (%)
Oil X	59.2
Oil X + EP	60.6
Oil X + NP	63.8
Oil X + DP	63.1

3.2.2. Centrifugation experiments

Centrifugation experiments were performed with oil X as reference and oil X treated with 3000 ppm in volume of EP, NP and DP. The concentration of unstable asphaltene aggregates larger than 200 nm centrifuged per unit of volume of crude oil as function of the aging time is represented for each system in Figure 8.

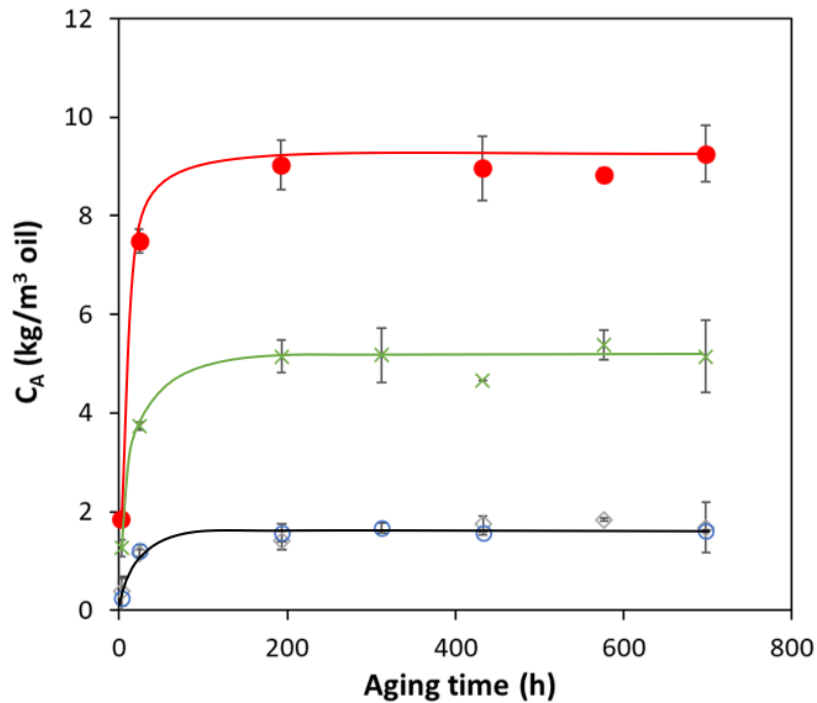


Figure 8. Concentration of unstable asphaltenes larger than 200 nm separated by centrifugation as a function of the aging time of prepared blends of crude Oil X + 60 vol % \pm 0.3% n-heptane: (red ●) nontreated oil X, (green ×) oil X + EP at 3000 ppm, (blue ○) oil X + NP at 3000 ppm and (grey ◇) oil X + DP at 3000 ppm. The solid lines are made to facilitate the reading of the trends.

The results indicate that the amount of separated asphaltene in the presence of EP is reduced by approximately 43% at equilibrium for a composition of 60 vol% of n-heptane compared to nontreated oil. Moreover, the results obtained by centrifugation with NP and DP are identical, as the presence of these amphiphiles stabilizes the asphaltene to an equivalent extent at the studied

antisolvent composition. These observations are in line with those made from microscopy detection time experiments.

3.2.3. QCR experiments

Titration experimentations of n-heptane in dead crude oil X with an immersed QCR sensor were carried out with EP, NP and DP. The changes in resonance frequency of the third overtone peak measured by the QCR for each system are presented in Figure 9.

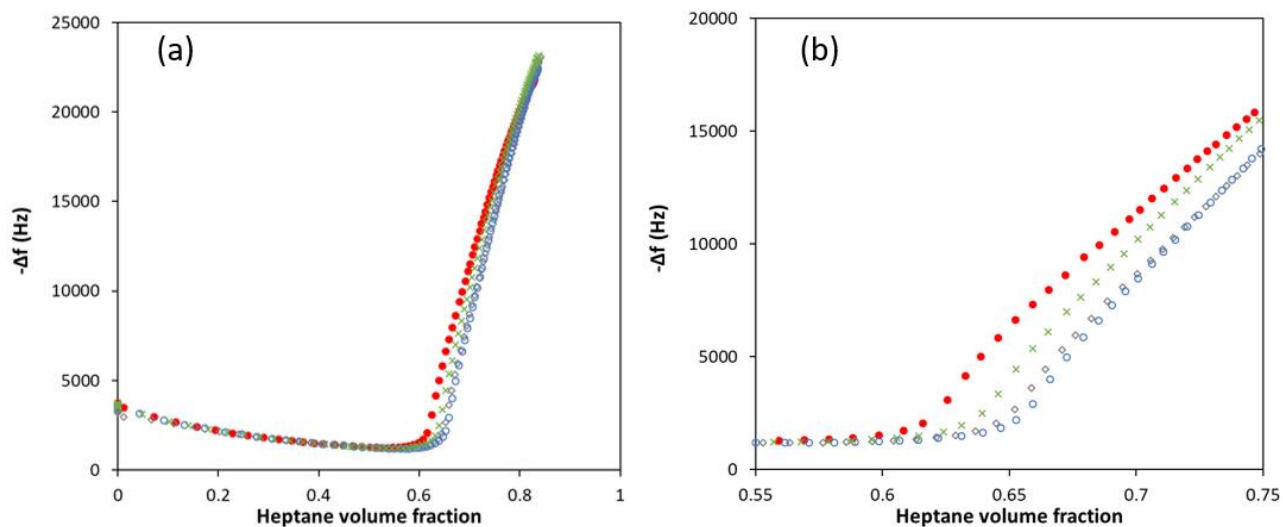


Figure 9. (a) shift of resonance frequency (3rd harmonic) recorded during continuous titration of crude oil X as a function of the volume fraction of n-heptane: (red ●) nontreated oil X, (green ×) oil X + EP at 3000 ppm, (blue ○) oil X + NP at 3000 ppm and (grey ◇) oil X + DP at 3000 ppm. (b) zoom of the frequency shift between 0.55 and 0.75 volume fraction of n-heptane.

The results show that all the tested p-alkylphenols have the effect of shifting the “onset” of destabilization towards higher n-heptane composition. EP shifts the “onset” of destabilization by +1.4%, while NP and DP shift the “onset” almost identically by +2.8% and +2.5% respectively, as seen in Table 5.

Table 5. "Onset" of destabilization from resonant frequency measurements.

Sample	n-heptane composition at "onset" of destabilization (%)
Oil X	55.2
Oil X + EP	56.6
Oil X + NP	58.0
Oil X + DP	57.7

The calculated deposited mass and deposition rate during the continuous titration of n-heptane in the presence of EP, NP, and DP are presented in Figure 10. Figure 10.a. shows that in the presence of p-alkylphenols, the cumulative deposition amount on the sensor surface remains lower throughout the titration compared to the oil free of amphiphile. However, even though p-alkylphenols delay the appearance of deposition, they sustain a maximum deposition rate of $5 \pm 0.4 \text{ g/m}^2/\text{day}$ for a longer duration than the nontreated oil, whose maximum deposition rate is similar ($5.2 \text{ g/m}^2/\text{day}$), as observed in Figure 10.b.

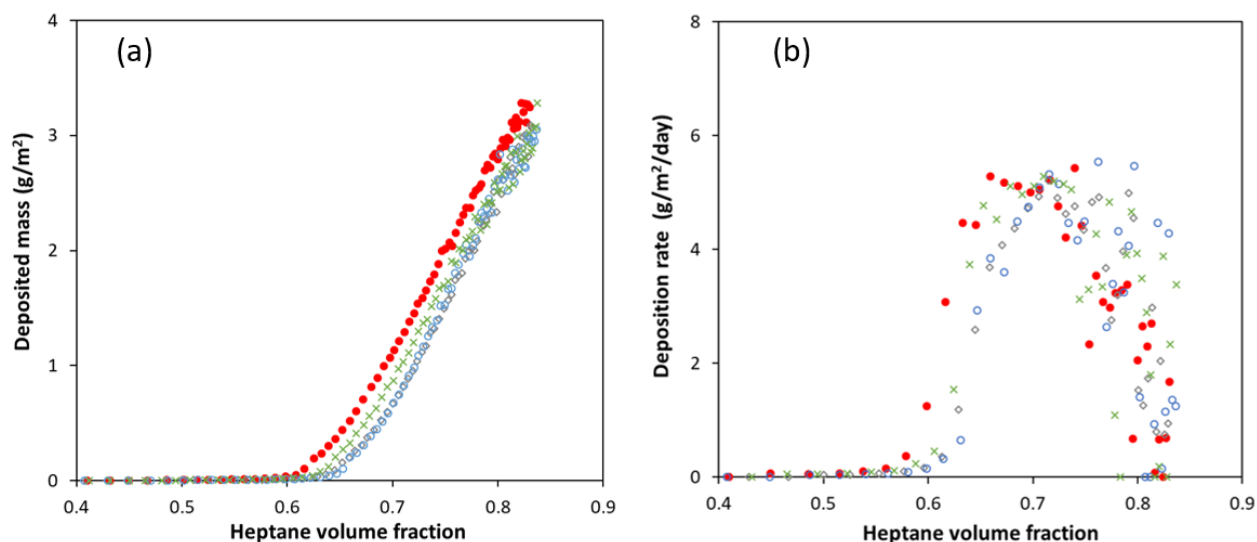


Figure 10. (a) deposited mass and (b) deposition rate, calculated during experimental titration of crude oil X with n-heptane. (red ●) nontreated oil X, (green ×) oil X + EP at 3000 ppm, (blue ○) oil X + NP at 3000 ppm and (grey ◇) oil X + DP at 3000 ppm.

3.2.4. Discussions

The overall results show that the selected p-alkylphenols interact with the asphaltenes and stabilize them. Despite its relatively short chain, EP demonstrates interaction with the asphaltenes and shifts their destabilization and deposition. Both NP and DP exhibit more significant dispersion effects due to the length of their longer alkyl chains, which allows for steric repulsion as suggested in the literature^{5;7}. However, the two p-alkylphenols exhibit similar effects on the destabilization, aggregation, and deposition of asphaltenes, despite the difference of 3 carbons in the alkyl chain.

4. Conclusions

The combination of optical microscope detection, centrifugation, and QCR methods allowed for the assessment of the effect of different amphiphile chemistries on the destabilization, aggregation, and deposition of asphaltenes. Several conclusions can be drawn from this study. Firstly, a polar group is required to interact with asphaltenes. Furthermore, it is noteworthy that the amphiphiles possess the capability to stabilize asphaltenes. This stabilization can be attributed to two mechanisms. Firstly, in the case of long-chain p-alkylphenols, their interaction with asphaltenes leads to the creation of an energy barrier through steric repulsion of the chains, as emphasized in previous studies^{5;7}. The second mechanism, which could explain the stabilizing effect of EP, involves its interaction with asphaltenes through its polar head group, saturating active sites (e.g., H-bonding sites) and limiting asphaltene self-association. Due to EP's short alkyl chain, its interaction with an asphaltene does not block the grafting of additional EP molecules by steric exclusion, unlike long-chain p-alkylphenols, which limit the number of amphiphile molecules on a single asphaltene. However, the results show that long-chain p-alkylphenols have a better effect on shifting the “onset” of destabilization and more effectively inhibiting deposition at lower antisolvent concentrations (<70 vol%). Moreover, it does not seem useful to lengthen the chain beyond 10 carbon atoms.

5. References

- (1) Wang, S.; Liu, J.; Zhang, L.; Masliyah, J.; Xu, Z. Interaction Forces between Asphaltene Surfaces in Organic Solvents. *Langmuir* **2010**, *26* (1), 183–190. <https://doi.org/10.1021/la9020004>.
- (2) Wang, S.; Liu, J.; Zhang, L.; Xu, Z.; Masliyah, J. Colloidal Interactions between Asphaltene Surfaces in Toluene. *Energy Fuels* **2009**, *23* (2), 862–869. <https://doi.org/10.1021/ef800812k>.
- (3) Vargas, F. M.; Gonzalez, D. L.; Creek, J. L.; Wang, J.; Buckley, J.; Hirasaki, G. J.; Chapman, W. G. Development of a General Method for Modeling Asphaltene Stability. *Energy Fuels* **2009**, *23* (3), 1147–1154. <https://doi.org/10.1021/ef800666j>.
- (4) Javanbakht, G.; Sedghi, M.; Welch, W. R. W.; Goual, L.; Hoepfner, M. P. Molecular Polydispersity Improves Prediction of Asphaltene Aggregation. *Journal of Molecular Liquids* **2018**, *256*, 382–394. <https://doi.org/10.1016/j.molliq.2018.02.051>.
- (5) Chang, C.-L.; Fogler, H. S. Stabilization of Asphaltenes in Aliphatic Solvents Using Alkylbenzene-Derived Amphiphiles. 1. Effect of the Chemical Structure of Amphiphiles on Asphaltene Stabilization. *Langmuir* **1994**, *10* (6), 1749–1757. <https://doi.org/10.1021/la00018a022>.
- (6) Chang, C.-L.; Fogler, H. S. Stabilization of Asphaltenes in Aliphatic Solvents Using Alkylbenzene-Derived Amphiphiles. 2. Study of the Asphaltene-Amphiphile Interactions and Structures Using Fourier Transform Infrared Spectroscopy and Small-Angle X-Ray Scattering Techniques. *Langmuir* **1994**, *10* (6), 1758–1766. <https://doi.org/10.1021/la00018a023>.
- (7) Goual, L.; Sedghi, M.; Wang, X.; Zhu, Z. Asphaltene Aggregation and Impact of Alkylphenols. *Langmuir* **2014**, *30* (19), 5394–5403. <https://doi.org/10.1021/la500615k>.
- (8) Hashmi, S. M.; Zhong, K. X.; Firoozabadi, A. Acid–Base Chemistry Enables Reversible Colloid-to-Solution Transition of Asphaltenes in Non-Polar Systems. *Soft Matter* **2012**, *8* (33), 8778–8785. <https://doi.org/10.1039/C2SM26003D>.
- (9) Huffman, M.; Fogler, H. S. Asphaltene Destabilization in the Presence of Dodecylbenzene Sulfonic Acid and Dodecylphenol. *Fuel* **2021**, *304*, 121320. <https://doi.org/10.1016/j.fuel.2021.121320>.

- (10) Barcenas, M.; Orea, P.; Buenrostro-González, E.; Zamudio-Rivera, L. S.; Duda, Y. Study of Medium Effect on Asphaltene Agglomeration Inhibitor Efficiency. *Energy Fuels* **2008**, *22* (3), 1917–1922. <https://doi.org/10.1021/ef700773m>.
- (11) Ismail, M.; Yang, Y.; Chaisontornyotin, W.; Ovalles, C.; Rogel, E.; Moir, M. E.; Hoepfner, M. P. Effect of Chemical Inhibitors on Asphaltene Precipitation and Morphology Using Ultra-Small-Angle X-Ray Scattering. *Energy Fuels* **2019**, *33* (5), 3681–3693. <https://doi.org/10.1021/acs.energyfuels.8b03055>.

Chapter 5. Understanding the mechanism of action of chemical additives on asphaltene deposition

1. Introduction

Asphaltenes are defined as the fraction of crude oil that is soluble in aromatic liquids, such as toluene, while being insoluble in lights alkanes. They are characterized as the heaviest and most polarizable polydisperse fraction of the crude oil. The solubility of asphaltenes is greatly influenced by temperature, pressure, and composition changes within the crude oil, leading to their destabilization and subsequent deposition in subsea wells, pipelines, and porous formations. During pressure depletion, the expansion of light alkanes affects the solubility of asphaltenes and causes their destabilization. Once asphaltenes separate from oil, they tend to flocculate and deposit. These deposition phenomena may have serious consequences, such as clogging pipelines, resulting in reductions of production and substantial financial losses.

In order to model the deposition of asphaltenes, previous authors employed various approaches and hypotheses¹⁻⁵. Nabzar and Aguilera¹ used a "colloidal approach" to demonstrate experimentally that the deposition kinetics of asphaltenes followed the same scaling laws as those of colloidal deposition in porous media. Authors proposed the general scaling laws for the deposition kinetics, given by:

$$\Omega \propto \forall \cdot \gamma^{-s} \tag{1}$$

where Ω is the capture efficiency, γ is the shear rate, exponent s being universal and dependent on the deposition regime. The pre-factor \forall contains the system characteristics (flow field around the collector and collector geometry). They emphasized that at low flow rates below a critical shear rate and in presence of antisolvent, the deposition takes place according to classical diffusion limited deposition (DLD, $s = 2/3$). At higher shear rates, the deposition process becomes more sensitive to the shear rate, and a new regime called shear limited deposition (SLD) was considered.

This regime results from the superposition of the previous DLD regime and a shear contribution that slows down the deposition kinetics proportionally to shear rate ($s = 2/3 + 1 = 5/3$).

However, Hashimi et al.² conducted an experimental study to measure asphaltene deposition by injecting oil-heptane mixtures into a metal pipe and measuring pressure drop assuming uniform deposition along the pipe. They observed that, for laminar flow at high flow rates, there was no deposition. To explain this observation, they suggested that this absence of deposition was due to a pore volume injection that was too short to observe deposition. They concluded that the effects at high flow rates could be explained by a diffusion-limited mechanism, and that the nomenclature proposed by Nabzal and al.¹ (Shear Limited Deposition) for this type of regime was not necessary. Moreover, in some cases, they reported a decrease in asphaltene deposition at low flow rates due to a significant increase in the local shear rate at the center of the pipe.

Eskin et al.³ proposed a model for asphaltene deposition based on experimental data obtained using a Couette device. The authors introduced the concept of a critical size for depositing asphaltenes and evaluated it by considering the forces exerted on a deposited particle at the surface. They suggested that this critical size is determined by the balance between the adhesion forces of particles to the surface (described by Van der Waals forces) and the drag forces. When the particle size exceeds this critical size, hydrodynamic forces dominate, and the particles are re-suspended in the flow stream. According to the model they proposed, they estimated that the size of unstable particles that deposit on the surface would be around a few tens of nanometers under flow conditions. However, the model has many fitting parameters (such as particle-particle collision efficiency, particle sticking probability, and intermolecular distance), and therefore the predictions made by this model may be subject to questioning.

Vilas Bôas Fávero et al.⁴ were the first to model one-dimensional mass-transfer deposition through a diffusion-limited mechanism in the viscous flow regime using a single fitting parameter: the diffusion coefficient of the deposited particles. The authors developed their approach based on a packed-bed experiments with stainless steel beads, in which they flowed different oil-heptane mixtures. The amounts of deposited asphaltenes were measured in different conditions by varying several parameters such as the injection rate of the antisolvent, the nature of the oils tested, n-alkane contents and the packed-bed lengths. Several of their results led them to propose a model based on a diffusion-limited deposition mechanism. These were mainly:

- (i) The deposition rate of unstable asphaltenes scaled with the square root of the fluid flow velocity in viscous flow regime.
- (ii) The asphaltene deposition profile along the packed bed matches theoretical behavior predicted by the diffusion-limited correlations for mass-transfer deposition.
- (iii) The deposition rate was independent of the bead material.

Saidoun⁵ revisited the model of Vilas Bôas Fávero by adding the kinetics of asphaltene destabilization and by considering aggregation kinetics as the fastest step. As a result, the limiting process became the destabilization kinetics, which Saidoun et al.⁶ expressed as time-dependent. By considering a time-dependent destabilization kinetics, the concentration of unstable asphaltenes that could deposit (C_A) became lower than the one used as an input parameter by Vilas Bôas Fávero in their model leading to a larger diffusion coefficient (D_A) according to the Stokes-Einstein law (Equation 2). Consequently, a hydrodynamic radius of the diffusing particles lower than the hundred nanometers initially suggested by the authors was found.

$$D_A = \frac{k_B T}{6\pi\eta_{liq}R_A} \quad (2)$$

From their proposed model that involves only 1 fitting parameter (the radius of particles that diffuse), Saidoun⁵ estimated the size of the deposited asphaltenes particles to be less than 20 nanometers and described them as clusters of asphaltene nanoaggregates that transform from stable to unstable. Moreover, in accordance with previous research concerning asphaltene diffusion-limited models, Saidoun⁵ showed that the deposition rate of unstable asphaltenes scales with the square root of the fluid flow velocity, indicating that mass-transfer is controlled by the diffusion of unstable primary particles.

One of the solutions used in the industry to prevent or inhibit the formation of deposits on surfaces is the injection of chemical additives. However, the results obtained by Saidoun raise a question about the mechanism of action of these chemical additives. Indeed, most chemical additives are selected based on their dispersing capability, limiting the size of asphaltenes. The issue is, if a chemical additive reduces the size of unstable asphaltene particles in a mass-transfer limited phenomenon, the diffusion coefficient of these particles should be larger, leading to a higher deposition rate according to the relationship demonstrated by the author:

$$Rate_{dep} \propto C_A D_A^{2/3} \quad (3)$$

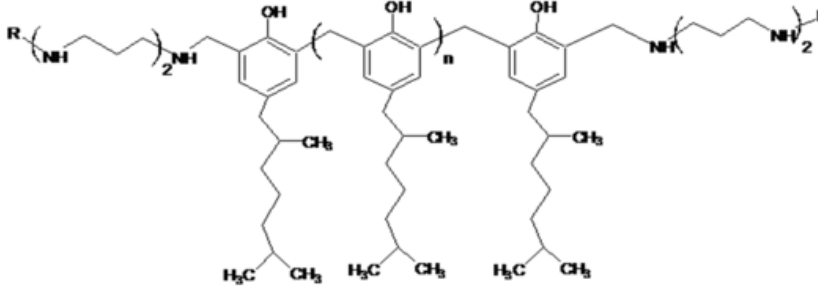
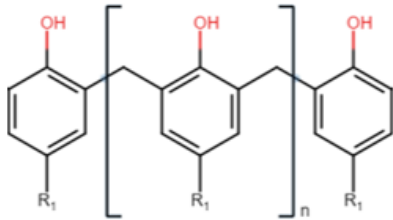
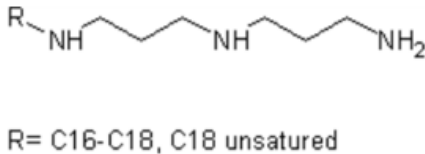
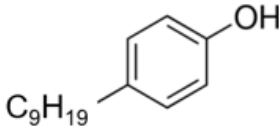
The objective of this work is to shed light on the mechanism of action of chemical additives that inhibit asphaltene deposition on surfaces. To achieve this, the cumulative amount of deposited unstable asphaltenes and the deposition rate were evaluated using a Quartz Crystal Resonator (QCR). The concentration gradient of diffusing particles was experimentally obtained through centrifugation measurements and continuously modeled as a function of the antisolvent volume fraction. Finally, using results of both centrifugation and QCR experiments, the mass-transfer limited model proposed by Saidoun⁵ was used to calculate the hydrodynamic radius of diffusing particles with or without the addition of chemical additives, in order to assess their influence on asphaltene deposition mechanisms.

2. Materials and methods

2.1. Materials

The characteristics of oil X and the n-heptane were presented in *Chapter 2*. Four different chemical additives provided by *TotalEnergies Additives & Fuels Solutions* were tested. Their chemical structures are presented in Table 1. The first one, named chemical additive A, is a commercial “asphaltene deposition inhibitor”, which is actually an alkylphenol resin modified by an alkyl polyamine. The structure of chemical additive A is presented in Figure 1. The second one, named chemical additive B, is a precursor of chemical additive A and corresponds to the alkylphenol resin part (polynonylphenol). The third one, named chemical additive C, is another precursor of chemical additive A and consists of the alkyl polyamine part. Finally, the last one, named chemical additive D, is the 4-nonylphenol, an amphiphilic compound.

Table 1. Structures of chemical additives.

Chemical Additive name	Structure
Chemical additive A	
Chemical additive B	
Chemical additive C	 <p>R= C16-C18, C18 unsaturated</p>
Chemical additive D	

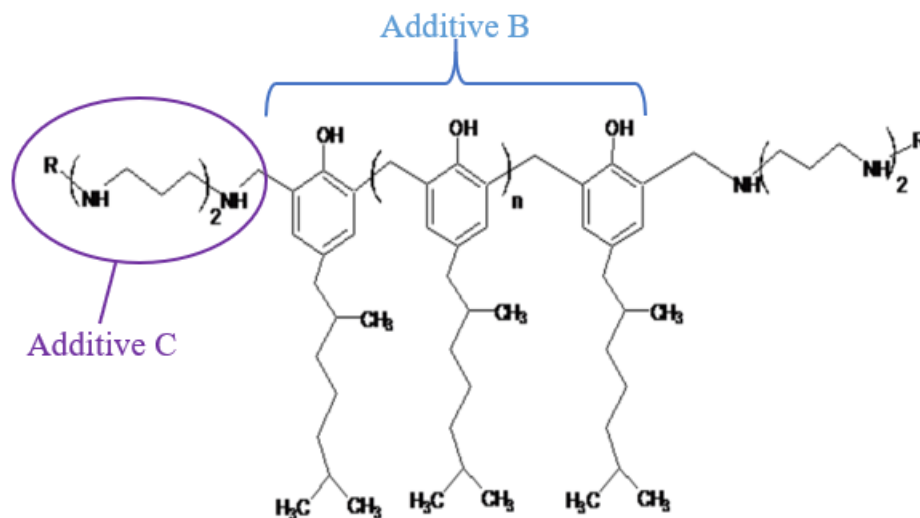


Figure 1. Comparison of structure of chemical additive A with B and C.

2.2. Methods

2.2.1. Experimental

The different chemical additives were characterized through centrifugation measurements to obtain the concentration of unstable asphaltenes available for diffusion. Additionally, titration measurements were conducted using n-heptane as an antisolvent. A totally immersed quartz crystal resonator sensor was employed to monitor the formation of unstable asphaltenes deposit on the probe surface. The experimental methods used here were described in *Chapter 2*. The concentration of chemical additives is set at 3000 ppm by volume, and it is kept constant during the titrations by adding 3000 ppm by volume into the antisolvent.

2.2.2. Modelisation of the concentration gradient of unstable asphaltene in the liquid phase

In the approach proposed by Saidoun et al.⁶ the destabilization of asphaltenes in a static solution, whose composition does not change over time, was mathematically modeled by a first-order reaction in which stable nanoaggregates (A_{stable}) destabilize with a destabilization rate constant k_D . These unstable particles are referred to as unstable primary asphaltene particles ($A_{unstable}$) and have a characteristic size between 2 and 10 nm. These unstable primary particles will then follow an aggregation process to form unstable aggregates ($A_{unstable}$) with k as the number of primary particle units according to the aggregation rate constant k_A . The aggregation process from stable clusters to agglomerated unstable clusters is described in Figure 2.

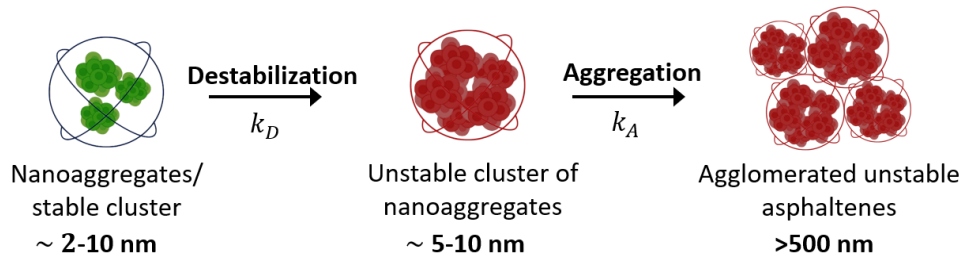


Figure 2. Kinetics of asphaltene destabilization and aggregation.

The authors showed that the deposition of asphaltenes is limited by the slow destabilization kinetic, in other words primary unstable particles have a relatively short lifespan in the "non-aggregated" state at n-heptane content larger than the "onset". This conclusion suggests that asphaltene particles separable by centrifugation which make a transition from a stable to unstable state quickly tend to aggregate reaching particle sizes larger than the cut-off size (200 nm).

The destabilization kinetics proposed by Saidoun et al.⁶ is as follows,

$$r_1 = \frac{dC_A}{dt} = k_D C_{A\infty} \quad (4)$$

Here, C_A is the concentration of unstable asphaltene in oil (m_A/V_{oil}), r_1 is the generation rate of unstable asphaltene and $C_{A\infty}$ is the mass concentration of unstable asphaltene at equilibrium (when time tends to infinite).

Centrifugation experiments were conducted to measure the quantity of separable unstable asphaltenes in oil-heptane mixtures with fixed compositions and varying aging times. These experiments were performed under static solution conditions where the antisolvent composition remained constant over time. The destabilization constant, k_D , was calculated by analyzing the change in unstable asphaltenes concentration ΔC_A over a time increment Δt , and the following equation was proposed by Saidoun et al.⁶ to represent this constant as a function of time:

$$k_D = \frac{1}{\tau} \left(1 - \frac{C_{Ai}}{C_{A\infty}} \right) e^{-\frac{t}{\tau}} \quad (5)$$

Here, τ is the time required to reach the equilibrium plateau.

Considering the following initial conditions,

$$\begin{aligned} t = 0 & \quad \Rightarrow \quad C_A(0) = 0 \\ t > 1000 \text{ h} & \quad \Rightarrow \quad C_A(t) = C_{A\infty} \end{aligned}$$

Integration of Equation 4 using k_D given by the Equation 5 leads to the expression of the concentration of unstable asphaltenes as a function of time t :

$$C_A(t) = C_{A\infty} \left(1 - e^{-\frac{t}{\tau}} \right) \quad (6)$$

In this expression, the parameters $C_{A\infty}$ and τ must be adjusted to match the concentration of unstable asphaltenes obtained experimentally over time in a mixture of fixed antisolvent composition. This behavior was obtained by carrying out centrifugation experiments with the same prepared mixture but at different periods.

In order to model the concentration of unstable asphaltenes for a mixture whose antisolvent composition varies continuously over time, it is necessary to represent the concentration of unstable asphaltenes at equilibrium $C_{A\infty}$ and the time required to reach this concentration τ as a function of antisolvent composition.

With this aim, Saidoun et al.⁶ proposed a power law function with two adjusted parameters (b and c) for representing time τ required to reach the plateau as a function of n-heptane composition expressed by its volume fraction ϕ_{C_7} . The equation is as follows:

$$\tau = b\phi_{C_7}^c \quad (7)$$

Then, a sigmoid function was proposed by the authors in order to represent $C_{A\infty}$ as a function of the volume fraction of antisolvent continuously added:

$$C_{A\infty} = \frac{C_{A\infty,\max}}{1 + i \times \exp\left(\frac{-(\phi_{C_7}-f)}{d}\right)} \quad (8)$$

where $C_{A(\max)}$ represents the maximum concentration of unstable asphaltenes corresponding to an infinite dilution at an infinite time, f corresponds to the inflection point of the sigmoid that characterizes the instantaneous “onset”, i and d are two parameters adjusted to the centrifugation experiments carried out in various mixtures with different compositions and correspond respectively to a scaling factor for the slope of the sigmoid (the larger i , the steeper the slope) and a translation parameter that controls the horizontal shift of the sigmoid function, influencing the point where the curve starts to rise.

$C_{A(\max)}$ is obtained from centrifugation measurement and f is obtained from the resonant frequency changes measured by QCR as described in previous chapters. The sigmoid function ultimately represents the concentration of unstable asphaltenes at equilibrium as a continuous function of antisolvent composition with only 2 interdependent parameters to adjust.

2.2.3. Correction factor to account for trapped liquid in fractal cluster

Several structural studies^{7,8,9,10} have shown that asphaltene nanoaggregates associate to form fractal clusters with a fractal dimension D_f , of approximately 2. This fractal dimension tends to increase when asphaltene clusters change from stable to unstable upon addition of alkanes⁸.

Fractal cluster contains solvent trapped within their structure. This trapped solvent affects the overall density of the clusters. Due to the presence of the trapped solvent, the effective density of

the fractal cluster, ρ_{eff} , is lower than the density of "dry" asphaltenes (ρ_{asph}), which is commonly accepted as 1200 kg/m³. The effective density can be expressed as follow:

$$\rho_{eff} = \left(\frac{\phi_{asph}}{\rho_{asph}} + \frac{(1 - \phi_{asph})}{\rho_{liquid}} \right)^{-1} \quad (9)$$

where ρ_{liquid} is the density of the trapped liquid solvent and ϕ_{asph} is the volume fraction of asphaltene components within a cluster.

In the case of suspensions of aggregates composed of hard spherical primary particles in contact, the volume fraction of asphaltene, ϕ_{asph} can be given by^{11,12}:

$$\phi_{asph} = \left(\frac{R_A}{R_p} \right)^{D_f - 3} \quad (10)$$

here, R_A is the hydrodynamic radius of asphaltene aggregates, R_p is the hydrodynamic radius of the primary units of asphaltene considered as nanoaggregates of 1.3 nm⁷ and D_f is the fractal dimension of the unstable clusters with a reported value around 2.1-2.8⁸.

As the centrifugation-based characterization of unstable asphaltenes concentration relies on the dried mass, Saidoun et al.⁵ suggested a dimensionless factor, denoted ψ , to correct for the swollen diffusing mass with respect to the solvent components of clusters.

The correction factor is given by:

$$\psi = x_{asph} + (1 - x_{asph}) \frac{\rho_{liquid}}{\rho_{asph}} \quad (11)$$

where the mass fraction of asphaltene nanoaggregates units within the fractal structure x_{asph} is determined as follow:

$$x_{asph} = \frac{\rho_{asph}}{\rho_{eff}} \phi_{asph} \quad (12)$$

2.2.4. Convective mass-transfer coefficient at the surface of the quartz sensor

To model the mass transfer at the surface of the quartz crystal resonator, each face of the sensor was assumed ideally smooth and surrounded by a semi-infinite liquid medium that flows parallel to the surface and exclusively downward. For a diffusion-limited mechanism the sticking reaction rate k_r constant is much greater than the mass transfer coefficient k_c ¹³:

$$k_r \gg k_c \quad (13)$$

In this context of a mass transport controlled mechanism, it is considered that a particle is stuck to the wall when the distance between the center of the particle and the surface is equal to the particle radius. In other words, the particle concentration at the surface $C_{A,surface}$ is equal to zero and the concentration gradient of unstable asphaltene particles available to deposit in the mass-transfer boundary layer becomes equal to the particle concentration in the liquid $C_{A,d,liquid}$ as follows:

$$\Delta C_{A,d} = C_{A,d,liquid} - C_{A,surface} \cong C_{A,d,liquid} \quad (14)$$

The concentration gradient of unstable asphaltene through a mass-transfer boundary layer will control the deposition rate as illustrated in Figure 3. The particle concentration available to deposit in the liquid at each time is obtained from Equation 6.

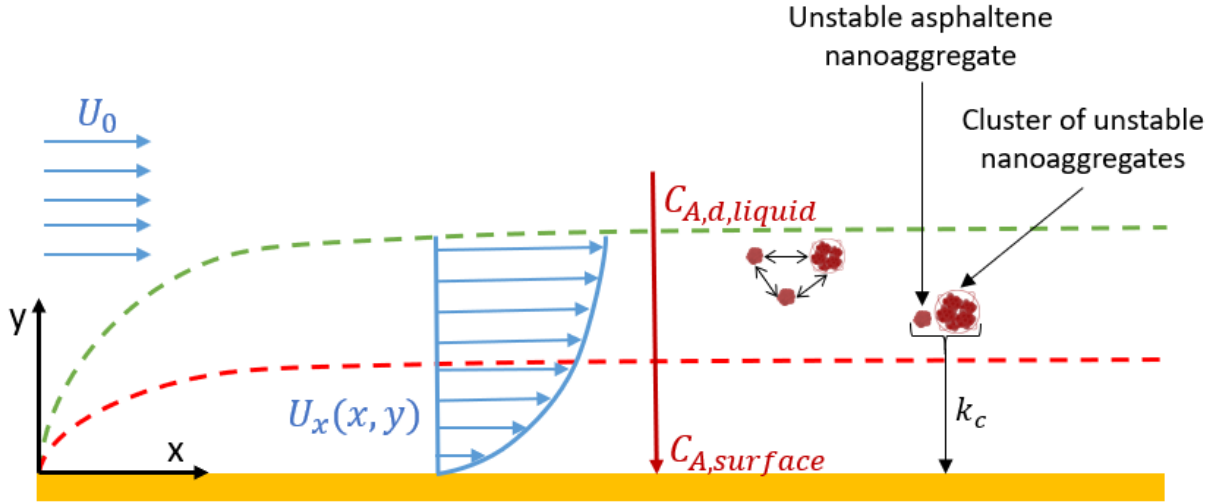


Figure 3. Schematic of unstable asphaltenes particles travelling at a velocity $U_x(x, y)$ in the momentum boundary layer (green dashed line) over a parallel solid surface and depositing through a mass-transfer boundary layer (red dashed line) controlled by the mass transfer coefficient k_c . $C_{A,d,liquid}$ and $C_{A,surface}$ are the liquid and surface concentrations of unstable asphaltenes particles respectively.

In this configuration, the deposition rate is given by:

$$Rate_{dep} = k_c C_{A,d,liquid} S_{QCR} \quad (15)$$

where $C_{A,d,liquid}$ is the concentration of dry unstable asphaltene particles available to deposit in the boundary layer and S_{QCR} is the quartz sensor surface area accounting for both immersed sides. k_c , the mass transfer coefficient at the surface of the quartz sensor, is a function of the hydrodynamic conditions, namely the fluid velocity U_0 , and the particle radius R_A .

In the case of a laminar ($Re < 2.10^5$) parallel stream with a superficial velocity U_0 , the mass transfer coefficient can be expressed as¹⁴:

$$k_c = \frac{D_A}{L} \overline{Sh} = 0.664 \frac{D_A}{L} Re^{1/2} Sc^{1/3} \quad (16)$$

where D_A is the diffusion coefficient, \overline{Sh} is the average Sherwood number, Re and Sc are respectively the dimensionless Reynolds and Schmidt numbers and L is the characteristic length equal to the QCR electrodes diameter (0.0125 m).

The dimensionless Reynold number is expressed as:

$$Re = \frac{U_0 L}{\nu_{liquid}} = \frac{\rho_{liquid} U_0 L}{\eta_{liquid}} \quad (17)$$

where, U_0 is the superficial velocity of the fluid, ν_{liquid} is the kinematic viscosity of the liquid (or viscosity diffusion rate) and it can be expressed as the ratio of the dynamic viscosity η_{liquid} to the density of the liquid ρ_{liquid} .

The dimensionless Schmidt number is the ratio of the viscosity diffusion rate to the molecular diffusion rate and is given by:

$$Sc = \frac{\nu_{liquid}}{D_A} = \frac{\eta_{liquid}}{\rho_{liquid} D_A} \quad (18)$$

Combining Equations 15 and 16 we get,

$$Rate_{dep} = 0.664 S_{QCR} D_A^{2/3} \left(\frac{U_0}{L}\right)^{1/2} \left(\frac{\rho_{liquid}}{\eta_{liquid}}\right)^{1/6} \psi C_{A,d,liquid} \quad (19)$$

Finally, the mass of deposit accumulated over time on sensor surface for a characteristic experimental run-time, t , is given by the following summation:

$$m_{dep}(t) = \int_0^t Rate_{dep}(t) dt \quad (20)$$

Because of the complexity of Equation 19 with multiple parameters varying implicitly with time, the integration in Equation 20 is calculated numerically using the Riemann summation method with N_t partitions of time (Δt). The cumulative amount of deposit is thus obtained by:

$$m_{dep}(t) = \sum_{t=0}^{N_t} Rate_{dep}(t) \Delta t \quad (21)$$

Saidoun⁵ used a dye tracing visual method to measure the superficial fluid velocity around the QCR as a function of the revolution speed of the magnetic stirrer. We invite readers curious about the details of the protocol used, as well as the approximations made by the author, to refer to his manuscript. Saidoun observed that superficial fluid velocity varied linearly with the stirring speed within the range studied.

The same glass vessel was used and the position of the disc was identical during our study, so the fluid velocity value was fixed in the following sections using the linear function proposed in the Figure 4.

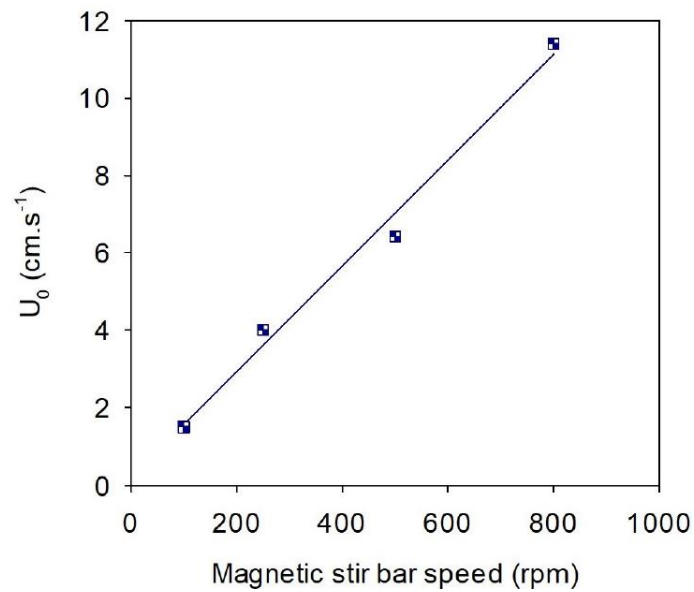


Figure 4. Average superficial velocities U_0 as a function of the revolution speed of the magnetic stirrer (reprinted from Saidoun et al.⁵).

3. Results and discussion

3.1. Evaluation of the chemical additive's interaction with QCR surface

Prior to the study presented in this manuscript, the interaction between the surface of the QCR and the chemical additives under investigation was verified. For that purpose, the chemical additives were diluted in toluene at 3000 ppm (in volume), and the mixture was left to equilibrate with the sensor during 1 hour at 60°C. A solution of pure toluene was used as a reference. Toluene was chosen as a substitute for the crude oil matrix because it is an aliphatic solvent and is known not to interact with the quartz surface¹⁵. The ratio of the shifts of resonance frequency and dissipation (3rd harmonic) is plotted in Figure 5. The results show very small variations in the ratio, and after a short equilibrium phase between the quartz and the surrounding fluid, the ratio tends towards a similar value regardless of the presence or absence of the chemical additives. These observations are consistent with the findings of Subramanian et al.¹⁶, who studied the effect of fatty-alkylamine (an amphiphilic compound) using QCM-D and found that it did not form a protective layer on a stainless-steel surface.

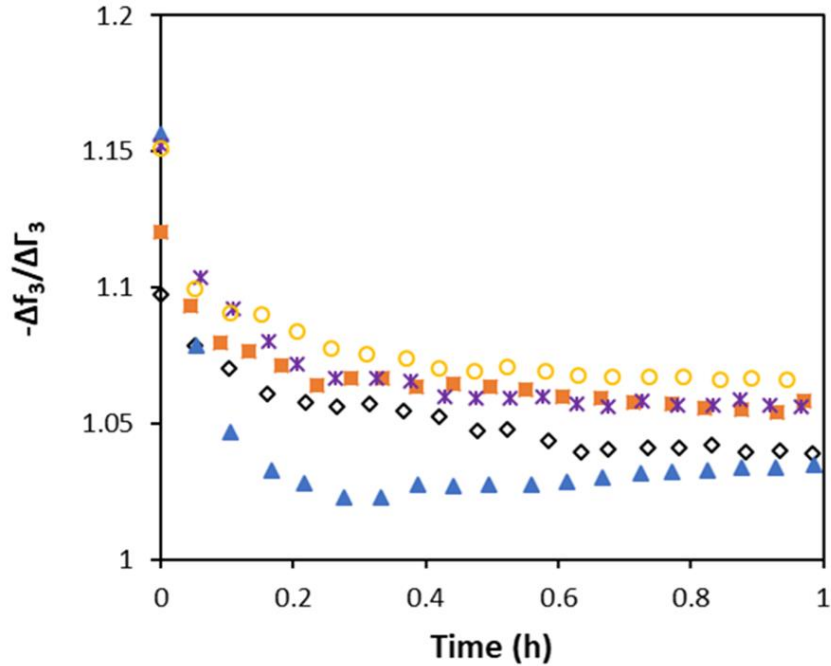


Figure 5. Ratio of the shifts of resonance frequency and dissipation (3rd harmonic), for QCR immersed in pure toluene (black ◇), toluene + 3000 ppmv of chemical additive A (orange ■), toluene + 3000 ppmv of chemical additive B (blue ▲), toluene + 3000 ppmv of chemical additive C (purple ✱), toluene + 3000 ppmv of chemical additive D (yellow ○), as a function of time at 60 °C and atmospheric pressure.

3.2. Concentration of unstable asphaltenes

The concentration of unstable asphaltenes particles by mass per volume of oil was obtained through centrifugation measurements using nontreated oil X. Experiments were carried out using different oil-heptane ratios and varying aging durations for specific oil-heptane ratios.

The concentration of unstable asphaltenes of each mixture as a function of the aging time is calculated using Equation 6.

The exponential form of the evolution of the concentration of unstable asphaltenes in the Equation 6 is controlled by two system dependent parameters: (i) the equilibrium concentration of unstable asphaltenes $C_{A\infty}$, which determines the value of the plateau, and (ii) the characteristic time for equilibration τ , which accounts for the aging time of the system.

$C_{A\infty}$, being given by the value of C_A on the plateau, the sole unknown parameter τ , is adjusted for each oil-heptane mixture to ensure that the predicted concentration of unstable asphaltenes matches the amount separated through centrifugation. The fitting of this parameter was performed using the least squares method in order to minimize the following objective function:

$$F_{obj} = \sum_{i=1}^N r_i^2 \quad (22)$$

Here, r_i are the residuals of the model defined as the difference between the observed value of the dependent variable and the value predicted by the model. The results of the modeling using Equation 6 for the nontreated oil X are presented in Figure 6.

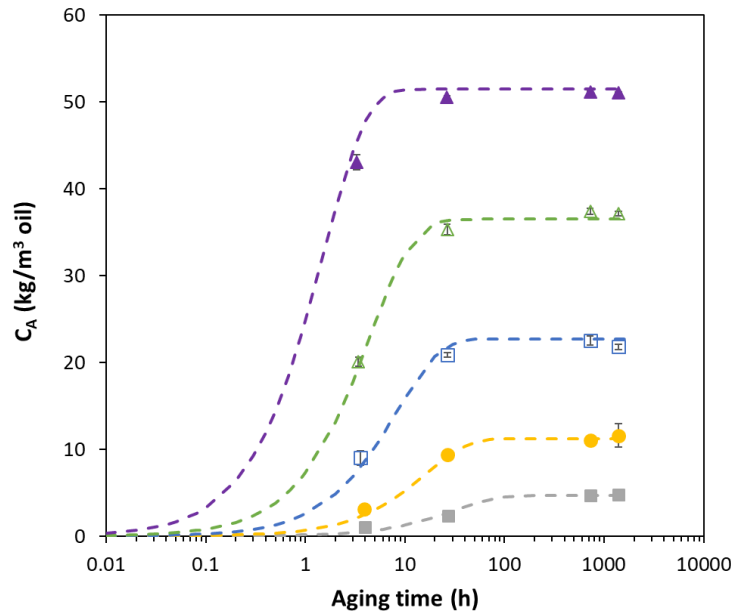


Figure 6. Concentration of unstable asphaltenes larger than 200 nm for nontreated oil X as function of aging time at multiple n-heptane volume fractions: (grey ■) 56.2 vol% n-C₇, (yellow ●) 61.1 vol% n-C₇, (blue □) 66.0 vol% n-C₇, (green △) 71.0 vol% n-C₇, (purple ▲) 80.7 vol% n-C₇. The dashed lines are calculated from Equation 6.

Given the trends in the experimental data, power functions would seem suitable for representing them. Nevertheless, the power law function suggests that the concentration of unstable asphaltenes at equilibrium increases continuously until a solvent content of 100% is reached. However, it is known that beyond a certain composition, the majority of asphaltenes become destabilized. This is confirmed by the presence of an inflection point in Figure 7-a. Therefore, the power function is unable to accurately represent this behavior, which is why a sigmoid function was preferred.

To establish continuity across the entire range of n-heptane content, the continuous dependencies of τ and $C_{A\infty}$ on mixture compositions (in terms of n-C₇ volume fraction) were achieved by adjusting both parameters to match the centrifugation data using Equations 7 and 8, respectively.

Finally, the values obtained by this method for $C_{A\infty}$ and τ are represented as a function of the n-heptane content in Figure 7 in order compared it to experimental values obtained from centrifugation measurements. From this figure, it can be seen that both equations are able to correlate $C_{A\infty}$ and τ parameter as a function of n-C₇ volume fraction.

Figure 7-a shows that as the antisolvent composition increases, the concentration of unstable asphaltenes at equilibrium also increases. Additionally, the time needed to reach equilibrium becomes shorter with an increase in the volumetric fraction of n-heptane (Figure 7-b). To explain this finding, Saidoun⁵ demonstrated through a sensitivity study of the particle generation rate constant that k_D increases as the n-heptane fraction is raised and as the aging time is reduced.

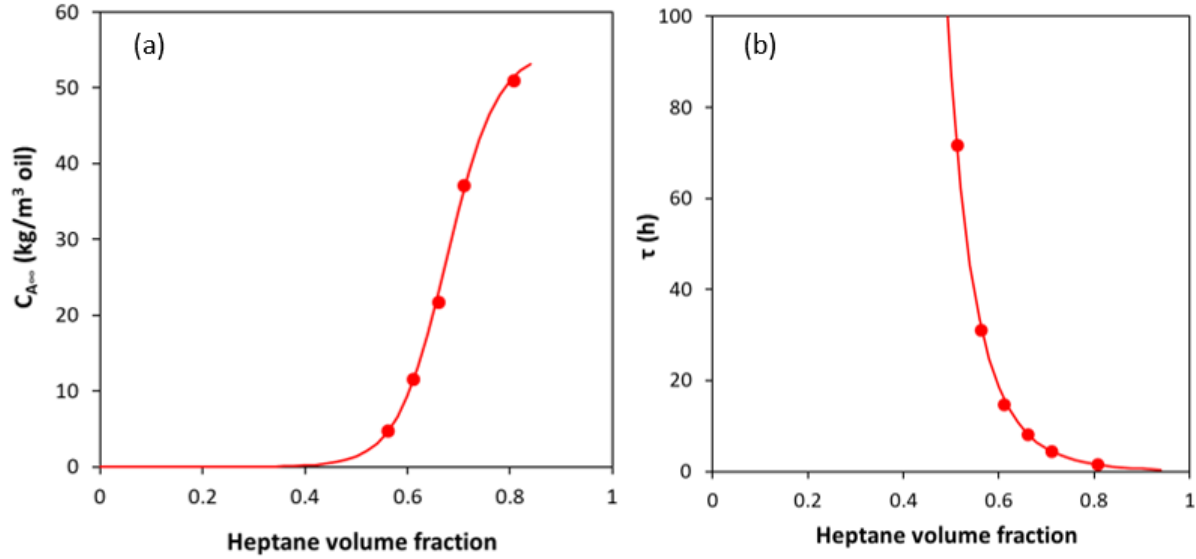


Figure 7. (a) Equilibrium concentration of unstable asphaltenes as a function of n-heptane volume fraction for nontreated oil X. The symbols correspond to the experimental data obtained by centrifugation measurements and the red solid line is calculated from Equation 8.

(b) Characteristic time of equilibration τ as a function of n-heptane volume fraction for nontreated oil X. The symbols correspond to the experimental data obtained by centrifugation measurements and the red solid line is calculated from Equation 7.

Using the proposed correlations for $C_{A_{\infty}}$ and τ , the concentration of unstable asphaltenes as a function of the n-heptane volume fraction was predicted using Equation 6 for a fixed aged time equal to 3.5 hours. The predicted values were then compared in Figure 8 to the experimental values obtained through centrifugation for mixtures aged for the same duration. This figure shows a notable alignment between the modeled curve, and the experimental values.

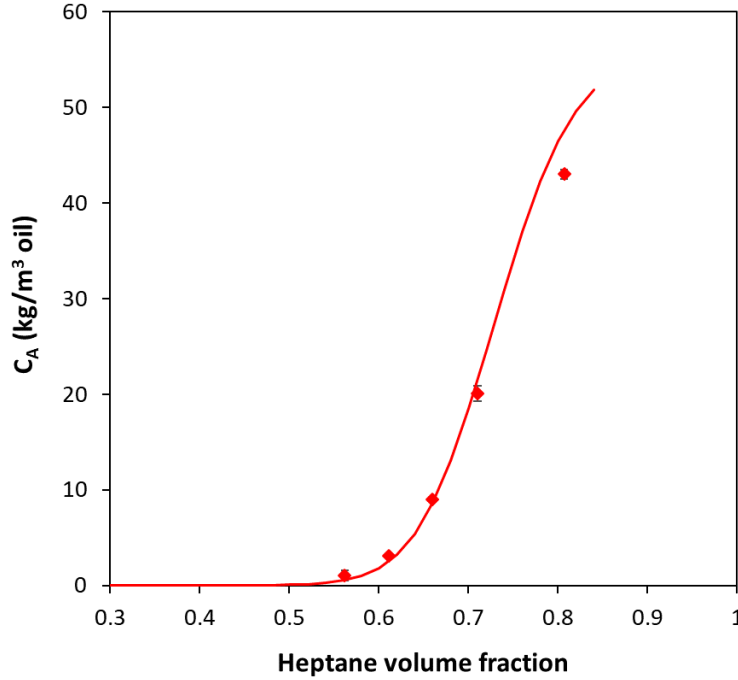


Figure 8. The red solid line is the concentration of unstable asphaltenes for the nontreated oil X as a function of n-heptane volume fraction calculated using Equation 6 for a 3.5 h aged mixture. The symbols represent the experimental data obtained by centrifugation with the same aging time for nontreated oil X.

In order to model the mass transfer during a continuous titration of antisolvent, the concentration profile of generated unstable asphaltenes, C_A and its derivative with respect of time need to be estimated. This can be achieved from Equation 6 with parameters $C_{A\infty}$ and τ correlated to volume fraction using Equations 7 and 8.

Because of the continuous injection of antisolvent, the volume fraction ϕ_{C_7} is a function of time, t , according to the following relation:

$$\phi_{C_7} = \frac{V_{C_7}}{V_{oil} + V_{C_7}} = \frac{q_{C_7}t}{V_{oil} + q_{C_7}t} \quad (23)$$

where V_{C_7} corresponds to the volume of n-heptane, V_{oil} is the volume of oil, and q_{C_7} is the injection rate of n-heptane.

The rate of change of the volumetric fraction of n-heptane is expressed as follow,

$$\frac{\partial \phi_{C_7}}{\partial t} = \frac{q_{C_7} V_{oil}}{(V_{oil} + q_{C_7} t_k)^2} \quad (24)$$

Consequently, $C_{A\infty}$ and τ , which depend on the antisolvent volume fraction, appears as an implicit function of time. Therefore, the derivation of C_A with respect to time during a titration experiment implies that Equation 6 needs to be treated as a composite function in order to derive it, utilizing the following chain rule:

$$\frac{dC_A}{dt} = \frac{C_{A\infty}}{\tau} \exp^{-\frac{t}{\tau}} + \left(\frac{\partial C_A}{\partial C_{A\infty}} \frac{\partial C_{A\infty}}{\partial t} \right) + \left(\frac{\partial C_A}{\partial \tau} \frac{\partial \tau}{\partial t} \right) \quad (25)$$

The derivative of C_A with respect to $C_{A\infty}$, is expressed as:

$$\frac{\partial C_A}{\partial C_{A\infty}} = 1 - \exp^{-\frac{t}{\tau}} \quad (26)$$

The derivative of $C_{A\infty}$ with respect to time is obtained from derivation of Equation 8:

$$\frac{\partial C_{A\infty}}{\partial t} = \frac{\partial C_{A\infty}}{\partial \phi_{C_7}} \frac{\partial \phi_{C_7}}{\partial t} = \frac{C_{A\infty, \max} i \times \exp^{-\frac{-(\phi_{C_7} - f)}{d}}}{d \left(1 + i \times \exp^{-\frac{-(\phi_{C_7} - f)}{d}} \right)^2} \frac{\partial \phi_{C_7}}{\partial t} \quad (27)$$

The derivative of C_A in Equation 6 with respect to τ , gives,

$$\frac{\partial C_A}{\partial \tau} = -C_{A\infty} \frac{t}{\tau^2} \exp^{-\frac{t}{\tau}} \quad (28)$$

The derivative $\partial\tau/\partial t$ is determined from derivation of Equation 7. It is expressed as,

$$\frac{\partial\tau}{\partial t} = \frac{\partial\tau}{\partial\phi_{C_7}} \frac{\partial\phi_{C_7}}{\partial t} = bc\phi_{C_7}^{c-1} \frac{\partial\phi_{C_7}}{\partial t} \quad (29)$$

A discretization of the time is used to resolve the quantity of unstable particles at a particular time t_k . Considering an extremely fast aggregation kinetics, above the asphaltene destabilization “onset”, generated particles are assumed to no longer exist in the form of primary units at the following time step t_{k+1} and are rather already considered larger entities⁵. Based on this assumption, the concentration of primary unstable asphaltenes C_1 can be written:

$$C_1(t) \approx \Delta C_{A_k} = C_A(t_{k+1}) - C_A(t_k) \quad (30)$$

Finally, the incremental concentration of unstable asphaltenes ΔC_A in the solution mixture upon an increment of time Δt while the addition of n-heptane is carried is given by:

$$C_1(t) \approx \frac{dC_A}{dt} \Delta t = \left[\frac{C_{A\infty}}{\tau} \exp^{-\frac{t}{\tau}} + \left(\frac{\partial C_A}{\partial C_{A\infty}} \frac{\partial C_{A\infty}}{\partial t} \right) + \left(\frac{\partial C_A}{\partial \tau} \frac{\partial \tau}{\partial t} \right) \right]_{t_k} \Delta t \quad (31)$$

In order to compare the values obtained from the analytical derivatives with results obtained by QCR measurements the increment of time Δt is chosen to correspond to the increment of time between each experimental measurement point of the QCR analyzer.

The generation rate of unstable asphaltenes in the solution per unit of time is calculated using Equation 23 and the result is showed in Figure 9. As the amount of n-heptane increase the quantity of unstable asphaltenes get larger starting from a minimum n-heptane composition (f in Equation 8), after the sharp increase a maximum is reached and the generation rate of unstable asphaltenes start to decrease.

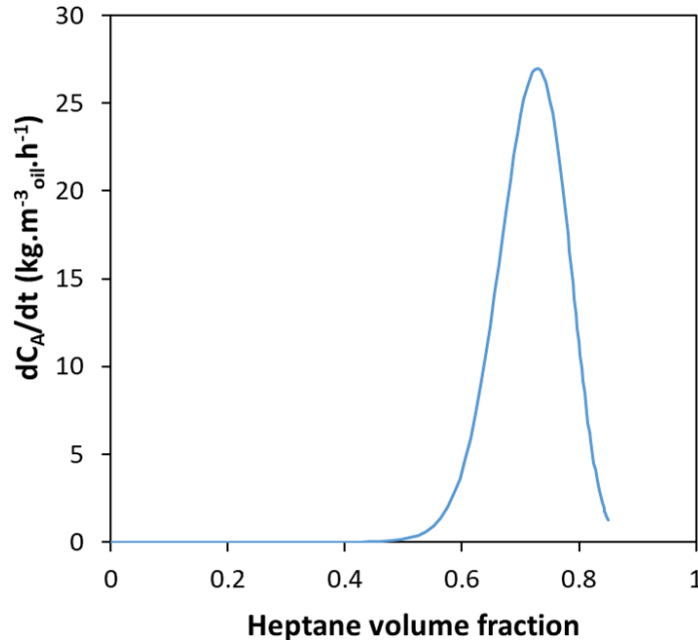


Figure 9. Generation rate of unstable asphaltenes $\frac{dC_A}{dt}$ as a function of n-heptane volume fraction in nontreated oil X during continuous addition of n-heptane.

3.3. Modeling deposition rate of unstable asphaltene particles by adjusting the diffusion coefficient

Saidoun⁵ postulated that the concentration of asphaltenes available to deposit $C_{A,d,liquid}$ was equal to the transient concentration of generated unstable particles C_1 , then Equation 19 becomes:

$$Rate_{dep} = 0.664s_{QCR}D_A^{2/3} \left(\frac{U_0}{L}\right)^{1/2} \left(\frac{\rho_{liq}}{\eta_{liq}}\right)^{1/6} \psi C_1 (1 - \phi_{C_7})_{t_k} \quad (32)$$

To account for the dilution effect of the solution during the continuous titration the concentration C_1 is multiplied by the volume fraction of oil in the mixture. After calculating C_1 from Equation 31, the only unknown parameter needed to calculate the deposition rate of unstable asphaltenes becomes the diffusion coefficient of primary particles diffusing toward the QCR surface that is directly correlated to the size of unstable particles according to Equation 2. Therefore, by

simultaneously fitting equations 6, 7 and 8 to the centrifugation data and equation 32 to the quartz crystal resonator experiments, it becomes possible to determine the size of unstable asphaltene particles diffusing to the quartz surface as a function of time/n-C7 concentration. For this application, the simplest approach would be to adjust the average particle size considering a constant value throughout the experiment. This data fitting was carried out using the titration experiment results for the oil without chemical additive. The result of this adjustment leads to an average value of 9.5nm for the unstable asphaltene aggregates diffusing toward the QCR surface. Using this fitted value, the deposition rate was first calculated using Equations 32. Then from the obtained deposition rate, the cumulative deposition mass was estimated from Equation 21. The results are compared to measurements in Figure 10-a and 10-b. These graphs show that, although the agreement is not perfect, the model is globally able to reproduce the experience by considering an average size of around 10 nm. This initial observation aligns with the findings of Saidoun⁵, indicating that it is the freshly destabilized clusters of nanoaggregates (less than twenty nanometers) that mainly contribute to the deposition, supporting the previously suggested assumption ($C_{A,d,liquid} = C_1$). However, it can be seen in Figure 10-a that the model is unable to capture the sharp increase of the deposition rate just after the “onset” when considering a constant hydrodynamic radius. This must mean that the size of the diffusing particles changes over experiment as a result of changes in composition and aging, while remaining in the range of around ten nanometers.

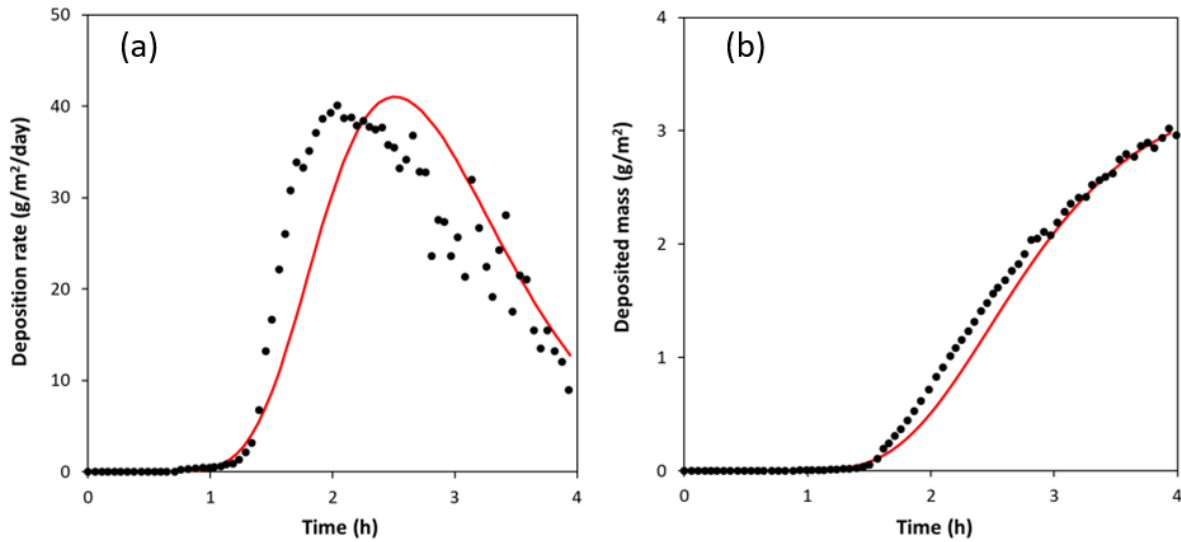


Figure 10. Asphaltene deposition rate (a) and deposited mass (b) on QCR sensor surface as a function of time during continuous titration of oil X with n-heptane. Symbols are experimental data and the solid lines are the computed values using Equations 32 (a) and 21 (b) with a fixed R_A of 9.5 nm.

To verify this hypothesis the fitting was repeated by considering a non-constant hydrodynamic radius of diffusing primary particles. By using the Stokes-Einstein (Equation 2) and fitting the hydrodynamic radius of the diffusing primary particles to the experimental data obtained from QCR. To achieve a good match between experiment and modeling, the particle size had to be adjusted point by point. However, to limit the noise associated with measurement and data derivation uncertainties, the experimental deposition rates were smoothed before being used to calculate the particles diameters. The results show a better match for the sharp increase of the deposition rate and the cumulative amount of deposit in Figure 11. These findings indicate that the average size of the diffusing particles varies during the continuous n-heptane addition. However, as shown in Figure 12, the size of the diffusing particles remains on the same order of magnitude as the size of stable asphaltene nanoaggregates clusters (<20 nm). A sensitivity analysis of the model was conducted to evaluate the effect of the experimental uncertainty on estimating the plateau value ($C_{A\infty}$) for the fitted hydrodynamic radii. The results are presented in Appendix B, and it can be concluded that the experimental uncertainty does not affect the trend of the fitted hydrodynamic radii during the titration and has a minor impact on the R_A value.

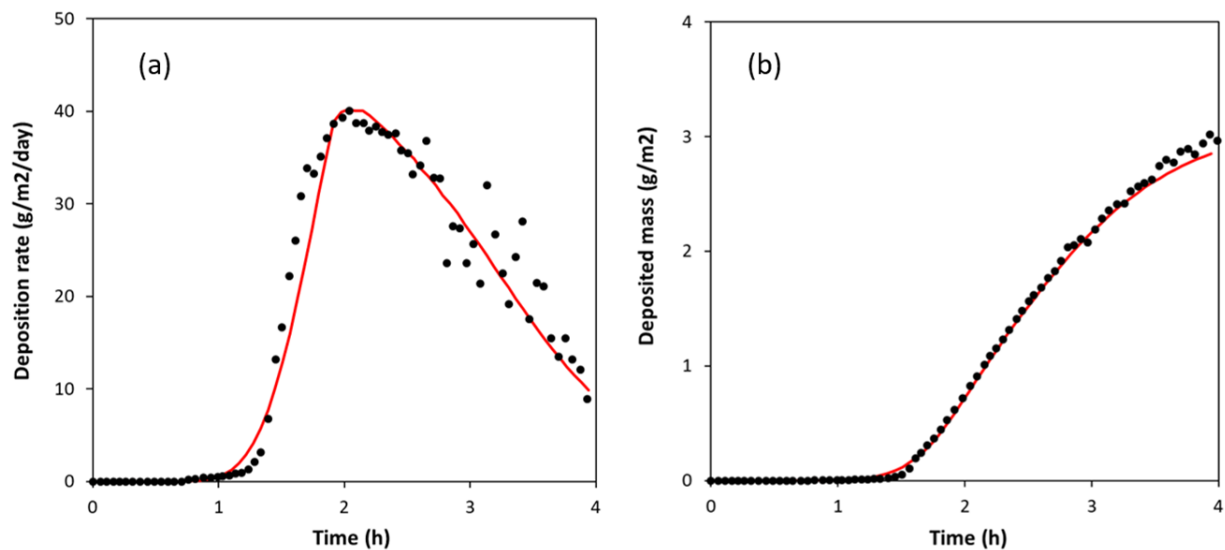


Figure 11. Symbols are experimental data obtained by QCR and the solid lines are the computed values of (a) the deposition rate using Equation 32 and (b) the cumulative mass of deposited asphaltenes using Equation 21 ; both as a function of time during continuous n-heptane addition and with a fitted R_A .

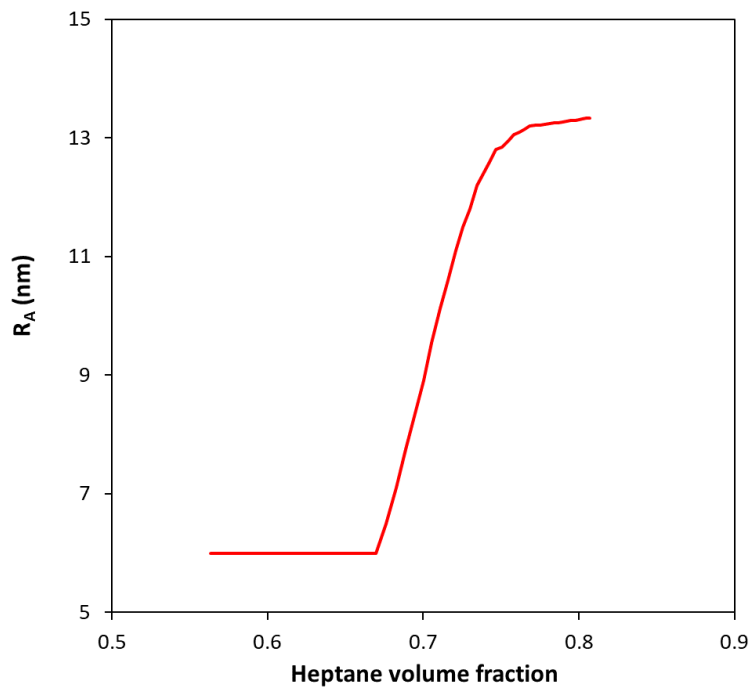


Figure 12. Mean hydrodynamic radius of diffusing primary particles during the continuous titration of oil X with n-heptane.

3.4. Effect of chemical additives

In order to study the effect of chemical additives on deposition mechanism, continuous addition of n-heptane in crude oil X with an immersed QCR sensor were carried out with chemical additives A, B, C, D, and compared with the nontreated crude oil X. During these experiments the shift in resonance frequency along various overtones (1 to 7) of the resonating sensor was recorded and analyzed for comparison. The results of the third overtone peak are presented in Figure 13. The shift in resonance frequency first decreases due to the dominant dilution effect caused by the addition of n-heptane. Then, the major change in the slope of the frequency can be explained by the fact that the mass deposition effect of asphaltenes takes precedence over the dilution effect. The values of the volumetric fraction of n-heptane at “onset” of destabilization in presence of the chemical additives are recorded in Table 2. The results indicate that the “onset” is significantly shifted towards higher n-heptane compositions in the presence of chemical additives D, A, and C in increasing order. This implies that these chemical additives stabilize the asphaltenes. Chemical Additive B, on the other hand, has the opposite effect. From the results of this experiment alone, it seems to promote asphaltene destabilization. However, the fact that the Δf_3 curves corresponding to oil alone and oil additivated with chemical additive B intersect shows that far from the “onset” it acts as a deposition inhibitor.

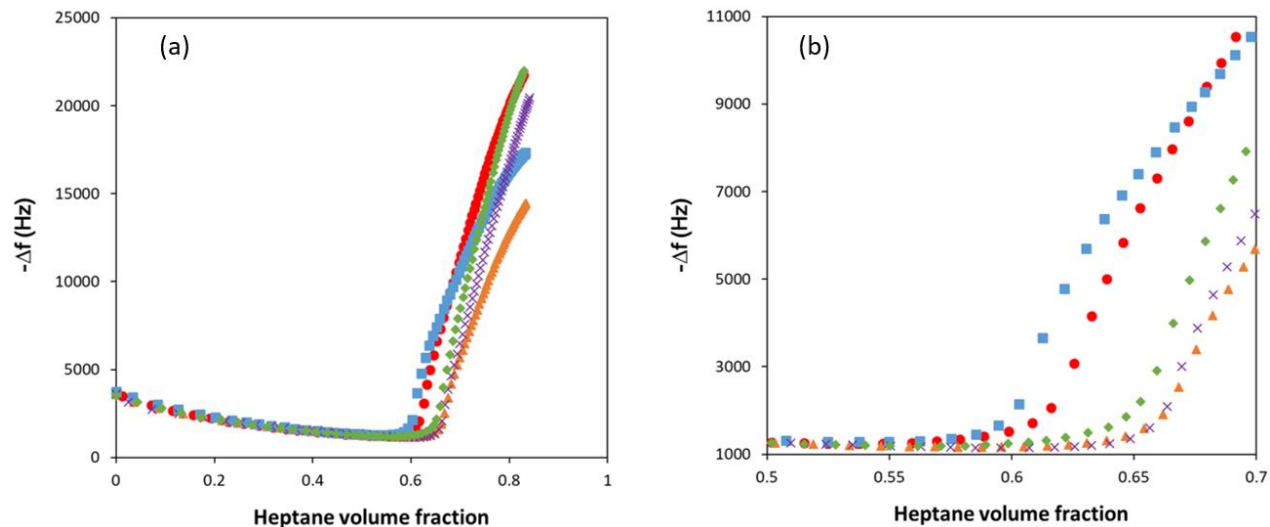


Figure 13. (a) Shift of resonance frequency (3rd harmonic) recorded during experimental titration of different crude oil X + chemical additive systems as a function of the volume fraction of n-heptane: (red ●) nontreated oil X, (orange ▲) chemical additive A at 3000 ppmv, (blue ■) chemical additive B at 3000 ppmv, (purple ×) chemical additive C at 3000 ppmv and (green ◆) chemical additive D at 3000 ppmv. A zoom of the frequency shift between 0.50 and 0.70 volume fraction of n-heptane is shown in the right-hand figure (b).

Table 2. “Onset” of destabilization from resonant frequency measurements.

Sample	Heptane volume fraction at inflexion point (%)
Nontreated oil X	55.2
Chemical additive A	58.7
Chemical additive B	55.0
Chemical additive C	60.7
Chemical additive D	58.0

At the same time, the concentrations of unstable asphaltenes at equilibrium were measured by centrifugation for various oil-heptane mixtures in the presence of the different chemical additives following the method presented in the *Methods* part. From these measurements, the characteristic

times to reach this equilibrium : τ and the concentration value when the plateau is reached: $C_{A\infty}$ were calculated and expressed continuously for each system as a function of the antisolvent content using Equations 7 and 8, respectively. The results are shown in Figure 14 (a) and (b). It can be seen in this figure that chemical additives do not qualitatively modify trends, but only quantitatively change values. In particular, the concentration of unstable asphaltenes is reduced by a factor of five in the presence of 3000 ppmv of chemical additive A across the entire composition range compared to nontreated oil. For the chemical additive B the curve for $C_{A\infty}$ overlap with nontreated oil up to 60% of n-C₇ but beyond that, the $C_{A\infty}$ value becomes much smaller than that measured for pure oil. It is even smaller than that obtained with the chemical additive C. Same as for nontreated oil the time required to reach equilibrium is shorter as the volumetric fraction of n-heptane increases whatever the chemical additive added. The time to reach equilibrium at low n-heptane content is much longer in the presence of additives A, C, and D compared to nontreated oil while $C_{A\infty}$ is lower. This observation suggests that these chemical additives not only reduce the total quantity of destabilized asphaltenes, but also affect destabilization kinetics by slowing down the process.

Centrifugation results in addition to QCR measurements shows that the A, C, and D chemical additives not only have an effect that delays the “onset” of asphaltenes destabilization but they also directly affect the kinetic beyond the “onset” as well as the total amount of unstable asphaltenes for a given volume fraction of n-heptane.

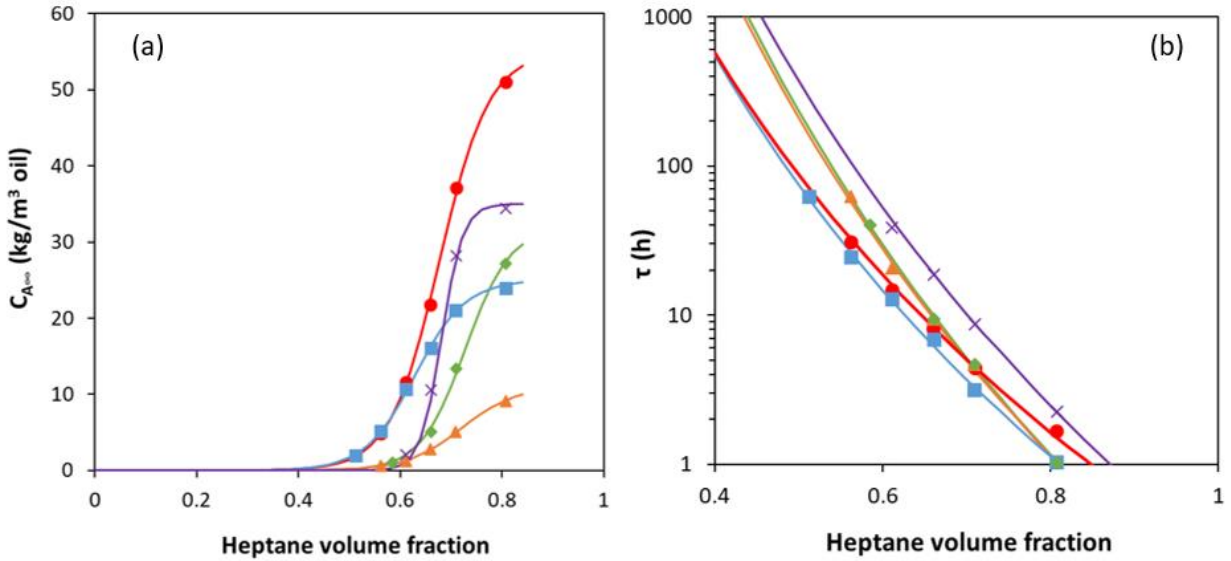


Figure 14. (a) Equilibrium concentration of unstable asphaltenes as a function of n-heptane volume fraction. The symbols correspond to the experimental data obtained by centrifugation measurements and the solid lines are calculated from Equation 8.

(b) Characteristic time of equilibration τ as a function of n-heptane volume fraction. The symbols correspond to the experimental data obtained by centrifugation measurements and the solid lines are calculated from Equation 7.

(red ●) nontreated oil X, (orange ▲) chemical additive A at 3000 ppmv, (blue ■) chemical additive B at 3000 ppmv, (purple ×) chemical additive C at 3000 ppmv and (green ◆) chemical additive D at 3000 ppmv.

To model the deposition rate considering a laminar flow, it was assumed that in presence of chemical additives the mass transfer remains diffusion-limited. In other words, the diffusivity of the depositing asphaltenes was expected to remain in the same order of magnitude as for nontreated oil. In the same way as for the pure oil, the modeled deposition rates were calculated using Equation 32 by adjusting the diffusion coefficient through the hydrodynamic radius using the Stokes-Einstein law (Equation 2). The experimental deposition rates obtained from QCR measurements during continuous titrations of oil X with n-heptane in the presence of the different chemical additives are represented by symbols in Figure 15. In the same figure, the modeled deposition rates based on combinations of Equations 31 and 32 using $C_{A\infty}$ and τ parameters obtained by fitting centrifugation data were represented by solid lines.

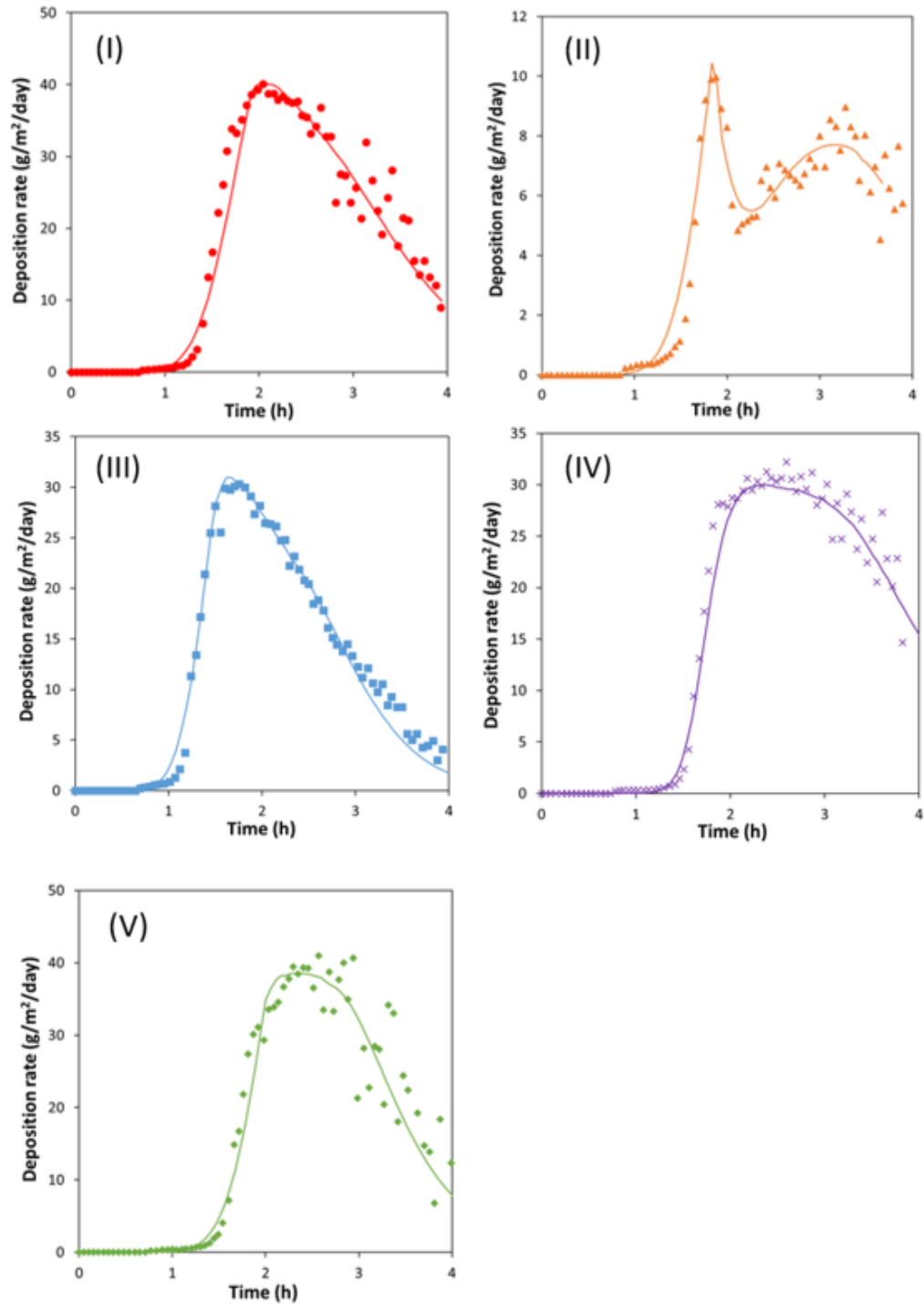


Figure 15. Symbols are experimental data obtained by QCR and solid lines are computed deposition rate with a fitted mean hydrodynamic radius.

(I) nontreated oil X, (II) chemical additive A at 3000 ppmv, (III) chemical additive B at 3000 ppmv, (IV) chemical additive C at 3000 ppmv and (V) chemical additive D at 3000 ppmv.

The modelled deposition rates adjusted with the mean hydrodynamic radii are shown in Figure 15. Comparison of the results obtained using this method show good agreement with the experimental data, despite the inconsistent behavior of some of the experimental data in Figure 15. For this reason, the modeled results for the different chemical additives were compared in Figure 15 instead of the experimental data. The deposition rates are shown in Figure 16.a, and the results indicate that nontreated oil, additive B, and additive D exhibit an increasing deposition rate followed by a maximum value and then a rapid decrease. For additive C, the deposition rate increases, reaches a plateau at the maximum, and then decreases slowly. Finally, chemical additive A shows an initial destabilization phase with an initially increasing deposition rate, followed by a sharp drop, and then a second destabilization phase with a relatively constant deposition rate. In order to ensure that the effect of chemical additive A on the deposition rate is not related to a measurement artifact, the chemical additive was tested at multiple concentrations (5000 and 20,000 ppmv). The results are presented in Appendix A and demonstrate the same behavior with two phases of destabilization whatever the amount of chemical additive used.

Figure 16.b shows the cumulative masses deposited on the sensor surface in the presence of the different chemical additives. Except for chemical additive B, all other chemical additives show a reduction in deposition compared to the nontreated oil. This result is directly correlated to experimental behavior found for the shift of resonance frequency of the quartz sensor in contact with titrated solutions. The most significant effect was obtained with chemical additive A that reduces the amount of deposited asphaltenes by a factor of 4 at 80 vol % of n-heptane compared to the nontreated oil.

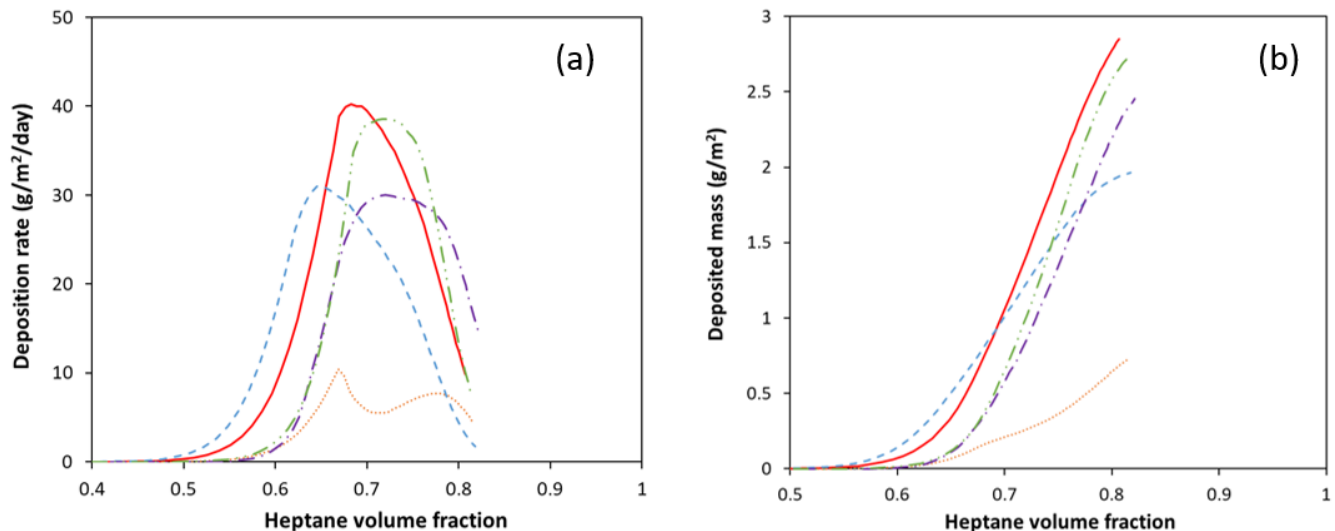


Figure 16.(a) deposition rate and (b) cumulative deposited mass as a function of n-heptane volume fraction in presence of the chemical additives.

(— red solid line) nontreated oil X; (⋯ orange dotted line) chemical additive A at 3000 ppmv; (--- blue dashed line) chemical additive B at 3000 ppmv; (-·-· purple dash-square-dot line) chemical additive C at 3000 ppmv; (-·-·- green dash-square-dot-dot line) chemical additive D at 3000 ppmv.

The fitted mean hydrodynamic radius of diffusing particles obtained after fitting Equation 32 to QCR and centrifugation experiments, is plotted in Figure 17 as a function of the volumetric composition of n-heptane. For all systems, R_A ranges from 2 nm to 15 nm, which remains of the same order of magnitude as of nanoaggregates and nanoaggregate clusters stabilized in oil. This result demonstrates that the primary particles, once destabilized, are indeed the ones involved in the deposition process. The chemical additives modify the size of particles that diffuse towards the surface. However, there isn't a change of several orders of magnitude. The diffusivity of unstable asphaltenes in the presence of chemical additives remains within the nanometer range (2-20 nm), similar to the nontreated oil. Therefore, the assumption that asphaltene deposition is still limited by diffusion, even in the presence of the tested chemical additives, is verified in both cases: with or without chemical additives.

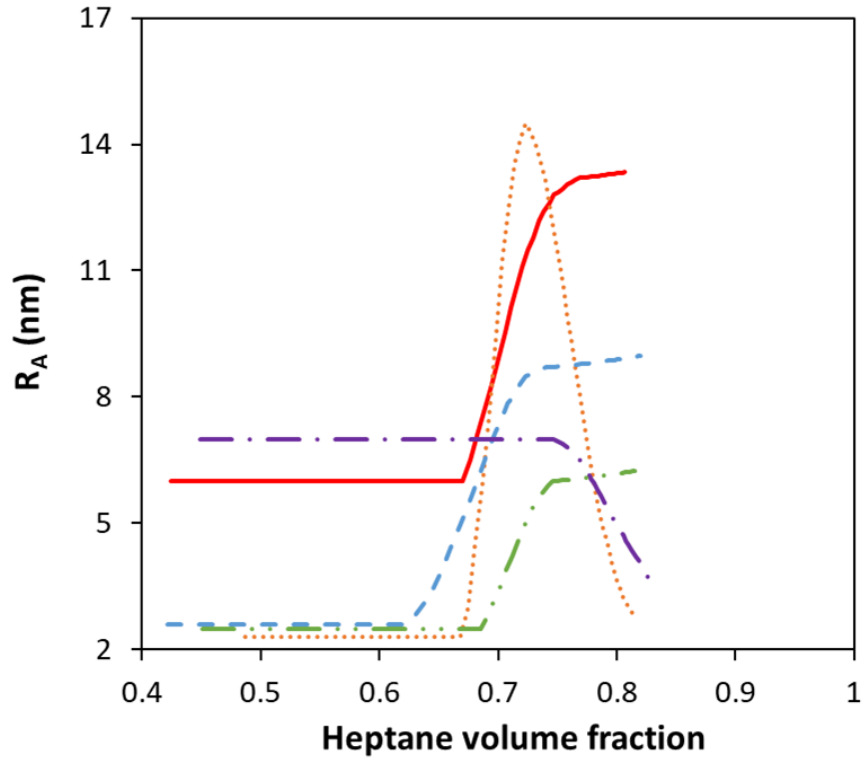


Figure 17. Mean hydrodynamic radius of diffusing primary particles as a function of n-heptane volume fraction in presence of chemical additives.

(— red solid line) nontreated oil X; (⋯ orange dotted line) chemical additive A at 3000 ppmv; (--- blue dashed line) chemical additive B at 3000 ppmv; (-.- purple dash-square-dot line) chemical additive C at 3000 ppmv; (-.-.- green dash-square-dot-dot line) chemical additive D at 3000 ppmv.

3.5. Discussions

In order to analyze the mechanisms of action of different chemical additives, the experimental results and modeled results have been summarized for each chemical additive in the same figure, including: (I) the resonant frequency changes raw data obtained from the QCR; (II) the experimental and modeled data of the concentration of unstable asphaltenes obtained through centrifugation for (which is of the same order of magnitude as the QCR titration time); (III) the deposition rate measured by the QCR; and (IV) the hydrodynamic radius fitted using the diffusion limited model. This analysis involves a juxtaposition of experimental and modeling outcomes with nontreated oil results for each chemical additive.

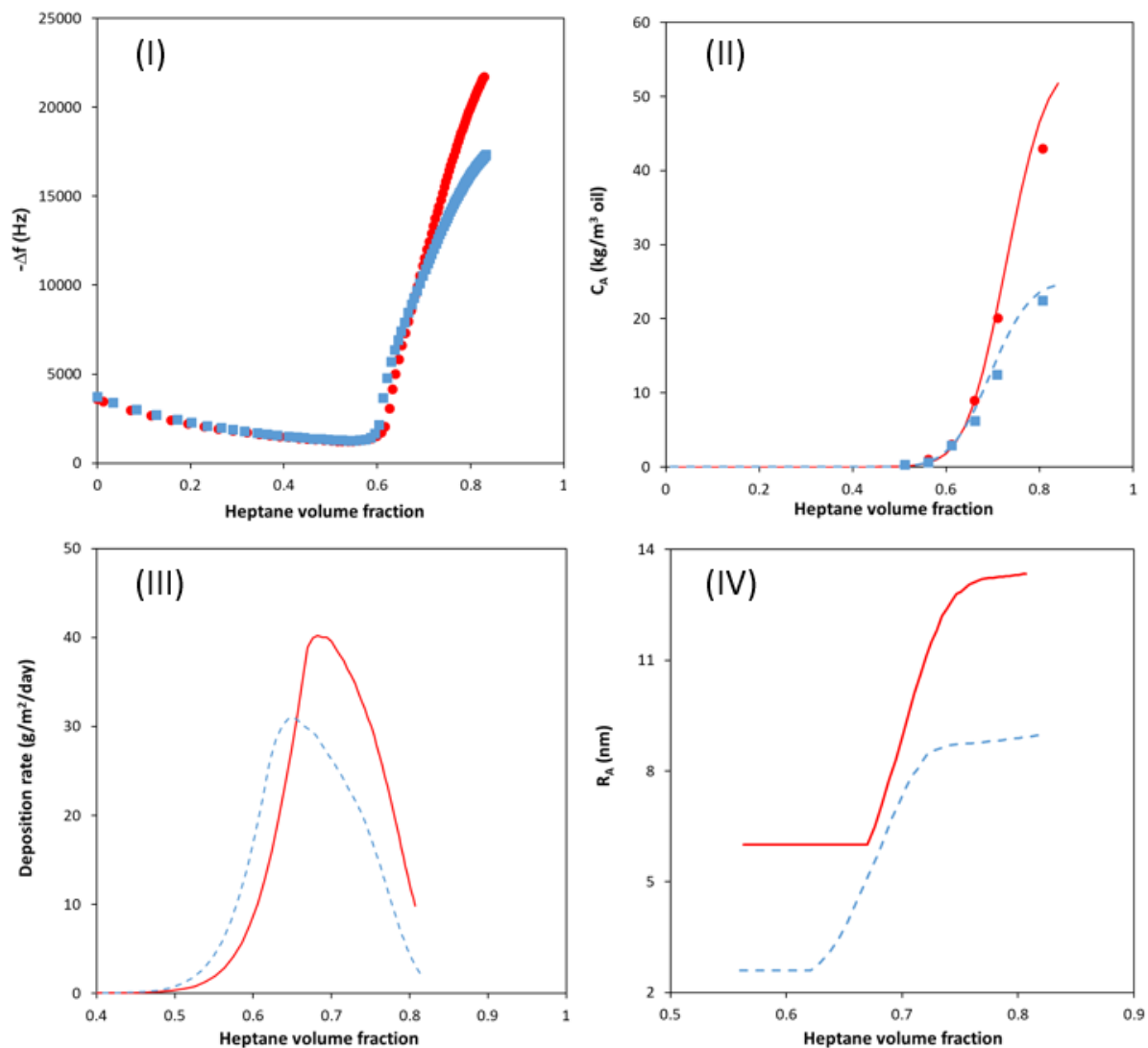


Figure 18. Results for oil X treated with 3000 ppmv of chemical additive B: (I) resonant frequency changes raw data obtained from the QCR; (II) experimental (symbols) and modeled data (lines) of the concentration of unstable asphaltenes obtained through centrifugation for $t = 3.5 h$ (III) deposition rate measured by the QCR; and (IV) the hydrodynamic radius fitted using the diffusion limited model.

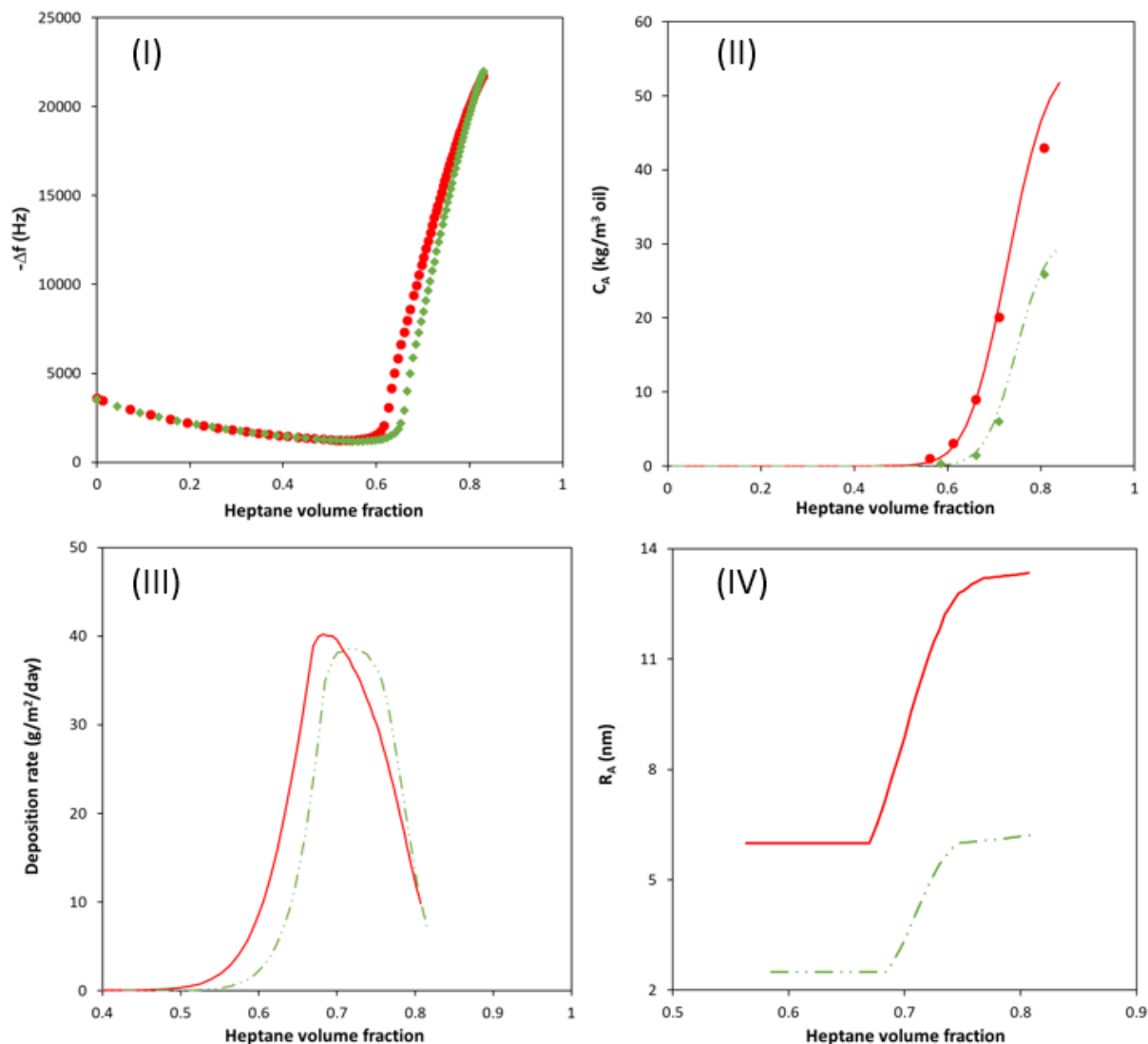


Figure 19. Results for oil X treated with 3000 ppmv of chemical additive D: (I) resonant frequency changes raw data obtained from the QCR; (II) experimental (symbols) and modeled data (lines) of the concentration of unstable asphaltenes obtained through centrifugation for $t = 3.5 h$ (III) deposition rate measured by the QCR; and (IV) the hydrodynamic radius fitted using the diffusion limited model.

Chemical additives B (Figure 18) and D (Figure 19) are the ones that inhibit deposition the least and display a behavior similar to that of nontreated oil. Chemical additive B exhibits an average particle size of 2.6 nm during the initiation of destabilization, and then the particle size increases monotonically resulting on a decreased deposition rate when n-heptane content becomes significant. Even though additive B tends to induce asphaltenes destabilization before the “onset”

of the nontreated oil, it still exerts a favorable inhibition impact on the amount of deposition occurring far from the “onset”.

Chemical additive D (4-nonylphenol), which can be considered as the "monomer" of B, has a similar effect to chemical additive B (polynonylphenol), but it keeps the particle size smaller during the decreasing deposition rate phase. At the beginning of deposition in the presence of chemical additives B and D, the size of diffusing particles is reduced and corresponds to the size of stable asphaltene nanoaggregates. Similar particle sizes have been reported by Goual et al.¹⁷ through conductivity measurements for asphaltenes treated with octylphenol and dodecylphenol in heptol with a fixed ratio of 80:20. At low asphaltene content, the authors observed sizes of 2 nm, and when the asphaltene concentration was increased, the particle sizes were around 8 nm (compared to approximately 10 nm for nontreated asphaltenes)¹⁷. The reduction in size of asphaltene particles can be explained by the steric repulsion generated by additives C and D, as well as by the active sites they block upon attaching to asphaltenes, as discussed in *Chapter 4* in the presence of alkylphenols.

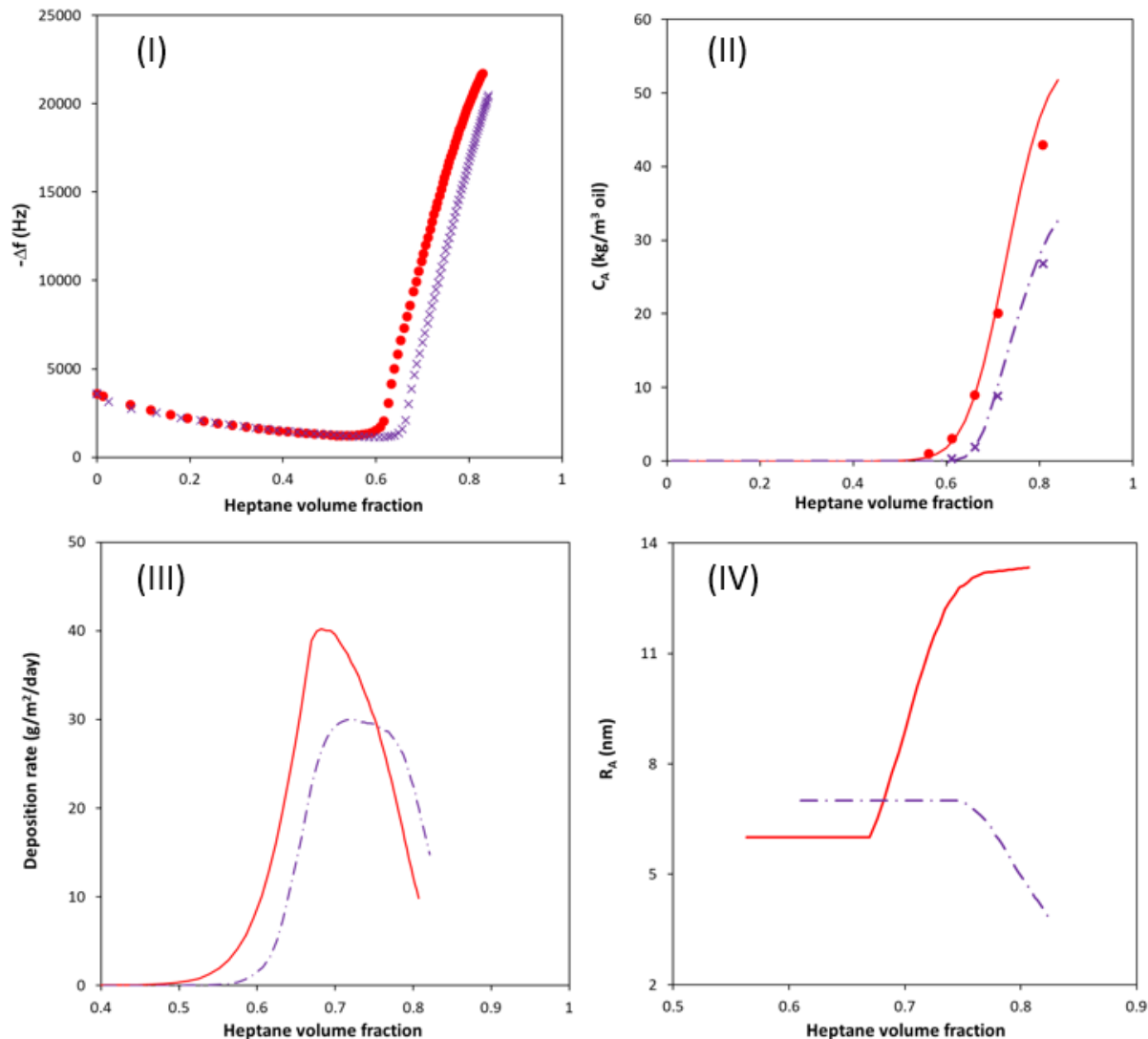


Figure 20. Results for oil X treated with 3000 ppmv of chemical additive C: (I) resonant frequency changes raw data obtained from the QCR; (II) experimental (symbols) and modeled data (lines) of the concentration of unstable asphaltenes obtained through centrifugation for $t = 3.5 h$ (III) deposition rate measured by the QCR; and (IV) the hydrodynamic radius fitted using the diffusion limited model.

A summary of the results obtained with chemical additive C is presented in Figure 20. In the presence of chemical additive C, the hydrodynamic radius of diffusing particles is maintained at 7 nm, then, at approximately 73 vol % of n-heptane, the size of diffusing particles decreases. Chemical additive C reduces the amount of the most unstable asphaltenes, but does not affect the size of the diffusing particles, which remains equivalent to that of nontreated asphaltenes below

73 vol % of n-heptane. However, above this composition, the asphaltenes stabilized by the chemical additive C become unstable and diffuse, resulting in a higher deposition rate than nontreated oil. The size of diffusing particles decreases despite the increase in the concentration of unstable particles. The mechanism of action of this chemical additive is not the same as in the presence of alkylphenol-type compounds.

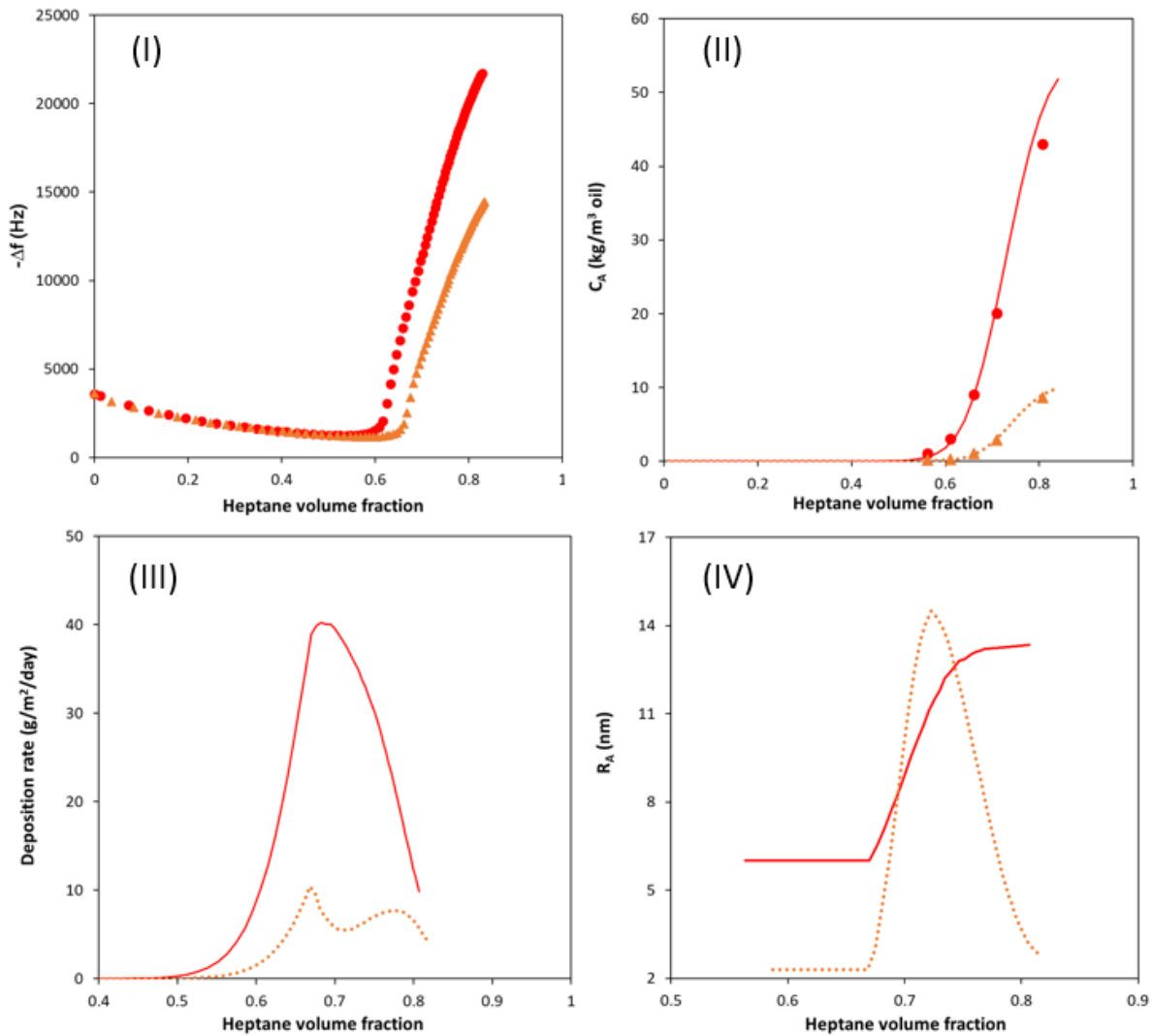


Figure 21. Results for oil X treated with 3000 ppmv of chemical additive A: (I) resonant frequency changes raw data obtained from the QCR; (II) experimental (symbols) and modeled data (lines) of the concentration of unstable asphaltenes obtained through centrifugation for $t = 3.5 h$ (III) deposition rate measured by the QCR; and (IV) the hydrodynamic radius fitted using the diffusion limited model.

Figure 21 presents a summary of the outcomes achieved with chemical additive A. Chemical additive A, which has a complex structure, exhibits two phases of destabilization resulting from a synergy of the effects of the two precursors (chemical additives B and C), leading to an initial increase in the size of diffusing particles followed by a decrease. One could envision that the structure of chemical additive A enables the stabilization of a broader distribution of asphaltenes, which could be explained by the two complementary chemical structures (chemical additives B and C) within the same framework that can interact with a wider range of asphaltenes chemistry such as H-bonding or acid-base interaction (the N-H bond of secondary amines can cleave, giving them a mildly acidic quality to react with asphaltenes, which, in contrast, exhibit a basic character^{18;19}). While comprehending and elucidating the mechanisms prompted by the introduction of chemical additive A in crude oil may prove challenging, the collective findings unequivocally highlight its paramount influence on both the generation of unstable asphaltene and the buildup of deposit. The combined synergy of the inhibitory effects of additives B and C brings about a substantial reduction in deposition on sensor surface.

4. Conclusions

The fitting of diffusion coefficients has revealed that the particles diffusing towards the surface have mean hydrodynamic radii of less than twenty nanometers, which is of the same order of magnitude as stable nanoaggregates clusters. The question arises that if the chemical additives limit the cluster size, this should generate more deposition since these particles would have higher diffusion coefficients in accordance with the Stokes-Einstein equation. However, measurements of unstable asphaltenes concentration have shown that the number concentration is reduced in the presence of chemical additives and almost negligible for additives A, C, and D at low n-heptane content. Therefore, the chemical additives stabilize the asphaltenes to a different degree depending on the amount of n-heptane in the system. With a limited number of unstable particles, the concentration gradient decreases, thus limiting deposition. The results in the presence of p-nonylphenol (chemical additive D) and polynonylphenol (additive B) show a limited reduction in deposited quantity compared to nontreated oil. These chemical additives have the effect of reducing the quantity of available particles and constraining the size of diffusing particles through

steric repulsion. However, as the available destabilized particle quantity increases, each stabilized particle will have more neighboring particles, and steric repulsion will become insufficient, leading to an increase in size. For chemical additives C and A, the mechanisms of action are more complex, and additional experiments are needed to clarify them. A study of fractal dimension, surface roughness, and asphaltene size in the presence of these chemical additives using scattering methods could provide answers.

5. References

- (1) Nabzar, L.; Aguilera, M. E. The Colloidal Approach. A Promising Route for Asphaltene Deposition Modelling. *Oil & Gas Science and Technology - Rev. IFP* **2008**, *63* (1), 21–35. <https://doi.org/10.2516/ogst:2007083>.
- (2) Hashmi, S. M.; Loewenberg, M.; Firoozabadi, A. Colloidal Asphaltene Deposition in Laminar Pipe Flow: Flow Rate and Parametric Effects. *Phys. Fluids* **2015**, *27* (8), 083302. <https://doi.org/10.1063/1.4927221>.
- (3) Eskin, D.; Ratulowski, J.; Akbarzadeh, K.; Pan, S. Modelling Asphaltene Deposition in Turbulent Pipeline Flows. *Can. J. Chem. Eng.* **2011**, *89* (3), 421–441. <https://doi.org/10.1002/cjce.20507>.
- (4) Vilas Bôas Fávero, C.; Hanpan, A.; Phichphimok, P.; Binabdullah, K.; Fogler, H. S. Mechanistic Investigation of Asphaltene Deposition. *Energy Fuels* **2016**, *30* (11), 8915–8921. <https://doi.org/10.1021/acs.energyfuels.6b01289>.
- (5) Saidoun, M. Investigations into Asphaltenes Destabilization, Aggregation and Deposition. Thesis, 2020.
- (6) Saidoun, M.; Favero, C. V. B.; Carrier, H.; Palermo, T.; El Ghazouani, J.; Daridon, J.-L. On the Controlling Kinetics of Unstable Asphaltenes (to be submitted). **2023**.
- (7) Barré, L.; Simon, S.; Palermo, T. Solution Properties of Asphaltenes. *Langmuir* **2008**, *24* (8), 3709–3717. <https://doi.org/10.1021/la702611s>.
- (8) Hoepfner, M. P.; Vilas Bôas Fávero, C.; Haji-Akbari, N.; Fogler, H. S. The Fractal Aggregation of Asphaltenes. *Langmuir* **2013**, *29* (28), 8799–8808. <https://doi.org/10.1021/la401406k>.
- (9) Roux, J.-N.; Broseta, D.; Demé, B. SANS Study of Asphaltene Aggregation: Concentration and Solvent Quality Effects. *Langmuir* **2001**, *17* (16), 5085–5092. <https://doi.org/10.1021/la0101651>.
- (10) Gawrys, K. L.; Matthew Spiecker, P.; Kilpatrick, P. K. The Role of Asphaltene Solubility and Chemical Composition on Asphaltene Aggregation. *Petroleum Science and Technology* **2003**, *21* (3–4), 461–489. <https://doi.org/10.1081/LFT-120018533>.

- (11) Snabre, P.; Mills, P. I. Rheology of Weakly Flocculated Suspensions of Rigid Particles. *J. Phys. III France* **1996**, *6* (12), 1811–1834. <https://doi.org/10.1051/jp3:1996215>.
- (12) Palermo, T.; Tournis, E. Viscosity Prediction of Waxy Oils: Suspension of Fractal Aggregates (SoFA) Model. *Ind. Eng. Chem. Res.* **2015**, *54* (16), 4526–4534. <https://doi.org/10.1021/ie504166n>.
- (13) Fogler, H. S. *Essentials of Chemical Reaction Engineering*, Second edition.; Prentice Hall international series in the physical and chemical engineering sciences; Prentice Hall: Boston, 2018.
- (14) Welty, J.; Rorrer, G. L.; Foster, D. G. *Fundamentals of Momentum, Heat, and Mass Transfer*; John Wiley & Sons, 2020.
- (15) Cassiède, M.; Mejia, A.; Radji, S.; Carrier, H.; Daridon, J.-L.; Saidoun, M.; Tort, F. Evaluation of the Influence of a Chemical Inhibitor on Asphaltene Destabilization and Deposition Mechanisms under Atmospheric and Oil Production Conditions Using QCM and AFM Techniques. *Energy Fuels* **2021**, *35* (21), 17551–17565. <https://doi.org/10.1021/acs.energyfuels.1c02570>.
- (16) Subramanian, S.; Buscetti, L.; Simon, S.; Sacré, M.; Sjöblom, J. Influence of Fatty-Alkylamine Amphiphile on the Asphaltene Adsorption/Deposition at the Solid/Liquid Interface under Precipitating Conditions. *Energy Fuels* **2018**, *32* (4), 4772–4782. <https://doi.org/10.1021/acs.energyfuels.8b00059>.
- (17) Goual, L.; Sedghi, M.; Wang, X.; Zhu, Z. Asphaltene Aggregation and Impact of Alkylphenols. *Langmuir* **2014**, *30* (19), 5394–5403. <https://doi.org/10.1021/la500615k>.
- (18) Peng, J.; Tang, G.-Q.; Kovscek, A. R. Oil Chemistry and Its Impact on Heavy Oil Solution Gas Drive. *Journal of Petroleum Science and Engineering* **2009**, *66* (1), 47–59. <https://doi.org/10.1016/j.petrol.2009.01.005>.
- (19) Hosseinpour, N.; Khodadadi, A. A.; Bahramian, A.; Mortazavi, Y. Asphaltene Adsorption onto Acidic/Basic Metal Oxide Nanoparticles toward in Situ Upgrading of Reservoir Oils by Nanotechnology. *Langmuir* **2013**, *29* (46), 14135–14146. <https://doi.org/10.1021/la402979h>.

6. Appendices

6.1. Appendix A

In order to confirm that the deposition rate profile obtained while using 3000 ppm by volume of chemical additive A in oil X during the continuous n-heptane titration was not influenced by experimental errors, supplementary measurements were performed on the QCR at progressively higher concentrations. The results are presented in Figure A-1. It becomes clear that a comparable pattern arises at both 5000 and 20,000 ppmv levels, exhibiting an initial phase characterized by a rapid deposition rate rise, succeeded by a decline, and subsequently followed by a resurgence, forming a secondary peak.

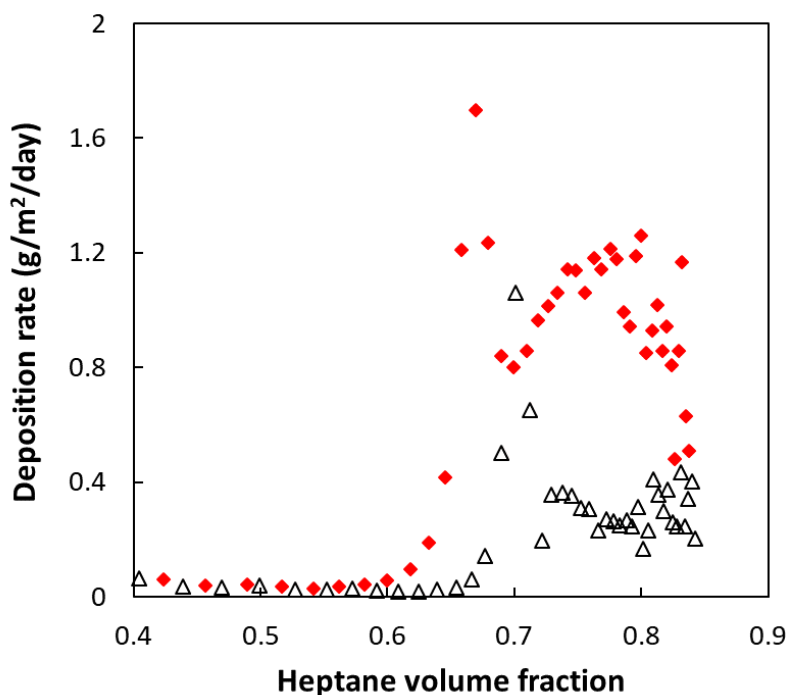


Figure A-1. Deposition rate measured by QCR during the continuous titration of oil X with n-heptane in the presence of the chemical additive A at: (red ♦) 5000 ppmv and (black △) 20,000 ppmv.

6.2. Appendix B

We observed that the main uncertainty associated with the experimental measurements was attributed to the value of the plateau measured by centrifugation. Considering the error bars from the plateau values, we estimated an error of $\pm 5\%$ of $C_{A\infty}$ at a given n-heptane composition.

Figure B-1 illustrates the impact of the relative error of $C_{A\infty}$ on the adjusted hydrodynamic radius during a continuous titration of oil X with n-heptane. A 5% variation in $C_{A\infty}$ does not affect the size of the diffusing particles at the beginning of the titration but has a relatively minor effect on the fitted hydrodynamic radius value as the concentration of particles available in the solution increases. The size of the diffusing particles at the end of the titration is 13.3 ± 1.2 nm, which is comparable to the size of stable clusters.

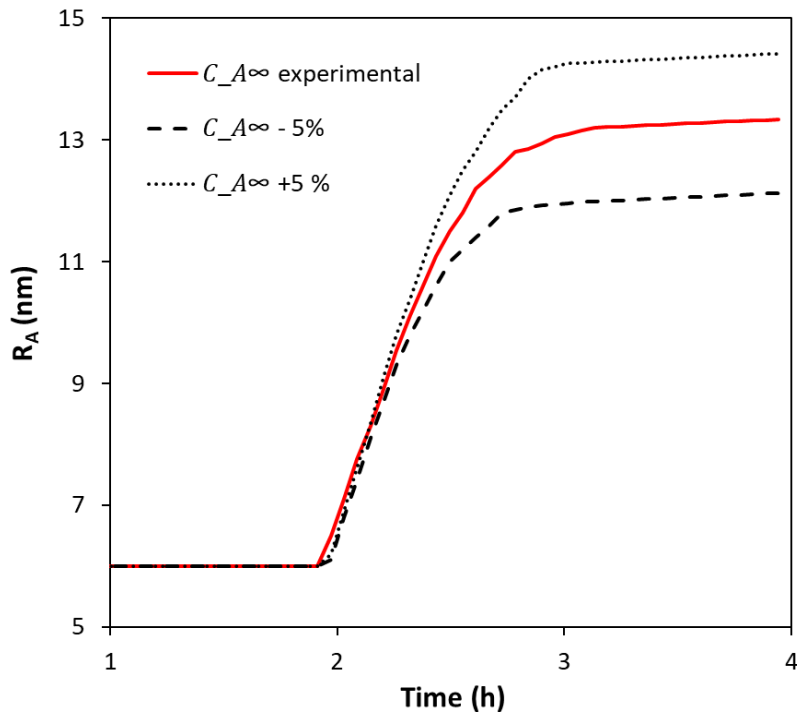


Figure B-1. Impact of the unstable asphaltene concentration at equilibrium incertitude for pure crude oil X.

Conclusions and Perspectives

In recent decades, the understanding of phenomena related to asphaltenes has improved, notably through the structural characterization of these molecules. In their natural state, asphaltenes self-associate to form stable nanoaggregates and clusters. When destabilized due to the volumetric expansion of light alkanes during oil depressurization, the asphaltenes flocculate and deposit on surfaces. This deposition hinders the proper flow of oil, leading to economic costs. To mitigate or inhibit the formation of asphaltene deposits, the petroleum industry employs the use of chemical anti-deposition additives, also known as asphaltene deposition inhibitors. Understanding the mechanisms of action of these deposition inhibitors is crucial to enhance their chemistries and adapt them based on encountered issues in oil reservoirs.

To shed light on the effects of chemical additives on destabilization, aggregation, and deposition, a multi-scale workflow has been proposed, spanning from the nanometer to micrometer scale. Experiments were conducted at atmospheric pressure in nondiluted oil, and asphaltene destabilization was induced by adding n-heptane.

The complementary techniques used are as follows:

- Centrifugation, a method for separating asphaltenes to obtain the concentration of unstable asphaltene aggregates in a given solution (oil-heptane), with controlled aging time.
- Quartz Crystal Resonator (QCR), an acoustic sensor detecting asphaltenes destabilization and measuring deposition on its surface at the nanoscale during continuous titration with antisolvent
- Optical methods, including detection time, for studying the kinetics of unstable asphaltenes aggregation.

In *Chapter 3*, the workflow, based on that set of robust and complementary techniques, was used to evaluate a commercial deposition inhibitor. The experiments assessed the chemical additive's

ability to shift destabilization towards higher antisolvent compositions and to reduce cumulative deposition on the acoustic sensor's surface. The utility of using complementary techniques was highlighted by studying both the chemical additive's effect on the liquid phase, including destabilization and aggregation kinetics, and its effect on deposition. Following this chapter, a working concentration was established for the rest of the thesis.

In *Chapter 4* the impact of the polarity of the functional group and the alkyl chain length of alkylbenzene-derived amphiphiles on their interaction with asphaltenes was evaluated. The results showed that a polar head was required for amphiphiles to interact with asphaltenes. Additionally, the effect of alkyl chain length was assessed within the alkylphenol family by varying the alkyl chain length from 2 to 12 carbons. Results indicated that asphaltene stabilization was more effective as the alkyl chain length increased, yet this effect seemed limited beyond around ten carbons. The suggested mechanism of asphaltene stabilization by amphiphiles is that these compounds chemically interact with asphaltenes through their polar heads, utilizing acid-base interactions or hydrogen bonding, and stabilize asphaltenes by both blocking active sites on asphaltenes and generating steric repulsion when the alkyl chain length is sufficient.

In *Chapter 5* mechanism of action of a commercial inhibitor and its chemical precursors was investigated. A model of diffusion-limited mass transfer was used to calculate particle size evolution during continuous antisolvent titration in the presence of chemical additives. Model input parameters, unstable asphaltenes concentration, and deposition rate, were obtained from centrifugation and QCR experiments, respectively. Results clearly demonstrated that the quantity of unstable asphaltenes was reduced in the presence of chemical additives, and the size of diffusing particles was also affected. However, even with chemical additives present, the size of diffusing particles remained in the range of stable nanoaggregates and clusters (<20 nm), indicating that freshly destabilized particles contribute to deposit formation.

The studies conducted during this thesis work have proven to be conclusive, and the proposed workflow meets industrial needs and constraints. For a deeper understanding, to verify the effect of short-chain p-alkylphenols, it would be interesting to work with molar concentrations,

controlling the amphiphile/asphaltene ratio to identify a concentration where active sites (e.g., H-bonding sites) become saturated. Analyzing the supernatant from centrifugation measurements of extracted asphaltenes in toluene treated with short-chain p-alkylphenols using Fourier transform infrared spectroscopy would help characterize the amphiphile-asphaltene interaction further¹. Furthermore, the versatile effects observed in the case of DDBSA depending on the studied oil could be investigated by testing the amphiphile interaction with different asphaltene fractions with varying heteroatom contents.

To confirm and delve further into the results obtained regarding the hydrodynamic radius of diffusing particles, it could be interesting to conduct Small-Angle X-Ray Scattering (SAXS) diffusion measurements. This way, the interaction of chemical additives with stable clusters could be investigated through fractal dimension, surface roughness, and size measurements. Additionally, by adopting an approach similar to Ismail and Hoepfner², it could be valuable to study the transition from stable (soluble) to unstable (insoluble) state of asphaltenes in the presence of chemical additives using Ultra-Small Angle X-Ray Scattering (USAXS).

References

- (1) Chang, C.-L.; Fogler, H. S. Stabilization of Asphaltenes in Aliphatic Solvents Using Alkylbenzene-Derived Amphiphiles. 1. Effect of the Chemical Structure of Amphiphiles on Asphaltene Stabilization. *Langmuir* **1994**, *10* (6), 1749–1757. <https://doi.org/10.1021/la00018a022>.
- (2) Ismail, M.; Yang, Y.; Chaisontornyotin, W.; Ovalles, C.; Rogel, E.; Moir, M. E.; Hoepfner, M. P. Effect of Chemical Inhibitors on Asphaltene Precipitation and Morphology Using Ultra-Small-Angle X-Ray Scattering. *Energy Fuels* **2019**, *33* (5), 3681–3693. <https://doi.org/10.1021/acs.energyfuels.8b03055>.